Membrane Emulsification and Filtration for Engineered Particles

by

Marijana M. Dragosavac

Doctoral thesis

Submitted in partial fulfillment of the requirements

for the award of

Doctor of Philosophy of Loughborough University

13th September 2011

Dad, thank you for telling me that Chemical Engineering is for me.

ACKNOWLEDGEMENTS

This thesis would be incomplete without an acknowledgement of those who contributed to its successful completion. When the journey towards this degree began in the autumn of 2008, the day that I write the acknowledgements section of my thesis seemed infinitely far away. At the start, the only encouragement I received was from my husband, Vladan, who was so far away but at the same time so close.

Yet throughout the journey, I've met many kindred spirits who have helped me along the way. Big thanks goes to people in the department Sean, Dave, Monika, Kim, Graham and Jim who all helped me with the things I did not have a clue but I was supposed to learn. Paul was there to save me from all the computer troubles but was there firstly as a friend. A big thanks goes to my second supervisor Dr Goran T. Vladisavljević who taught me almost everything I know about science, membrane and microchannel emulsification, and who was and still is a valuable person to discuss the work, helping me improve as a researcher.

It was very scary to come alone so far away from home and I still remember the first night here, but I was so lucky to find Winn and John in Loughborough who made me feel like at home. They accepted me as a member of the family and there are no words to explain how valuable they were to me to survive my first year here.

So many new friends came along the way Sara, Giuseppe, Nati, Idil, Milena, Gi, Mike, Basti, Amy, Mariapia, and many others who helped me realize that there is life outside the research too.

Professor Richard G. Holdich deserves a paragraph to himself. When I met him as a visiting researcher in 2007 I never thought I would do a PhD in Loughborough, he suggested me to do so and I came and now I am writing this. It would be impractical to list all that I've learned from him, but suffice it to say, he has taught me more than any teacher I had before him, but above all he showed me to be patient and modest. He was there to support me in times when I was thinking that I was not good enough for this degree by not letting me put my head down and for that I thank him the most.

I am grateful to Faculty of Technology and Professors Milan Sovilj, Zavargo Zoltan and Radovan Omorjan for giving me the time off to pursue this degree. Professor Milan

Sovilj deserves big thanks also for believing in me as a researcher and giving me an opportunity to start my work in academia as well as giving me an opportunity to visit Loughborough in 2007. A big thanks goes to Professor Miodrag Tekić for all advices and help that he gave me when I needed it while working at Chemical Engineering department at Faculty of Technology in Novi Sad.

Finally, I have to thank my family. First on the list, of course, is my husband Vladan. Of the six years we've been married, I've been away from him three but, nevertheless, our love never faded away, and he has encouraged me every step of the way. Only he understands how I felt when making the late phone calls while feeling blue but his words, even just over the phone, gave me the strength to carry on.

My dad Marijan deserves special thanks since I would not be here if he did not advice me that Chemical Engineering was much better for me than Chemistry that day when we were together and I had to choose what to study. He is a valuable person to talk to every time when making some hard decisions. Every time when I needed to talk my mum Milka was there, and I know she worried a lot since I was so far away. But even so far away I felt that she was watching over me. My sister Nena was there when the sister's advice was needed and was a good companion to visit various places and do various things in England. And my brother Saša cared for me too. Also my grandparents, Đorđe i Dušica, were in my thoughts and I missed them so much. My mother in law, Angelina, was important along the way providing me with my favourite cake every time on my way back to Loughborough which reminded me of home when so far away. Even though not with us any more, I will never forget my father in law Jovan who was every time helping me to test the cakes before I had to take them to Loughborough.

ABSTRACT

In many applications employing particles, the distribution of particle sizes has significant influence on the properties of the resultant material. Membrane emulsification (ME) is a method for manufacturing uniformly sized emulsion droplets where a dispersed phase is forced through a membrane into the continuous phase. It is the shear applied on the membrane surface that detaches the droplets thereby generating an emulsion. Formulation of the dispersed and the continuous phase influences the final droplet size of the emulsion. Therefore one of the aims of this research is to broaden the existing knowledge on particle production by membrane emulsification using nickel microengeneered disk membrane with cylindrical pores and the Dispersion Cell.

The Dispersion Cell was successfully used to produce W/O/W emulsions (the oil phase was pumpkin seed oil). Also W/O emulsions (the water phase was acidified sodium silicate) were produced and additionally solidified in order to manufacture solid silica particles with high surface area and internal porosity. The particles were additionally functionalized using 3-aminopropyltrimethoxysilane and turned into ion exchange material capable to sorb copper. Since the silica particles do not swell such ion exchange material might be interesting for applications in nuclear industry.

Having in mind an industrial application of membrane emulsification the Dispersion Cell cannot be used due to the problems with the scaling up. Therefore two novel systems: Oscillating and Pulsating were developed and reported for continuous production of the particles. Both systems were commissioned using sunflower oil for production of O/W emulsions. Additionally the Pulsating system was successfully used for production of complex coacervates.

In the Oscillating system the nickel membrane was in the shape of a candle and the shear on the membrane surface was induced by vertical oscillations of the membrane. In the Pulsating system a tubular nickel membrane was used and the shear on the membrane surface was applied by oscillations of the continuous phase. The scaling up of both Oscillating and Pulsating system can be achieved by providing a larger membrane area (elongating the membrane) as well as connecting the membranes in parallel.

It was successfully shown that a simple force balance can be used to model the size of emulsion droplets as a function of the shear stress. The average shear stress worked better when modelling the droplet sizes in the Dispersion Cell, but the correction for the droplet neck had to be taken into consideration when higher dispersed phase flow rates were used. In the Oscillating and Pulsating systems it was the maximal shear stress that gave the better prediction, but in both systems it was clear that additional forces were present which influenced the final droplet size.

An alternative field of application for the Dispersion Cell, relevant to the tests of functionalized silica particles, was investigated. The Dispersion Cell was modified into a continuous flow stirred cell with a slotted nickel membrane on the bottom. The continuous flow stirred cell is shown to be an effective technique for both mass transfer kinetics as well as equilibrium data acquisition – combining both into a single step, and simplifying ion exchange analysis. To commission the system the commercial ion exchange resin (Dowex 50W-X8) was used. Once determined, the design parameters can readily be used to model ion exchange contacting in a well mixed system, column operations or any process that requires ion exchange material. Using the continuous flow stirred cell it was shown that the silica particles produced using the Dispersion Cell and functionalized using 3-aminopropyltrimethoxysilane were capable to sorb copper.

As a part of the collaboration within the DIAMOND (Decommissioning, Immobilisation And Management Of Nuclear wastes for Disposal) project a novel ion exchange material (copper hydroxide acetate suitable for iodide sorption) produced in the Department of Chemistry (Loughborough University) was successfully tested using the continuous flow stirred cell and equilibrium and mass transfer parameters were determined.

The continuous flow stirred cell is particularly relevant to instances when the mass of ion exchange material available for the testing is low (less than 1g) and when dealing with hazardous or expensive materials. It is a technique employing microfiltration and ion exchange (or sorption), of the engineered particles that could be produced by membrane emulsification described in this thesis.

TABLE OF CONTENTS

List of figures

List of tables

List of symbols

$\overline{q}$	Average mass of copper per unit mass of resin	g g^{-1}
μ_L	Dinamic viscosity of the suspending fluid	Pa s
a	Amplitude of oscillation	m
A	Total surface area of the resin particle	m^2
A_s	Interfacial area	m^2
b	Langmuir constant related to the energy of sorption	m^3 g^{-1}
b_h	Blade height	m
C	Sorbate concentration in the liquid phase	g m^{-3}
C_e	Equilibrium copper concentration in the liquid phase	g m^{-3}
C_{eq}	Final copper concentration in batch experiments in the liquid	g m^{-3}
C_o	Copper concentration in feed	g m^{-3}
C_{oi}	Initial copper concentration in batch experiments in the liquid	g m^{-3}
C_{ox}	Initial sorbate concentration/sorbate concentration in the feed stream	g m^{-3}
CV	Coefficient of variation	-
d	Mean droplet diameter/size	m
D	Stirrer width	m
D_{eff}	Effective diffusion coefficient of copper inside the particle	m^2 s^{-1}
D_{liq}	Diffusion coefficient of copper in the liquid phase	m^2 s^{-1}
D_m	Effective diameter of the membrane	m
d_p	Pore diameter	m
$d(v,0.5)$	Mean droplet diameter by volume	m
$d(n,0.5)$	Mean droplet diameter by number	m
d_m	Diameter of the tubular membrane	m
f	Frequency of the oscillation	s^{-1}
F	Volumetric flow rate of the effluent	m^3 s^{-1}
F_b	Buoyancy force	N
F_{ca}	Capillary force	N
F_d	Drag force	N
F_I	Inertial force	N
F_L	Dynamic lift force	N

F_{neck}	Static pressure difference force	N
F_o	Volumetric flow rate of the feed	$m^3\ s^{-1}$
G	Interfacial free energy	N m
g	Gravitational acceleration	$m\ s^{-2}$
J	Transmembrane flux	$m^3\ m^{-2}\ h^{-1}$
J_d	Dispersed phase flux	$m^3\ m^{-2}\ s^{-1}$
k	Mass transfer coefficient in liquid phase	$m\ s^{-1}$
k_p	Fraction of active pores	-
L	Pore spacing	m
m	Total mass of the resin	kg
m_{si}	Mass fraction of silica present in the liquid	-
N	Total number of pores in the membrane	-
q	Sorbate concentration on the solid phase	$g\ g^{-1}$
Qc	Volumetric flow of the continuous phase	$m^3\ s^{-1}$
Q_d	Total volumetric dispersed phase flow rate	$m^3\ s^{-1}$
q_e	Sorbate concentration on the solid phase in equilibrium	$g\ g^{-1}$
q_m	Maximal amount of sorbate that can be sorbed on the sorbent	$g\ g^{-1}$
P	Pressure	Pa
P_o	Saturation pressure	Pa
R	Sauter mean radius	m
r	Radial distance from the centre of particle	m
r_c	Radial distance from the membrane centre	m
R_g	Universal gas constant	$J\ kg^{-1}\ K^{-1}$
r_p	Pore radius	m
Re	Reynolds number	-
Re_{slip}	Reynolds number at $v = v_{slip}$	-
Re_t	Reynolds number in the tubular membrane	-
R_f	Total fouling resistance	$m^2\ m^{-3}$
R_m	Membrane resistance	$m^2\ m^{-3}$
r_p	Pore radius	m
r_{trrans}	Transitional radius	m
S	Stoichiometric value for iodide in reaction with copper hydroxide acetate	$g\ g^{-1}$

Sc	Schmidt number	-
Sh	Sherwood number	-
T	Tank width	m
t	Time	s
t_d	Droplet formation time	s
t_{neck}	Necking time	s
T_s	Saturation temperature	K
V	Volume of the liquid in the cell	m^3
$\overline{V}$	Molar volume of condensed liquid	$m^3\ kg^{-1}$
V_{crit}	Droplet volume predicted by the model	m^3
V_d	Droplet volume	m^3
V_p	Cumulative pore volume	m^3
V_{voids}	Void volume within the silica particle	m^3
V_{solid}	Solid volume within the silica particle	m^3
v_{slip}	Relative particle-liquid velocity (slip velocity)	$m\ s^{-1}$
V_t	Mean velocity of continuous phase	$m\ s^{-1}$
x	Formed (predicted) droplet diameter	m
X	Tube immersed deepth	m
x_p	Particle (xerogel/hydrogel) diameter	m
ΔP	Transmembrane pressure	Pa

Greek symbols

$\dot{\gamma}$	Shear rate	s^{-1}
τ	Sheer stress on the membrane surface	Pa
τ_{av}	Average shear stress	Pa
τ_{max}	Maximal shear stress	Pa
τ_w	Wall shear stress (due to the continuous phase flow)	Pa
μ	Dynamic viscosity of the continuous phase	Pa s
γ	Equilibrium interfacial tension	$N\ m^{-1}$
δ	Boundary layer thickness	m
δ_f	Film thickness	m

ε	Porosity of the membrane	-
ε_s	Internal voidage (porosity) of silica particles	-
v_o	Peak velocity	m s^{-1}
ρ	Liquid density / continuous phase density	kg m^{-3}
ρ_d	Acidified sodium silicate density	kg m^{-3}
ρ_{oil}	Dispersed phase density (oil)	kg m^{-3}
ρ_s	Density of swollen particle	kg m^{-3}
ρ_{si}	Solid silica density	kg m^{-3}
ρ_t	Absolute silica density	kg m^{-3}
ω	Angular velocity	rad s^{-1}
ω_f	Angular frequency	rad s^{-1}

1. INTRODUCTION

In the physical sciences, a particle represents a small localized object to which can be ascribed several physical properties such as volume or mass. Particles may be solid, but they also may be liquid droplets dispersed in another immiscible liquid or air. There is a great market demand for uniform particles both organic and inorganic which can have potential application in various industries (food, pharmaceutical, chemical etc.). An emulsion is a dispersion of one liquid in another where the liquids are not miscible, or are slightly soluble, and they play a valuable role in the production of the particle. Emulsion droplets are already particles but, even more, the droplets after production may be converted into solid particles by applying an additional treatment (reacting, setting, solidifying, polymerising, etc.).

Conventional emulsification processes such as rotor/stator devices or high-pressure homogenizers apply more energy than needed to disrupt the droplets (Karbstein, Schubert 1995), and the droplet break-up is mainly due to the turbulent eddies. If more energy than needed is applied this leads to droplets with a wide size distribution which in some applications is not acceptable.

By contrast, membrane emulsification (Kandori, Kisi & Ishikawa 1992); is a mild dispersion process to produce a monosized emulsion of one liquid phase in a second immiscible liquid phase using low energy per unit volume (Vladisavljević & Williams 2005). The dispersed phase is pressed through the membrane into the continuous phase and it is widely accepted that shear on the membrane surface needs to be applied in order to produce uniform droplets and the growth and detachment of the droplets is a complex phenomenon dependent on the process conditions including the formulation of the dispersed and the continuous phases.

Having in mind great potential application of membrane emulsification in various industries this thesis reports possible applications of membrane emulsification (using microengineered nickel membranes) by investigating different emulsions formulations, and also reports two novel systems suitable for industrial application.

The formulation of the dispersed phase and the continuous phase influences the final droplet size in membrane emulsification. The Dispersion Cell (first reported by Kosvintsev *et al.* 2005) in combination with the disk hydrophilic nickel membrane (for

the work with O/W and W/O/W emulsions) or hydrophobic membrane (for the work with W/O emulsions) was used to study the influence of the emulsion formulation on the final droplet size. In the Dispersion Cell the rotation of the paddle placed on top of the membrane induces the shear on the membrane surface which enables the droplet detachment, and the following applications were investigated here:

- O/W emulsions

  oil in water emulsions play an important role in the food industry since many flavour oils are composed of apolar, volatile molecules and they are subjected to considerable losses especially during harsh processes. Therefore flavour encapsulation within the oil droplets is nowadays widely used.

  Stabilisation of sunflower droplets using Tween 20 and sunflower droplets containing 10 wt.% oil using mixture of Gum Arabic and gelatine (complex coacervation) was investigated.
- W/O/W emulsions

  water in oil in water emulsions have a potential for encapsulation and release of substances with promising application in food, cosmetic, and pharmaceutical industries. W/O/W emulsion are very interesting for reduction of the fat content in food and therefore attract great interest specially because of the possibility for encapsulation of a water soluble substance within the internal water phase and production of functional food. Hence W/O/W emulsions were investigated. The oil phase was sunflower oil or pumpkin seed oil, PGPR (polyglycerol polyricinoleate) was used to stabilise W/O emulsion (first emulsification step) and Tween 20 was used to stabilise W/O/W (second emulsification step).
- W/O emulsions

  water in oil emulsions can be used for encapsulation or dissolving water soluble substance within the water droplets. In this thesis W/O emulsion route is reported for production of solid silica particles. Span 80 was used as an emulsifier for stabilising the water droplets in kerosene.

The industrial application of the Dispersion Cell is less good due to the problem of batch size of the system. Nevertheless it represents a valuable and effective tool for

formulation development. For the industrial application two novel systems for membrane emulsification are proposed: Oscillating and Pulsating.

Both systems have been commissioned using sunflower oil for production of O/W emulsion. In the Oscillating system the nickel membrane was in a shape of a candle and the shear on the membrane surface was induced by moving the membrane up and down by adjusting the frequency and amplitude while in the Pulsating system the membrane was in a shape of a tube and the continuous phase was pulsed. The productivity increase using the Oscillating or Pulsating system can be achieved by providing larger membrane area. The model that takes into consideration maximal shear stress was successfully applied to predict the droplet size both in Oscillating and Pulsating systems, while the model with average shear stress was able to predict the droplet size in the Dispersion Cell.

The thesis was undertaken as a part of a DIAMOND project (Decommissioning, Immobilisation And Management Of Nuclear wastes for Disposal) funded by the EPSRC and the nuclear industry which shows a great interest in inorganic ion exchange resins. Malik *et al.* (2009) have reported that it is possible to produce crosslinked polystyrene co-divinylbenzene sorbent microspheres with median diameter between 40 and 300 μm in a Dispersion Cell. Organic resins have a tendency to swell and degrade which makes them incompatible for use in the nuclear industry therefore, inorganic ion exchange resins, due to easier disposal, are interesting for nuclear industry. Highly uniform droplets of acidified sodium silicate were successfully produced using the Dispersion Cell and they were solidified forming spherical silica particles. Additionally the silica particles were functionalized with 3-aminopropyltrimethoxysilane and were capable to sorb copper.

As a complementary project, relevant to the use of the particles and especially relevant to nuclear laboratory testing, the Dispersion Cell was used as a continuous stirred system (with slotted microporous filter) for determining the sorption capacity of ion exchange material as well as mass transfer properties (Dragosavac, Holdich & Vladisavljević 2011) using commercial ion exchange material DOWEX 50W-X8. The developed system proved to be very convenient for quick lab tests especially in the cases when the amount of material is limited. Once the system was commissioned, it was used to test novel ion exchange material (copper hydroxide acetate) for the removal

of iodide from water. Copper hydroxide acetate was produced by Andy Butterworth and Dr Sandie Dann at the Department of Chemistry at Loughborough University and the experiments were undertaken as a part of the collaboration within the DIAMOND project. Beside copper hydroxide acetate functionalized silica particles were also tested using the continuous stirred cell.

Hence, this thesis builds on the existing work on membrane emulsification using the Dispersion Cell, with particular strengths in showing how it can be used to make complex and functional particles, modelling the conditions required to make particles at a desired size and structure and use of the same cell for determination of mass transfer properties suitable for ion exchange modelling.

Some of the work reported here was published in peer reviewed papers and presented at national and international conferences; see the list in appendix 4D.

2. LITERATURE REVIEW

Most oils are less dense than water, and if mixed together after a while oil will simply rise up to the surface of the water. In emulsions, one liquid phase (dispersed phase) is dispersed as droplets in another liquid phase (continuous phase). If left without surfactant the droplets of the dispersed phase will coalesce, which implies that the emulsions are thermodynamically unstable. The thermodynamic instability of the emulsions comes from the excess free energy at the interface between two phases. The cohesive forces between molecules within the individual phases exceed the adhesive forces between two phases. With the increase of the interfacial area, the interface free energy increases and the system becomes more thermodynamically unstable (Becher 2001). The change in interfacial free energy can be expressed by the following equation:

$$dG = \gamma dA_s \qquad \textbf{Eq. 1}$$

Where G is the interfacial free energy, γ is the interfacial tension, called surface tension if one of the phases is a gas, and A_s is the interfacial area. High interfacial area in emulsions leads to thermodynamical instability, the system aims to reduce the interface by various destabilizing mechanisms eventually leading to a complete phase separation. The main destabilizing mechanisms between dispersed droplets are coalescence or bursting (Becher 2001).

According to the liquid phase forming the dispersed phase, single emulsions are divided into oil in water (O/W) and water in oil (W/O). Also emulsions of emulsions also exist (multiple emulsions) which are generally prepared in a two step procedure where a single emulsion is firstly prepared followed by dispersing into an outer continuous phase. Multiple emulsions are divided into W/O/W (water in oil in water) and O/W/O (oil in water in oil). All types of emulsions have potential applications in food, cosmetic, pharmaceutical and chemical industries, and size and size distribution as well as formulation of the droplets play an important role in many applications. Therefore, the possibility to control the size and size distribution is of great importance (Becher 2001). Depending on the mean droplet diameter, emulsions can be divided into nano- (10–100 nm), mini- (100–1000 nm) and macro-emulsions (greater than 500 nm) and the work reported in this thesis will tackle only macro-emulsions.

In most cases the –stable" emulsions are caused by the presence of an emulsifying agent residing at the liquid-liquid interface. A surfactant (surface active agent) is an amphiphilic molecule, i. e. with hydrophilic head and hydrophobic tail therefore each part of the molecule is dissolvable in a different phase. By addition of the surfactant: the interfacial tension defined by the interfacial free energy *G* can be considerably reduced, surface elasticity can be increased, electric double layer repulsions can be increased (if surfactant is ionic) (Schramm 2005). Surface active agents can be classified into two main categories: low-molecular weight surfactants and polymeric surfactants. Further criteria for classification are, for example, the subdivision by charge of the hydrophilic part: non ionic (no charged headgroups), anionic (negative charge in the headgroups), cationic (positive charge in the headgroups) or amphoteric (both positive and negative charges in the head groups, pH-triggered). But the very well known classification is the hydrophilic-lipophilic balance (HLB) concept firstly introduced by Griffin (1949).The method is based on the rule established by Bancroft (1913 and 1915), which states that the phase in which the surfactant is soluble to a higher extent forms the continuous phase. For non-ionic surfactants which are used in this thesis the HLB number can be simply calculated from molecular weight of the molecule and its hydrophilic portion according to the equation:

$$HLB = 20 \times \frac{M(hydrophilic.portion)}{M(entire.molecule)} \qquad \textbf{Eq. 2}$$

Only materials with HLB numbers in the range 4–6 are suitable as emulsifiers for W/O emulsion, whereas only those with HLB number in range 8–18 are suitable for the preparation of O/W emulsions (Becher 2001).

Figure 1 shows the surfactants used in this thesis for stabilizing W/O, W/O/W and O/W emulsions. As mentioned earlier surfactant molecules have both hydrophilic and hydrophobic parts therefore either in water phase or oil phase a molecule will be partly attracted, and partly rejected, therefore it assembles at the interface between the phases with the hydrophilic head turned into the water phase and hydrophobic tail oriented toward the oil phase.

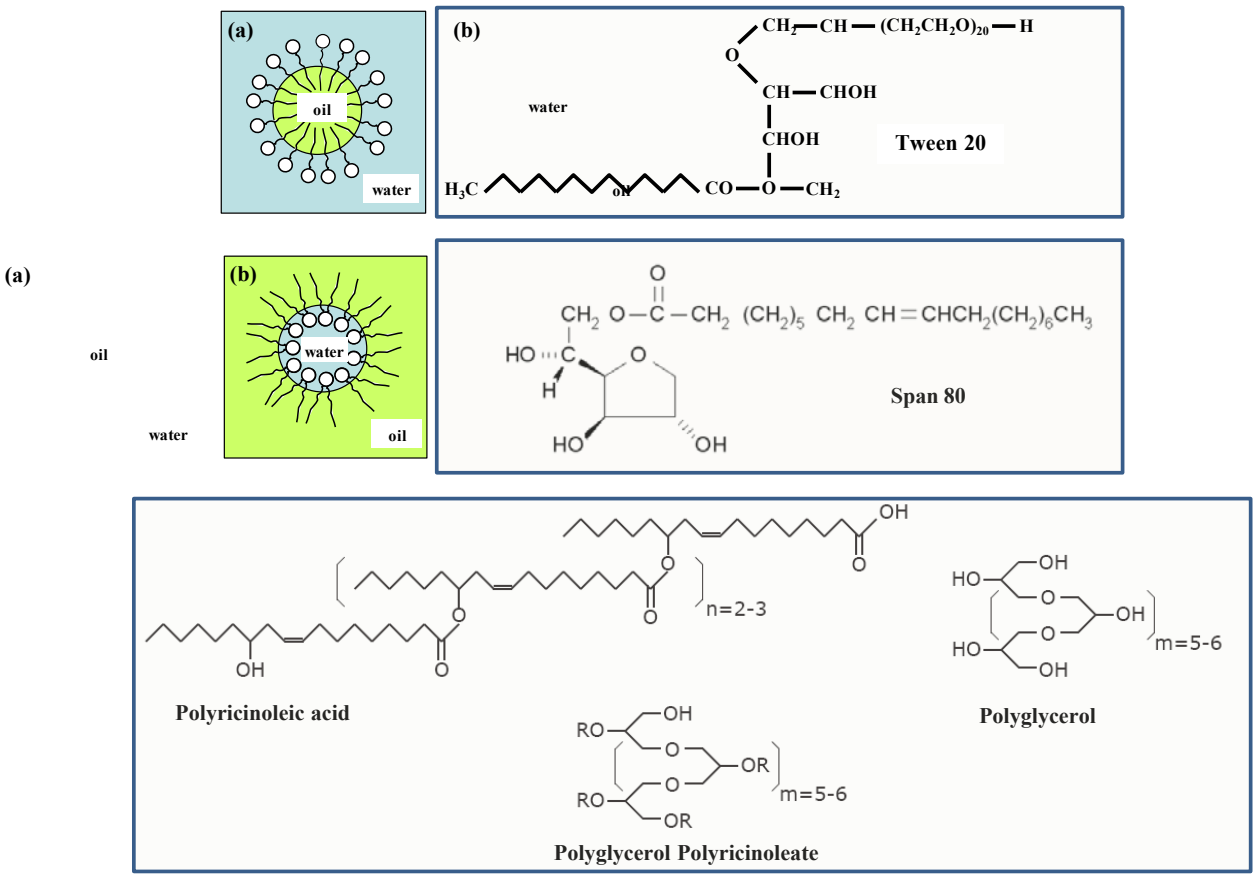

Figure 1 Surfactants used in this thesis: (a) Tween 20 water soluble, (b) Span 80 and PGPR (Polyglicerol Polyricinoleate) oil soluble surfactants.

The greatest effect a surfactant can have (Schramm 2005), whether in interfacial tension lowering, suspension stabilizing, as a delivery vehicle, or in promoting foam stability, is when it is at or above the CMC (critical micelle concentration). Care has to be taken when selecting the surfactant for drop by drop emulsification. As shown by van den Graaf *et al.* (2005) surfactants with fast adsorption kinetics are better used in order to stabilize the droplet within the droplet formation time. On the other hand the presence of surfactant may adversely affect the membrane properties (e. g. wetability).

2.1 CONVENTIONAL EMULSIFICATION METHODS

There are many conventional ways for preparing emulsions. In such devices a premix emulsion is necessary, which is produced by gentle mixing, followed by homogenization which will lead to further reduction of the droplet size. In general, homogenization is an intense process: it introduces a large amount of energy into the premix emulsion to break up the droplets into smaller ones. Examples of

homogenization systems that are used in practice are presented in Figure 2 and are (Karbstein, Schubert 1995):

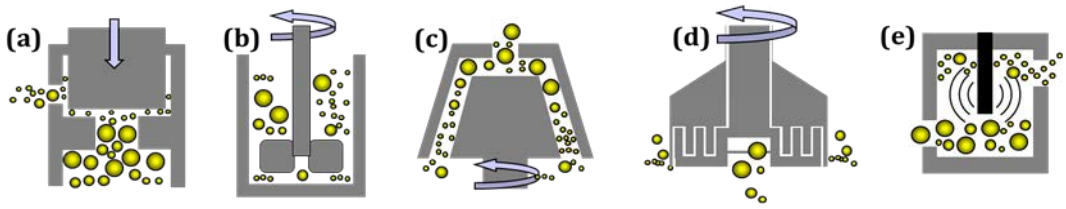

Figure 2 Conventional devices for production of emulsions.

- High-pressure systems (Figure 2 a). Premix is pushed through a small valve at high pressure. Due to the high shear and extension rates in the valve, large droplets break up into smaller.

- Rotor-stator systems (Figure 2 (b), (c) and d):

    - *Stirring vessels* (Figure 2 (b)). The droplets break up is due to the paddle stirring. The average input per unit volume is quite low and they are suitable for production of coarse emulsions, and mainly used as batch systems.

    - *Colloidal mill* (Figure 2 (c)). Premix is pushed through the gap between a cylindrical or conical stator and rotor. Due to the shear and extension exerted by the rotor, large droplets break up into smaller ones. A laboratory homogeniser uses a very similar principle to this.

    - *Toothed disk dispersing machines* (Figure 2 (d)). Premix is pushed through the gap between several pairs of concentrically arranged disks of various design, one of which rotates due to shear and large droplets break up.

- Ultrasound systems (Figure 2 (e)). Premix is placed in a vessel with an ultra sound device. Due to the intense turbulence caused by the ultrasound waves, the droplets break up into smaller ones.

Conventional homogenizers, as illustrated above, are very convenient for production of small size droplets. For production of larger droplets low shear needs to be applied, but

conventional homogenisation in that case produces droplets with a wide size distribution. Such a product is often unstable and has unsatisfactory properties.

2.2 DROP-BY-DROP EMULSIFICATION

2.2.1 Membrane emulsification

Membrane emulsification (ME) is a relatively new method (Kandori, Kishi & Ishikawa 1992) for producing micron-sized emulsion droplets of a predefined size, based on the extrusion of the dispersed phase into the continuous phase liquid through a microporous membrane. The membranes for membrane emulsification can be divided into two main categories: tortuous pore channel membranes (SPG first membranes used for membrane emulsification, α-Al_2O_3, Zr_2O_3, silica membranes…) and microengeneered sieves (van Rijn *et al.* 1999; Kosvinstev *et al.* 2005), stainless steel membranes (Schandler & Windhab 2006)). The disadvantage of the tortuous membranes is the low flux (Vladisavljević & Schubert 2003) due to the thick membrane and a small number of active pores while the microengeneered sieves have high flux (Holdich *et al.* 2010) they are thin and the number of active pores is higer than for tortuous membranes. Two methods of operation are used for membrane emulsification: direct ME – the passage of pure disperse phase through the membrane (Joscelyne & Trägårdh 2000) and premix ME (Suzuki *et al.* 1996) - the passage of coarse pre-emulsified mixture through the membrane, or membrane homogenization.

Literature reviews about membrane emulsification are available (Joscelyne & Trägårdh 2000; Vladisavljević & Williams 2005) and they all agree that there are several factors influencing the final droplet size: shear on the membrane surface, dispersed phase flux, surfactant concentration, membrane wettability, membrane pore size (droplet size is directly proportional to the membrane pore radius and the proportionality constant equals 3–20 (Peng & Williams 1998; Vladisavljević & Williams 2005)), as well as viscosities of both continuous and dispersed phase. In order to detach droplets from the membrane surface and allow better control over the droplet size distribution, the shear stress is usually controlled at the surface of the membrane.

The surface shear can be created by recirculating the continuous phase in cross-flow (Figure 3 (a)) (Nakashima *et al.* 2000; Joscelyne & Trägårdh 2000), by vibrating (Kelder *et al.* 2007) or rotating the membrane (Figure 3 (b) and (e)) (Vladisavljević & Williams 2006; Schadler & Windhab 2006; Aryanti et.al 2009), by vibrating an element

(e.g. a wire or plate) in the continuous phase at a short distance from the membrane (Figure 3 (c)) (Hatate et.al 1997; Clair *et al.* 2003) or by stirring the continuous phase using a stirring bar (Figure 3 (f) and (g)) (Higashi & Setoguchi 2000; Ma *et al.* 1997) or a paddle stirrer (Figure 3 (d)) (Kosvintsev *et al.* 2005; Stillwell et. al. 2007; Dragosavac et. al. 2008), oscillating the membrane (Figure 3 (h)) (Holdich *et al.* 2010) or combining the cross-flow with pulsation of the continuous phase (Figure 3 (i)) (this thesis).

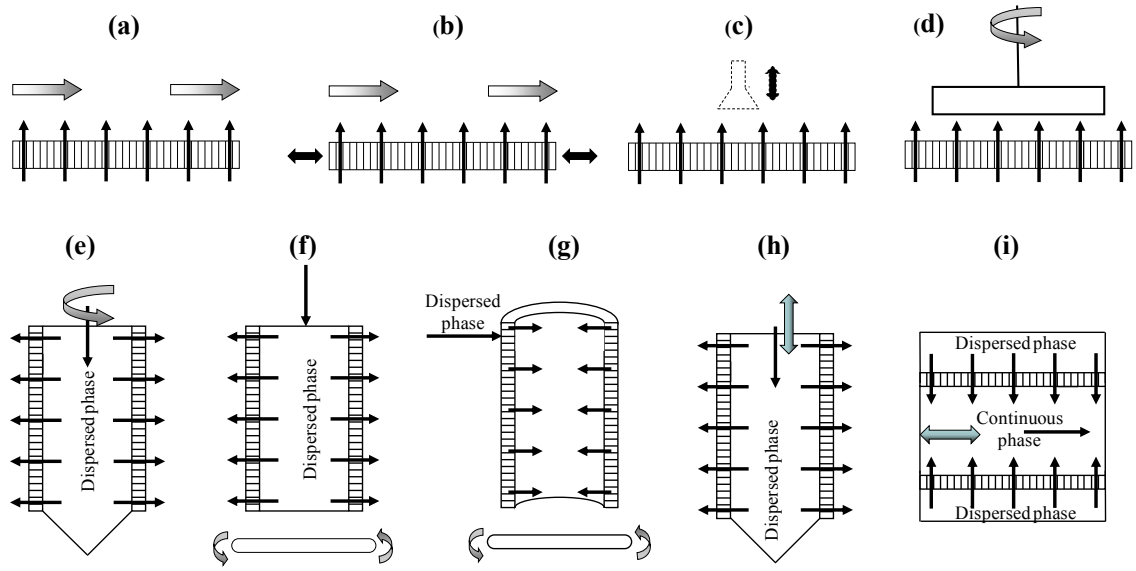

Figure 3 Formation of surface shear in membrane emulsification.

Each system has potential advantages and disadvantages and Table 1 lists potential advantages and disadvantages of the various techniques used for generation of surface shear in membrane emulsification.

Table 1 Comparison of different techniques for creation of shear stress at the membrane surface in membrane emulsification

	Potential advantages	**Potential disadvantages**	**References**
Cross-flow, tortuous membranes	Easy scale-up, constant shear stress at the membrane surface, modules widely available	Droplets can be damaged during recirculation in pipes and pumps, long operation times for concentrated emulsions	Nakashima *et al.* 2000; Joscelyne & Trägårdh 2000

	Potential advantages	Potential disadvantages	References
Cross-flow + membrane vibration	Additional control over droplet detachment, decrease in mean droplet size as compared with a simple cross-flow	Complicated design, no evidence that droplet size monodispersity is improved	Kelder *et al.* 2007
Vibration in continuous phase	Simple set-up	Poor control of shear stress, suitable only for small scale applications	Hatate et.al 1997; Clair *et al.* 2003
Rotating microengineered membrane	Suitable for creation of fragile particles and viscous emulsions	Complicated and expensive design, high power consumption	Vladisavljević & Williams 2006; Schadler & Windhab 2006; Aryanti et.al 2009
Stirring, tubular SPG membrane	Volume of continuous phase liquid can be as low as several mililitres	Maximum transmembrane pressure restricted to several bars, non-uniform shear stress at the membrane surface, batch operation	Higashi & Setoguchi 2000; Ma *et al.* 1997
Stirring, flat microengineered membrane	High injection rates of dispersed phase through the membrane	Mean droplet size in product emulsions above 20 μm, batch operation, non-uniform shear stress at the membrane surface	Kosvintsev *et al.* 2005; Stillwell et. al. 2007; Dragosavac et. al. 2008
Oscillating candle microengineered membrane	High productivity, easy scale up	Need for removal of produced droplets if high amounts are produced	Holdich *et al.* 2010
Cross-flow + pulsation of the continuous phase tubular membrane	High productivity, easy scale up	Too long membrane can vibrate and therefore reduce the uniformity of the dropelts	This thesis

The main application areas of membrane emulsification are production of particles such as: double emulsions (Vladisavljević *et al.* 2004; Vladisavljević *et al.* 2006b; van der

Graaf *et al.* 2005; Surh *et al.* 2007), creation of droplets for biphasic enzymatic reactions (Giorno *et al.* 2003), and production of solid microparticles (Vladisavljević, Williams 2005), such as solid lipid microcapsules (Kukizaki, Goto 2007), polymeric microspheres (Ma *et al.* 2003), silica particles (Fuchigami *et al.* 2000), and gel microbeads (Zohou *et al.* 2009). This thesis will tackle production of O/W, W/O/W, W/O emulsions and will also explore the possibility of droplets solidification.

2.2.2 Microfluidic and Microchannel emulsification

Microfluidic devices such as T-, Y- shaped microchannel junctions (see Figure 4 (a) and (b) respectively), in which a cross-flow is used, and flow-focusing devices (Figure 4 (c) and (d)) in which co-flow of phases exerts extensional shear have been reported for production of highly uniform droplets. In microfluidic devices it is the shear that governs the droplet detachment as in the case of membrane emulsification. The great advantage of microchannel junctions as well as flow-focusing devices is that they provide a controllable generation of core-shell droplets and multiple emulsion droplets with a controlled number of inner droplets in the outer drop (Vladisavljević *et al.* 2010).

Microchannel emulsification emerged as a relatively new technique for preparation of monodisperse emulsions where the droplets are spontaneously created. Kawakatsu *et al.* (1997) reported use of grooved microchannel arrays (Figure 4 (e)) while several years later Kobayashi (2002) reported use of straight through microchannel arrays. The difference from membrane emulsification is that it is not the shear forces that governs the droplet size but the microchannel geometry, and to a lesser extent the to-be-dispersed-phase flow (Van Dijke et. al, 2008). Interfacial tension is used as a driving force for droplet formation; and less energy (a factor of 10–100 less) as compared to the conventional techniques is needed (Sugiura et. al, 2001), for the production of various products such as O/W emulsions, W/O emulsions, lipid microparticles, polymer microparticles or microcapsules (Sugiura et. al, 2004). The disadvantage of the systems is a problem with scaling up and industrial application, but on the other hand the droplets produced are highly uniform as can be seen in Figure 5.

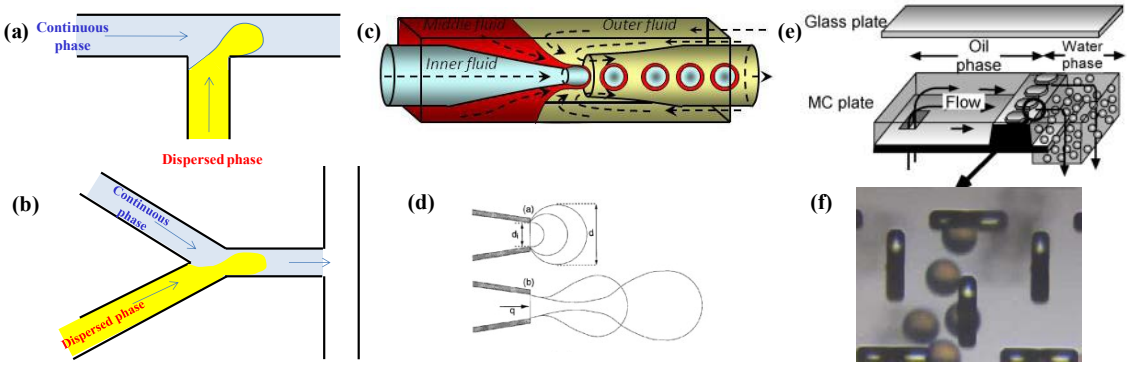

Figure 4 Some examples of microfluidic devices which are capable of producing monodisperse droplets. (a) T-Junctions (b) Y-Junctions (c) Flow–focusing microcapillary device (Vladisavljević *et al.* (2010)) (d) Co-flow system (droplet growth (a) and separation (b)) (Umbanhowar *et al.* 2000) (e) Grooved microchannel (Sigura *et al.* , 2004) (f) Straight-through microchannel device with asymmetric arrays. (Vladisavljević & Dragosavac 2010, Unpublished material.)

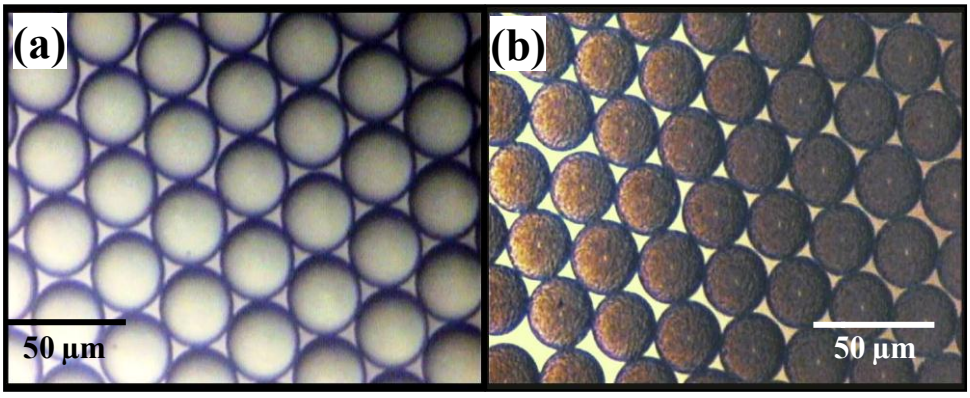

Figure 5 Emulsions produced by straight through microchannels with asymmetric arrays (continuous phase 2% Tween 20): (a) O/W – O-sunflower oil, (b) W/O/W – O-5% PGPR in pumpkin seed oil. CV<4%. (Vladisavljević & Dragosavac 2010, Unpublished material).

2.2.3 Drop by drop production of W/O/W emulsions

Multiple emulsions (Seifriz 1925) have attracted significant interest in the past several decades. They have potential applications in the pharmaceutical industry, such as carriers of active pharmaceutical ingredients, e.g. in drug delivery systems (Nakano 2000); cosmetics, e.g. deposition of water soluble benefit agents onto skin (Vasudevan & Naser 2002); and the food industry, e.g. encapsulation of flavours (Merchant *et al.*

1998; Dalgleish 2006), production of food with lower fat content (Okonogi *et al.* 1994) and protection of sensitive and active food components from a local harsh environment (Daisuke *et al.* 2004). Multiple emulsions are very suitable for encapsulation of hydrophilic bioactive components, such as: vitamin B (Owusu *et al.* 2004), immunoglobulin (Chen *et al.* 1999), insulin (Cournarie *et al.* 2004) and amino acids (Owusu *et al.* 2004; Weiss *et al.* 2005), and they are also useful for preparation of delivery systems that contains lipophilic encapsulants, such as flavour (Cho & Park 2003) and both lipophilic and hydrophilic bioactive components in the same system (Owusu *et al.* 2004).

Multiple emulsions are complex systems where both water-in-oil (W/O) and oil-in-water (O/W) emulsion types exist simultaneously (Muschiolik 2007). Water-in-oil-in-water (W/O/W) emulsions (Figure 6) contain small primary water droplets within larger oil droplets while the oil droplets are dispersed within the secondary continuous water phase. They are usually prepared in a two step procedure using conventional homogenization technology. The first step is preparation of the primary W/O emulsion using an oil soluble surfactant under high-shear conditions to obtain small droplets (typically less than 1 μm). It is necessary to expend significant energy in this system to provide large interfacial energy associated with the production of small droplets. In the second step of the emulsification process, when the W/O/W droplets are produced, controlled shear needs to be applied as there is a requirement not to rupture the primary emulsion (Garti 1997), which would lead to a lowering of the encapsulation efficiency. Also, many ingredients suitable for multiple emulsions are temperature and shear sensitive, and application of high shear would lead to deterioration in their properties (van der Graaf 2005).

If low shear needs to be applied in the second stage of emulsification, in order to prevent breakage of inner W/O droplets, conventional homogenisation in agitation devices, rotor-stator systems or high pressure homogenizers provides large and non-uniform W/O/W droplets. Such a product is often unstable and has unsatisfactory properties. A narrow droplet size distribution can be obtained if the energy density (a measure of the energy input per cubic metre) in the space between rotor and stator is well controlled (Schubert, Armbruster 1992), which is hard to achieve.

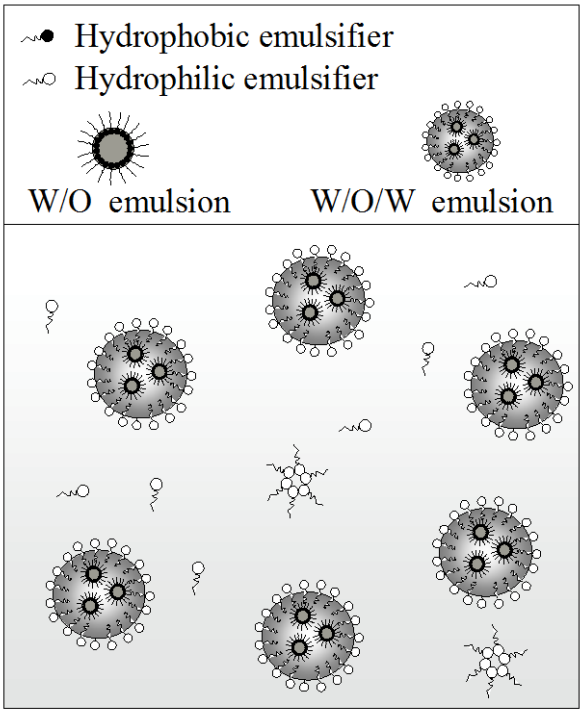

Figure 6 Schematic representation of multiple W/O/W emulsions.

Membrane emulsification process applies low mechanical stress (Schröder *et al.* 1998) or even no shear (Kosvintsev *et al.* 2008), and has low energy input compared with conventional emulsification methods providing a better control of droplet size representing a very good solution for production of multiple emulsions (especially if used for second emulsification stage). Cross-flow ME, where dispersed phase is pressed through the microporous membrane while continuous phase flows along the membrane surface, is not convenient for production of larger droplets due to the need to recycle the dispersion over the membrane surface leading to damage to the previously formed droplets within the pump and fittings of the system (Gijsbertsen-Abrahamse *et al.* 2004). Membranes with interconnected pores, like the Shirasu Porous Glass (SPG) and α-aluminium oxide (α-Al_2O_3) membranes are not appropriate for production of droplets greater than 60 μm (Vladisavljević *et al.* 2004) due to their small maximum pore size. Also due to large thickness of the membrane and low percentage of active pores (Schröder, Schubert 1999), flux through the membrane is very low, usually up to 0.1 $m^3\ m^{-2}\ h^{-1}$. The thinner the membrane, the larger the flux through the pores, resulting in a higher droplet production rate (Gijsbertsen-Abrahamse *et al.* 2004; Schröder & Schubert 1999). Flux through SPG membrane can be increased to above 200 $m^3\ m^{-2}\ h^{-1}$ using premix membrane emulsification with a size distribution span of

0.3 (Vladisavljević, Shimizu & Nakashima 2004). New developments in nano- and micro-engineering produced microsieves (van Rijn *et al.* 1999) provide higher droplet production in direct ME (Wagdare *et al.* 2010).

Another method of producing W/O/W emulsions is by extruding O/W emulsion through microfabricated channel arrays (Kawakatsu, Trägårdh & Trägårdh 2001; Lambrich *et al.* 2004; Sugiura *et al.* 2004). In 1997 the Nakajima group first demonstrated the controlled formation of micrometre-sized oil-in-water (O/W) and water-in-oil (W/O) emulsions in a silicon microchannel array device (Kawakatsu, Kikuchi & Nakajima 1997). A higher degree of control over the structure of resultant double emulsions can be achieved using microfluidic devices (for example, ability to create core/shell droplets (Utada *et al.* 2005)), but at very small production scales. The two most commonly used microfluidic geometries are T-junction (Thorsen *et al.* 2001) and flow focusing channel (Gañán-Calvo & Gordillo 2001) and both geometries were used for production of multiple emulsions. Okushima *et al.* (2004) generated monodisperse double emulsions with 100% entrapment efficiency and a controlled number of inner droplets encapsulated in each larger droplet using two T-junctions in series with alternating wetabilities. Chu *et al.* (2007) produced triple emulsions using capillary microfluidics in hydrodynamic flow focusing system, but again the droplet throughput was very small due to the fact that all droplets were produced by one channel. The main advantage of membrane systems is the fact that the droplets are formed simultaneously from thousands, or even hundreds of thousands, of pores.

2.2.4 Drop by drop production of silica particles

Recently the production of porous inorganic materials with high surface area and internal porosity has attracted lot of attention. Silica is an inorganic material that does not swell in solvents, has very good mechanical and thermal stability as well as good dispersion characteristics in various solvents. Colloidal silica with a mean particle size ranging from about 5 to 100 nm has a wide range of applications as thickener, adsorbent, molecular sieve, abrasive, additive, catalyst support, coating film or glass precursor (Iler 1979). In addition to colloidal silica, there is significant commercial interest in porous spherical silica particles for use in analytical and preparative columns, requiring particle diameters greater than 1 μm. Such particles, if additionally functionalized, can have potential application as ion exchange (Jal, Patel & Mishra

2004), biochemical sensors (Buranda *et al.* 2003), packing materials in chromatography columns (Ide *et al.* 2010), drug delivery systems (Barbé *et al.* 2004), and catalysts (Suzuki *et al.* 2007). Particle size and pore structure of silica particles directly influences mass transfer rate to, and from, the silica particle and its control is important in processes such as ion exchange, catalysis, chromatography, and drug delivery. Silica particles for larger-scale use, as scavengers in pharmaceutical processing or column applications, including ion exchange and adsorption, require much larger particle size: up to 100 μm in diameter. In these applications uniform spherical particles is preferred to angular crushed solids, to minimise pressure drop and provide reproducible behaviour.

Silica particles can be produced from organic silicon compounds, e.g. siliciumalkoxide, such as tetraethyl or tetramethyl ortosilicate (TEOS and TMOS) or inorganic materials (sodium silicate). Sodium silicate is the cheapest source of silicon for silica particles. To produce silica gel sodium silicate solution can be diluted with an acid to form silicic acid ($Si(OH)_4$) which then through condensation polymerisation loses water and creates –Si–O–Si – bonds. Upon drying the formed hydrogel shrinks to a xerogel. A surfactant can be dissolved in the silica source to additionally tailor the internal gel structure (surfactant templating method) (Lin, Mou 2002). The characteristics of a produced dried gel are determined by the physical and chemical conditions at each step of the process of preparation.

To form spherical silica particles acidified sodium silicate solution can be dispersed into the immiscible organic phase liquid, water in oil (W/O) emulsion route (Titulaer, Jansen & Geus 1994), or spray dried (Iler 1979). In the W/O emulsion route, the droplets of sodium silicate solution are dispersed in an appropriate immiscible organic solvent either by bulk emulsification, or by drop-by-drop emulsification. The dispersed droplets actually represent microreactors in which condensation polymerisation occurs. Anderson *et al.* (2007) used the W/O emulsion route in combination with solvent evaporation to produce spherical silica particles. They applied stirring to produce the emulsion and reported particles of up to 40 μm with a relatively broad size distribution. Size and uniformity of the silica particles produced depends largely on size and uniformity of the silica precursor droplets and, therefore, the controllable drop-by-drop emulsion formation is preferred. Several single channel microfluidic technologies have been reported for production of spherical silica particles: Chen *et al.* (2008) injected a dispersed aqueous phase (a mixture of silica sol, acrylamide and initiator) through a

needle into a cross-flowing oil phase to produce porous silica particles by calcination of polyacrylamide-silica composite particles. Carroll *et al.* (2008) injected silica precursor (acidified TEOS solution with triblock copolymer) using a flow focusing oil, while Chokkalingam *et al.* (2010) fabricated silica particles by self-synchronized pairwise production of droplets of different solutions (acidified TEOS solution and ammonia solution) using a microfluidic cross junction followed by *in situ* droplet merging. Produced particles were above 10 μm and very uniform, with a coefficient of variation of less than 5%, but reported productivity was below 0.02 mL min^{-1}. Microchannel emulsification (Kobayashi, Nakajima & Mukataka 2003), where the dispersed phase is pressed through uniformly sized microchannel arrays fabricated on a silicon microchip into the continuous phase, can be used for fabrication of uniform droplets. The disadvantage of this process is low productivity which does not exceed 0.025 mL min^{-1} for grooved-type plate and 1 mL min^{-1} for straight-through microchannel plate. Productivity of the process is crucial in industrial applications and, therefore, microfluidic devices or microchannel emulsification are not promising due to their limited ability to scale for production purposes.

Production of spherical silica particles using W/O emulsion route and membrane emulsification has been reported by several authors (Table 2) but membranes with tortuous pores were used. These membranes can be easily fouled by the precursor solution and the reported mean particle size did not exceed 5 μm. These sizes may be appropriate for analytical column use, but for larger scale „process" column applications particle diameters between 10 and 100 μm are desirable. Cross-flow membrane emulsification, where the shear is induced by the recycled flow of continuous phase, is not convenient for the production of droplets larger than 20 μm, due to droplet break up in the pump and fittings.

Table 2 Silica particles produced using W/O emulsion route and membrane emulsification (DP: dispersed phase, CP: continuous phase).

Membrane (µm)	Particle size (µm)	Emulsion formulation	Post-emulsification treatment	Ref.
Anodic porous alumina 0.125	0.05-0.2	DP: 1 M Na_2SiO_3 in water CP: 2 wt % Tween 85 in mixture of hexane and cyclohexane (1:4 by volume)	Emulsion mixed with 4 wt % aqueous $(NH_4)_2CO_3$ solution	(Yanagishita *et al.* 2004)
SPG / 1.5 Silica monolithic / 2	Up to 3	DP: Colloidal silica (SiO_2: 20%; mean diameter of silica beads: 10–20 nm) CP: 1 wt % Span 20 in kerosene	Emulsion mixed with 0.5 M aqueous NH_4Cl solution	(Hosoya *et al.* 2005)
SPG 0.98–2.7	Up to 1	DP: Na_2SiO_3 + sulfonic acid in water, final pH 2 CP: 2–10 wt % PE–64 in toluene	Not given	(Kandori, Kishi & Ishikawa 1992)
Sol-gel derived macroporous glass SPG Pore size not given	Up to 3	DP: Colloidal silica CP: Span 20 in toluene	Dripping 2M NH_4OH into emulsion	(Fuchigami, Toki & Nakanishi 2000)

2.3 ION EXCHANGE AND SEEDED MICROFILTRATION

2.3.1 Ion exchange

There are many definitions for ion exchange resins, the most general one is:

Ion exchange resins are insoluble materials carrying reversibly fixed ions. These ions can be stoichiometrically exchanged for other ions of the same sign (Zagorodni 2007).

Ion exchange polymers, are cross-linked polymers carrying fixed functional groups or sites (Zagorodni 2007).

The most basic classification of ion exchange resins distinguishes cation and anion exchangers. If an ion exchanger bears negatively charged functional groups and carry exchangeable cations they are called cation exchangers, but if they carry exchangeable anions then they are called anion exchangers.

The largest group of ion exchangers available today is synthetic organic resins and they are supplied as beads. Their matrix is a flexible network of hydrocarbon chains and within that network at different positions fixed ionic charges exist. They are commonly prepared from styrene and different levels of the cross-linking agent divinyl-benzene, but there are also phenolic and acrylic resins. The amount of cross-linking agent regulates mechanical strength (higher amount of cross-linking agent higher mechanical strength), permeability, water retention capacity (swelling) and total capacity of the resin.

Conventionally, the amount of cross-linking agent is expressed as percentage of cross-linking reagent introduced in a reaction mixture at the synthesis stage. For example Dowex 50W-X8 contains 8% of divinyl-benzene molecules. But cross-linking process can never be perfect so it can happen that cross-linking molecule gets connected only to one end of polymeric chain and that it is not in a good position to be connected to another chain. Cross-linking is not perfect but it is sufficient to consider the material homogenous.

The main advantages of synthetic organic ion-exchange resins are (Inglezakis, Poulopoulos 2006):

- high capacity

- wide application
- low cost for production

The ion exchangers have found a large implementation in many different processes, but their main application is the separation of dissolved ions. Zagorodni (2007) gave following classification of ion exchange processes:

- **Purification of solvent** – performed when the solvent is the desired product, and all the dissolved ions are considered as contaminants. The raw material is usually a solution of one or more ionic substances. A typical example is the water purification for the electronic industry. The requirement is a zero-content of dissolved substances, i.e. all ions present in the raw solution must be removed and disposed.

- **Purification of solution** is performed when the product is a solution of certain composition and the raw material is the same or similar solution but containing an undesirable solute. A typical example is the decontamination of an industrial waste stream by removal of one or more toxic substances. Another example is the removal of toxic substances from blood during a haemodialysis treatment.

- **Extraction** is performed when a dissolved compound has to be extracted from a solution and the exhausted solution has no value. The typical example is the extraction of gold from seawater. The product (gold) is highly valuable while the treated seawater can be disposed back to the sea without any additional care.

- **Separation** is obviously applicable to all the described cases. However, the case of two products of interest – an ionic substance or a mixture of target ions and a solution or a solvent – can be named only as separation. The term **separation** also includes cases where several ions of interest are obtained as different products. A typical example is obtaining different amino acids from a mixture prepared by hydrolysis of proteins. Another example is the classical analytical ion exchange chromatography in which all compounds should be separated prior to a final detection procedure.

Application of the ion exchanger determines type of ion exchange material and method for the practical application. When we are talking about ion exchangers some of the most important properties to be considered in use of ion exchange resins are:

- Complete insolubility
- Resistance to oxidation
- Heat stability
- Exchange capacity
- Exchange rates
- Resin volume changes
- Physical stability (the most important)

The revival of interest in inorganic exchangers began in the early 1960s. This was associated with the fact that ion exchangers with a fairly high thermal stability and resistance to ionising radiation were needed for many branches of industry; furthermore, an extremely high partition coefficient was observed in certain inorganic sorbents even for alkaline earth metal cations, which are comparatively difficult to separate. After the synthesis by Clearfield and Stynes (1964) of the cryptocrystalline acid zirconium phosphate, which is now one of the most familiar inorganic ion exchangers, the stream of studies devoted to ion exchange on inorganic materials increased significantly.

Natural inorganic exchangers can be classified into three main categories: zeolites, oxides and clay minerals. Synthetic inorganic exchangers can be classified into the following categories: zeolites, hydrous oxides, acidic salts of polyvalent metals, salts of heteropoly acids, hexacyanoferrates and other ionic compounds (Baacke, Kiss 1990; Lieser 1991; Weiss 1991). Inorganic exchangers have interesting properties such as resistance to decomposing in the presence of ionizing radiation or at high temperatures, which have made them interesting for the treatment of nuclear waste. Some studies of natural zeolites and some hydrous oxides have been made for their profitable use in waste treatment. Clinoptilolite and chabazite have been investigated for the separation of transition metals from mixed metal contaminated effluents (Ouki, Kavannagh 1997), also phlogopite mica and mordenite have been studied for Cs and Sr sorption (Liang, Hsu 1993; Komarneni, Roy 1988). Clinoptilolite has been extensively used in radioactive waste decontamination (Hutson 1996).

In recent years, there has been pronounced tendency to utilize mechanically stable synthetic or natural solid matrices by immobilization of organofunctional groups in many applications, such as chemically bonded phase in chromatography, extraction of cations from aqueous and non-aqueous solvents, catalytic or ion-exchange reactions,

electronics, ceramics and also in bioengineering. The systematic use of immobilization of organofunctional groups has increased in the past three decades, mainly on silica, because this support offers pronounced advantages over other organic/inorganic supports as listed below (Jal, Patel & Mishra 2004):

- Immobilization on silica results in great variety of silylating agents, allowing pendant functional groups in the inorganic framework
- Attachment is easier on silica surface than on organic polymeric supports, which have a high number of cross-linking bonds, requiring hours to reach equilibrium for surface activation
- Silica gel being the most popular substrate for surface studies because it is the first commercially available high specific surface area substrate with constant composition, enabling easy analysis and interpretation of results
- Silica gel has high mass exchange characteristics and no swelling
- Silica support has great resistance to organic solvents
- Silica has very high thermal resistance

2.3.2 Sorption and ion exchange

The term –sorption" includes the uptake of gaseous or liquid components of mixtures from external and/or internal surface of porous solids. On the other hand ion exchangers take ions from solution and release an equivalent amount of other ions with same sign. Ion exchange is a similar process to sorption, because there is a mass transfer of the species from the liquid phase to the solid in both cases and they are basically diffusion processes. Although ion exchange is similar to sorption since a substance is captured by a solid in both processes, there is a characteristic difference between them: ion exchange is a stoichiometric process in contrast to sorption. It means that in ion exchange process, for every ion that is removed, another ion of the same sign is released, while during the sorption no replacement takes place (Helfferich, 1995).

2.3.3 Mechanism of ion exchange process

The following steps that take place during the ion exchange (Figure 7) and the slowest of these steps will be the limiting step for the ion exchange (Zagorodni (2007)):

- The first step is diffusion of the first ion form the bulk of the solution towards the phase film (process 2 in Figure 7) this step is easily manipulated because diffusion transport in the bulk solution can be assisted with agitation.

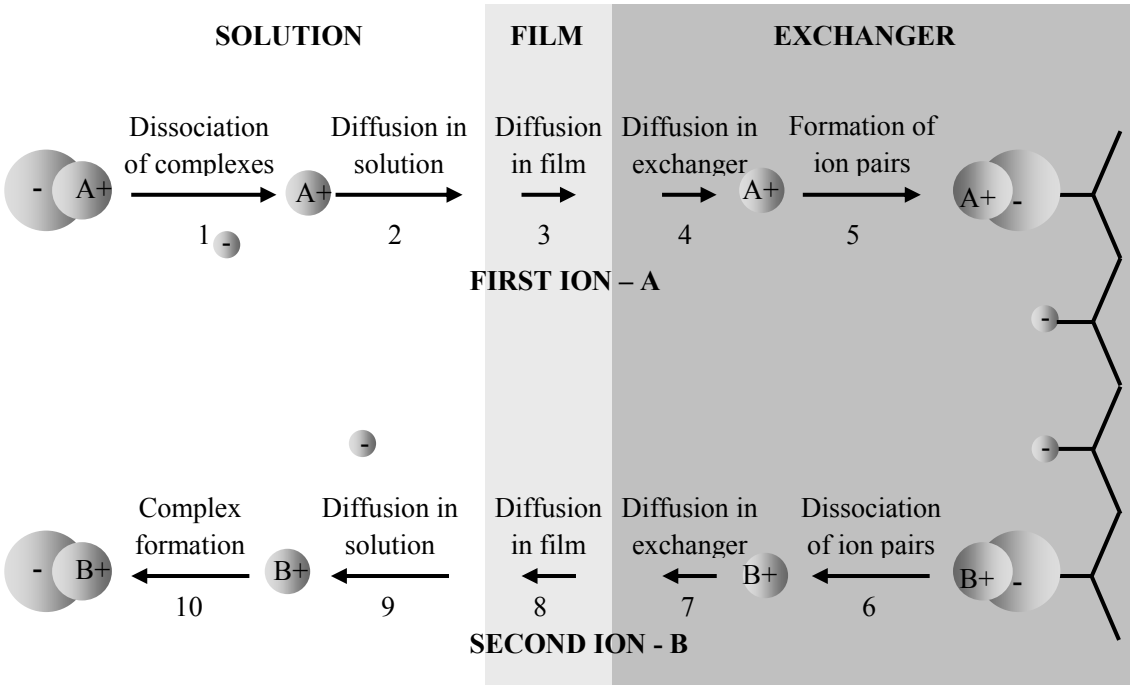

Figure 7 General mechanism of the ion exchange process. (1) dissociation of the dissolved complexes containing first ion; (2) diffusion of the first ion from solution towards the inter-phase film; (3) diffusion of the first ion through the inter-phase film; (4) diffusion of the first ion inside the material phase; (5) association between the first ion and functional group; (6) dissociation of the associates between the second ion and functional group; (7) diffusion of the second ion inside the material phase towards the surface; (8) diffusion of the second ion through the interphase film (9) diffusion and random distribution of the second ion in the solution; (10) formation of the second ion complex in the solution (Zagorodni 2007).

- Next step is diffusion of the ion through the Nernst film (Concept of diffusion layer – originally developed by Nernst. The convection of the solution by turbulent or laminar flow recedes continuously from the bulk solution to the solid surface. Film concept replaces this situation by a zone of defined thickness –film thickness" without any convection and with a sharp boundary separating it from the complete agitated solution. Quite commonly Sherwood dimensionless

number $Sh = \frac{k \cdot 2R}{D_{liq}}$ is used for describing the film thickness) – process 3. No convection can be established here. The mass transfer is solely defined by mobility of the ion. The film thickness can be reduced by increasing the agitation speed in the solution, but it can never be completely removed.

- When the ion has passed the boundary between the film and solid, the ion diffuses inside the phase of material (process 4). This is controlled only by properties of the ion and material. The only driving force is the concentration gradient.

- And finally there is bonding of the ion on to the resin (process 5) where the chemical reaction takes place.

- Processes from 6-10 are associated with the leaching out of the ions attached on the resin.

2.3.4 Equilibrium

A common way to represent equilibrium in sorption and ion-exchange systems is the equilibrium isotherm. The equilibrium isotherm represents the distribution of the sorbed material between the sorbed phase and the solution phase at equilibrium. The isotherm is characteristic for a specific system and a particular temperature.

The main difference between sorption and ion exchange is that while there is only one isotherm at a specified temperature for sorption, more than one isotherm can exist at a specific temperature for different normalities of the solution in the exchange of the ions of different valences due to the concentration – valence effect (Inglezakis & Poulopoulos 2006 and Helfferich 1995). Chemical equilibrium in processes of sorption and ion exchange is represented with isotherm where sorbates are simultaneously sorbed and desorbed from the surface at constant temperature and pH. Time taken to equilibrium regarding the ion exchangers depends on the characteristics of the ion exchanger and ion that is sorbed on the ion exchanger.

At constant pH and temperature the single solute sorption can be described by the function:

$$q = f(C) \qquad \textbf{Eq. 3}$$

where q is the sorbate concentration on the solid phase and C is the sorbate concentration on the liquid phase. There are many equations of sorption isotherms (Limousin *et al.* 2007) but the most common and the most used one is the Langmuir isotherm.

2.3.4.1 Langmuir isotherm

Sorbents that exhibit the Langmuir isotherm behaviour are supposed to contain fixed individual sites, each of which equally sorbs only one molecule, forming thus a monolayer, namely, a layer with the thickness of a molecule:

$$\frac{q_e}{q_m} = \frac{bC_{eq}}{1 + bC_{eq}} \qquad \textbf{Eq. 4}$$

where q_e is the sorbate concentration on the solid phase in equilibrium with the sorbate concentration in the liquid phase at the interface C_{eq}, q_m is the maximal amount of sorbate that can be sorbed on the sorbent and it corresponds to the concentration of sorbate at the interface at monolayer coverage and represents the highest value of q that can be achieved as C is increased. b is a Langmuir constant and it is related to the energy of sorption which increases as the strength of sorption increases.

The parameter of Hall, for predicting the exchange efficiency of the process, is determined by using the following equation (Hall *et al.* 1966):

$$R_L = \frac{1}{1 + bC_{ox}} \qquad \textbf{Eq. 5}$$

where C_{ox} is the initial metal ions concentration in the solution. Also when the dimensionless sorption capacity (q/q_o) is plotted against the dimensionless concentration (C/C_{ox}) for different R_L values, the shape of isotherm can be developed and used to predict if the process of sorption is favourable or unfavourable. The effect of R_L can be interpreted according to the classification in Table 3.

Table 3 Effect of R_L on exchange efficiency of ion exchanger

Value of R_L	**Exchange efficiency**
R_L>1	Unfavourable
R_L=1	Linear
0<R_L<1	**Favourable**
R_L=0	Irreversible

2.3.5 Column techniques

The two most common methods of studying ion exchange are batch operation and fixed-bed column operation. Batch operation (ion exchanger and solution are simply mixed together and agitated) is rarely used in industrial processes, but it is well suited for laboratory experiments due to the simplicity of the experimental apparatus (Lehto, Harjula 1995). The main disadvantage of batch process is that it cannot separate the ions completely and that the process itself is discontinuous and requires phase separation at the end of the process.

On the other hand fixed-bed columns have several advantages: there is a constant removal of counter ion that is released during the ion exchange which enhances the process (counter ion can be attached back onto the ion exchanger), ions that have to be retained on ion exchanger move with the solution through the column and coming in contact with fresh portions of the material so the driving force for sorption of ions onto ion exchanger increases while the concentration of ions fall through the fixed-bed column. Fixed-bed process can be described as a large number of successive batch operations in series (Lehto, Harjula 1995).

2.3.6 Membrane filtration

Membrane filtration is defined as a pressure- or vacuum-driven separation process in which particulate matter larger than a certain size is rejected by an engineered barrier primarily through a size exclusion mechanism. Two most important parameters are: water flux and rejection. In recent years use of membrane processes for treatment of waste waters has been widely investigated.

Depending on the pore size, membrane processes can be divided into:

- Microfiltration – MF,

- Ultrafiltration – UF,
- Nanofiltration – NF and
- Reverse osmosis – RO.

Separation may be based on **exclusion and diffusion** or on **sieving mechanisms** when particles bigger than pore diameter of the membrane are retained by the membrane. The difference between four membrane processes is presented in Table 4.

Table 4 Comparing Four Membrane Processes (Wagner 2001). HMWC – high molecular weight component, LMWC – low molecular weight component.

	Microfiltration (MF)	**Ultrafiltration (UF)**	**Nanofiltration (NF)**	**Reverse osmosis (RO)**
Pore size (µm)	>0.1	0.1 – 0.001	<0.002	<0.002
Approximately molecular weight	>100,000	>10,000	<20,000	<1000
Rejection	Suspended solids, emulsions, bacteria, red blood cells, blue indigo dye.	Macro molecules, polysaccharides, colloidal silica, viruses, gelatine, milk proteins.	HMWC, mono-, di- and oligosaccharides, multivalent ions.	HMWC, LMWC, aqueos salt, lactose (sugars), monovalent ions.
Operating pressure (bar)	<2	1 – 10	5 – 35	15 – 150
Flux (L m^{-2} h^{-1})	>100	<100	<100	<10

A common problem that is related to membrane filtration is fouling of the membrane. During the filtration there is a sharp decline of flux compared to initial clean water flux. After this sharp fall of flux, the rate of decline reduces until the steady state is reached. This shows that there is high fouling rate at the start of the filtration and that equilibrium fouling layer thickness may be reached when no further growth of the thickness of the fouling layer occurs later. There are two fouling mechanisms: internal and external (Tarleton & Wakeman 1993). During internal fouling fine particles from the feed stream are captured into pores which can lead to blocking of the pores. This generally happens with filters with significant depth and open pore structure such as conventional microfiltration membranes (Figure 8).

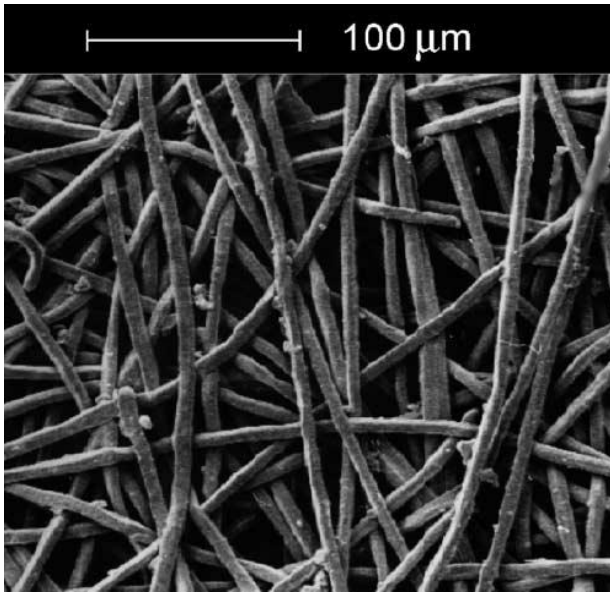

Figure 8 Photograph and pore size distribution of commercial metal microfiltration membrane (Holdich *et al.* 2003).

During external fouling cake is formed on the membrane surface. As a result of membrane fouling resistance to permeate flow increases and the flux reduces. Darcy‘s law represents how the flux is reduced if the resistance is increased:

$$J = \frac{\Delta P}{\mu_L (R_m + R_f)} \qquad \textbf{Eq. 6}$$

where J is transmembrane flux, R_m is membrane resistance, R_f is total fouling resistance and ΔP is applied transmembrane pressure and μ_L is viscosity of the suspending fluid.

According to Holdich et. al. (1998) a membrane that contains uniform pores, not connected to each other and pass directly from one side to another side of the membrane can be used to reduce internal clogging/fouling. A –surface microfilter" such as this does not require a tortuous flow channel to achieve its pore size rating (Figure 9). The reason to use the slots and not the circular pores is more likely clogging of the circular pores (Holdich 2002).

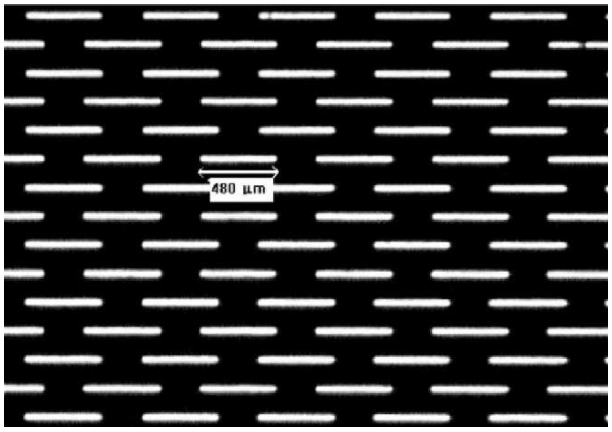

Figure 9 Photograph and pore size distribution of –surface microfilter" (Holdich *et al.* 2002).

2.3.7 Seeded microfiltration

From Table 4 it can be seen that RO and NF are capable of retaining metal ions from aqueous streams while UF and MF are not capable of retaining the metal ions due to the nature of their membranes where pore size is bigger than the size of the hydrated metal ion. In order to use UF and MF for separation of metal ions precipitation or binder enhancement are required in order to separate metal ions.

If UF or MF can be used for separation of metal ions from a solution that would mean that a lower pressure can be used instead of a high pressure when RO or NF is used, and such change would lead to lowering of operating costs. Several hybrid membrane processes based on the use of binders/sorbents (chelating agents, micelles, ion exchange resins, powdered activated carbon, etc.) together with UF or MF have been developed and reported. This process is called –seeded filtration". Michaels (1968) reported for the first time removing metal ions from aqueous streams by binding metal ions to dispersed material coupled with ultrafiltration process. The main advantage of this separation method is the high efficiency and a lower cost of the process compared with classical sorption in a fixed bed system. The sorbents can be used as very fine particles that increase the interfacial area and the rate of the process is enhanced (Nadav 1999).

3. MODELLING

3.1 MEMBRANE EMULSIFICATION

3.1.1 Dispersed droplet size modelling

There are numerous forces acting on the droplet forming at the pore as a result of the membrane emulsification. These forces can be divided in two main groups: (a) forces ***holding*** the droplet and (b) forces ***detaching*** the droplet from the pore (Figure 10).

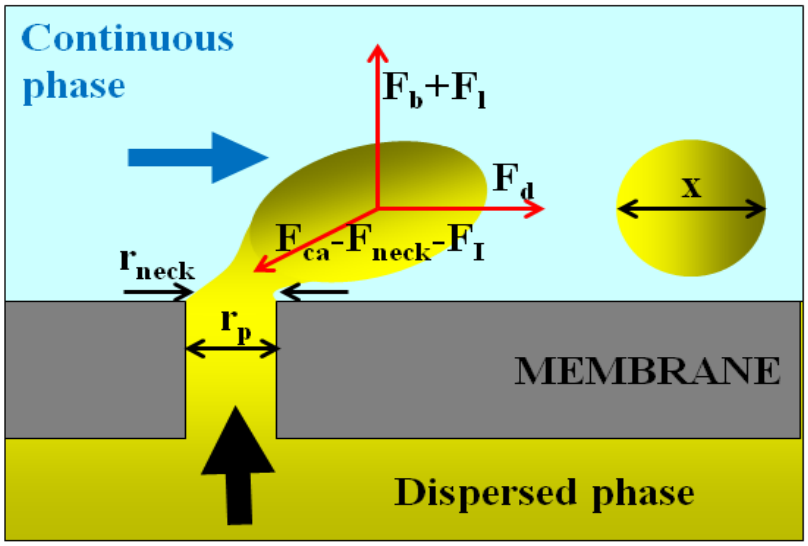

Figure 10 Forces acting on the droplet during its formation at a pore.

Capillary force $\boldsymbol{F_{ca}}$ (Eq. 7) is the main force that keeps the droplet on the membrane surface. Main detaching force is a viscous drag force $\boldsymbol{F_d}$, (Eq. 8) induced by the continuous phase flow, while other detaching forces acting on the forming droplets are: static pressure difference force $\boldsymbol{F_{neck}}$ cased by the pressure difference between continuous and dispersed phase, dynamic lift force $\boldsymbol{F_L}$, caused by the laminar velocity profile, inertial force $\boldsymbol{F_I}$, induced by the mass of the dispersed phase flowing out of the pore (which during generation of the 100 µm droplets is 3 orders magnitude less than the shear drag force, and for 200 µm droplets 2 orders of magnitude). Buoyancy force $\boldsymbol{F_b}$ also exist ($F_b = \frac{1}{6}\pi g x^3(\rho - \rho_{oil})$ which is not necessarily detaching force and can be neglected for the droplets smaller than 500 µm (Kosvintsev *et al.* 2008), which occurs due to the density difference between dispersed and continuous phase (Peng & Williams 1998, Joscelyne & Trägårdh 2000, Schröder, Behrend & Schubert 1998).

$$F_{ca} = 2\pi r_p \gamma \qquad \textbf{Eq. 7}$$

$$F_d = 9\pi\tau \cdot x\sqrt{\left(\frac{x}{2}\right)^2 - r_p{}^2} \qquad \textbf{Eq. 8}$$

where r_p is the pore radius, τ is the shear stress, γ is the interfacial tension and x is the formed droplet diameter.

The general equation used in this study was introduced in the previous work (Kosvintsev *et al.* 2005). The initial, and simplest, approach is where the droplet diameter is calculated from a force balance of two main forces: the capillary force F_{ca} and the drag force F_d acting on a strongly deformed droplet at a single membrane pore

$$F_{ca} = F_d \qquad \textbf{Eq. 9}$$

At the moment the detaching forces prevail droplet is detached from the membrane surface. Rearranging the Eq. 9 substitution and solving for a quadratic gives the resulting droplet diameter

$$x = \frac{\sqrt{18\tau^2 r_p^2 + 2\sqrt{81\tau^4 r_p^4 + 4r_p^2\tau^2\gamma^2}}}{3\tau} \qquad \textbf{Eq. 10}$$

The shear stress at the membrane surface varies, τ, with the radial distance from the centre of the membrane, r_c, according to the equations (Nagata 1975):

For $r_c < r_{trans}$ $\qquad \tau = 0.825\mu\omega r\frac{1}{\delta}$ $\qquad$ **Eq. 11**

For $r_c > r_{trans}$ $\qquad \tau = 0.825\mu\omega r_{trans}\left(\frac{r_{trans}}{r}\right)^{0.6}\frac{1}{\delta}$ $\qquad$ **Eq. 12**

For the simple Dispersion Cell (Figure 14), the shear stress τ at the base of a paddle stirred vessel must be determined in order to predict the droplet size (Eq. 10). It can be argued that the appropriate shear stress to use is either the average, or maximum, value. The maximum value of the shear stress τ_{max} determined from a stirred system, such as the Dispersion Cell, is given from knowledge of the location of the transitional radius r_{trans} along the paddle blade radius

$$\tau_{\max} = 0.825\mu\omega r_{trans}\frac{1}{\delta} \qquad \textbf{Eq. 13}$$

The transitional radius, r_{trans}, is the point at which the rotation changes from a forced vortex to a free vortex

$$r_{trans} = \frac{D}{2}1.23\left(0.57+0.35\frac{D}{T}\right)\left(\frac{b_h}{T}\right)^{0.036} n_b^{0.116}\frac{\mathrm{Re}}{1000+1.43\mathrm{Re}} \qquad \textbf{Eq. 14}$$

where b_h is the blade height, T is the tank width, D is the stirrer width and n_b is the number of blades. The Reynolds Number is defined by $Re = \rho\omega D^2/(2\pi\mu)$, where ρ is the continuous phase density, ω is the angular velocity and μ is the viscosity of continuous phase. Figure 11 shows change of local shear stress on membrane surface at different rotation speeds.

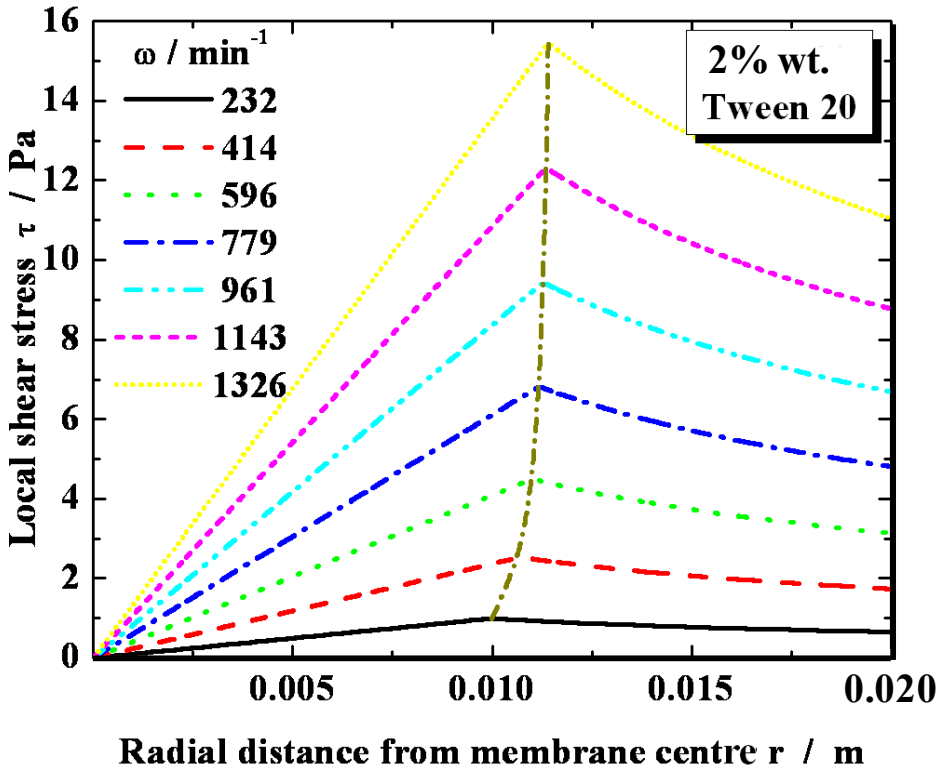

Figure 11 Local shear stress at different rotation speeds. Dash dot dash line connects transitional radiuses. For the calculations boundary condition is assumed to be no-slip at the wall of the cell.

The boundary layer thickness, δ is defined by the equation (Landau & Lifshits 1959)

$$\delta = \sqrt{\frac{\mu}{\rho\omega}} \qquad \textbf{Eq. 15}$$

where ω is angular velocity. The approach based on Eqs. (10)-(15) will be called Model A. The alternative approach is to use the average shear in Eq. (10) for the stirred cell, where the average shear is given by (Dragosavac *et al.* 2008)

$$\tau_{av} = \frac{\int_0^{r_{trans}} 0.825\mu\omega r \frac{1}{\delta}(2\pi r)dr + \int_{r_{trans}}^{D_m/2} 0.825\mu\omega r_{trans}\left(\frac{r_{trans}}{r_c}\right)^{0.6} \frac{1}{\delta}(2\pi r)dr}{\pi D_m^2/4} = \quad \textbf{Eq. 16}$$

$$= \frac{6.6}{D_m^2}\mu\omega\frac{1}{\delta}\left\{\frac{r_{trans}^3}{3} + \frac{r_{trans}^{1.6}}{1.4}\left[\left(\frac{D_m}{2}\right)^{1.4} - r_{trans}^{1.4}\right]\right\}$$

where D_m is the effective diameter of the membrane, i.e. the diameter exposed to the continuous phase. For the experimental equipment used, D_m=3.3 cm. Use of Eqs. (10), (14) and (15) will be called Model B.

However, Eq. (10) does not take in to account the ‗neck', which exists between the forming droplet and the membrane pore. This can be included by introducing another force: the so-called Static force, F_{neck}. As shown previously, there is a static pressure difference due to pressure between the inside and outside of the droplet which can be expressed as

$$F_{neck} = \frac{4\gamma}{x}\frac{\pi}{4}d_p^2 \quad \textbf{Eq. 17}$$

where the neck diameter is approximated to the membrane pore diameter (d_p). The force due to interfacial tension (capillary force) is

$$F_{Ca} = \pi d_p \gamma \quad \textbf{Eq. 18}$$

It is possible to modify the capillary force in order to consider the neck

$$F_{Ca} - F_{neck} = \pi d_p \gamma\left(1 - \frac{d_p}{x}\right) \quad \textbf{Eq. 19}$$

When the droplets are in a region close to the pore diameter, the expression considering the neck underestimates the net capillary force, and the correction for this neck static pressure is no longer applicable. In such cases it is preferable to use the uncorrected expression, Eq. (18).

Hence, it is possible to write a force balance using all of the above equations

$$F_{Ca} - F_{neck} = F_D \qquad \textbf{Eq. 20}$$

where the drag force (Eq. (8)) can be calculated using the maximal (Eq. (13)) or average shear stress (Eq. (16)) and this modelling approach will be called Model C.

3.1.2 Oscillating system

When considering an Oscillating membrane (Figure 21) the equation for the shear rate ($\dot{\gamma}$) with respect to time is (Jaffrin 2008)

$$\dot{\gamma} = v_o \left(\frac{\omega_f \rho}{2\mu} \right)^{1/2} \left[\sin(\omega_f t) - \cos(\omega_f t) \right] \qquad \textbf{Eq. 21}$$

and the equation for shear stress will be

$$\tau = \mu\dot{\gamma} = v_o \left(\frac{\omega_f \mu \rho}{2} \right)^{1/2} \left[\sin(\omega_f t) - \cos(\omega_f t) \right] \qquad \textbf{Eq. 22}$$

In Eq. (21) and Eq. (22) the term ω_f is the angular frequency, and it is determined during oscillation from the following equation

$$\omega_f = 2\pi f \qquad \textbf{Eq. 23}$$

where f is the frequency of the oscillation. The peak velocity, v_o, is related to both the angular frequency and the amplitude a of oscillation by the equation

$$v_o = \omega_f a \qquad \textbf{Eq. 24}$$

The droplet formation time t_d, useful for comparison of the number of times an emerging droplet is subject to maximum shear, is obtained from a material balance (Schröder, Behrend & Schubert 1998; Vladisavljević & Schubert 2002).

$$t_d = \frac{2\varepsilon k d(v,0.5)^3}{3 d_p^2 J_d} \qquad \textbf{Eq. 25}$$

where k is the fraction of pores taking part in the emulsification, $d(v,0.5)$ is the mean droplet diameter by volume, J_d is the dispersed phase flux and ε is the porosity of the membrane surface.

3.1.3 Pulsating system

When modelling the droplet size in the Pulsating system an additional shear that originates from the flow of the continuous phase is also present. In the experiment the volumetric flow rate of the continuous phase was 3.33×10^{-7} or 6.66×10^{-7} m^3 s^{-1} and Reynolds number ($Re_t = 4\cdot Qc\cdot\rho/(d_m\cdot\mu\cdot\pi)$ where Qc is volumetric continuous phase flow rate, ρ is continuous phase density, μ is coefficient of dynamic viscosity of the continuous phase and d_m is membrane diameter) was 28 and 56 respectively meaning that the flow of the continuous phase was laminar. For the laminar flow (Re_t<2300) wall shear stress is given by following equation (Vladisavljević & Schubert, 2003b):

$$\tau_w = \frac{8\mu V_t}{d_m} \qquad \textbf{Eq. 26}$$

where μ is dynamic viscosity the continuous phase, V_t is the mean velocity of the continuous phase ($Vt=Qc/A$; A is the cross-sectional area of the membrane). For both flow rates of the continuous phase wall shear stress induced by the flow of the continuous phase were 0.01 and 0.02 Pa respectively. Shear induced by the pulsations can be calculated on the same way as in the case of the oscillations (Eq. (22)) and was varied in the range between 1 and 8 Pa. Even when the higher cross-flow velocity was used in combination with the lowest shear induced by the pulsation the shear induced by the flow of the continuous phase did not exceeded 2%. Therefore in all the calculations the wall shear stress induced by the flow of the continuous phase in the Pulsating system was neglected.

The intention was to compare the performance of dispersion generation between a stirred, but stationary membrane system, one that uses oscillation of the membrane but stationary continuous phase and Pulsating system where the membrane is stationary and continuous phase pulsates. If the droplet size is dependent only on the shear conditions at the membrane surface then it should be possible to calculate the shear stress in the

Oscillating system or in Pulsating system using Eq. (22) and obtain comparable results with the stirred stationary membrane system, provided that oscillation of the membrane or pulsation of the flow can be used to generate droplets of a reasonable degree of uniformity.

3.2 ION EXCHANGE AND SEEDED MICROFILTRATION

For ion exchange, several studies (Van Nguyen *et al.* 2009; Weng *et al.* 2007; Popuri *et al.* 2009) reported kinetic analyses of contact time results based on the application of kinetic, or pseudo-kinetic, modelling. However, such models require equilibrium constants and activity coefficients for metal ion, or yield pseudo-rate constants, specific to a single experiment. Rate parameters obtained from each experiment were different and therefore, the application of these kinetic models to generate designs is limited. More applicable models are based on a mass balance combined with diffusion controlled mass transfer. Film and pore diffusion are the two main mass transfer mechanisms (Helfferich 1995). For systems with high feed concentration film diffusion is normally neglected and pore diffusion is the limiting mechanism. Often, in the literature pore diffusion models are based on a single effective diffusion coefficient in the solid phase (Holdich, Cumming & Perni 2006), or different solid phase diffusivities such as the diffusion within the pores of the resin and the surface diffusion within the resin (Yiacoumi & Tien 1995). However, it is not easy to separate the effects of the different solid phase diffusional resistances (pore and surface) and for all practical purposes a single effective diffusion coefficient in the solid phase may be sufficient for design.

In order to predict the behaviour of the seeded MF process, a conventional mass transfer model was applied based on mass transfer resistance within the aqueous film surrounding the particles together with diffusional resistance within the particle. However, the analysis was coupled with a material balance to account for the continuous nature of the process.

3.2.1 Continuous stirred tank reactor (CSTR)

When ion exchange is not present in the Dispersion Cell and there is continuous feed flow and continuous effluent flow in and from the Dispersion Cell, the whole system acts as continuous stirred thank reactor (CSTR) which is described in numerous reaction engineering literature (Fogler 2005, Levenspiel 1999) and a mass balance for such a system can be described as follows:

$$F_o C_o = FC + V\frac{dC}{dt} \qquad \textbf{Eq. 27}$$

where F_o is a volumetric flow rate of feed and F is a volumetric flow rate of effluent ($m^3\ s^{-1}$), C_o is concentration of copper in feed ($kg\ m^{-3}$) and C is concentration of copper in effluent ($m^3\ s^{-1}$). V is volume of Dispersion Cell (m^3). For a constant flow feed and effluent flow rate are equal so Eq. 27 can be simplified as follows:

$$V\frac{dC}{dt} = F(C_o - C) \qquad \textbf{Eq. 28}$$

Equation can be solved by integration and obtained equation is:

$$\frac{C}{C_o} = 1 - e^{-\left(\frac{F}{V}\right)t} \qquad \textbf{Eq. 29}$$

3.2.1.1 Seeded microfiltration

Mass transfer in seeded microfiltration is much faster compared with that obtained in fixed bed ion exchange columns (Holdich, Cumming & Perni 2006), which makes it useful in laboratory experiments for estimating the mass transfer coefficient and intraparticle diffusivity. The following assumptions are made in modelling: isothermal operation, rapid chemical reaction of binding the copper to ion exchange resin, sorption equilibrium described by the Langmuir isotherm, ideal mixing in the system with continuous flow, mass transfer of copper through external aqueous phase film by film diffusion and through pores represented by a single internal diffusion coefficient.

The mass balance of copper for sorption in a well-mixed continuous flow stirred cell can be expressed as follows:

$$V\frac{dC}{dt} = F(C_o - C) - m\frac{d\bar{q}}{dt} \qquad \textbf{Eq. 30}$$

where V is the liquid volume in the cell, C is the concentration in the solution at time t (both in the cell and the exit), C_o is the concentration in the feed stream, F is the volume feed flow rate, m is the total mass of the resin in the cell, and $\bar{q}$ is the average mass of sorbed copper per unit mass of the resin. $\bar{q}$ can be obtained by integrating the local mass throughout the resin from r=0 to r=R

$$\bar{q}(t) = \frac{3}{R^3}\int_0^R q(r,t) r^2 dr \qquad \textbf{Eq. 31}$$

where R is the Sauter mean radius of the resin particles and r is the radial distance from the centre of particle. Fick's second law for diffusion of copper inside a spherical particle is given by:

$$\frac{\partial q}{\partial t} = \frac{1}{r^2}\frac{\partial}{\partial r}\left(D_{eff} r^2 \frac{\partial q}{\partial r}\right) \qquad \textbf{Eq. 32}$$

where D_{eff} is the effective diffusion coefficient of copper inside the particle. The total mass of copper entering the solid phase per unit time is

$$m\frac{d\bar{q}}{dt} = kA(C - C_e) \qquad \textbf{Eq. 33}$$

where A is the total surface area of the resin particles, C_e is the equilibrium concentration of copper in the liquid phase at the interface and k is the mass transfer coefficient in the liquid phase. According to the film theory (Helffrich 1995)

$$k = \frac{D_{liq}}{\delta_f} \qquad \textbf{Eq. 34}$$

where D_{liq} is the diffusion coefficient of copper in the liquid phase and δ_f is the film thickness (distance over which liquid phase diffusion takes place). The Frössling equation (Frössling 1938) can be used to evaluate k, using Sherwood, Particle Reynolds and Schmidt dimensionless numbers:

$$Sh = 2 + 0.6\,\mathrm{Re}_{slip}^{0.5}\, Sc^{0.33} \qquad \textbf{Eq. 35}$$

$$Sh = \frac{k \cdot 2R}{D_{liq}} \qquad Sc = \frac{\mu}{D_{liqu}\rho} \qquad \mathrm{Re}_{slip} = \frac{v_{slip} 2R\rho}{\mu} \qquad \textbf{Eq. 36}$$

where μ is the liquid dynamic viscosity, ρ is the liquid density and v_{slip} is the relative particle-liquid velocity (slip velocity). Harriott (1962) suggested that at the just suspended conditions, e.g. at the minimum agitation conditions at which all particles attain complete suspension, the slip velocity is of the order of the terminal velocity (Heywood 1948).

We have assumed in our modelling that v_{slip} was equal to the terminal particle velocity, due to relatively low agitation speed in the cell. The concentration of copper in the liquid phase at the interface can be found from Eq. (4) by assuming that at the interface the liquid phase is in equilibrium with the surface layer of the solid phase:

$$C_e = \frac{q\big|_{r=R}}{b\left(q_m - q\big|_{r=R}\right)} \qquad \textbf{Eq. 37}$$

The total surface area of the resin particles, A can be expressed in the terms of the Sauter mean radius:

$$A = \frac{3m}{\rho_s R} \qquad \textbf{Eq. 38}$$

Therefore, the mass rate of copper entering the particle is given by:

$$m\frac{d\overline{q}}{dt} = A\rho_s D_{eff}\left.\frac{\partial q}{\partial r}\right|_{r=R} = \frac{3}{R}mD_{eff}\left.\frac{\partial q}{\partial r}\right|_{r=R} \qquad \textbf{Eq. 39}$$

and hence, Eq. (30) can be rewritten as:

$$V\frac{dC}{dt} = F(C_o - C) - \frac{3}{R}mD_{eff}\left.\frac{\partial q}{\partial r}\right|_{r=R} \qquad \textbf{Eq. 40}$$

For solving the differential Eq. (40) the boundary conditions have to be specified. At the beginning of the process, there is no copper in the liquid phase inside the cell:

$$q\left(t = 0, 0 \le r \le R\right) = 0 \qquad C\left(t = 0\right) = 0 \qquad \textbf{Eq. 41}$$

The concentration gradient is zero in the centre of the bead ($r = 0$):

$$\left.\frac{\partial q\left(t \ge 0\right)}{\partial r}\right|_{r=0} = 0 \qquad \textbf{Eq. 42}$$

and for the full radius of the bead ($r = R$) boundary condition is

$$\left.\frac{\partial q(t \geq 0)}{\partial r}\right|_{r=R} = \frac{k}{D_{eff}\rho_s}(C - C_e) \qquad \textbf{Eq. 43}$$

The system of Eqs. (30)-(40) must be solved simultaneously in an equation solver capable of solving partial differential equations. For solving of such system PDESOL (Numerica, Dallas, USA) was used subject to boundary conditions Eqs. (41)-(43). PDSOL file is given in Appendix C.

4. EXPERIMENTAL

4.1 DISPERSION CELL

4.1.1 Membranes

The emulsions in the Dispersion Cell were produced using a flat disk membrane, (Figure 12) under the paddle blade stirrer, which was supplied by Micropore Technologies Ltd. (Loughborough, UK). The membranes used were nickel membranes containing uniform cylindrical pores with a diameter of 10, 15, 20, 30 or 40 μm and a pore spacing of 200 μm. In some of the experiments a ring membrane (Figure 12(a)) was also used. The ring membrane has active pores just in an area of a narrow ring around the transitional radius (Eq. (14)) where the shear on the membrane surface reaches the maximal value.

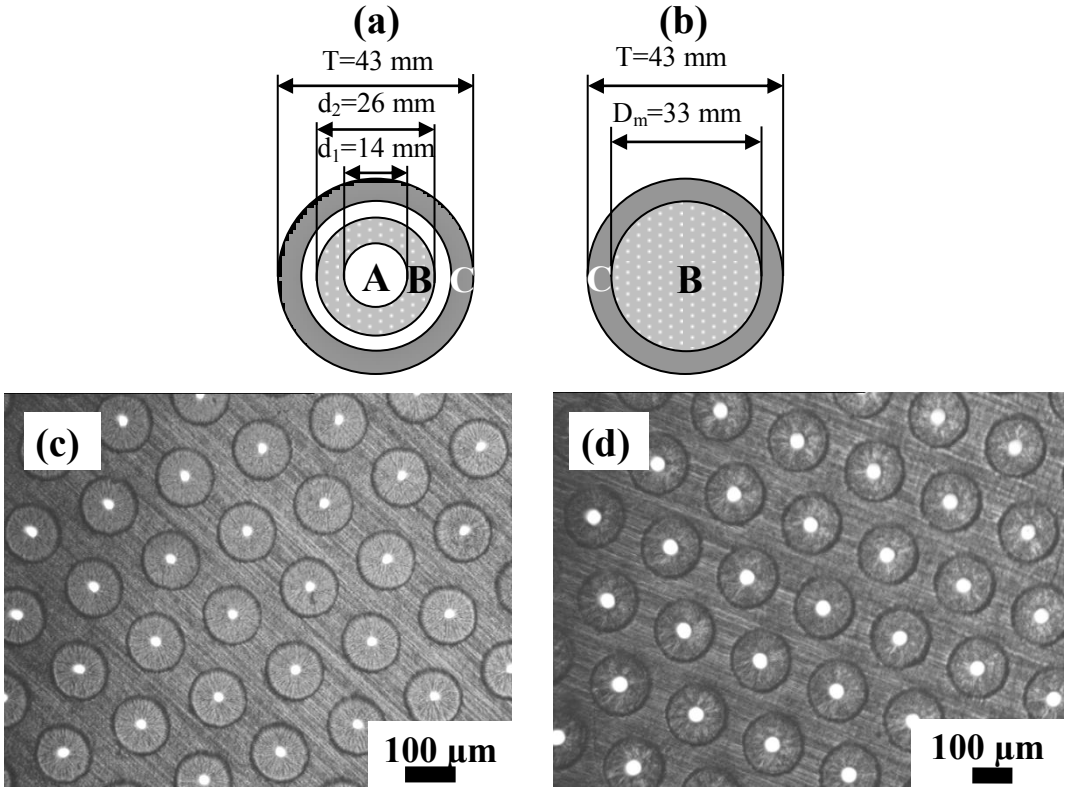

Figure 12 Schematic illustration of (a) ringed and (b) whole membrane. Photomicrograph of (c) 20 and (d) 40 μm membrane.

For production of O/W and W/O/W hydrophilic membranes were used while for the W/O hydrophobic membranes with PTFE coating were used. If hydrophobic, prior to the experiment the membrane was soaked at least 30 min in kerosene (to increase the

hydrophobicity) or in 2 wt.% wetting agent if hydrophilic (to increase hydrophilicity). A perfectly ordered hexagonal array of pores with a pore at the centre of each hexagonal cell can be seen on the micrograph in Figure 12(c) and (d).

The porosity of a membrane ε with the hexagonal pore array is given by:

$$\varepsilon = \frac{3\left(\frac{d_p^2\pi}{4}\right)}{\frac{3\sqrt{3}}{2}L^2} = \frac{\pi}{2\sqrt{3}}\left(\frac{d_p}{L}\right)^2 \qquad \textbf{Eq. 44}$$

and the calculation of the porosity is explained in Figure 13.

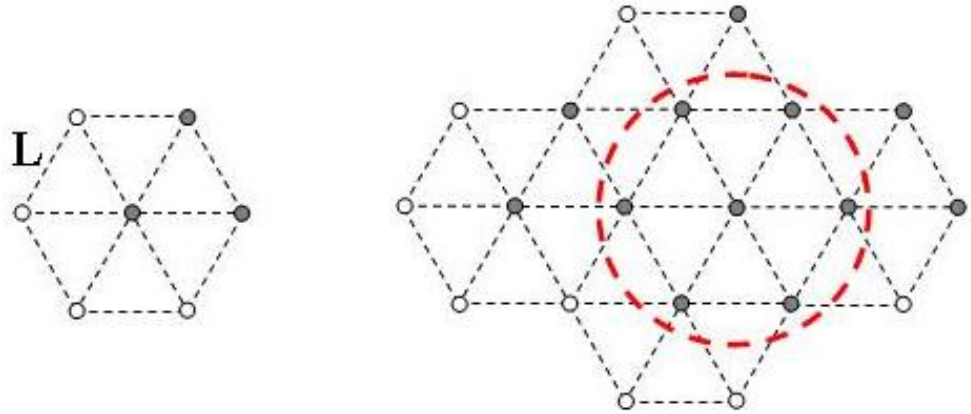

Figure 13 Calculation of the porosity for the membrane with hexagonal pore array.

where d_p is the pore diameter and L is pore spacing. The porosity of the used membranes was between 0.2 and 3.6%, respectively.

4.1.2 Formulation and experimental procedure

Emulsification using a stationary disk membrane was performed using a Micropore Technologies Ltd. Dispersion Cell. No matter the formulation of the emulsion the following general experimental procedure may be established when working with the Dispersion Cell (Figure 14).

The Dispersion Cell uses a 24 V DC motor to drive a paddle-blade stirrer, which provides the shear at the membrane surface. Stirrer speed settings ranging from 2 to 12 V were used, which are expressed in the results section as either angular velocities (180 – 1400 rpm) or their corresponding (maximum) shear stress (1-20 Pa) (Eq. (13)). Prior to the experiment the base of the Dispersion Cell was filled with the continuous phase

and the feed line was filled with continuous phase too (Table 5) using the pump. Depending on the investigation the pump was either a peristaltic pump (Watson-Marlow-Bredel Pump 101U/R, Cornwall, UK) providing the constant flow rate of 0.5–50 mL min^{-1}, corresponding to the dispersed phase fluxes of 30–3200 L m^{-2} h^{-1} or syringe pump (Harvard Apparatus model 11 Plus, US) providing the constant flow rate of 0.01–50 mL min^{-1}, corresponding to the dispersed phase fluxes of 0.6–3200 L m^{-2} h^{-1}. The use of the syringe pump was crucial when testing the validity of the models given in Chapter 3 since very low flow rates had to be used since the models do not take into consideration the flow rate of the dispersed phase. Once it was ensured that the feed line was free from air bubbles the membrane, with the shiny side up, was placed into the base. The PTFE sealing ring (good also for the use with the kerosene because it does not swell) was placed on top of the membrane and the glass cell was tightened to the base followed by placing the stirrer on top of the glass cell. The continuous phase was filled up to the desired volume (Table 5) and then the dispersed phase was injected.

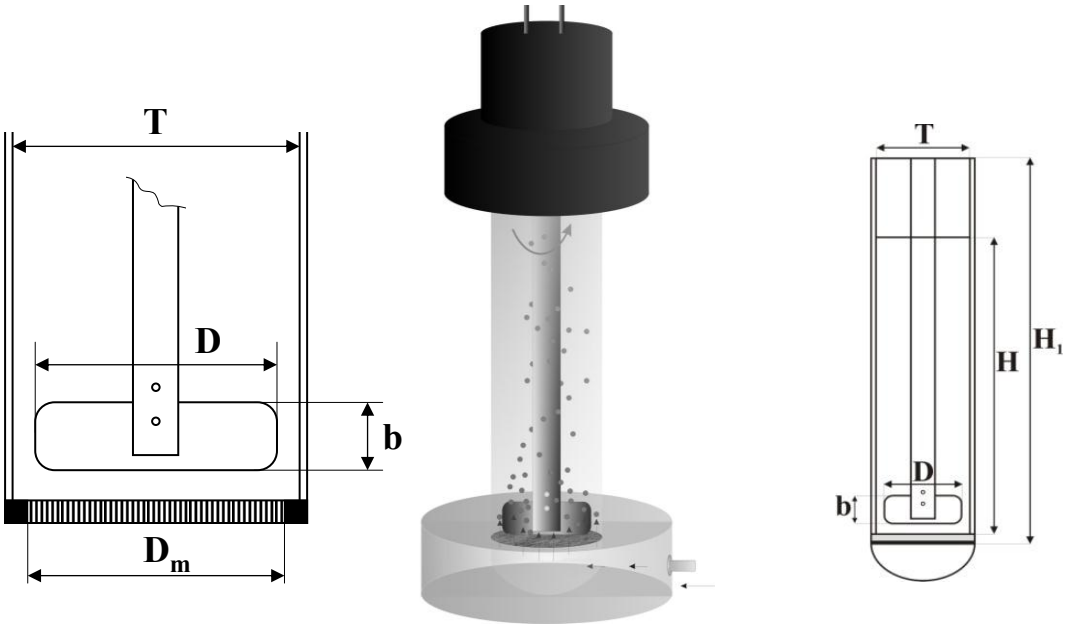

Figure 14 Schematic illustration of Dispersion Cell with simple paddle used (b = 12 mm, D = 30 mm, D_m = 33 mm, T = 40 mm, H_1=166 mm , H=130 mm).

Several types of the emulsions were produced using the Dispersion Cell and the basic formulations with membrane characteristics are given in Table 5.

Table 5 Formulations of the emulsions produced using the Dispersion Cell together with the used membranes. DP: dispersed phase, CP: continuous phase. O – sunflower oil; O_1 – sunflower oil with 5 wt.% PGPR; O_2 – pumpkin seed oil with 5 wt.% PGPR; W_1 – pure DI water; W_2 – 2 wt.% Tween 20; W_s – acidified sodium silicate; O_k – 2 wt.% Span 80 in Kerosene

Emulsion type	DP	Final content of DP (vol%)	CP	Initial volume of CP (cm^3)	Membrane type	Membrane pre experimental treatment	Pore sizes of the used membranes (μm)
O/W	O	6.25	W_2	150	Whole / hydrophilic	30 min soaked in wetting agent	10
$W_1/O_1/W_2$	W_1/O_1	5	W_2	125	Whole / hydrophilic	30 min soaked in wetting agent	10, 20, 30, 40
$W_1/O_2/W_2$	W_1/O_2	5	W_2	125	Whole / hydrophilic	30 min soaked in wetting agent	10, 20, 30, 40
W_s/O_k	W_s	9 / 33	O_k	100	Whole and ring / hydrophobic	30 min soaked in kerosene	15

4.1.2.1 O/W emulsions

Membranes with a 10 μm pore size, and 200 μm spacing between the pores, were supplied by Micropore Technologies Ltd. for the production of all the emulsions. In the majority of the experiments the dispersed phase was injected through the membrane pores using a very low flux of 30 litres of dispersed phase injected per square metre of membrane area per hour (L m^{-2} h^{-1}), and employed to minimise any "push-off" effect, but it was possible to achieve 3200 L m^{-2} h^{-1}. The continuous phase volume was 150 cm^3 and 10 cm^3 of dispersed phase was injected for each experiment.

4.1.2.2 W/O/W emulsions

The oil phase (O) in $W_1/O/W_2$ emulsions was 5 wt.% PGPR (polyglycerol polyricinoleate from Stepan Limited, UK) dissolved in unrefined pumpkin seed oil

(density of 913 kg m^{-3} at 298 K, GEA Tovarna Olja, Slovenia) or refined sunflower oil (food grade from a local supermarket). The inner aqueous phase (W_1) was pure (demineralised) water. The outer aqueous phase (W_2) for stabilising the W_1/O emulsions contained 2 wt.% Tween® 20 (polyoxyethylene sorbitan monolaurate from Fluka, UK). In some experiments PVA, poly(vinyl) alcohol 98% hydrolyzed molecular weight 13000-23000 g/mol, Sigma-Aldrich Company Ltd., UK, was added to investigate the effect of continuous phase viscosity on droplet break-up behaviour. The formulation of the product emulsions and the range of the mean particle sizes obtained are listed in Table 6.

Table 6 The composition of $W_1/O/W_2$ emulsions prepared in this work.

Inner aqueous phase, W_1	Pure Milli - Q water
Oil phase	5 wt.% PGPR dissolved in unrefined pumpkin seed oil or refined unflower oil
Outer aqueous phase, W_2	2 wt.% Tween® 20 dissolved in Milli–Q water, in some experiment PVA was added
Volume percent of inner aqueous phase in W_1/O emulsions (vol.%)	0 or 30
Volume percent of W_1/O emulsion droplets in $W_1/O/W_2$ emulsions (vol.%)	5
Mean size of outer droplets	102-422 and 134-433 μm for the pore size of 20 and 40 μm, respectively

The density of oil and continuous phase was measured using an Anton Paar digital density meter (model DMA 46, Graz, Austria). The oil viscosity was measured using HAAKE RheoStress® model RS600 rheometer with sensor C60/1° Ti and a gap of 51 μm (Thermo Electron, Karlsruhe, Germany). The continuous phase viscosities were measured with a Cannon-Ubbelohde model 9721-K50 viscometer (CANNON® Instrument Company, USA). The equilibrium interfacial tensions at the oil/water interface were measured by the Du Nouy ring method using a White Electric Instrument tensiometer (model DB2KS). The physical properties of the surfactant

solutions and the equilibrium interfacial tensions for the two different oils used are listed in Table 7.

$W_1/O/W_2$ emulsions were prepared by a two-step emulsification procedure. The W_1/O emulsion was prepared by means of a homogeniser (Ultra Turrax®, model T25, IKA Works, USA) at 24,000 rpm for 5 min which ensured that the mean droplet size of inner oil droplets was about 0.5 μm (Vladisavljević & Schubert 2003). The W_1/O emulsion was injected through the membrane (pre-soaked in a proprietary wetting agent for at least 30 min to increase the hydrophilicity of the surface) using a peristaltic pump (Watson-Marlow-Bredel Pump 101U/R, Cornwall, UK) at the constant flow rate of 0.5–50 mL min^{-1}, corresponding to the dispersed phase fluxes of 30–3200 L m^{-2} h^{-1}. Rotation speed of the stirrer placed on top of the membrane ranged from 230 to 1330 rpm (equal to shear stresses between 1 to 18 Pa (Eq. (13)). The initial volume of the solution in the cell was 125 cm^3 and the experiments were typically run until the dispersed phase concentration reached 5 vol.%. Once the desired amount of oil had passed through the membrane, both the pump and the agitator were switched off and the droplets were collected and analyzed. The membrane was cleaned with 8 M NaOH in an ultrasonic bath for 5 min followed by treatment in 10 vol.% HCl solution for 5 min.

Table 7 Density and viscosity of aqueous surfactant solutions used in this work and equilibrium interfacial tension at oil/aqueous phase interface. O_1 – sunflower oil with 5 wt.% PGPR; O_2 – pumpkin seed oil with 5 wt.% PGPR; W – pure DI water.

Aqueous phase	Density (kg m^{-3})	Viscosity (mPa s)	Oil phase	Interfacial tension (mN m^{-1})
2 wt. % Tween	1000	1.01	O_2	1.5
2 wt. % Tween	1000	1.01	W/O_2	1.0
2 wt. % PVA in 2% Tween 20	1005	1.92	W/O_2	0.5
2 wt. % Pluronic F-68	1000	1.28	O_2	6.0

Aqueous phase	Density (kg m^{-3})	Viscosity (mPa s)	Oil phase	Interfacial tension (mN m^{-1})
2 wt. % Pluronic F-68	1000	1.28	W/O_2	3.7
2 wt. % Pluronic F-68	1000	1.28	O_2 + 5% PGPR	3.0
Demineralised water	997	0.891	O_2	11.0
Demineralised water	997		W/O_2	3.0
2 wt. % Tween	1000	1.01	O_1	5.0
2 wt. % Tween	1000	1.01	W/O_1	0.8
Demineralised water	997	0.891	O_1	22.0
Demineralised water	997	0.891	W/O_1	5.3

4.1.2.3 W/O emulsions

4.1.2.3.1 Preparation of silica particles.

The silica precursor was prepared by diluting sodium silicate solution (28 wt % SiO_2, 14 wt % Na_2O, Fisher Scientific UK) down to 10 or 15 wt % SiO_2 using Mili-Q water (18.2 MΩ cm). Once diluted the solution was stirred for 30 min. Due to the gelling, the sol had to be prepared prior to the experiment by adding the diluted sodium silicate, with 10 or 15 wt. % SiO_2, dropwise to 1 M H_2SO_4 (Fisher Scientific UK). Approximately 17 mL of diluted sodium silicate was added to 25 mL of H_2SO_4 under vigorous stirring until the desired pH was achieved. Formulation of the water phase is given in Figure 15.

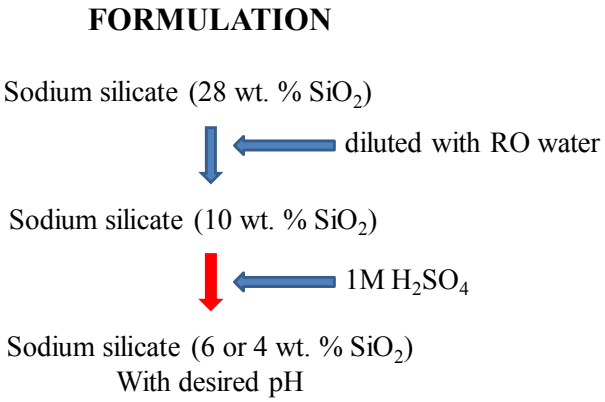

Figure 15 Formulation of the water phase (silica precursor) in W/O emulsions.

The gelling time is a function of pH, therefore, the right pH of the silicate solution after dilution with acid had to be selected. Condensation polymerization rate has a minimum at pH 2, at the isoelectric point (Iler 1979), and increases with increase of the pH. If the polymerization is too slow, the rate of particle growth is also slow and particles forming the gel will be small resulting in a more compact and microprous gel. To measure the gelling time of the solutions, 4 mL of the solutions with the pH of 1.5, 2.5, 3.5 and 4.5 were placed into plastic tubes and closed. The longest gelling time (longer than 24h) had a solution with pH of 1.5 while the solution with pH 4.5 gelled in 30 min. If the gelling time is long, droplet coalescence or breakage is more likely during the mixing stage. A pH of 3.5 was selected for most of the experiments, since it allowed the injection of up to 50 cm^3 of dispersed phase using the lowest flow rate used (1 mL min^{-1}) without fear of membrane blocking by the gelling solution. At this pH significant gelling did not take place until after 1 hour. Both sodium silicate and sulfuric acid were used without any purification.

The continuous phase was prepared by dissolving 5 wt% Span 80 in low odour kerosene (both supplied by Sigma Aldrich, UK). Span 80 was the emulsifier used to stabilise the aqueous sol droplets formed in the kerosene. The inlet hose was filled with the continuous phase prior to each experiment to ensure that the air was not entrapped within the oil phase. The cell was filled with 100 cm^3 of continuous phase and in most experiments 10 cm^3 of dispersed phase (silica precursor solution) was injected through the membrane pores using a Harvard Apparatus model 11 Plus syringe pump. After production, the silica droplets were transferred to a Teflon beaker and kerosene was added to dilute the volume concentration in order to minimise droplet coalescence.

Before the transition of the droplets into gel was complete the emulsion had to be subjected to continuous stirring to prevent settling and coalescence of the droplets. The stirring rate during gelling was found to be of great importance. If too high stirring was applied particles suffered attrition during solidification, therefore, 170 rpm was determined to be the most appropriate rate for the experiments: sufficient to keep the droplets suspended and separated, without causing shear deformation, or crushing, of the forming particles. When droplets of dispersed phase were initially injected into the kerosene solution it became milky white, and stirring was maintained until the kerosene solution became transparent again, and the hydrogel was formed. All the diluted solutions injected into the continuous phase were clear and transparent without any visible particulates, hence the milky colouration was believed to be due to water transport within the Span 80 stabilised continuous phase.

4.1.2.3.2 Washing of silica particles.

After the gelling, it was noticed that beside the spherical silica particles, needle shapes of silica were also created. So, to separate the spherical particles, a microfiltration cell was used (Figure 16). The microfiltration cell is the Dispersion Cell apart from the use of a slotted membrane attached at the bottom of the cell (Figure 16). The slotted membrane was provided by Micropore Technologies Ltd. Slots were 4 μm wide and 250 μm long meaning that even the smallest silica particles were maintained above the membrane. The advantage of the slotted membrane over a regular membrane is that the pores cannot be clogged with the small particles, as is the case with conventional membranes (Holdich *et al.* 2003; Yilmaz Ipek *et al.* 2007; Dragosavac, Holdich & Vladisavljević 2011). The silica particles were retained by the membrane while the needle-like material passed through the pores. All filtrate collected during the filtration was dried to identify the amount of silica lost as needles. No spherical particles were observed in the filtrate and the amount of needle-like silica in the filtrate was less than 2% of the total particle mass being filtered. In order to remove Span 80 and kerosene, from the particles, acetone washing was used. Once the kerosene was filtered off, the cell was partially filled with acetone and the spherical silica particles were washed with acetone. For filtrate removal a peristaltic pump (Watson-Marlow-Bredel Pump 101U/R, UK) was used which was operated at 0.1 mL min^{-1}. Each batch of spherical silica particles was continuously washed with at least 250 cm^3 of fresh acetone followed by

water washing. After washing the particles appeared fully white and looked to be surfactant free (if not washed in acetone they appeared yellowish). In order to be fully sure whether the particles are surfactant free the batch of particles produced using silica precursor solution of pH = 3.5 with the mean particle diameter of 40 μm was separated into two samples. One sample was only dried at the room temperature while the other sample was dried at the room temperature followed by calcining at 550^{o}C with a ramp step of 20^{o}C min^{-1} for 6 hours.

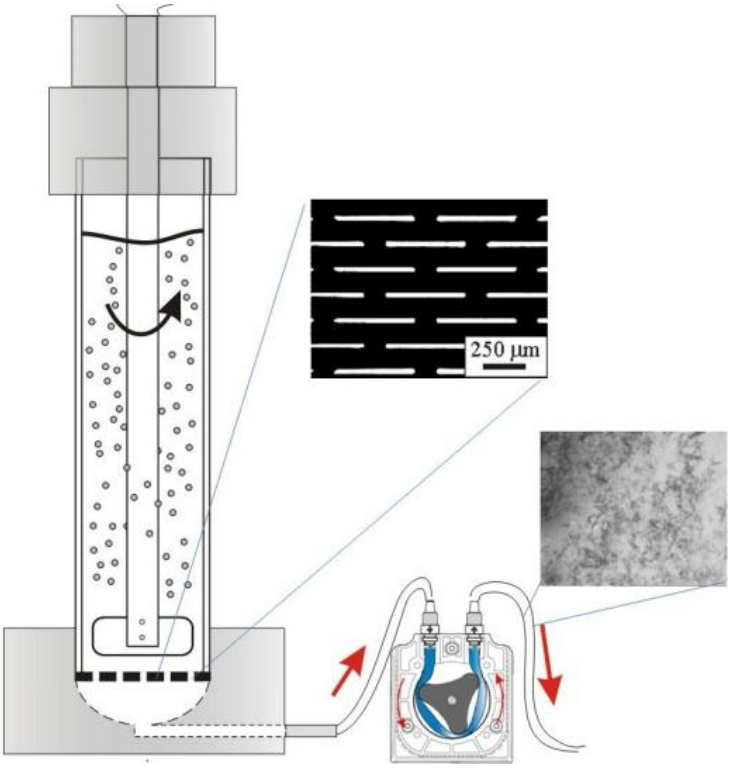

Figure 16 Schematic illustration of: microfiltration system together with slotted pore membrane and photomicrograph of the filtrate.

After drying both samples were analyzed using the BET surface analysis and EDX analysis. The non calcined sample had a specific surface area of 550 m^2 g^{-1}, total pore volume of 0.293 cm^3 g^{-1} and average pore radius of 1.1 nm (according to the BJH method (Barret, Joyner & Halenda 1951). Once the sample was calcined the specific surface area increased to 785 m^2 g^{-1}, total pore volume increased to 0.453 cm^3 g^{-1} while the average pore radius was 1.3 nm. The analysis showed that even the particles appeared to be white the surfactant was not fully removed from the pores. BET analysis for calcined and non-calcined silica particles are presented in Figure 17 and it can be seen that the samples are different. EDX analysis (Figure 18) confirmed the non-

calcined particles had carbon molecules present on the surface of the samples. Therefore it was decided that the particles, after washing in acetone and drying at the room temperature, should be calcined in order to complete the removal of the surfactant, and kerosene, from the surface of the particles.

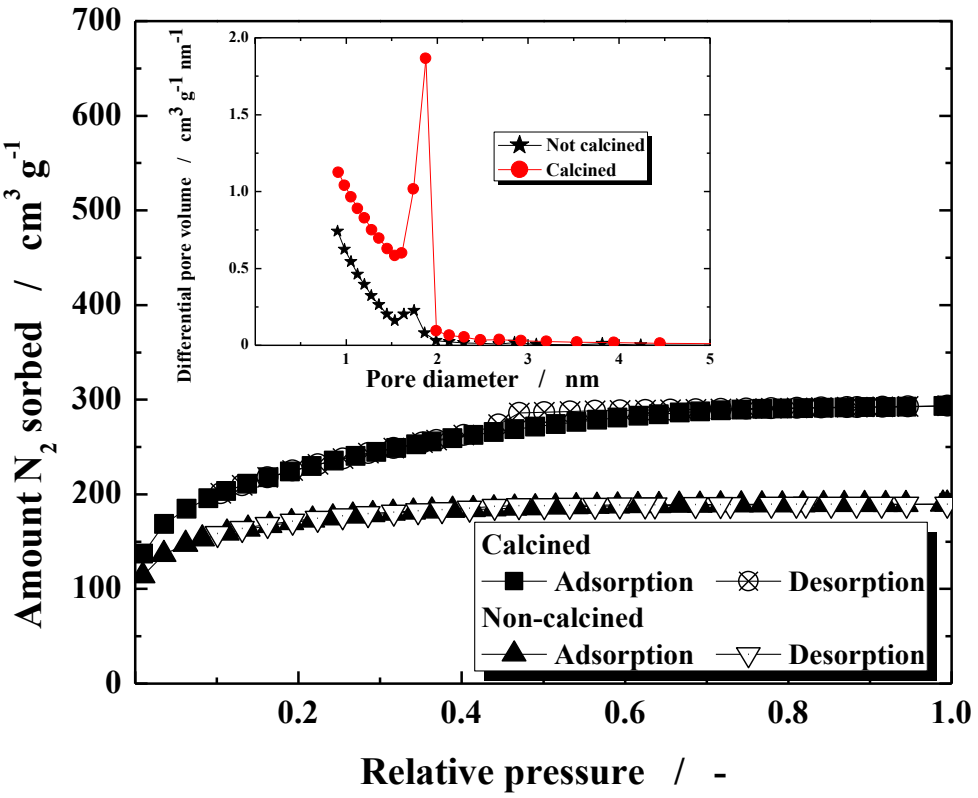

Figure 17 BET nitrogen sorption–desorption isotherm of silica particles (calcined and not calcined) with an average size of 40 μm. Both samples were washed with acetone and water and dried from water at a room temperature. Inset graph represents pore size distribution calculated using BJH method (Barret, Joyner & Halenda 1951) according to the desorption isotherm both for calcined and non-calcined silica particles.

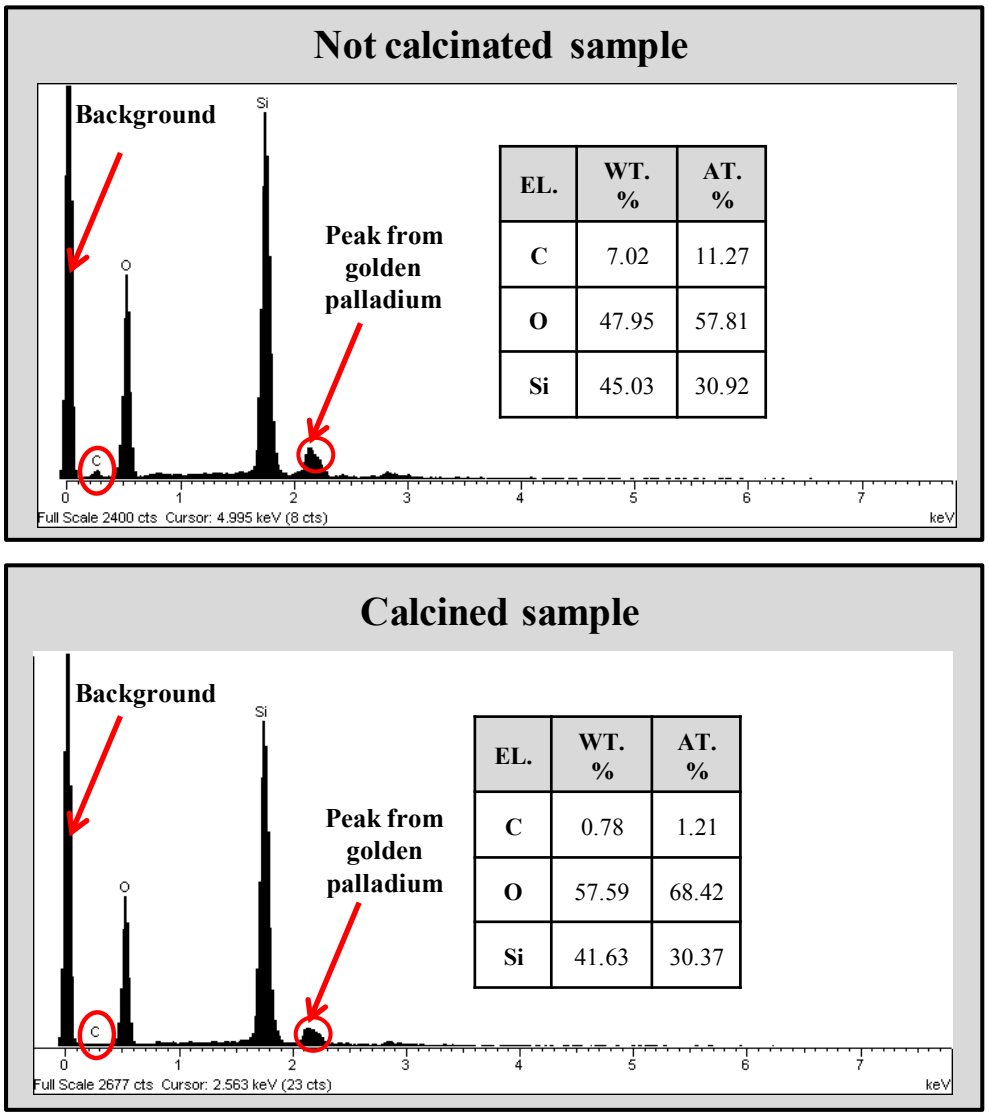

Figure 18 The Energy Dispersive Spectrum (EDS) of both calcined and non-calcined silica particles with average size of 40 µm.

4.1.2.3.3 Fuctionalization of the silica particles

There are numerous ways that the silica surface can be functionalized by immobilization of organofunctional groups for the sorption of the heavy metals from the water solutions (Jal, Patel & Mishra 2004). 3-aminopropyltrimethoxysilane has been reported in literature as effective silica surface modifier which enables removal of heavy metals from water solutions (Ozmen *et al.* 2009, Walcarius, Etienne & Bessière 2002, Manu, Mody & Bajaj 2010, Blitz *et al.* 2007). To functionalize the silica particles we followed the procedure given in previous papers. 3-aminopropyltrimethoxysilane was used here to utilize produced silica particles. 10 g of silica particles, with a specific

surface area of 360 $m^2 g^{-1}$ was first washed with a mixture of nitric and hydrochloric acid in a ratio of 1:3 for 2 h in order to remove possible metal impurities. The particles were then filtered, dried in a vacuum at 420 K, and refluxed in a mixture of 80 cm^3 of toluene and 10 cm^3 of 3-aminopropyltrimethoxysilane for 24 h (Figure 19).

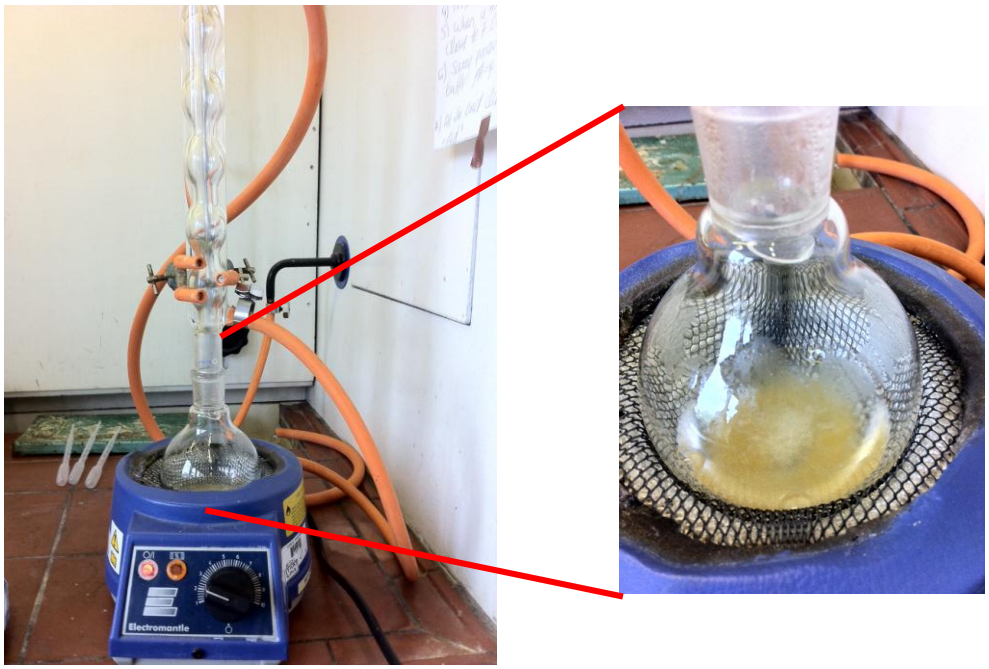

Figure 19 Refluxing of silica particles.

After refluxing, the particles were collected by filtration, washed with ethanol and then transferred to a Soxhlet extractor (Figure 20) and washed with toluene for 24 h, to eliminate possible traces of 3-aminopropyltrimethoxysilane and were dried at room temperature. After production functionalized silica particles were tested for sorption of copper ions from water solution (see Chapter 4.5.1.1.4).

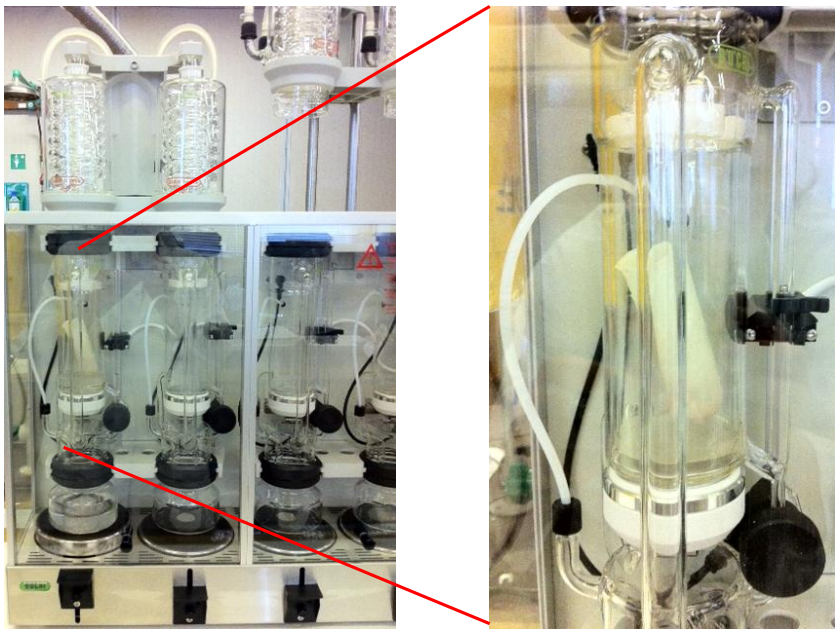

Figure 20 Toluene washing for 24h to remove 3-aminopropyltrimethoxysilane.

4.2 OSCILLATION MEMBRANE SYSTEM

4.2.1 Module and membranes (with experimental procedure)

The dispersed phase for the oil in water emulsions was commercially available food grade sunflower oil. The continuous phase was purified water (obtained from a reverse osmosis system) containing 2 wt.% Tween 20 surfactant (polysorbate 20 or polyoxyethylene sorbitan monolaurate) obtained from Sigma Aldrich.

The Oscillating system used to produce the suflower oil in water emulsions is presented in Figure 21 and was supplied by Micropore Technologies Ltd. For the Oscillating system a hydrophilic nickel membrane was in the form of the candle (Figure 21), with an external diameter of 15 mm and working length of 57 mm. Pore size was 10 μm and the pore spacing was 200 μm. At the bottom end of the membrane a stainless steel cap sealed off the membrane tube, and the cap had a pointed end to reduce turbulence during oscillation. At the top of the membrane candle there was a 1/8 inch BSP fitting to enable the candle to be attached to the injection manifold, to which an accelerometer was fixed. The injection manifold had internal drillings to allow the passage of the oil phase to be injected, which was provided by a syringe pump (Harvard Apparatus 11 Plus). The accelerometer (PCB Piezotronics model M352C65) was connected to a National Instruments Analogue to Digital converter (NI eDAQ-9172) which was

interfaced to a LabView executable program running on a PC. The information provided by the program from the accelerometer was the frequency and amplitude of the oscillation: the frequency being determined by the direction of travel, and the amplitude was deduced from the acceleration measurement. The oscillation signal was provided by an audio generator (Rapid Electronics), which fed a power amplifier driving the electro-mechanical oscillator on which the inlet manifold was mounted. Frequencies were in range between 10 and 90 Hz while the amplitude ranged between 0.1 and 6.5 mm. Before each experiment, it was important to ensure that no air gaps or bubbles were entrapped within the oil phase. For that reason the membrane was immersed into the continuous phase and the continuous phase was sucked into the membrane and injection manifold with syringes. When air was completely removed, the injection tube was attached to the pump and the oil phase was introduced very slowly to the membrane. Oscillation did not start unless the oil phase emerged on the membrane surface in order to prevent premixing within the membrane. In each experiment the volume of the continuous phase was 200 cm^3 which allowed the membrane to be fully covered with continuous phase even when highest amplitude (6.5 mm) was used.

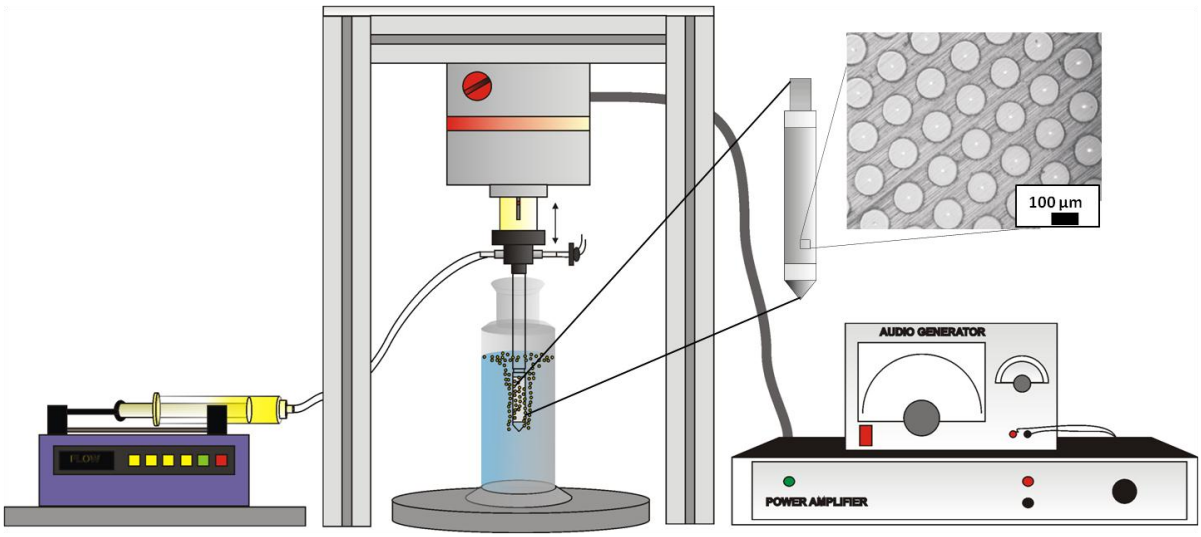

Figure 21 Schematic illustration of the Oscillating membrane system together with the candle membrane (External diameter 15 mm and working length 57 mm. Pore size 10 µm and the pore spacing 200 µm).

4.3 PULSATING SYSTEM

4.3.1 Module and membranes (with experimental procedure)

As a dispersed phase for the oil in water emulsions food grade sunflower oil was used. The continuous phase was purified water containing 2 wt.% Tween 20 surfactant (polysorbate 20 or polyoxyethylene sorbitan monolaurate) obtained from Sigma Aldrich. The Pulsating system was also tested for complex coacervation and for those experiments the dispersed phase was 10 wt.% peppermint oil dissolved in a commercially available food grade sunflower oil, while the continuous phase was mixture of gelatin and gum arabic at 40^{o}C with pH = 3.8 which was adjusted by lactic acid.

The membrane used was in the shape of a tube (Figure 22(a)) with the outer diameter of 20 mm and working length of 70 or 170 mm. For injecting both the dispersed (Figure 22 (e)) and continuous phase (Figure 22 (f)) peristaltic pumps were used. There was no recirculation of the continuous phase and the entire product was collected in the stirred tank (Figure 22 (d)) where the emulsion was slowly agitated in order to prevent coalescence. It is important to ensure that no air remains entrapped in the system since it can cause a production of small air bubbles which can favour the coalescence of oil droplets. To prevent the presence of air within the system both outer and inner sides of the membrane were filled with the continuous phase prior to the experiment and all the air was released through the purging valve (Figure 22 (c)). An accelerometer (PCB Piezotronics model M352C65) was connected to a National Instruments Analogue to Digital converter (NI eDAQ-9172) which was interfaced to a LabView executable program running on a PC. The information provided by the program from the accelerometer was the frequency and amplitude of the oscillation: the frequency being determined by the direction of travel, and the amplitude was deduced from the acceleration measurement.

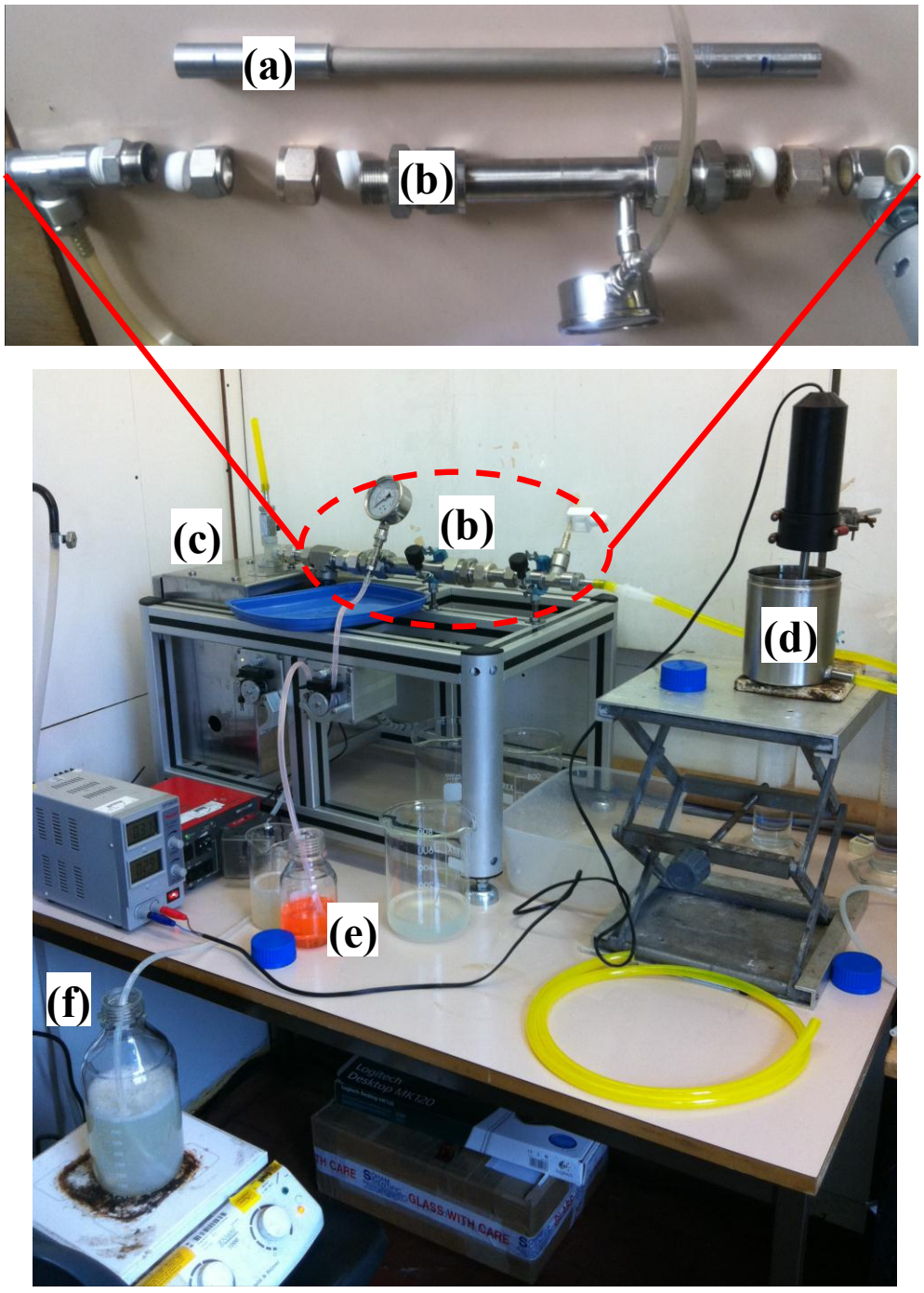

Figure 22 Photograph of the Pulsating membrane system (b-f) together with the tubular membrane (a) (External diameter 15 mm and working length 170 mm. Pore size 20 µm and the pore spacing 200 µm). Setup for the complex coacervation.

The oscillation signal was provided by National Instrument frequency generator, which fed a power amplifier driving the electro-mechanical oscillator which was connected to a bellows designed for use in a diaphragm pump, which was submerged in the

continuous phase – hence its oscillation provided a pulsation. Frequencies were in range between 8 and 100 Hz while the amplitude ranged between 0.25 and 5 mm. Compared to the Oscillating system where the membrane was moving, in the Pulsating system the membrane was fixed still and the continuous phase was pulsed. The drop generation within the Pulsating system is presented in Figure 23.

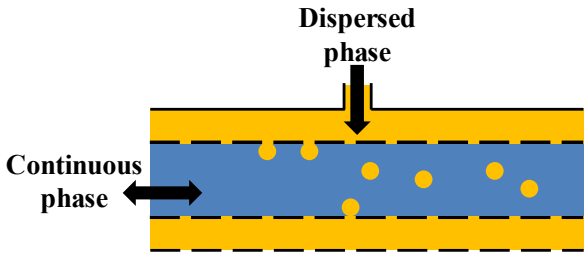

Figure 23 Droplet generation in Pulsating system.

4.4 MEMBRANE CLEANING

All the membranes used were nickel membranes but shaped differently (disk, candle or tube). The cleaning procedure depended on which type of emulsion was being produced W/O or O/W requiring a hydrophilic or hydrophobic membrane, respectively. The cleaning procedure is presented in Figure 24.

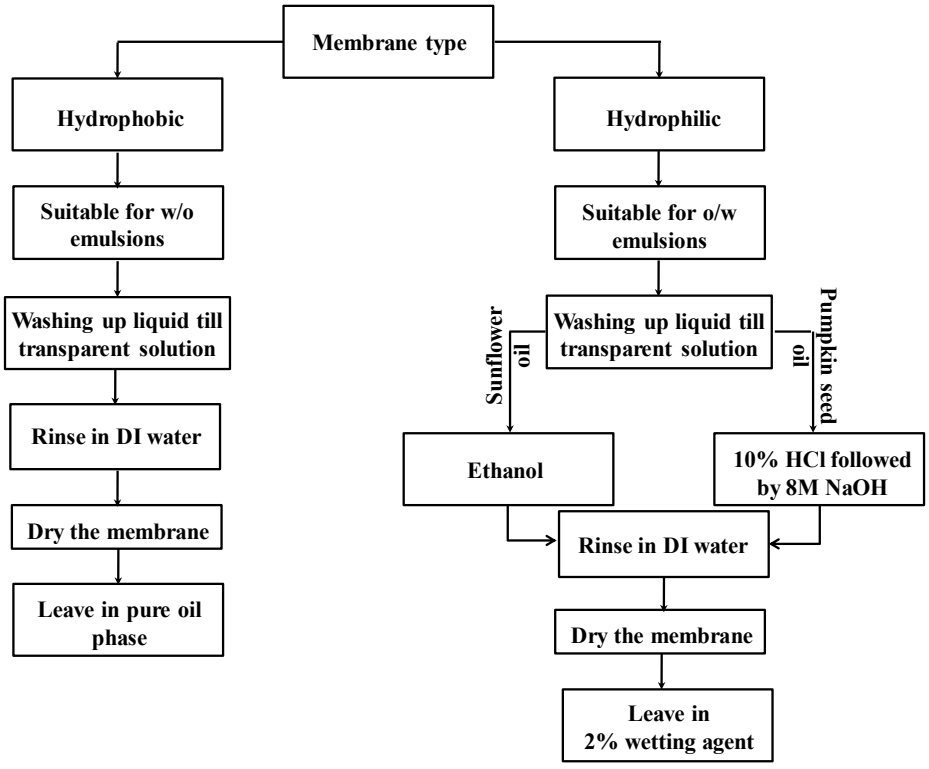

Figure 24 Membrane cleaning procedure.

4.5 ION EXCHANGE

4.5.1 Development of the technique to determine mass transfer and equilibrium data using the stirred cell with continuous flow

4.5.1.1 Materials and methods

4.5.1.1.1 Liquid phase

All the chemicals used were of analytical grade, supplied by Sigma Aldrich, UK. The solutions of copper ions were prepared by dissolving appropriate amounts of $Cu(NO_3)_2.6H_2O$ in deionised water. The copper concentration used in the feed solution with the continuous flow experiments was in the range between 19 and 636 g m^{-3} while for the batch experiments it was in the range between 10 and 11300 g m^{-3}. The ionic strength in the liquid phase was adjusted by $NaNO_3$ and kept at 0.2M, unless stated differently. The pH was kept constant at 4.5 ± 0.1 by adjustment using 0.4M NaOH and was measured directly in the cell using a pH meter (PW9420 Philips, UK). The pH adjustment was needed only at the very beginning of the experiment, when the resin swapped hydrogen form to the sodium form because of the high content of sodium ions present in the solution. This is a rapid process (Morig, Gopala Rao 1965), and the time taken was neglected from subsequent kinetic modelling.

4.5.1.1.2 Ion Exchange Resin (Dowex 50W-X8)

Two different sizes of ion exchange resin beads Dowex 50W-X8 (100-200 and 200-400 mesh) were obtained from Sigma Aldrich. Dowex 50W-X8 is a strong acid cation polystyrene resin containing 8% divinylbenzene. The size distribution of Dowex resin particles was determined by a laser diffraction particle size analyser (Malvern Mastersizer S, UK). The cumulative size distribution curves for both sizes of Dowex 50W-X8 particles are presented in Figure 25(a) while microscopic photographs of the resin particles are shown in Figure 25(b). The particle size range of Dowex 50W-X8 particles with 100-200 and 200-400 mesh was 101-679 and 34-517 μm, respectively. Probably, the diameters larger than those stated by the manufacturer are a consequence of the resin swelling. The Sauter mean radius of Dowex 50W-X8 particles with 100-

200 and 200-400 mesh was 87 and 42 μm, respectively (3 independent samples were analysed and a mean value is calculated). These Sauter mean radii were used in Eqs. 31, 36, 38 and 40 for the prediction of copper concentration in the effluent.

(a)

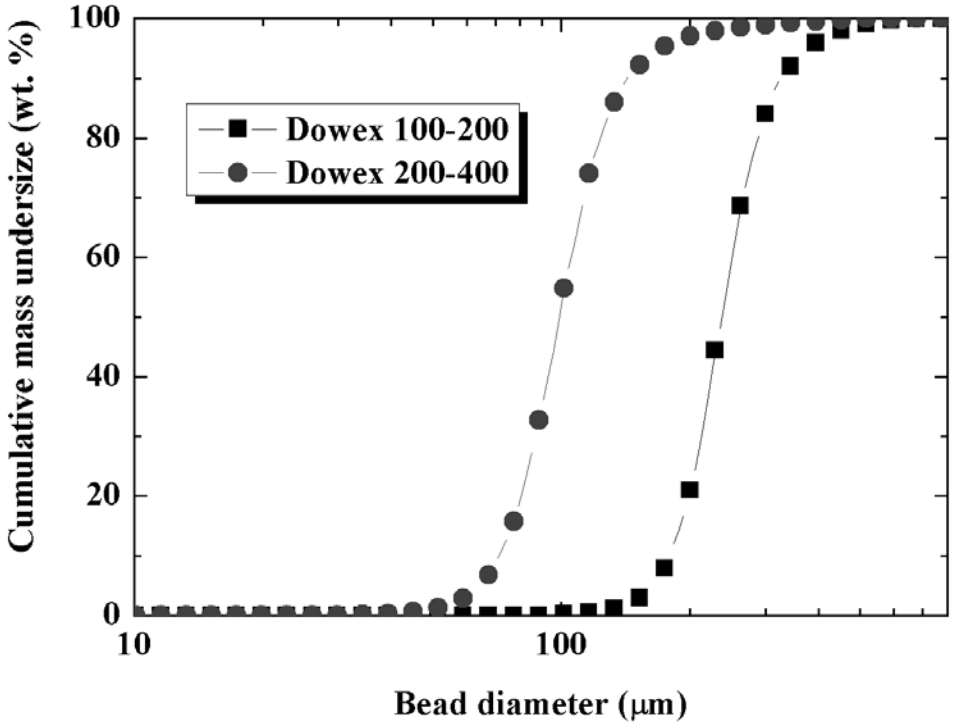

(b)

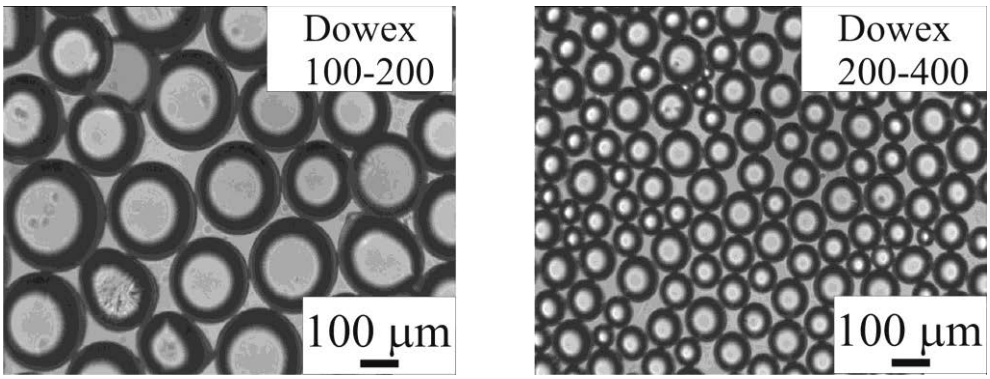

Figure 25 (a) Cumulative distribution curves of Dowex 50W-X8 particles. (b) Microscopic photographs of dry resins.

Prior to each use the ion exchange resin was soaked for about 1 h in deionised water to swell. Most of the water was then removed from the resin by decanting and the resin was washed several times with 1 M HNO_3 followed by washing with deionised water.

The remaining amount of water was removed by placing the ion exchange resin in a vacuum drier at 50°C overnight and kept in a desiccator before use. In all experiments 1g of resin (dry mass) was used.

4.5.1.1.3 Batch sorption experiments

The batch sorption experiments were carried out in a series of flasks containing different initial copper (II) concentration in the liquid phase (Figure 26). In Table 8 the content of each flask is presented. In all the solutions the pH and ionic strength were kept constant. After equilibration (the flasks were sealed and left to shake for one month at the room temperature), the liquid phase was separated from the solid phase and analysed. This represents the conventional approach to the determination of sorption equilibrium isotherm. The equilibrium sorption capacity was calculated using the following mass balance equation:

$$q_e = \frac{(C_{oi} - C_{eq})V}{m} \qquad \textbf{Eq. 45}$$

where q_e is the equilibrium sorption capacity, C_{oi} and C_{eq} are the initial and final concentration of copper (II) in the liquid phase, respectively, V is the volume of the liquid phase, and m is the mass of dry resin used. A control experiment with copper (II) solution in the absence of any resin confirmed that there was no copper sorption onto the walls of a flask.

Figure 26 Equipment for batch sorption experiment (shaker).

Table 8 Content of each flask for batch experiments (sorption of copper ions on Dowex 50W-X8).

Flask	V / m^3	m / kg	C_o / g m^{-3}	$C_{o,Na}$ / g m^{-3}
1	0.05	0.001	11300	3790
2	0.08	0.005	870	3760
3	0.08	0.005	430	3680
4	0.08	0.005	230	3670
5	0.08	0.005	120	3780
6	0.08	0.005	70	3680
7	0.08	0.005	35	3800
8	0.08	0.005	20	3650
9	0.08	0.005	10	3770

4.5.1.1.4 Continuous flow experiments (combined micro filtration and sorption or "seeded microfiltration")

All continuous flow experiments were carried out at room temperature in a microfiltration cell (Figure 27(a)) provided by Micropore Technologies Ltd, Loughborough, UK. Fresh copper solution was continuously delivered to the cell from a feed tank by a peristaltic pump (Watson-Marlow Ltd, UK). In all experiments the liquid phase flow rate was constant at 7.8 mL min^{-1} (1.3×10^{-7} m^3 s^{-1}). A two blade paddle stirrer attached to the laboratory power supply (Instek Laboratory DC, UK) provided agitation in the cell at a constant speed of 270 rpm. In all experiments the volume of the liquid phase in the cell was 140 mL. A slotted-pore metal membrane (Figure 27(b)) with an effective diameter of 3.2 cm was fitted to the bottom of the cell. The pore width and length was 8 and 400 μm, respectively. This pore width was fine enough to keep even the smallest resin particles in the cell. As shown in Figure 25(a), the smallest particle size for Dowex 50W-X8 200-400 was 34 μm.

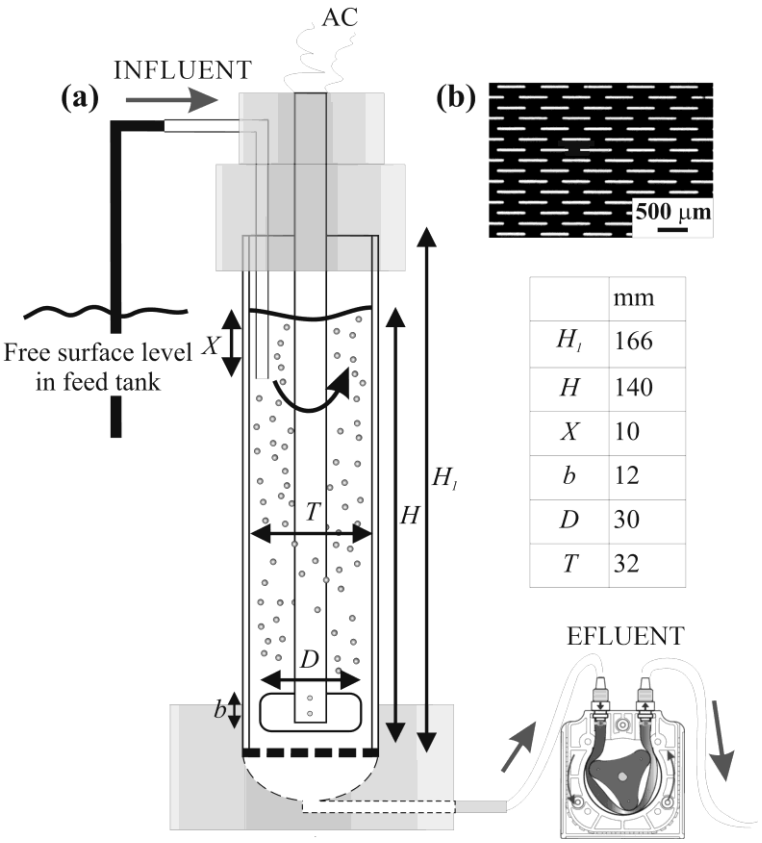

	mm
H_l	166
H	140
X	10
b	12
D	30
T	32

Figure 27 (a) Schematic diagram and geometry of seeded microfiltration system; (b) Microphotograph of the slotted pore membrane used in this work.

For the tests, the cell was filled with a pure buffer solution (0.2 M $NaNO_3$) and fresh wetted resin was added to the cell. Before immersion in the buffer solution the tube from the feed tank was filled with the feed copper solution and clamped. The clamp on the tubing was released after starting the pump. At predetermined times 10 mL of effluent samples were collected and at the end of the experiment all samples were analysed as described in following Chapter 4.5.1.1.5. In all experiments the pH of the liquid phase was maintained constant at 4.5 but this was needed only at the very beginning of the experiment.

Figure 28 compares the Cu(II) concentrations in the effluent when the inlet tube was only 40 mm above the membrane surface (the tube immersion depth X = 100 mm) and when the tube immersion depth was 10 mm in the absence of any resin in the cell. When the immersion depth was 100 mm the experimental response curve exceeds the model prediction for ideal continuous stirred tank (CST) indicating that bypassing occurred in the cell. When the immersion depth was 10 mm corresponding to the optimal position of the inlet tube the experimental curve matches very well the model

prediction for ideal CST and this immersion depth was kept in all future continuous flow experiments.

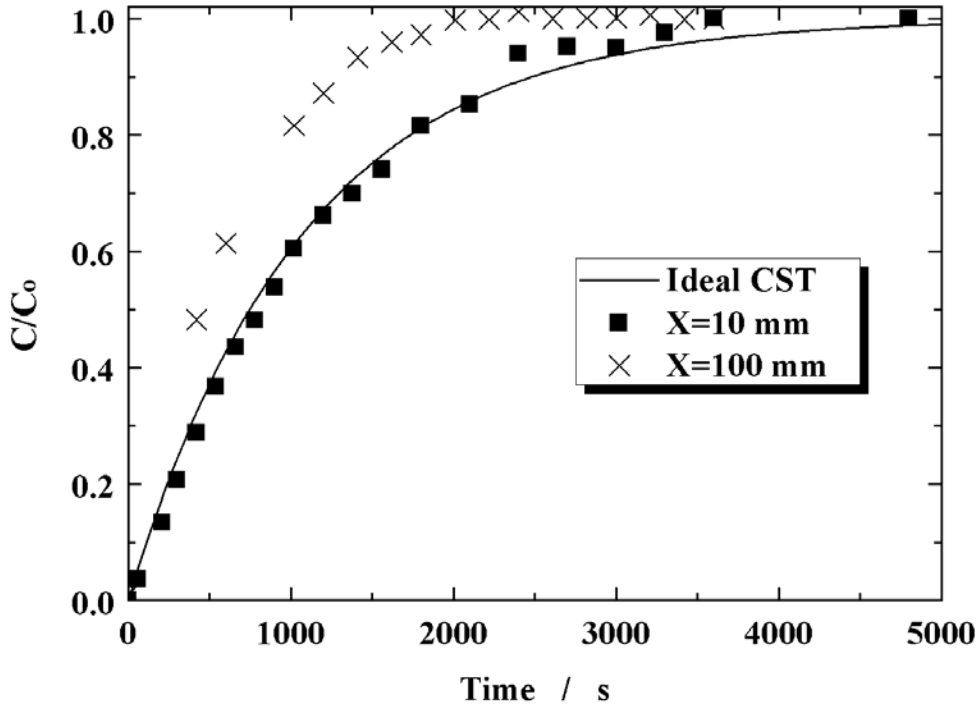

Figure 28 Influence of positioning the inlet tube in the cell. No ion exchange resin in the cell. Inlet copper concentration C_o = 78 ppm, Flow rate F=1.3×10^{-7} m^3 s^{-1}. (×) inlet tube immersed to deep in the cell X = 100 mm; (■) inlet tube immersed X = 10 mm from the liquid level in the cell.

4.5.1.1.5 Analytical procedure

The copper and sodium concentrations in the samples were determined using an Atomic Absorbance Spectrophotometer (AAS) (Spectra AA-200 Varian, UK) operating at a wavelength of 244.2 nm for copper and 330.2 nm for sodium. Calibration was performed before each experiment. The samples were analysed automatically based on the calibration curve and the mean value of 3 independent samples was used. More information on the experimental procedure using the Atomic Absorbance Spectrophotometer is given at Appendix A.

4.5.2 Determining mass transfer kinetics and equilibrium data for copper hydroxide acetate using "seeded microfiltration"

4.5.2.1 Materials and methods

4.5.2.1.1 Liquid phase

The solutions of iodide ions were prepared by dissolving appropriate amounts of KI (supplied by Sigma Aldrich, UK) in deionised water. The iodide concentration used in the feed solution for continuous flow experiments was in the range between 250 and 2000 g m^{-3} while for the batch experiments was in the range between 250 and 9000 g m^{-3}. The ionic strength was not adjusted and the pH of the solutions was 6.3.

4.5.2.1.2 Ion Exchange Resin (Copper hydroxide acetate)

Copper hydroxide acetate $Cu_2(OH)_3(CH_3COO)H_2O$ is produced by titration of the $Cu(CH_3COO)_2$ with NaOH (Butterworth *et al.* 2010) and represents one of the fundamental compounds from the family of the $M_2(OH)_3X$ Layered Hydroxide Salts (LHSs), where X is an exchangeable anion (e.g. NO^{3-}, CH_3COO^-,Cl^-, SO_4^{2-}, RSO_2O^-) and M is a transition metal (II) cation (e.g. Cu, Co, Ni, Mn, Zn).

If LHS is synthesized using large exchangeable anions such as acetate they are less stable and prone to anion exchange with smaller species. In copper hydroxide acetate the acetate anion is held electrostatically within the layers and a water molecule is bonded directly to the copper cation (Figure 29). This results in a much larger gallery spacing of ~9.3Å that in theory is more susceptible to exchange with smaller anions (Butterworth *et al.* 2010). It is the gallery spacing that governs which anions from the solution will be exchanged with the acetate anion.

The copper hydroxide acetate used in this thesis was produced by Andrew Butterworth (Chemistry Department, Loughborough University) and was given in order to determine the exchange capacity and mass transfer properties of the sample. Microscopic photographs of the copper hydroxide acetate particles are shown in Figure 30 and the cumulative size distribution curve for copper hydroxide acetate particles is presented in Figure 31.

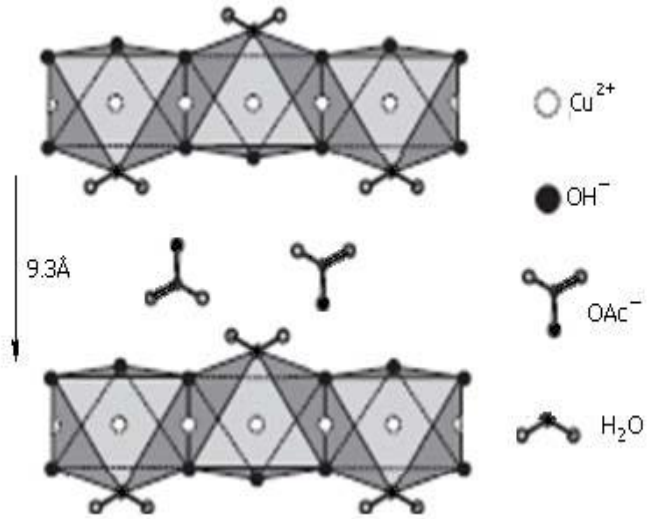

Figure 29 The structure of copper hydroxide acetate (Butterworth *et al.* 2010).

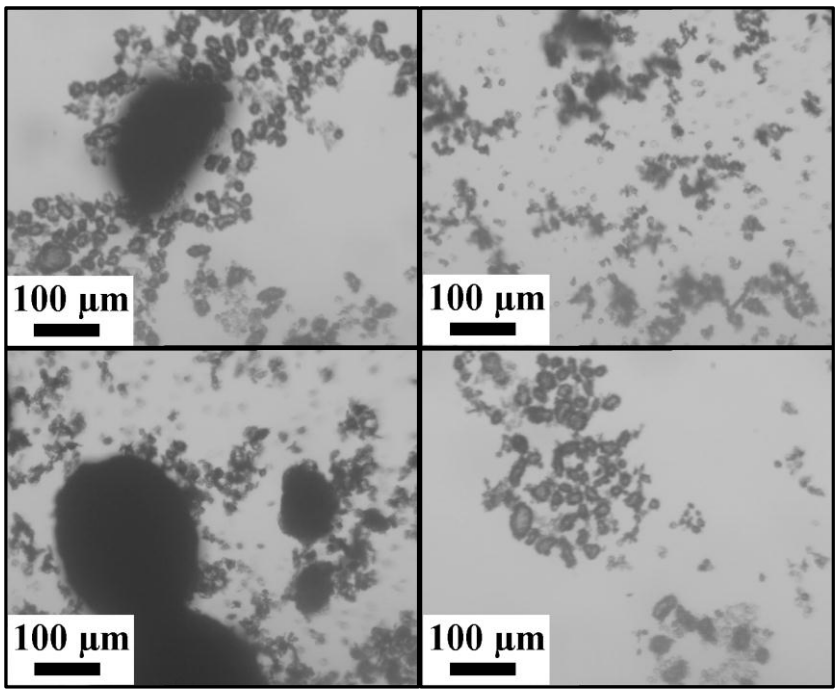

Figure 30 Four different microphotographs of the copper hydroxide acetate particles dispersed in water.

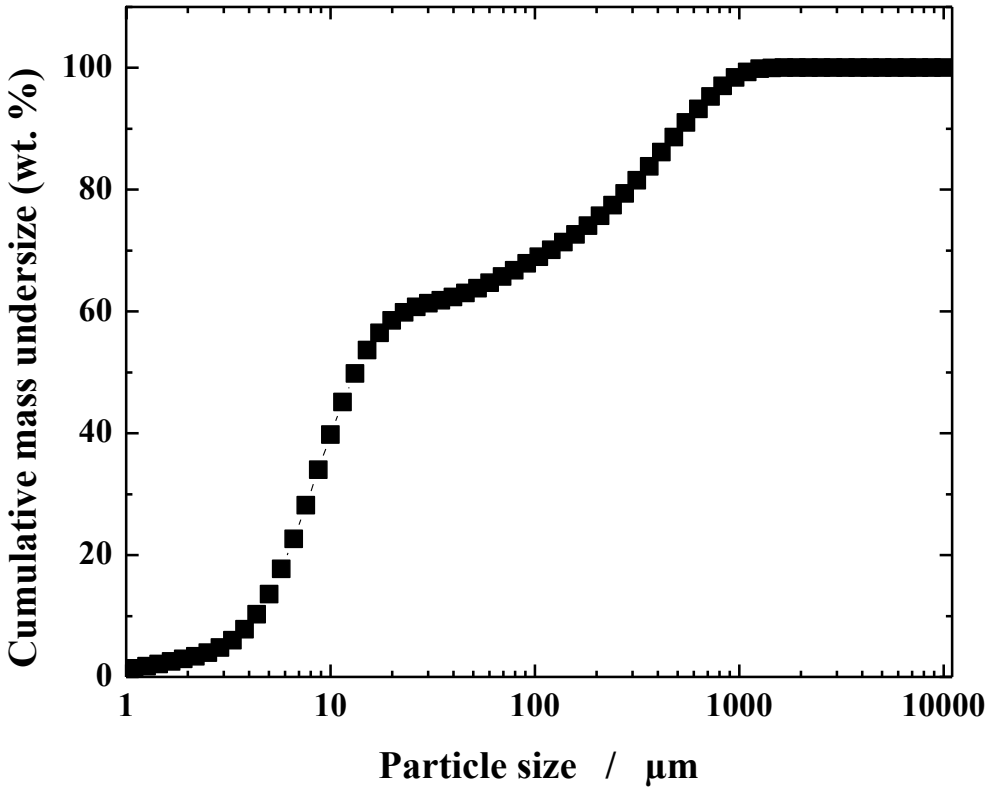

Figure 31 Cumulative distribution curve of the copper hydroxide acetate particles dispersed in water.

The Sauter mean diameter of the copper hydroxide acetate particles was 10 μm, (3 independent samples were analysed and a mean value is calculated). This Sauter mean radius was used in Eqs. (31), (36), (38) and (40) to predict the iodide concentration in effluent.

4.5.2.1.3 Batch sorption and continuous flow experiments

The batch sorption experiments were carried out in series of flasks containing different initial iodide concentration (C_o) in the liquid phase. In Table 9 content of each flask is presented. In all the solutions the pH was 6.3.

After equilibration (the flasks were sealed and left to shake for one month at the room temperature), the liquid phase was separated from the solid phase and analyzed. This represents the conventional approach to the determination of sorption equilibrium isotherm. The equilibrium sorption capacity was calculated using the following mass balance Eq. (45).

Table 9 Contents of each flask for batch experiments (sorption of iodide ions on copper hydroxide acetate)

Flask	$V\ 10^3$ (m^3)	$m\ 10^3$ (kg)	C_o (g m^{-3})
1	0.1	5	9000
2	0.1	5	4500
3	0.1	5	2000
4	0.1	5	1500
5	0.1	5	250

Continuous flow experiments were done as described in Chapter 4.5.1.1.4. The only change was that the cellulose nitrate membrane (Whatman, with average pore size 0.45 μm) was added on top of the metal membrane to prevent the loss of particles smaller than the membrane slots. Prior to use the cellulose nitrate membrane was wetted using ethanol. Flux was monitored during the experiments and no significant decay was observed. At predetermined times 10 mL of effluent samples were collected and at the end of the experiment all samples were analysed using an iodide selective electrode. For each sample the iodide concentration was measured 3 times and average value is reported.

5. RESULTS

5.1 MEMBRANE EMULSIFICATION

5.1.1 Dispersion cell

5.1.1.1 O/W emulsion

Figure 32 compares the results from the Dispersion Cell system, i.e. the stationary membrane with rotating paddle stirrer to create the shear (Figure 14), with the three models: (A) which uses peak (maximal) shear in the force balance equation; (B) which uses average shear in the force balance and (C) which employs peak or average shear, but also takes into account the neck formation of the droplet at the pore opening. It is clear that the experimental data is very close to the model based on average shear. During these experiments the oil flux rate was very low, at 30 L m^{-2} h^{-1}, so that any effect due to droplet "push-off" was minimised and drop growth before detachment was also low. The droplet size is influenced by the injection rate of the phase being dispersed (Egidi *et al.* 2008): increasing injection rate giving increasing droplet size. Hence, for these tests the injection rate was kept very low to minimise these effects, so that the influence of shear on the droplet detachment could be investigated for the paddle stirred system.

It appears that the average shear model works better in the paddle stirred system, where the droplets are detached by shear only in one direction and if formation of the neck is taken into consideration the experimental data match almost perfectly with the model. The span of the droplet size distribution in the Dispersion Cell is given in Figure 33 and in most of the cases was around 0.56, but it is obvious that under the conditions of too high shear (12 Pa) span increased which can be attributed to the droplet break up due to the too high stirring speed.

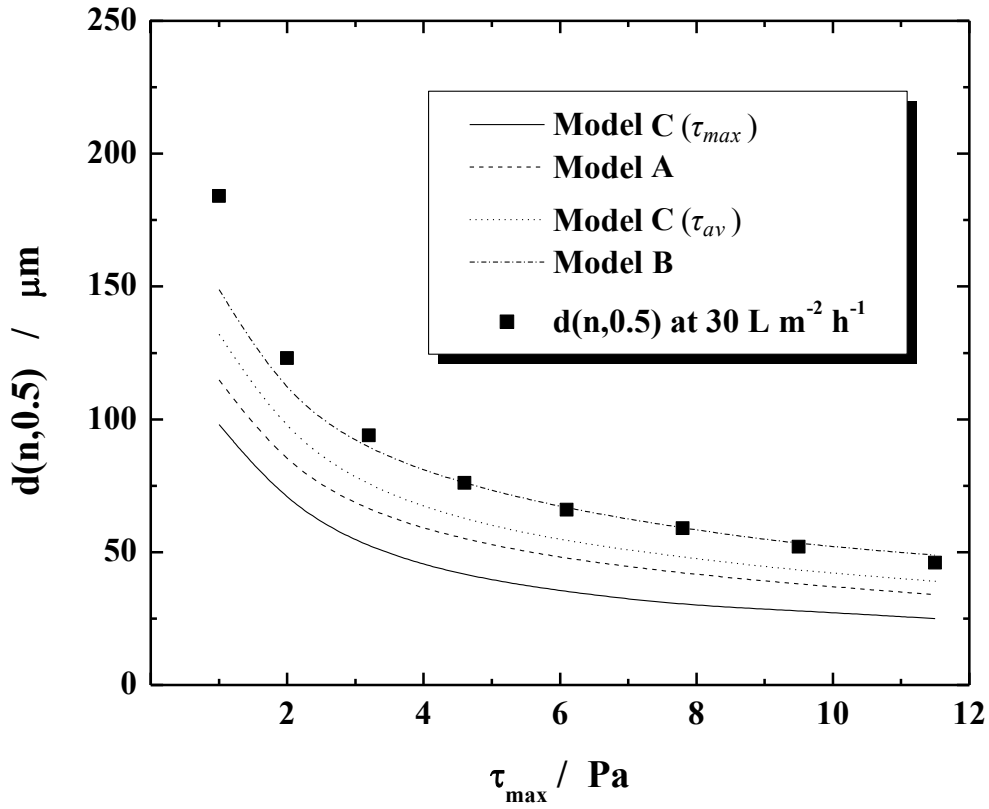

Figure 32 Comparison of experimental droplet diameters produced in Dispersion Cell and predicted values calculated using different models: the values of *d(n,0.5)* were obtained at 30 L m^{-2} h^{-1} and Model C uses Eqs. (17)-(20) and Eq. (8) with either τ_{max}, or τ_{av}, Model B is based on Eqs. (10) and (16) ($\tau = \tau_{av}$) and Model A uses Eqs. (10) and (13) ($\tau = \tau_{max}$). Dispersed phase: sunflower oil.

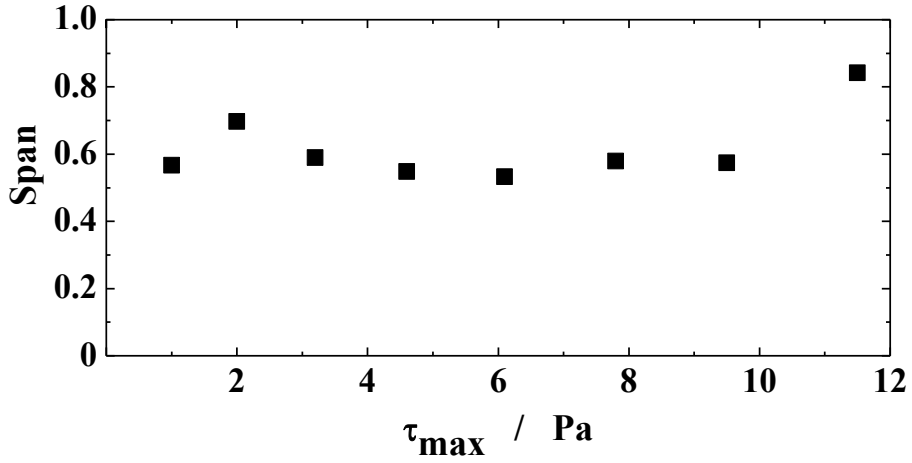

Figure 33 Span of particle size distribution as a function of a shear stress.

5.1.1.2 W/O/W emulsion

5.1.1.2.1 Influence of pore size and dispersed phase flux

Figure 34 shows the effect of dispersed phase flux on the droplet size for four different rotational speeds using the 20 μm membrane with 200 μm pore spacing. With increasing transmembrane flux up to 2000 L m^{-2} h^{-1} increasing droplet diameter is observed. Further increase over 2000 L m^{-2} h^{-1}, as can be seen from Figure 34, had an insignificant effect on the droplet size which remained almost constant for all rotation speeds. Such insignificant influence of the transmembrane flux at higher values of transmembrane flux was observed in the previous study of O/W emulsions (Dragosavac *et al.* 2008). Droplets produced at high rotation speed (high shear stress) had smaller droplet diameter than the ones produced at low rotation speed (low shear stress) which is in agreement with the literature (Nakashima, Shimizu & Kukizaki 1991, Dragosavac *et al.* 2008, Vladisavljević & Schubert 2003, Kosvintsev *et al.* 2005 and Egidi et.at 2008). The membrane used had 200 μm pore spacing and therefore it is expected that droplet sizes above 200 μm would require significant droplet deforming to take place. As can be seen from Figure 34 in the case when rotation speed was 230 rpm droplets greater than 300 μm were formed. At low rotation speed, droplet formation time is longer and therefore the droplet produced at those conditions will have a bigger diameter. At the same time, if droplet detachment time is considered as a constant (Xu *et al.* 2005), an increase in flux will increase the droplet size. Even at high transmembrane fluxes it is reported that not all pores of a membrane are active (Vladisavljević & Schubert 2002), providing more space for droplets to grow on the membrane. From Figure 34 it can be seen that at the lowest rotation speed (230 rpm) droplets were in the range between 300 and 422 μm.

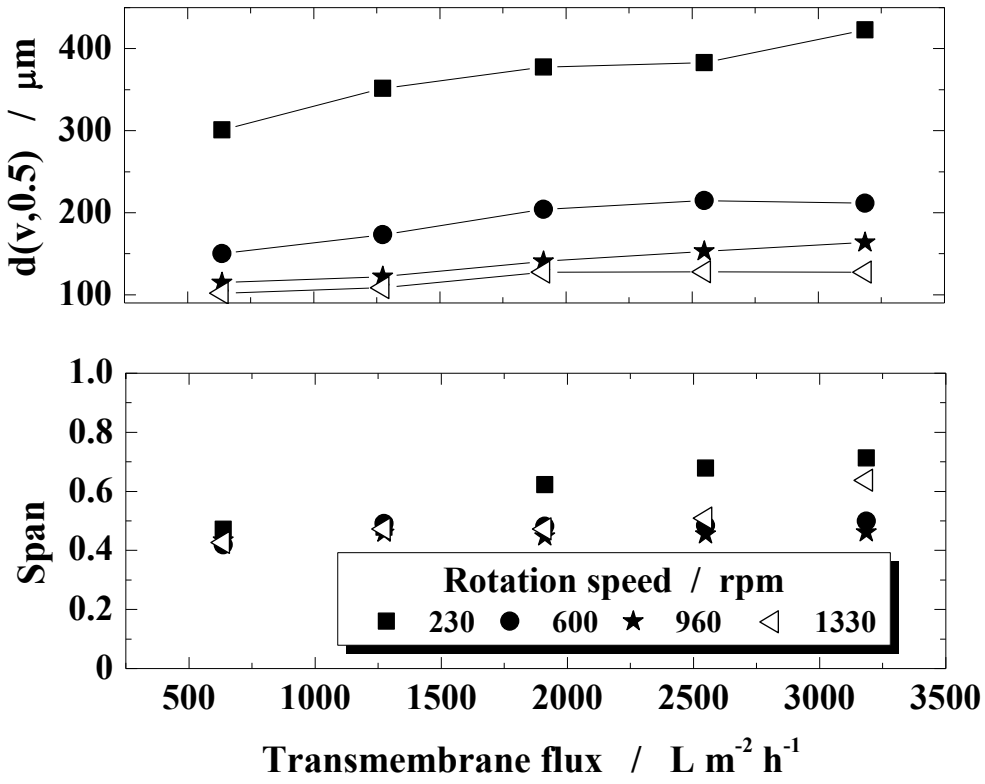

Figure 34 Variation of volume median diameter and span of particle size distribution with dispersed phase flux for the membrane with 20 µm pore size. (Disperse phase: water-in-pumpkin seed oil, continuous phase: 2% Tween 20).

Figure 34 shows that uniform droplets with span values less than 0.5 were obtained for almost all fluxes except the extreme cases of very low, and very high, rotation speed and high transmembrane flux. Another combination that also did not give droplets with narrow size distribution was high rotation speed with high transmembrane flux. Increase of the span from 0.5 to 0.63 with an increase of rotation speed from 960 to 1330 rpm could be consequence of partial droplet break up into smaller daughter droplets under the influence of high shear forces (Vladisavljević &Williams 2005).

Previous work using a membrane with much smaller inter-pore spacing (Egidi *et al.* 2008) suggests that there may be a "push-off" force that has an effect on droplet growth, and the span may decrease with increasing transmembrane flux. In this investigation using a much larger pore spacing such behaviour was not observed.

The influence of pore size on droplet diameter was also investigated since it is another important parameter that affects the droplet size. The effect of pore size on the mean

droplet size is not so pronounced than when the multiple emulsions were produced (Dragosavac *et al.* 2008). Figure 35 shows the results obtained with multiple emulsions containing sunflower oil and pumpkin seed oil at high transmembrane flux. As can be seen there is no significant difference between 10 and 20 μm membrane, and 30 and 40 μm membrane therefore 20 and 40 μm membranes were chosen for further investigations.

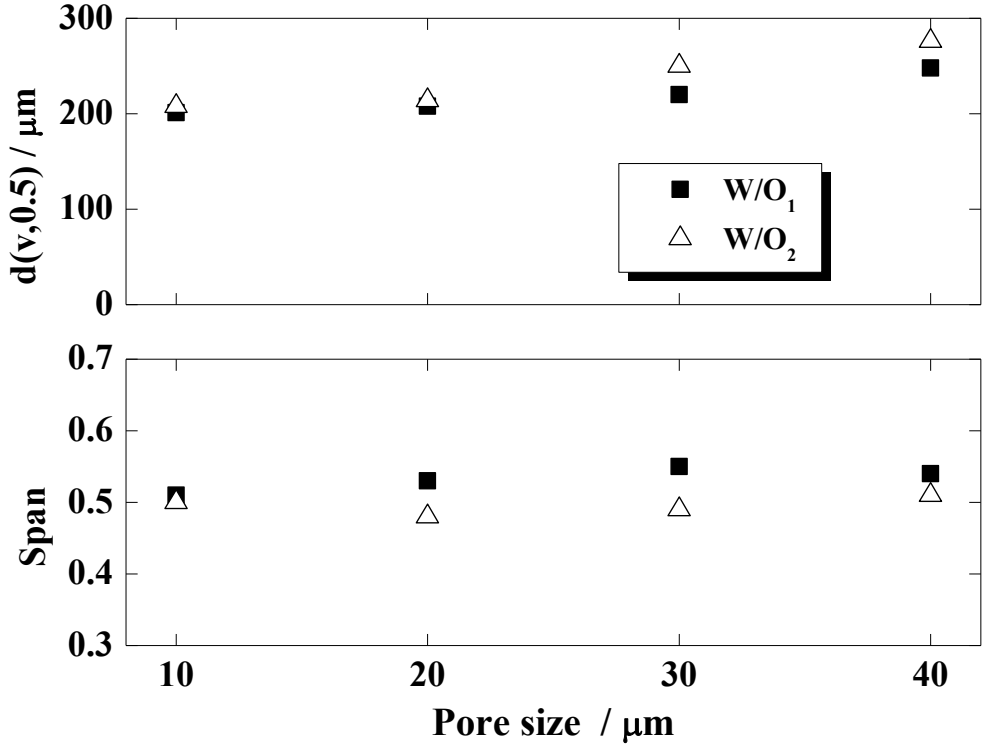

Figure 35 Variation of volume median diameter and span of particle size distribution for different membrane pore size and oil type. (Transmembrane flux = 2550 L $m^{-2}h^{-1}$, rotation speed = 600 rpm, continuous phase: 2% Tween 20). O_1-sunflower oil, O_2-pumpkin seed oil (both oils had 5 wt.% PGPR).

The limited variation of droplet size with membrane pore size is surprising and may be due to the nature of the membrane: each pore opening is set slightly below the surface of the membrane, by about 8 μm. This recess is of little consequence for the 20 μm (and larger) sizes, but is strongly significant for the 10 μm pore opening. Hence, if the dispersed phase can partially wet the membrane surface the droplets will spread slightly wider than the pore opening prior to the detachment.

Figure 36 compares 20 and 40 μm membrane. When 40 μm membrane was used droplets ~1.3 times bigger were produced. Larger droplet diameter in the case of

W/O/W emulsion using sunflower oil compared to pumpkin seed oil can be explained by a higher interfacial tension (Table 7).

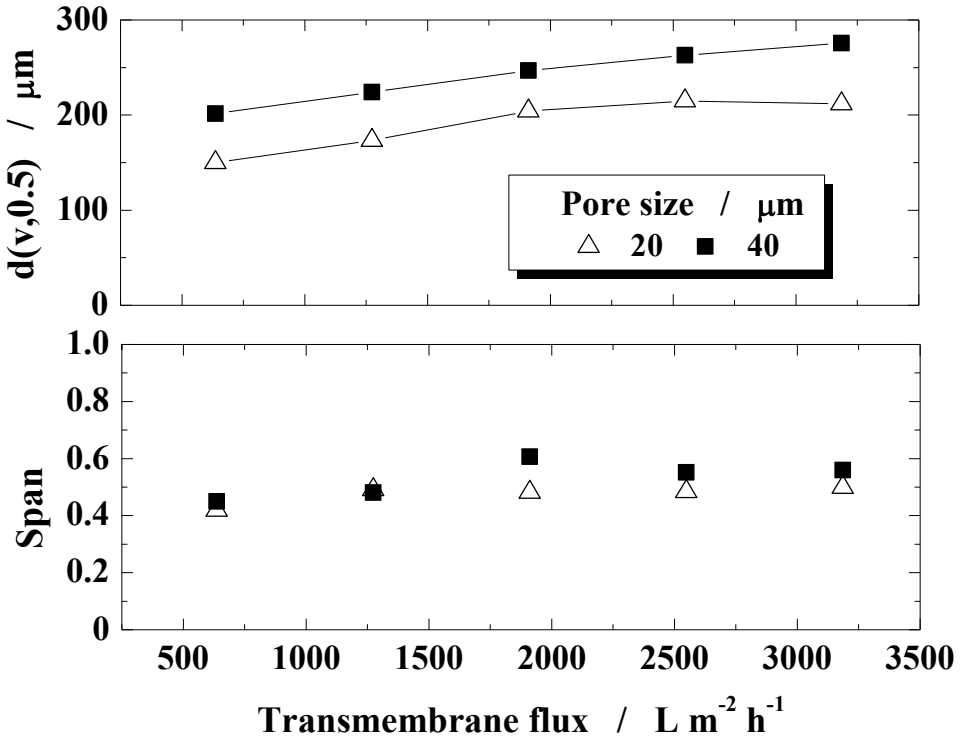

Figure 36 Variation of volume median diameter and span of particle size distribution with dispersed phase flux and pore size. (**Disperse phase: water-in-pumpkin seed oil**, rotation speed = 600 rpm, continuous phase: 2% Tween 20).

In this work a maximum transmembrane flux of 3200 L m^{-2} h^{-1} was achieved, and the lowest span was 0.46 when the stirrer had a rotation speed of 960 rpm. For comparison, in repeated premix emulsification using a 10.7 µm tortuous SPG membrane a maximum flux of 230 m^3 m^{-2} h^{-1} was reached with a span of 0.34, but several passes through the membrane were employed (Vladisavljević, Shimizu & Nakashima 2006).

5.1.1.2.2 Influence of dispersed phase

Figure 37 presents experimental results for production of single emulsions at a deliberately low transmembrane flux (30 L m^{-2} h^{-1}). When low transmembrane flux is used ―push-off" force (Egidi *et al.* 2008), which may influence the droplet size, can be neglected. As presented in Figure 37, the mean particle size increased with increasing mean pore size of the membrane. However, the ratio of mean particle size to the mean

pore size decreased with increasing the pore size. The mean pore size varied from 10 to 40 μm, the ratio $d(v,0.5)/d_p$ was in the range from 8.1 to 3.8 for sunflower oil and from 8.7 to 4.1 for pumpkin seed oil. In direct SPG membrane emulsification, $d(v,0.5)/d_p$ is normally 3.1–3.7 (Vladisavljević, Shimizu & Nakashima 2006b).

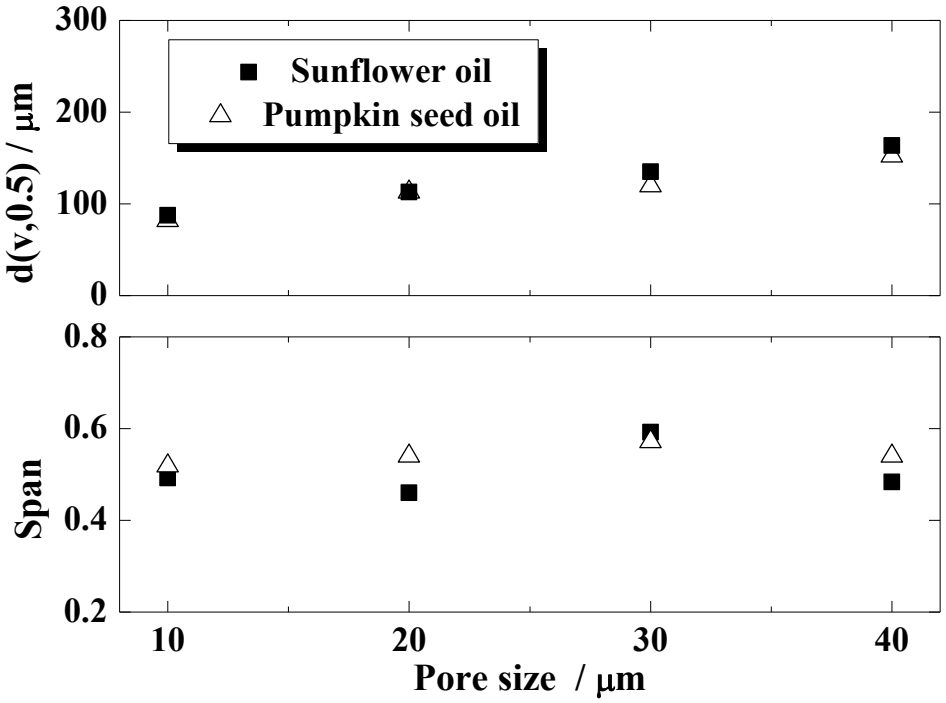

Figure 37 Variation of volume median diameter and span of particle size distribution for different membrane pore size and oil type. (Transmembrane flux = 30 L m^{-2} h^{-1}, rotation speed = 600 rpm, continuous phase: 2% Tween 20, **dispersed phase: pure oil**).

When single emulsions were produced at low transmembrane flux (30 L m^{-2} h^{-1}) and 600 rpm there was almost no difference between droplets of emulsions from sunflower, or pumpkin seed oil. The droplet diameters were in range between 80 and 160 μm and the span did not exceeded 0.6. At low transmembrane flux, and constant droplet detachment time, the droplets formed are smaller due to the smaller amount of dispersed phase that comes out from the pore before the droplet is quickly detached from the membrane surface. Such conditions prevail as long as the membrane does not become wetted with oil phase.

The same set of experiments was repeated but instead of pure oil phase the dispersed phase was W/O emulsion (Figure 38). As the mean pore size varied from 10 to 40 μm,

the ratio $d(v,0.5)/d_p$ was in the range from 6 to 7.9 for $W/O_1/W$ emulsion and from 7.8 to 25 for $W/O_2/W$ emulsion. At the same time, broader distributions were obtained at 30 L m^{-2} h^{-1} both for sunflower oil and pumpkin seed oil. When sunflower oil was used, the span was in a range between 0.91 (using a 10 μm membrane) and 0.74 (using 40 μm). On the other hand, when pumpkin seed oil was used the span was in a range between 1.51 (using 10 μm) and 1.47 (using 40 μm). The W/O/W emulsions have much lower interfacial tension than O/W emulsions (Table 7) hence the droplets produced would be expected to be smaller than for a single emulsion. On the contrary, experimental results show that the droplet size increased when multiple emulsions are produced. Droplet size for $W/O_1/W$ ranged from 59 to 275 μm while for $W/O_2/W$ droplets these were between 232 and 311 μm at 30 L m^{-2} h^{-1}. Such behaviour can be explained by looking at the composition of the emulsions: a significant additional compound in the formulation of W/O/W emulsions is PGPR (5%), an emulsifier added to the oil phase in order to stabilize the inner water droplets. If the membrane surface is ideally covered by a hydrophilic layer the oil droplet is limited to only the region around the pore opening, as reported by Christov *et al.* (2002) and the droplet formed on the pore would have a small diameter. When the oil phase has internally dissolved emulsifier, in this case PGPR which is a lipophilic emulsifier with hydrophilic head and hydrophobic tail, the process of droplet growth is different. During growth of the oil droplet at the pore surface, molecules of PGPR may orient toward the hydrophilic membrane thus expanding the contact line of the droplet/membrane over a larger surface. As the droplet grows larger, a larger area is occupied. Since the pore spacing is sufficient, the droplet is formed not just from one pore, but from a hydrophobised domain created due to interactions of PGPR molecules with the membrane. If droplets of single emulsions (W/O_1) and multiple emulsion ($W/O_1/W$) using sunflower oil are compared (Figure 37 and Figure 38) droplets of multiple emulsion are larger and less uniform.

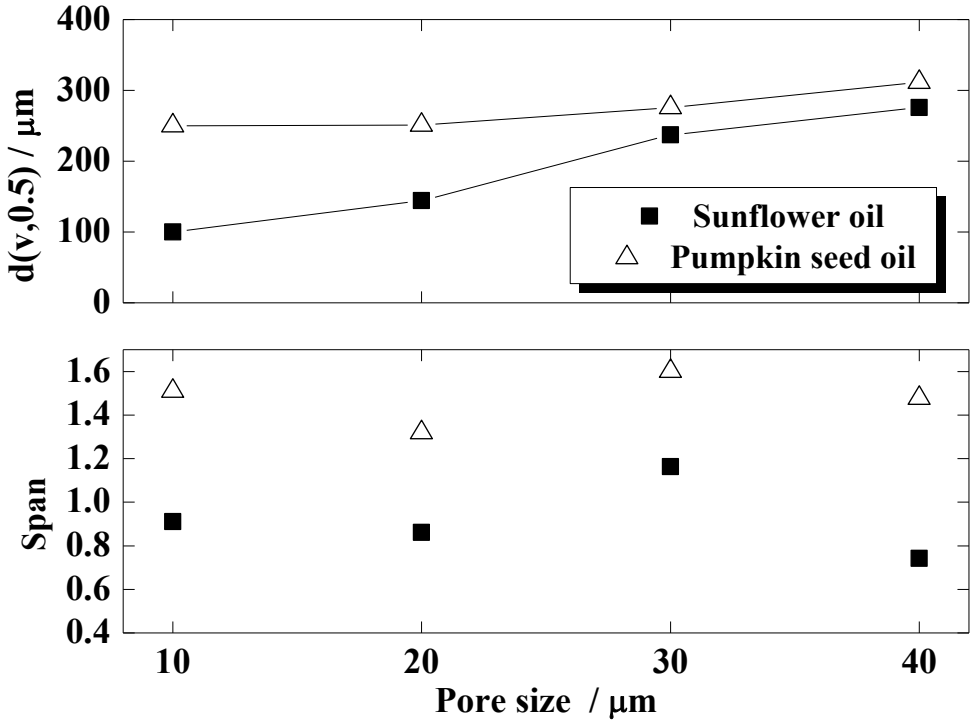

Figure 38 Variation of volume median diameter and span of particle size distribution for different membrane pore size and oil type. (Transmembrane flux = 30 L m^{-2} h^{-1}, rotation speed = 600 rpm, continuous phase: 2% Tween 20, dispersed phase: water-in-oil emulsion).

Unrefined pumpkin seed oil is rich in many compounds that can be sorbed on the membrane surface, such as free fatty acids, minerals, phospholipids, chlorophyll, and aromatic components (Murkovic *et al.* 2004). The sorption of these components as well as molecules of PGPR on the membrane surface may lead to partial membrane wetting by the oil phase. Hence, droplets of multiple emulsions using pumpkin seed oil ($W/O_2/W$) are larger than ones obtained from sunflower oil.

5.1.1.2.3 Influence of emulsifier

Ideally, the emulsifier molecules should not sorb to the membrane surface electrostaticaly. Such interactions could cause alteration of the membrane surface from hydrophilic to hydrophobic (Tong *et al.* 2000). Therefore, Tween 20 and Pluronic F68 were used as water soluble surfactants, as they are both nonionic surfactants with no affinity to sorb to the membrane surface.

In order to determine the effect of internal water phase and effect of PGPR molecules on the membrane surface and the droplet size four different tests were performed using a new membrane with 15 μm pores and 200 μm pore spacing, and the results are presented in Figure 39. After each experiment the membrane was ultrasonicated for 5 min in NaOH, then dried, followed by ultrasonication for 5 min in 10% HCl and dried again. After washing in the base and acid the membrane was left in the wetting agent for 1h. In all experiments 2% Pluronic F68 was used as the continuous phase.

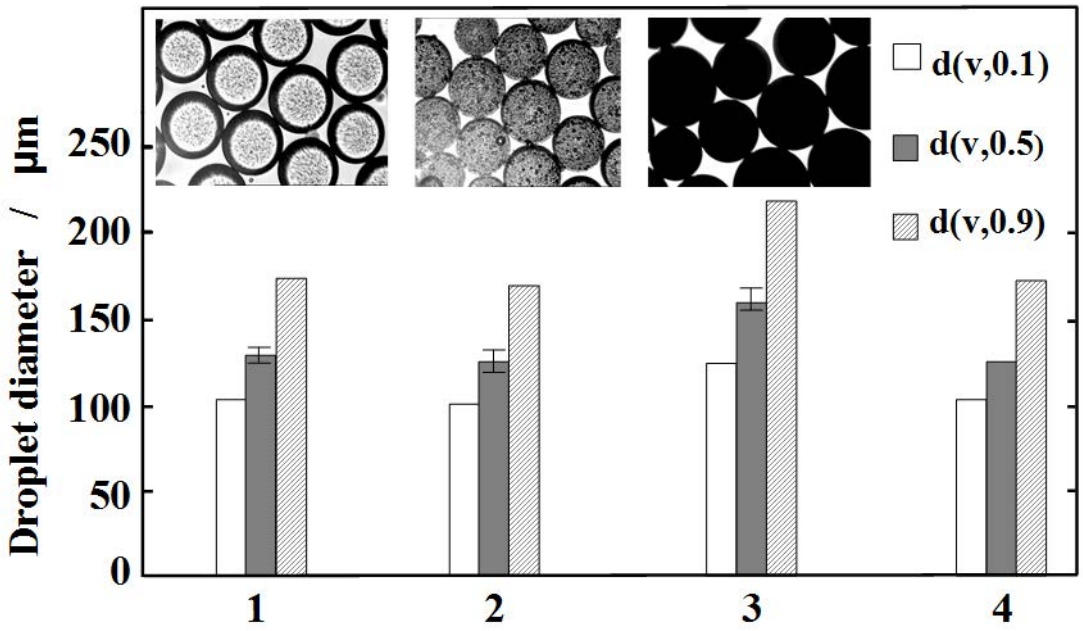

Figure 39 Effect of PGPR and internal water phase on the droplet size and appearance in 4 consecutive sets of experiments with the same membrane. Disperse phase: 1: Pure pumpkin seed oil (O_2); 2: 5% PGPR dissolved in pumpkin seed oil; 3: W/O_2 emulsion with 30% water phase and 5% PGPR in pumpkin seed oil, and 4: Experiment with pure pumpkin seed oil performed after previous experiments. Pore size = 15 μm, pores spacing = 200 μm, transmembrane flux = 640 L m^{-2} h^{-1}, rotation speed = 600 rpm, continuous phase: 2% Pluronic F68.

In the first experiment pure pumpkin seed oil was used as the dispersed phase. The experiment was repeated three times and the average value for *d(v,0.5)* is presented (the error bars indicate the highest and the lowest values obtained). *d(v,0.1)* and *d(v,0.9)* are presented for information. The average droplet size produced using the new membrane was 124 μm and the repeatability of the experiment was good (Figure 39). The first

photomicrograph presented in Figure 39 (top left corner) with almost transparent droplets corresponds to the pure pumpkin seed oil injected into the continuous phase. In the second experiment 5% of PGPR was dissolved in the oil phase (oil with PGPR was heated up to 50^{o}C and left overnight to be mixed), but no internal water phase was present. Again experiments were repeated three times, and the average value is presented for *d(v,0.5)*, and the error bars indicate the highest and the lowest values obtained. The average droplet size when the PGPR was dissolved in oil was 126 μm. Comparing the droplet sizes with, and without, PGPR almost no difference was observed. Interfacial tension of pure pumpkin seed oil is twice that when PGPR is dissolved (Table 7) and smaller droplets would, therefore, be expected when PGPR is present in the oil phase. As can be seen from Figure 39 almost the same droplet size was obtained with and without PGPR. The same droplet size indicates that the PGPR molecules may wet the membrane but not significantly since the uniformity of the droplets did not deteriorate. The third experiment involved the use of an inner water phase. Again three experiments were conducted, the average value for *d(v,0.5)* is reported and the error bars present the highest and the lowest values obtained. From Figure 39 it can be seen that the droplet size increases by approximately 20 μm. Such increase clearly shows that the presence of the internal water phase, together with PGPR molecules, wet the membrane resulting in the increase of droplet size. A question arose as to whether the molecules of PGPR sorb on the membrane surface irreversibly. In the final experiment the pure pumpkin seed oil was used again as dispersed phase. As it can be seen from Figure 39 the droplet size was no different from the first experiment showing that the cleaning of the membrane was efficient and that PGPR molecules were successfully removed by it. At the same time, the reproducibility of all experiments shows that the period for which the membrane was left in the wetting agent (1 h) was sufficient for the molecules of the wetting agent (used to increase the hydrophilicity of the membrane) to sorb onto the membrane surface.

When single emulsions were produced (Dragosavac *et al.* 2008) different hydrophilic surfactants were successfully used to regulate the droplet size. Figure 40 shows the influence of surfactant in the continuous phase on droplet size and droplet uniformity with increasing transmembrane flux while a rotation speed of the stirrer was 600 rpm. As reported earlier, Pluronic F68 was successfully used as an emulsifier for single emulsions (Dragosavac *et al.* 2008, Wulff-Pérez *et al.* 2009) so it was investigated here

as a stabilizer for the droplets of multiple emulsions. As can be seen when 2% Tween 20 was used with increasing transmembrane flux from 640 to 3200 L m^{-2} h^{-1} the droplet diameter increased from 150 to 211 µm, and span in all cases did not exceeded 0.5. Using 2% Pluronic F68 for the same operating conditions the droplet diameter increased and was between 235 and 303 µm while span increased, but was in most experiments less than 0.5. Figure 40 shows that droplet size can be regulated using different surfactants. The biggest droplets were obtained with Pluronic F68 as emulsifier, a consequence of the higher interfacial tension (Table 7).

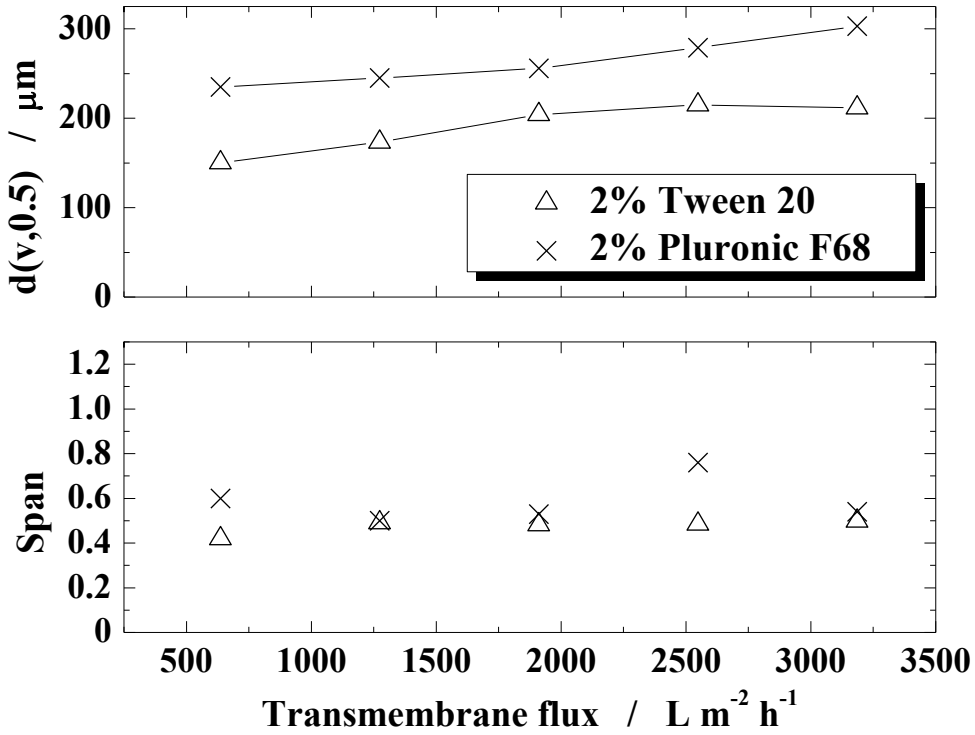

Figure 40 Variation of volume median diameter and span of particle size distribution with dispersed phase flux for 2% surfactant solutions (disperse phase: water-in-pumpkin seed oil, pore size = 20 µm, rotation speed = 600 rpm).

As a rule, the faster the emulsifier molecules sorb to the newly formed droplet surface, the smaller the mean droplet size of the resultant emulsion will be. The effective diffusion coefficient of Pluronic F68 is reported as 1.9×10^{-11} m^2 s^{-1} (Soong *et al.* 2010) while for Tween 20 Luschtinetz and Dosche (2009) reported a value of 7.7×10^{-11} m^2 s^{-1}. Since the loading of the interface with surfactant is directly proportional to the effective diffusion coefficient (van der Graaf *et al.* 2004), it will take longer for Pluronic F68 molecules to stabilise the forming oil droplet which may also explain the larger

diameters presented in Figure 40 and the slightly poorer span values. With increase of transmembrane flux from 2550 L m^{-2} h^{-1} to 3200 L m^{-2} h^{-1}, when the continuous phase included 2% Pluronic F68, droplet size increased from 279 to 303 μm but the span reduced from 0.76 to 0.54. Since the pore spacing of the membrane was 200 μm, then the ‘push-off’ force may be beginning to have an effect. However, the peristaltic pump capacity did not permit the testing of higher flow rates.

An increase in the viscosity of the continuous phase often increases the stability and shelf life of multiple emulsions. Therefore, 2% PVA was added to the continuous phase. The viscosity doubled (Table 7), and the increase of viscosity should lead to a decrease in the droplet size. As can be seen from Figure 41, with the addition of PVA the droplet size increased from 150 to 210 μm and the span of particle size distribution increased from 0.42 to 0.52.

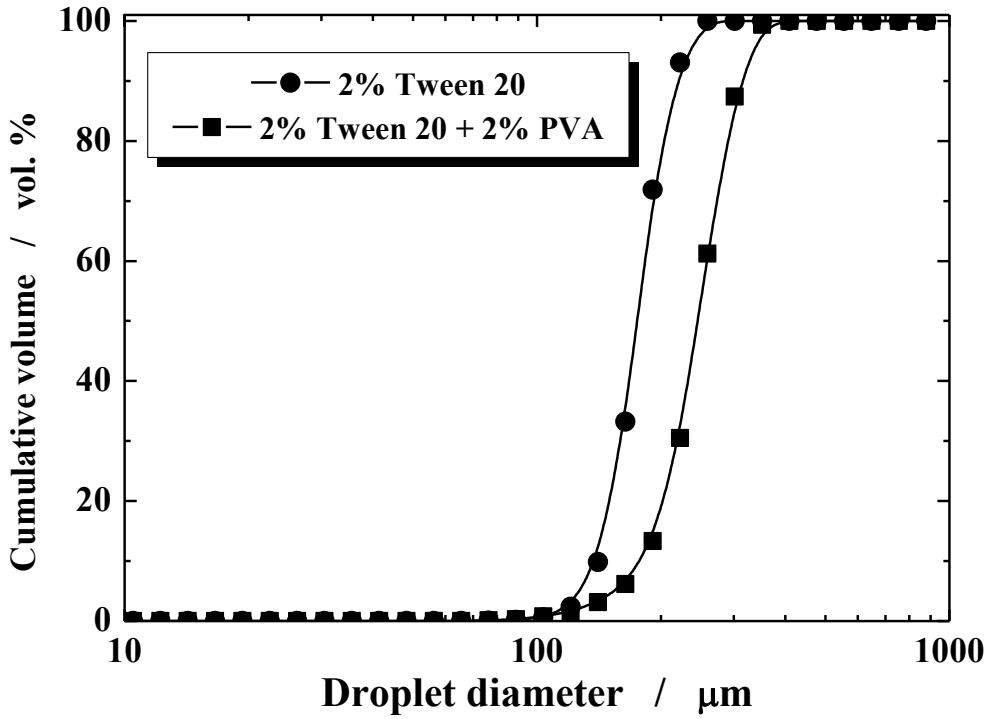

Figure 41 Variation of droplet size distribution with addition of PVA (disperse phase: water-in-pumpkin seed oil, pore size = 20 μm, rotation speed = 600 rpm, transmembrane flux = 640 L m^{-2} h^{-1}).

With the increase of the continuous phase viscosity the diffusional mobility of the surfactant molecules decreases, longer time is needed for stabilization of the droplet and therefore the droplet diameter is bigger. Similar findings were obtained by van

Dijke *et al.* (2010) by microchannel emulsification: using hexadecane as a dispersed phase and increasing the viscosity of the continuous phase from 0.9 to 7.8 mPa s they obtained droplets with increasing size (from 35 to 42 μm) while the CV increased with the increase of the viscosity of continuous phase from 2.5 to 9.5%.

5.1.1.2.4 Influence of surface shear stress

It is widely accepted that shear stress on the membrane surface has to be applied in order to produce uniform droplets (Peng, Williams 1998). Using an SPG membrane with mean pore size of d_p = 5.4 – 10.7 μm Vladisavljević *et al.* (2006) produced W/O/W emulsion by direct membrane emulsification where mean droplet size was d_d = 19.5 – 32 μm and the span of the particle size distribution was 0.28. Kobayashi *et al.* (2005) using microchannel (MC) with oblong section (42.8 × 13.3 μm) produced W/O/W emulsion where mean droplet size was 41.8 μm and the CV was 6.8%. In cross-flow systems and MC emulsification the shear stress is uniformly distributed on the whole membrane surface, therefore, it is expected that the uniformity of the droplets would be high. The shear stress in the Dispersion Cell is not constant over the whole membrane surface and has the highest value at the transitional radius (Eq. (14)) between a free and forced vortex (Kosvintsev *et al.* 2005).

Figure 42 demonstrates the influence of the rotation speed on the droplet size for multiple emulsions of pumpkin seed oil at oil flux of 640 L m^{-2} h^{-1}. As found earlier for single emulsions (Dragosavac *et al.* 2008; Kosvintsev *et al.* 2005), mean droplet size decreases with increasing shear stress. The shear stress on the membrane surface does depend on the distance from the axis of rotation and reaches its greatest value at the transitional radius (Figure 11).

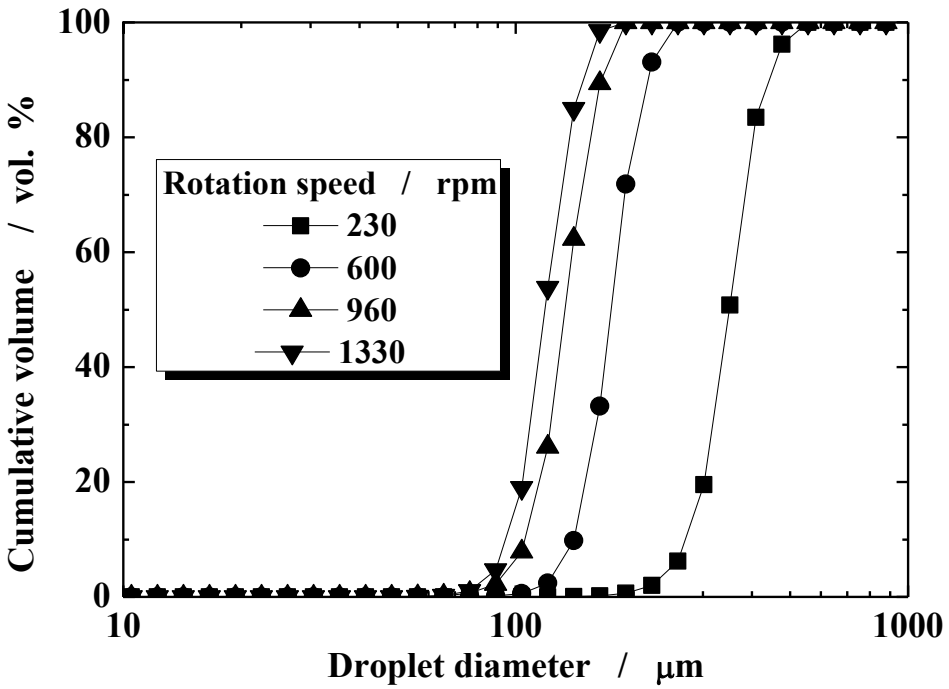

Figure 42 Variation of droplet size distribution with rotational speed (dispersed phase: water-in-pumpkin seed oil, continuous phase: 2% Tween 20, dispersed phase flux = 640 L m^{-2} h^{-1}, pore size = 40 μm).

Since the shear stress on the membrane surface is not constant, the average shear stress is more representative in the case of the whole membrane which was used here. Since the model does not take into consideration the flow rate of the discontinuous phase, it is expected that the model will predict the droplets produced using a very low flow rate, as shown in Figure 43. Droplets produced using the higher flow rate followed the same trend as the ones produced at lower transmembrane flux: increase of rotation speed decreased the droplet size, but the sizes of droplets produced at the higher transmembrane flux caused deviation from the model. The detachment of the droplet is not instantaneous but requires a finite time t_{neck}, the necking time, during which an additional amount of dispersed phase flows into the droplet. Therefore, the resultant droplet volume, V, is larger than the one estimated by the force balance model and can be expressed as (van der Graaf *et al.* 2004): $V_d = V_{crit}+(t_{neck}/k_p)(Q_d/N)$ where V_{crit} is the droplet volume predicted by the Model B (Eq. (10) and Eq. (16)), k is the fraction of active pores, Q_d is the total dispersed phase flow rate and N is the total number of pores in the membrane. For example for the data in Figure 43 obtained at 3185 L m^{-2} h^{-1}, the above equation gives values of t_{neck}/k in the range from 0.13 s at 1330 rpm to 2.6 s at

230 rpm. The fraction of active pores *k* usually ranges from 2 to 50%, which means that t_{neck} should vary from 0.003-0.07 s at 1330 rpm to 0.05-1.3 s at 230 rpm.

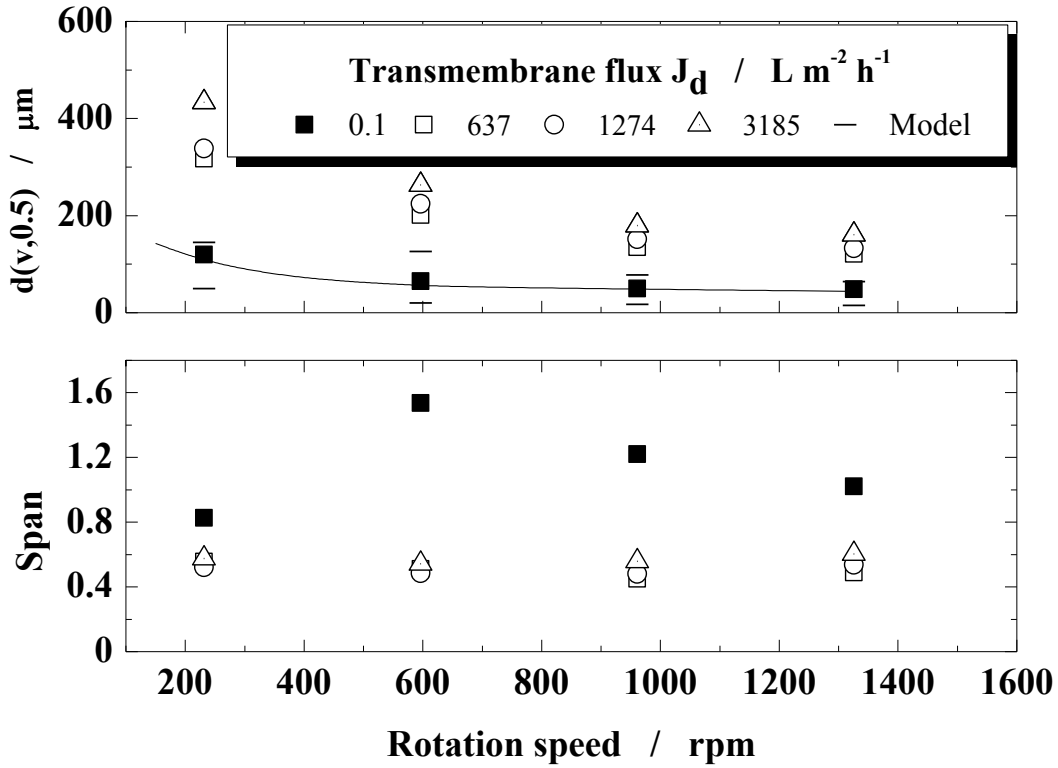

Figure 43 Experimental droplet diameters of water-in-(pumpkin seed oil)-in-water multiple emulsions produced. (Pore size = 40 µm, continuous phase: 2% Tween 20). Horizontal lines (-) represent *d(v,0.1)* and *d(v,0.9)* for the transmembrane flux 0.1 L m^{-2} h^{-1}. Line represents the Model C (τ_{av}).

Figure 44 supports the observation that the droplet size is influenced by shear stress. Photomicrographs correspond to the cumulative curves in Figure 42. As can be seen from the micrographs, the droplets have a dark colour due to the small water droplets entrapped within the oil phase scattering the transmitted light. These photographs were taken immediately after the experiment.

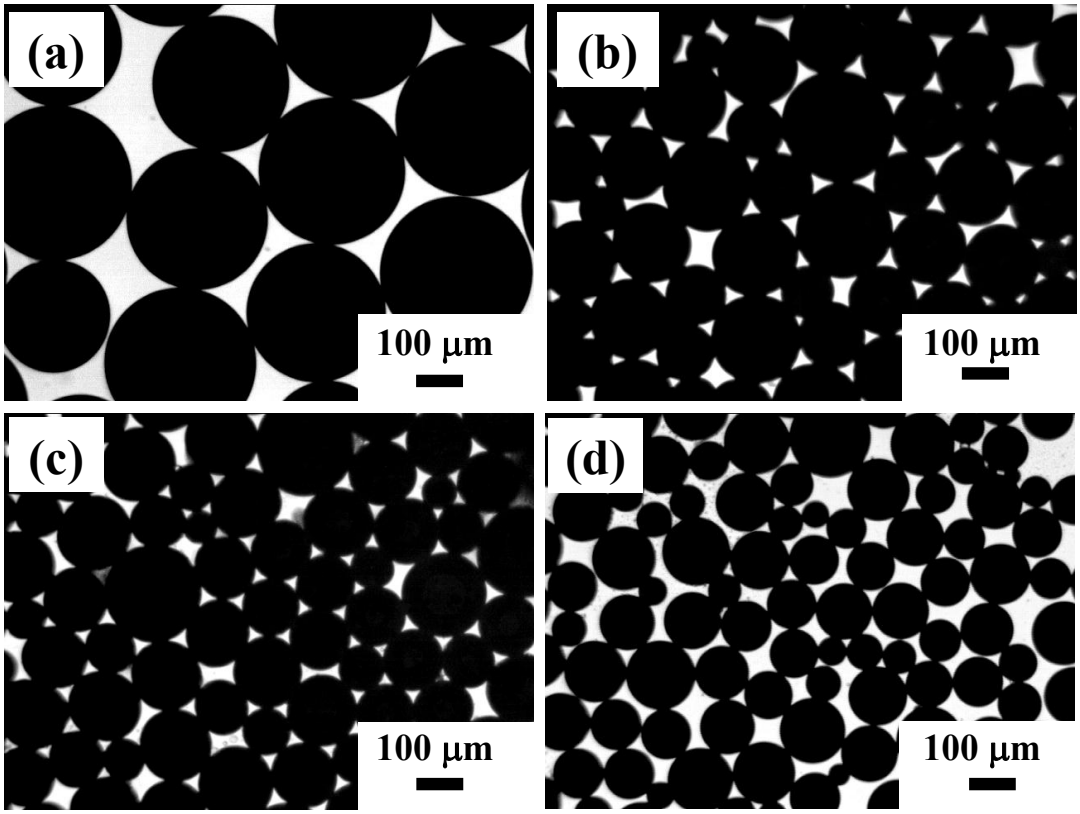

Figure 44 Photomicrographs of droplets formed with 40 µm membrane, dispersed phase: water-in-pumpkin seed oil, continuous phase: 2% Tween 20, transmembrane flux = 640 L m^{-2} h^{-1}: (a) 230 rpm (1 Pa); (b) 600 rpm (5 Pa); (c) 960 rpm (11 Pa); (d) 1330 rpm (18 Pa). Value in the brackets correspond to maximal shear stress.

5.1.1.3 W/O emulsion – silica particle production

The aim was to produce uniform spherical silica particles, within the size range of 30 to 70 µm, with controllable internal porosity, starting from sodium silicate and sulfuric acid, using stirred cell membrane emulsification. No literature data on production of W/O emulsions (acidified sodium silicate/kerosene) using the Dispersion Cell and hydrophobic membranes (Figure 12 and Figure 14) was available, and the reproducibility of the experiments had to be tested. For the tests, the paddle rotation was set to 875 rpm while the flow rate of the dispersed phase was set to 5 mL min^{-1} (corresponding to a flux of 350 L m^{-2} h^{-1}). Four experiments were conducted and the mean droplet sizes (*d*) as well as coefficient of variations (*CV*) are presented in Figure 45. In the experiments, marked as 1 and 2 the volume of dispersed phase injected

through the membrane was 10 cm^3 while in the experiments 3 and 4 it was 50 cm^3. Due to the nature of the emulsion it was not possible to analyse it using the Malvern Mastersizer S since it was equipped only with the water sampling cell therefore the microphotographs were analysed using ImageJ software. To be consistent in the analysis all the droplets and particles were analysed using ImageJ. Detailed explanation of the ImageJ use is given in Appendix B.

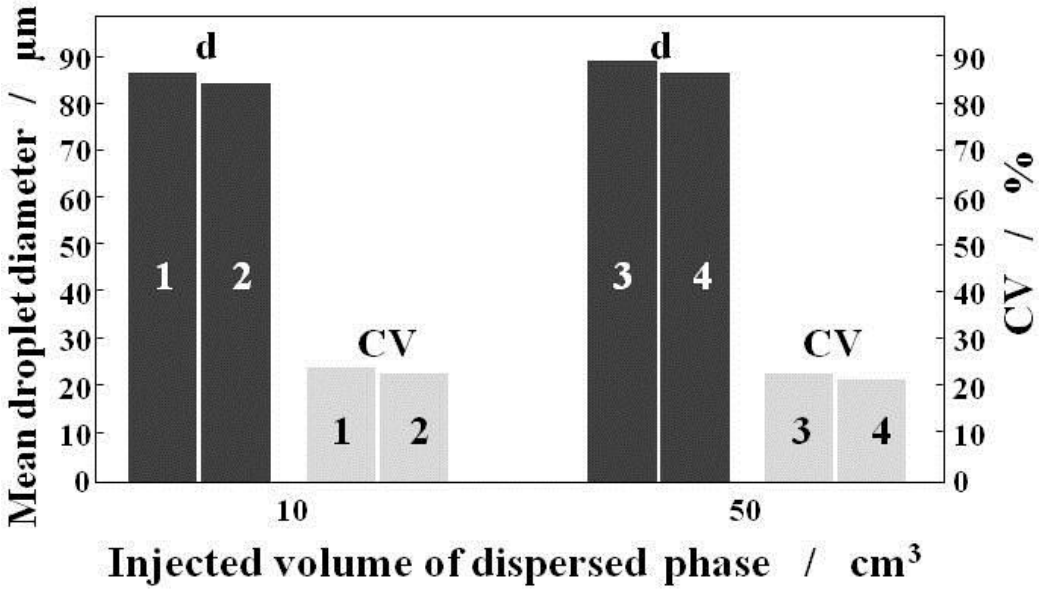

Figure 45 Repeatability of the repeated experiments: 10 cm^3 of dispersed phase was injected into the continuous phase in the exp. 1 and 2 while 50 cm^3 was injected in the exp. 3 and 4. ω = 875 rpm and J_d = 350 L m^{-2} h^{-1}. *d* represents mean droplet size and *CV* represents coefficient of variation. For each experiment at least 700 droplets were calculated.

After each experiment the membrane was sonicated for 30 min in a warm detergent solution in order to remove any remaining solution, washed with clean water and dried with compressed air. It was soaked for one hour in kerosene prior to an experiment in order to increase the hydrophobicity of the membrane. As can be seen from Figure 45, the mean droplet size (*d*) as well as coefficient of variation (*CV*) remained almost unchanged no matter the volume of dispersed phase injected into the continuous phase. This provides evidence that the experiments were reproducible and give a mean droplet size (*d*) of just below 90 µm and coefficient of variation (*CV*) in the range between 22.5 and 23.5% for the described combination of rotation speed and flow rate. Furthermore, these experiments demonstrate that neither the dispersed phase, nor surfactant (Span 80), sorbed onto the membrane surface within the time allowed for the experiments:

such an effect would have caused membrane „wetting‘ with a consequential increase in droplet size (and probably increasing of *CV*).

5.1.1.3.1 Influence of shear stress and flow rate on the droplet size

As commented earlier when using the Dispersion Cell for production of emulsions the two main parameters affecting the droplet size are paddle rotation speed and flow rate of the dispersed phase (Kosvintsev *et al.* 2005; Dragosavac *et al.* 2008; Stillwell *et al.* 2007). Figure 46 illustrates both influences: shear stress as well as flux of the dispersed phase, on droplet size. The error bars in Figure 46 represent one standard deviation from the mean value, and the theoretical prediction based on Eq. (10) and Eq. (16) is shown by the curve. As can be seen from the figure, the rotation speed represents an effective way to control the droplet size. An increase of the rotation speed increases the shear stress on the membrane surface and the droplet formation time shortens, therefore, the droplets produced at higher rotation speed have a smaller diameter. Using a flow rate of 5 mL min^{-1} and a rotation speed from 200 to 1400 rpm, droplet sizes in the range between 240 and 65 µm were produced.

Eq. (10) and Eq. (16) give good prediction of the droplets produced at a very low flow rate (1 mL h^{-1} equivalent to approximately 1 L m^{-2} h^{-1}). Several variations of the force balance model have been developed for predicting the droplet size in the Dispersion Cell (Kosvintsev *et al.* 2005; Dragosavac *et al.* 2008; Egidi *et al.* 2008). Kosvintsev *et al.* (2005) used maximal shear stress in the force balance model and Dragosavac *et al.* (2008) used average shear stress. Egidi *et al.* (2008) added the „push-off" force to the force balance model to predict the droplet size at high flow rates when the space between the pores is small. The shear stress on the membrane surface does depend on the distance from the axis of rotation and reaches its greatest value at the transitional radius (Kosvintsev *et al.* 2005). Since the shear stress on the membrane surface is not constant the average shear stress is more representative in the case of the whole membrane which was used here. Since the model does not take into consideration the flow rate of the discontinuous phase, it is expected that the model will predict the droplets produced using a very low flow rate, as shown in Figure 46. In the case of the very low flow rate, the volume of sulfuric acid used to initialize the gelling was replaced with dionised water, in order to avoid particle gelling during injection through the membrane. Such replacement was necessary, since the experiment had to

last for several hours in order to produce enough droplets for analysis, and if the solution was acidified the sodium silicate would gel within the tubing and membrane. These experiments were performed solely to assess the validity of the force balance model with this system. Droplets produced using the higher flow rate followed the same trend as the ones produced at lower transmembrane flux: increase of rotation speed decreased the droplet size, but the sizes of droplets produced at the higher transmembrane flux caused deviation from the model as seen in the case of W/O/W emulsions.

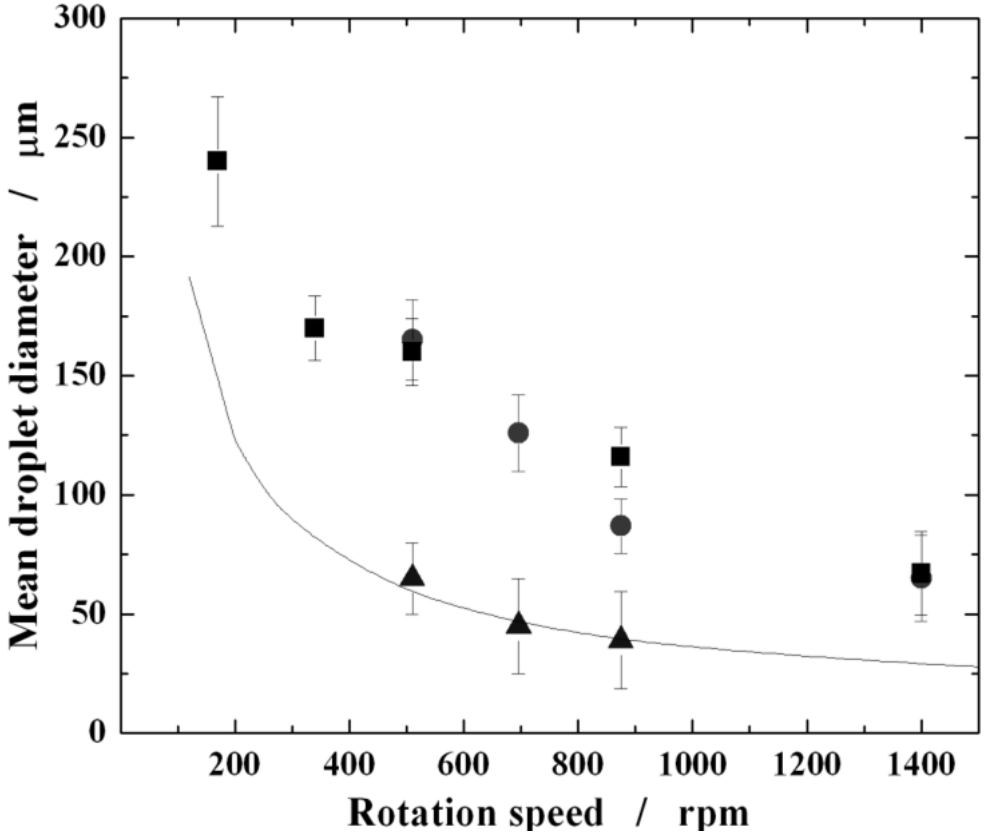

Figure 46 Experimental droplet diameters of produced water-in-oil emulsions as a function of rotation speed. Line represents the model Eq. (10) and Eq. (16) for predicting the droplet size. (■) 6 wt % SiO_2 (Sodium silicate + 1 M H_2SO_4) injected at 350 L m^{-2} h^{-1}. (●) 4 wt % SiO_2 (Sodium silicate + 1 M H_2SO_4) injected at 350 L m^{-2} h^{-1}. (▲) 6 wt % SiO_2 (Sodium silicate + distilled water) injected at 1 L m^{-2} h^{-1}.

Again the resultant droplet volume, V, is larger than the one estimated by the force balance model and can be expressed as (van der Graaf *et al.* 2004): $V = V_{crit}+(t_{neck}/k_p)(Q_d/N)$ where V_{crit} is the droplet volume predicted by the model, k_p is the fraction of active pores, Q_d is the total dispersed phase flow rate and N is the total

number of pores in the membrane. For the data in Figure 46 obtained at 350 L m^{-2} h^{-1}, the above equation gives values of t_{neck}/k in the range from 0.08 s at 1400 rpm to 3.4 s at 200 rpm. The fraction of active pores k usually ranges from 2 to 50%, which means that t_{neck} should vary from 0.002–0.08 s at 1400 rpm to 0.07–1.7 s at 200 rpm. Another reason for the deviation between the model predictions and experimental data at 350 L m^{-2} h^{-1} is insufficient coverage of the droplet surface with Span 80 molecules during formation of the droplets. The model calculations are made using the equilibrium interfacial tension which is lower than the actual interfacial tension during drop formation. Less coverage of the droplet surface by surfactant leads to greater interfacial tension force and the resultant droplet is larger.

It is clear that too low and too high rotation speed is not recommended for production of uniform droplets, as shown by the longer error bars in Figure 46. The decrease in uniformity probably originates from droplet breakup: at low rotation speed large droplets are created which are more susceptible to breakage by the stirrer, and at high rotation speed breakage is quite likely. Other dispersed phase injection rates were tested, but a dispersed phase flow rate of 5 mL min^{-1} gave the most uniform droplets regardless of paddle rotation speeds. No major difference in droplet uniformity and mean droplet diameter was observed for the droplets containing 4 and 6 wt.% SiO_2. Both solution have similar viscosity and density, therefore, the final droplet size should be the same and Figure 46 confirms this prediction. The higher content of silica was used in further experiments, since it is likely to give stronger silica particles. Concentrations higher than 6 wt.% SiO_2 were not used, since it was observed that the solutions were not clear after the addition of sulfuric acid.

In some applications the restriction of active membrane area to a ring encompassing the transitional radius may help to improve the uniformity of the formed droplets (Stillwell *et al.* 2007 and Thompson, Armes & York 2011). The argument here is that the shear stress on the membrane surface due to the stirring is not uniform under the paddle, and the region where the shear reaches its maximum will provide the most consistent region of shear. A ringed membrane was tested for production of the droplets, but no significant improvement in uniformity was observed in this case (data not shown).

5.1.1.3.2 Shrinking of the particles during drying

The produced droplets were transferred into a Teflon beaker, and stirred using a low rotation speed in order to allow gelling and formation of a hydrogel. A teflon baker was used since it was noticed that if the droplets of silica precursor were stirred in a glass beaker they tended to stick to the glass during gelling. Once gelled, the hydrogel particles were dried to form a xerogel. Figure 47 illustrates the shrinkage of the dispersed phase droplets and their transformation; firstly into the hydrogel and then to the xerogel forms. During condensation polymerization the droplets will shrink due to water loss as the hydrogel is formed. To remove kerosene and Span 80 a suspension of gel particles was transferred into a microfiltration cell and kerosene was filtered, followed by washing in acetone and then water. Washed particles were left to completely dry for several days at room temperature. During this drying stage liquid present in the pores is removed, the structure compresses and the porosity is reduced, at least to some degree, by the surface tension forces as the liquid is removed leaving spherical silica particles (xerogel). Drying at room temperature was followed by calcination, but further shrinkage of the dried silica particles was not observed. Shrinkage of the droplets during the drying process can be seen in Figure 47. The markers in Figure 47 represent the final particle size of the gel (hydrogel or xerogel) as a function of the initial droplet size and the lines fit the experimental data.

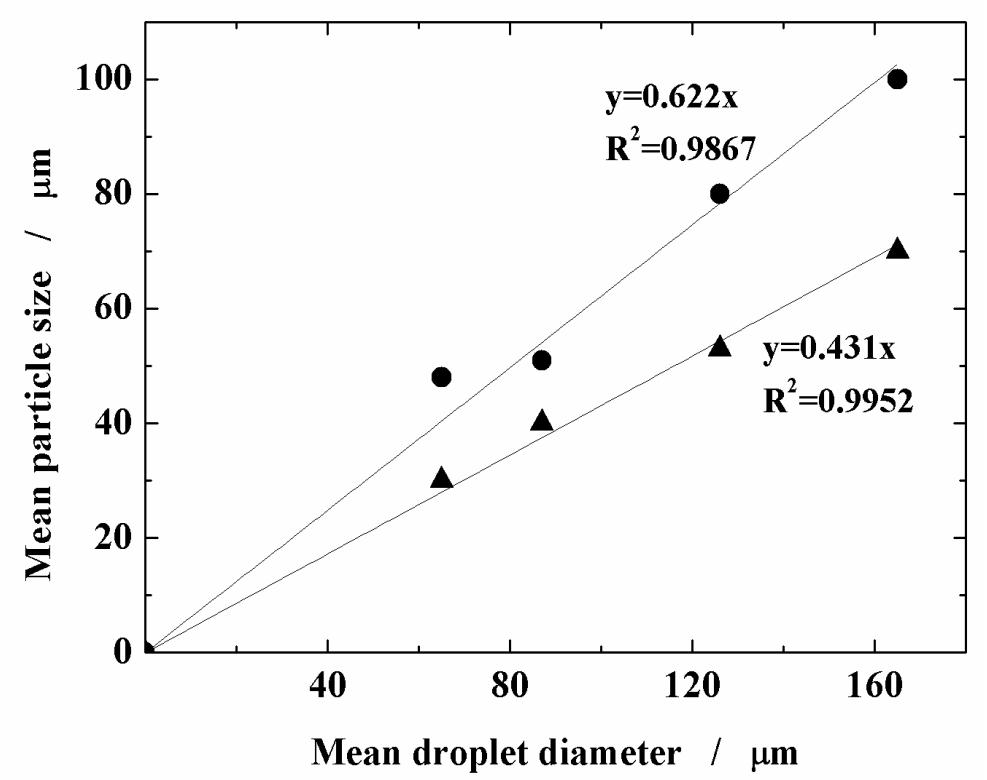

Figure 47 Relationship between the particle diameter in the resultant gels and the droplet diameter. (6 wt % SiO_2 (Sodium silicate + 1 M H_2SO_4) injected at 350 L m^{-2} h^{-1}). (●) Hydrogel. (▲) Xerogel.

Final particle size was found to be an approximately linear function of the initial droplet size. Final silica particles (xerogel) were 2.3 times smaller than initial droplet size. However, the particles are still very significantly bigger than would be predicted by a mass balance of the silica used in their formation. For example, the 120 μm droplets would give rise to xerogel particles of 37 μm based solely on a material balance on the silica present. Clearly, the larger observed size of 52 μm, is due to a significant amount of internal porosity, or voidage. This is discussed further after the dried particle characterization results. Figure 48 compares the *CV* for droplets, hydrogel and xerogel particles as a function of rotation speed.

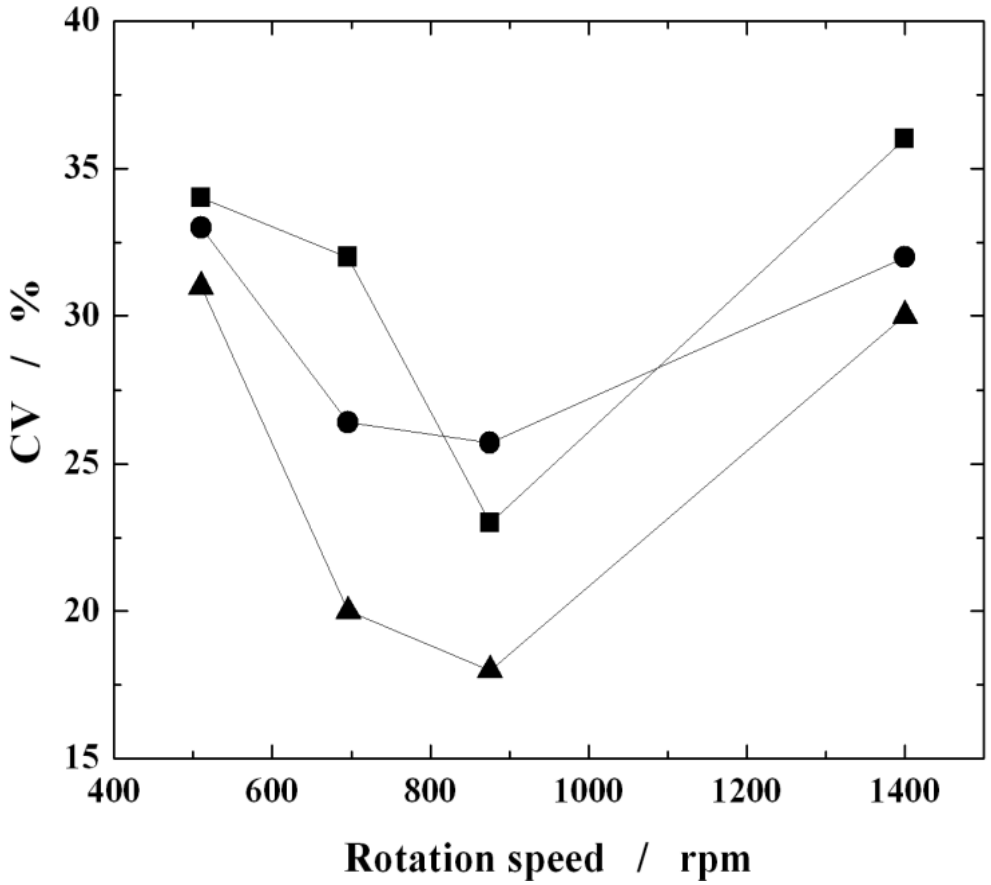

Figure 48 The coefficient of variation of silica particles in various stages during production as a function of rotation speed. (6 wt % SiO_2 (Sodium silicate + 1 M H_2SO_4) injected at 350 L m^{-2} h^{-1}). (■) Droplets of acidified sodium silicate solution in kerosene immediately after production. (●) Hydrogel particles. (▲) Xerogel particles.

It can be seen that the most uniform droplets were produced at an intermediate rotation speed of 875 rpm. It is interesting to note that with the loss of water the particles became more uniform as illustrated in Figure 48. Improvement in uniformity with the loss of water is also visible from Figure 49 where the particles (Figure 49 (c) and (d)) produced from the droplets (Figure 49 (a) and (b)) are presented. Using a 15 µm membrane, spherical silica particles in the range between 30 and 70 µm with a $CV < 20$ % were produced.

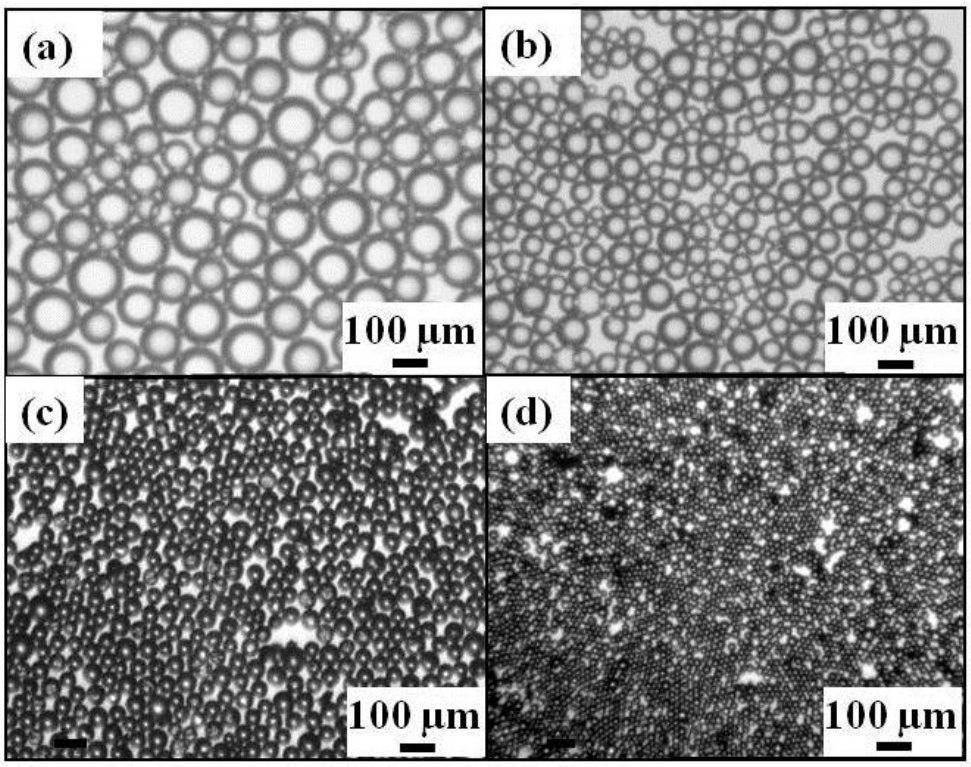

Figure 49 Optical micrographs of acidic sodium silicate droplets in kerosene produced at (a) 500 rpm and (b) 875 rpm. Optical micrographs of calcined silica particles produced from these droplets are shown in Figure (c) and (d), respectively.

5.1.1.3.3 Influence of the stirring speed, heating and air exposure during the gelling phase on the final silica particles

The very important phase during the production of silica particles is the transformation of silica precursor droplets to the hydrogel – gelling phase. The gelling phase is also known as a sticky phase since the particles become sticky and tend to attach to each other as well as to the walls of the beaker. Earlier was mentioned that the Teflon beaker was selected since the particles tended to stick to the glass walls possibly due to forming silanol bonds. In order to try to minimize the possibility of particles sticking to each other they had to be stirred during the gelling phase. Figure 50 shows the case when the stirring speed during the gelling time was set to be 500 rpm. Formed hydrogel particles were crushed and not too many particles actually retained the spherical shape. It was found that the rotation speed of 170 rpm retained the particles suspended and it was enough to prevent the settling, therefore, it was selected as the stirring speed in all experiments.

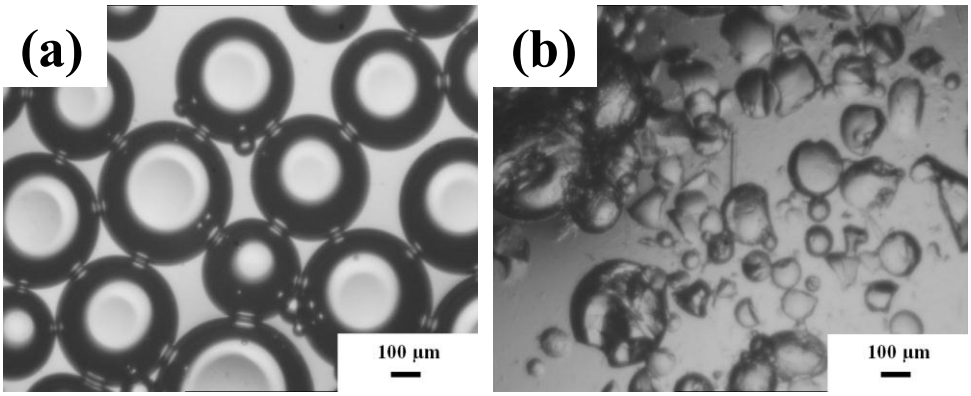

Figure 50 Influence of too high stirring speed during the gelling time on the final particle shape. (a) Inintial droplets produced using flow rate of 5 mL min^{-1} and 300 rpm. (b) Hydrogel.

It is interesting to notice that the spherical particles can be produced also without any stirring during the gelling phase as shown in Figure 51.

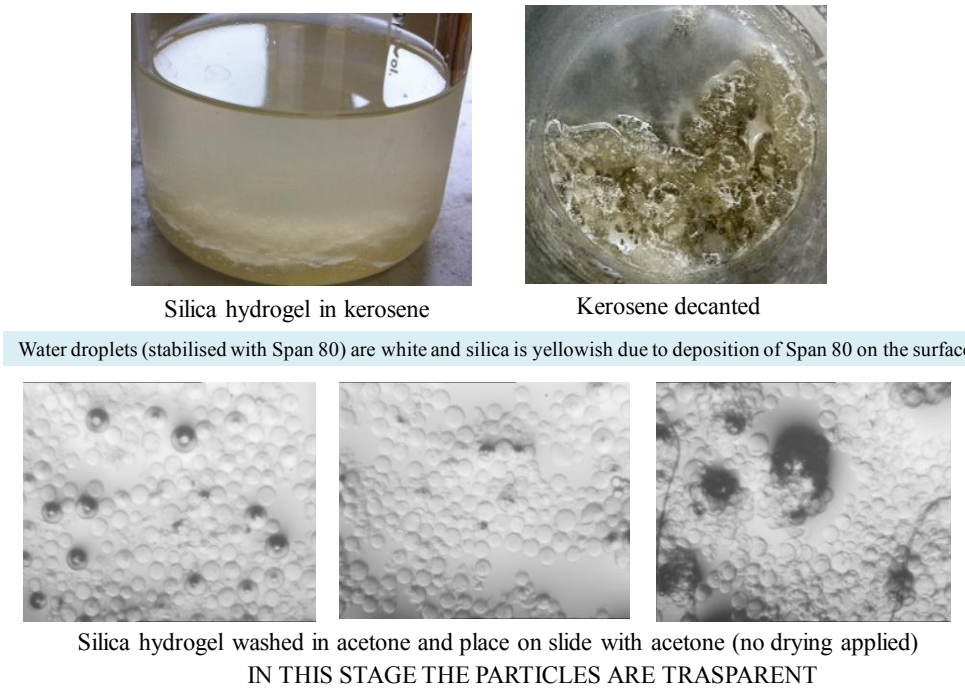

Figure 51 Hydrogel produced without stirring during the gelling phase.

It was also noticed that too early exposure to air once the droplets of acidified sodium silicate were produced can lead to breakage of the spheres. The newly formed surfaces appeared to be smooth with sharp edges as it can be seen in Figure 52. The droplets in Figure 52 were taken from the beaker immediately after the production and placed on the microscope slide. It can be seen that the largest droplet which is most likely to stand

out from the kerosene solution on the slide after 10 min standing on the slide cracks and splits during solidification (Figure 52 (a)) as the reaction progresses other droplets start to crack too (Figure 52 (d)).

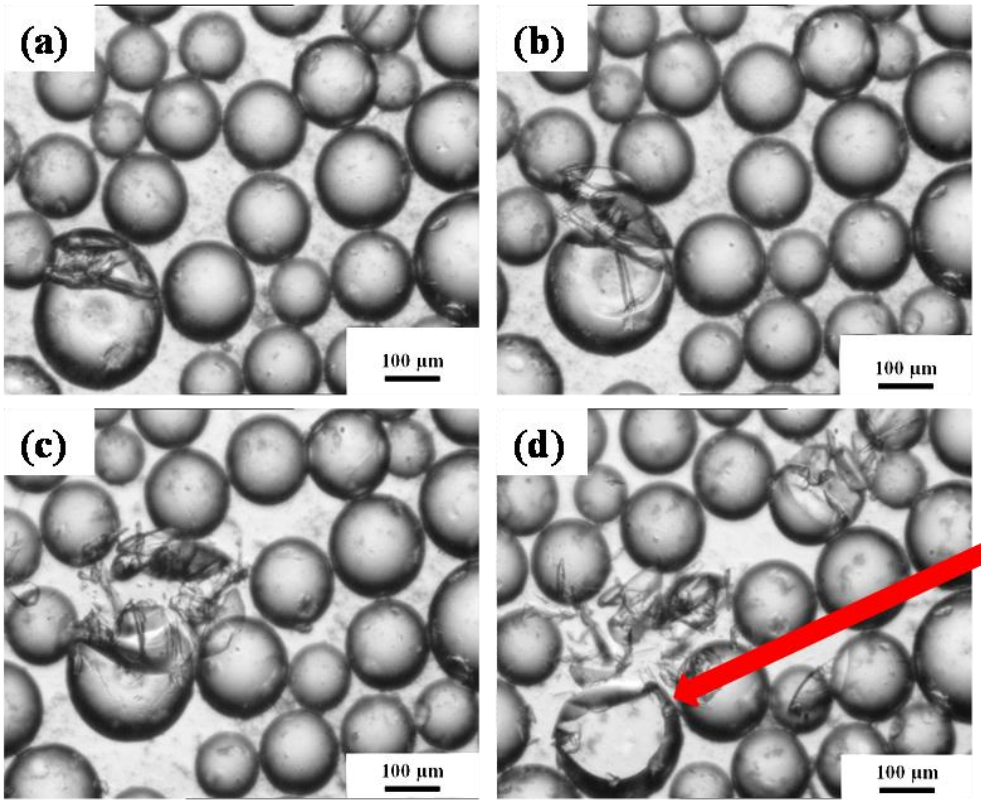

Figure 52 Too early exposure to the air (too fast solidification). (a) 10 min, (b) 15 min, (c) 25 min and (d) 35 min.

In an attempt to try to speed up the process of solidification of silica particles the droplets after the production were heated (Figure 53(a)). The heating was applied 3h after the droplets were produced (solidification process already started so the droplets/particles are not too fragile) and was continued over 12 h.

When heating was applied the solid silica particles were obtained much faster than in the case when no heating was applied. Solid silica particles were obtained after one day compared to the non heated ones where it took 3 days to get the solid particles, if the initial sodium silicate had a pH = 3.5. The resultant particles which were heated (Figure 53 (a)) are crushed and bruised whilst the ones that were not heated (Figure 53 (b)) maintained the spherical shape. With an increase of temperature the condensation reaction speeds up and water is removed more quickly from the droplets, therefore, it is possible that the changes in the shape of the particles are due to the faster removal of

water. Due to this, it was decided that all experiments should be run at room temperature.

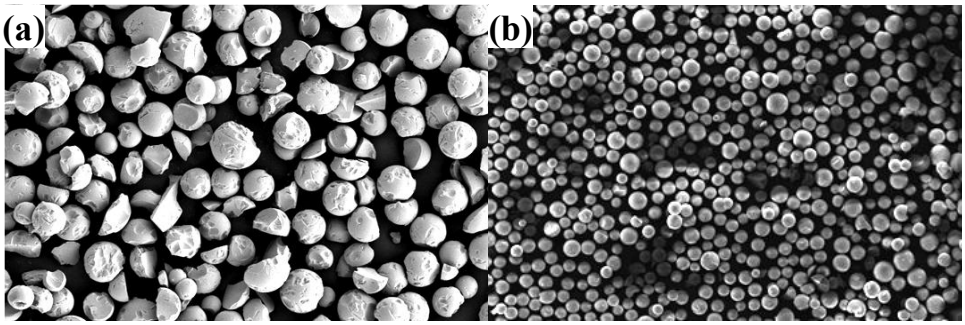

Figure 53 Influence of the heating during the gelling phase on the final shape of the particles. (a) During the gelling phase droplets were exposed to the heating (60^{o}C over 12 h). (b) Droplets were not exposed to the heating.

5.1.1.3.4 Surface analysis of produced silica particles

On the surface the presence of pores is visible on an SEM. To confirm the composition of the particles EDX elemental analysis was performed. Ten random silica particles were scanned and the averaged result of Energy Dispersive Spectrum is presented in Figure 54. As can be seen, the particles consist of silicon and oxygen with signals at 1.8 and 0.5 ekV respectively. At 0 and 2.2 ekV two signals can be seen: the first one comes from the background (i.e. the plate on which the particles were placed), while the other one comes from the golden palladium (mixture of gold and palladium) which was used to coat the particles prior to SEM analysis in order to reduce the charge interference. The surface structure of the silica particles after calcination was imaged by SEM (operated at 2.6 kV) and microphotographs are presented in Figure 55. The silica particles are almost perfectly round as can be seen from Figure 55(a) and (b), while the close-up of the particle surface shows a cloudy and corrugated external and internal surface morphology (Figure 55(c) and (d)).

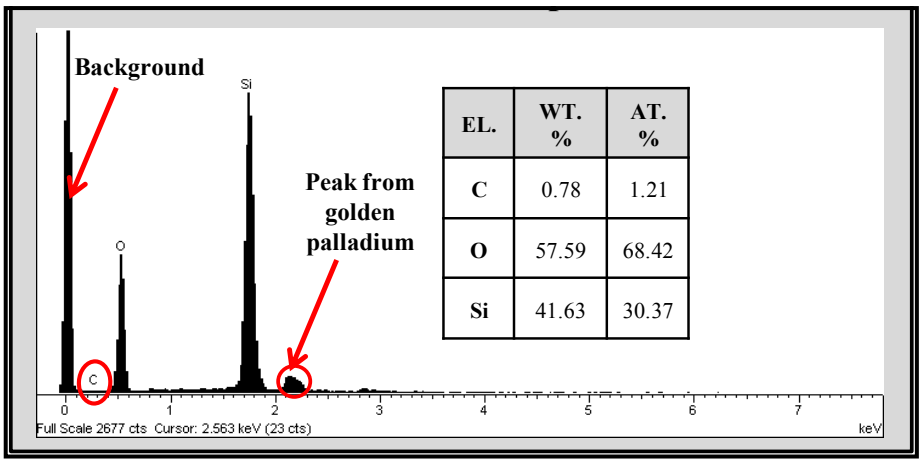

EL.	WT. %	AT. %
C	0.78	1.21
O	57.59	68.42
Si	41.63	30.37

Figure 54 The Energy Dispersive Spectrum (EDS) of silica particles with average size of 40 µm.

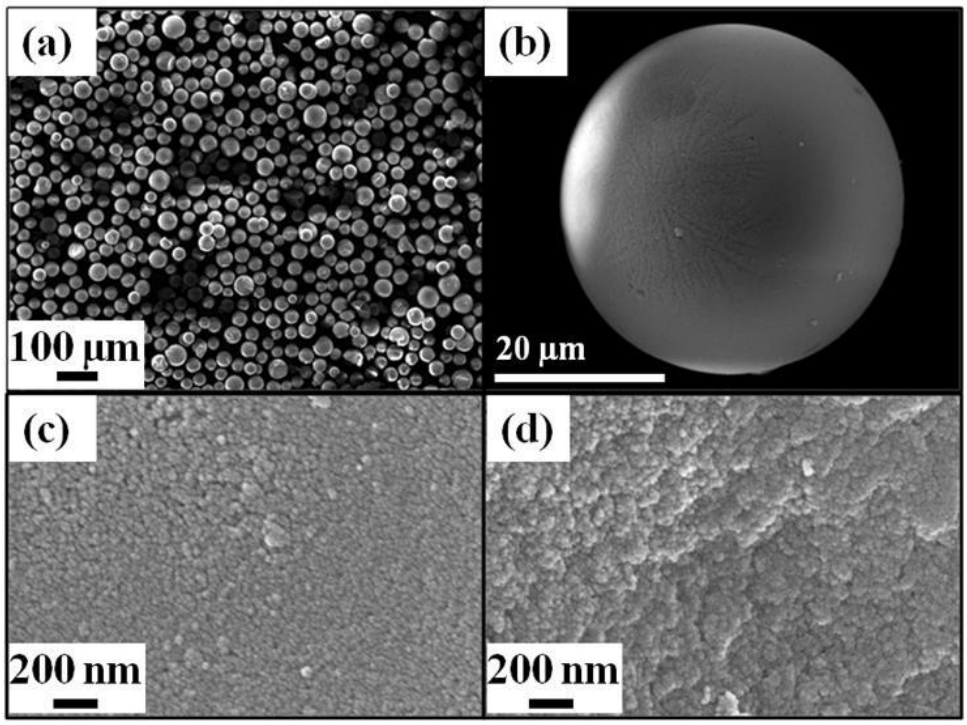

Figure 55 (a) Scanning electron micrograph (SEM) of the silica particles with an average size of 40 µm. (b) SEM of a single silica sphere. (c) Field emission gun (FEG) SEM of a silica sphere external surface structure. (d) FEG SEM of a broken silica sphere.

Gel formation is based on establishment of chemical bonds between neighboring particles and the particle size is a function of the pH of a silica precursor (Iler 1979). According to Iler (1979) after gelation, but before complete drying, the structure and chemistry may be altered by varying pH, salt concentration, temperature and/or pore

fluid composition in a process called aging. Muñoz-Aguado *et al.* (1995) found that if gellation is performed under acid conditions (pH≤7) final xerogel pore size depends mainly upon pH. In order to modify the internal porosity the pH of the dispersed phase was increased to 4.5 and aged in acetone. The particles were compared with the particles formed from the solution at pH 3.5 and hydrogel aged in water. The systematization of pores according to Dubinin (1968): where micropores have diameter smaller than 3 nm and mesopores have diameters in the region between 3 and 200 nm is used in the discussion below. Figure 56 (a) shows a nitrogen sorption–desorption isotherm of the silica synthesized under a pH of 3.5 aged for 7 days in water and dried and calcined. The sorption isotherm shows a steep rise in the low-pressure region at a normalized pressure of about $p/p_0 < 0.05$ and according to IUPAC (Sing *et al.* 1985) it is the type I isotherm which could be interpreted as an indication of the presence of micropores in the analyzed silica. The inset in Figure 56(a) shows the pore size distribution calculated from the desorption isotherm according to the BJH method (Barret, Joyner & Halenda 1951). The sample shows a wide pore size distribution in the micropore range with a distribution maximum at a pore radius of 1.5 nm. Figure 56(b) represents the silica sample produced from the acidified sodium silicate solution with a pH 4.5 aged for 7 days in acetone dried and calcined.

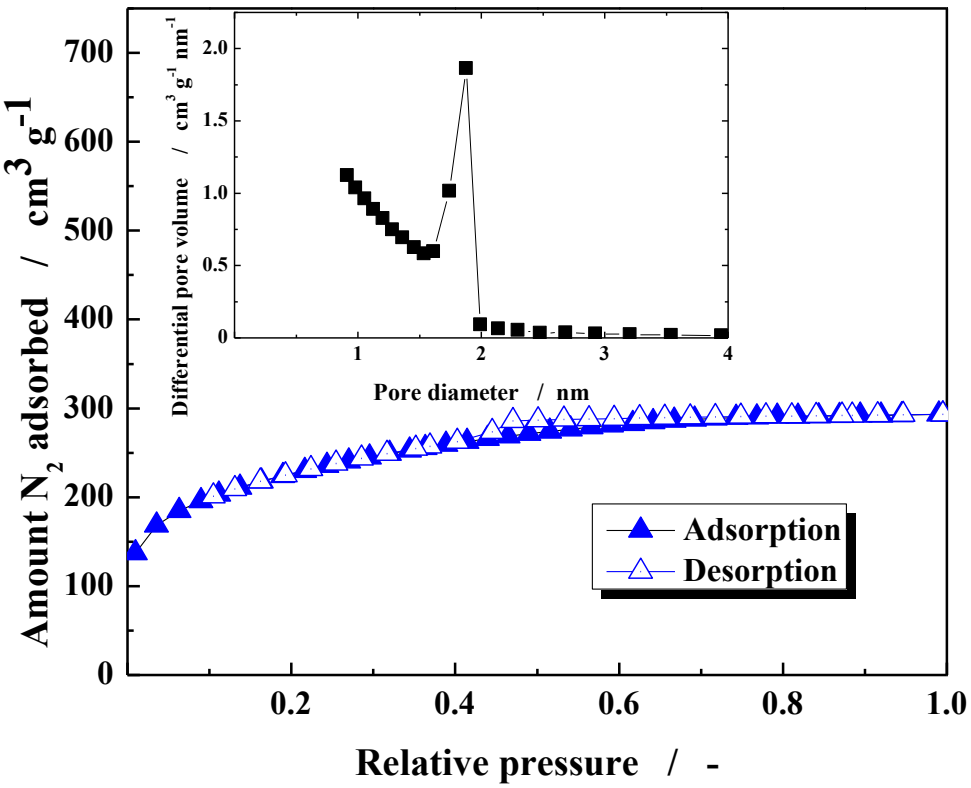

Figure 56 (a) BET nitrogen sorption–desorption isotherm of silica particles with an average size of 40 µm. Specific surface area was 760 m^{-2} g^{-1}. Initial sodium silicate solution had pH=3.5, and produced hydrogel was aged 7 days in water followed by vacuum drying on 100°C and calcination for 6h at 550°C. Inset graph represents pore size distribution calculated using BJH method according to the desorption isotherm.

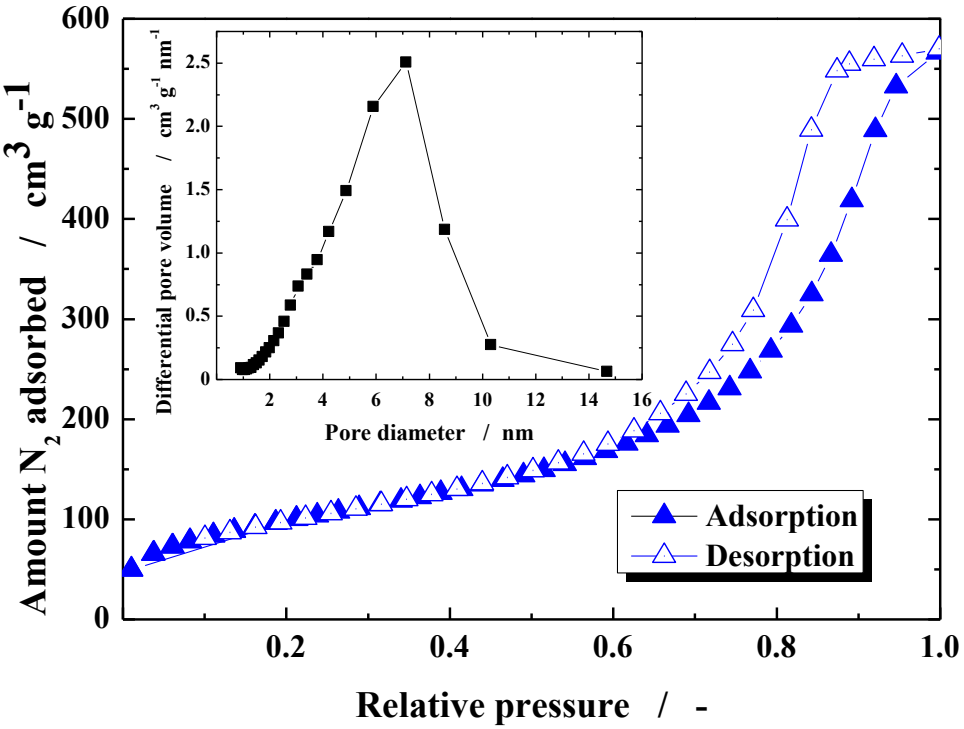

(b) BET nitrogen sorption–desorption isotherm of silica particles with an average size of 40 µm. Specific surface area was 360 m^{-2} g^{-1}. Initial sodium silicate solution had pH=4.5, and produced hydrogel was aged 7 days in water followed by vacuum drying at 100°C and calcination for 6h at 550°C. Inset graph represents pore size distribution calculated using BJH method according to the desorption isotherm.

The sorption isotherm has a characteristic hysteresis loop appearing between a relative pressure of p/p_0 = 0.60 and p/p_0 = 1 caused possibly by capillary condensation corresponding to a type IV isotherm according to IUPAC (Sing *et al.* 1985) indicating the presence of mesopores. The inset in Figure 56(b) illustrates the pore size distribution (according to the BJH method (Barret, Joyner & Halenda 1951)) of the sample with a distribution maximum at a pore radius of 6 nm. The results obtained are in accordance with the literature, since Muñoz-Aguado & Gregorkiewitz (1997) reported that gelling reactions in the acid region is approximately second order with respect to silica concentration and a bimolecular condensation reaction is the rate determining step. So the mechanism can be described by the following reaction sequence:

$$\equiv Si-OH + OH^- \xrightarrow{fast} \equiv Si-O^- + H_2O \qquad \textbf{Eq. 46}$$

$$\equiv Si-OH + {}^-O-Si\equiv \xrightarrow{slow} \equiv Si-O-Si\equiv + OH^- \qquad \textbf{Eq. 47}$$

and it combines OH^- catalysis (Eq. (46)) with bimolecular condensation (Eq. (47). When such mechanisms prevail, then according to Muñoz-Aguado and Gregorkiewitz (1997), a microporous texture is expected for the silica matrix.

The specific surface area of the sample aged in water at pH = 3.5 was 760 $m^2\ g^{-1}$ (± 21 $m^2\ g^{-1}$) with a cumulative pore volume (V_p) of 0.45 $cm^3\ g^{-1}$ (± 0.02 $cm^3\ g^{-1}$), determined using the BET multipoint method (Brunauer, Emmett & Teller E, 1938). In the case of the sample aged in acetone at pH=4.5 the specific surface area decreased to 360 $m^2\ g^{-1}$ (± 16 $m^2\ g^{-1}$) while the cumulative pore volume increased to 0.88 $cm^3\ g^{-1}$ (± 0.03 $cm^3\ g^{-1}$). Note that the specific surface area of the particles using the Mastersizer 2000 S (Malvern Instruments, UK) was determined to be just about 0.1 $m^2\ g^{-1}$ which is negligible with respect to the internal surface area. The absolute density ρ_t of the samples aged in water, or acetone, was measured using a Helium Pycnometer 9200 (Micromeritics, US) and was not found to differ significantly: 2070 kg m^{-3} (±40 kg m^{-3}). According to the cumulative pore volume (V_p) and the absolute silica density (ρ_t), the internal voidage ($\varepsilon_s = V_p/(V_p + 1/\rho_t)$) of the samples aged in water and acetone is 47 and 63%, respectively.

The analysis above compares favourably with a material balance based on the information contained in Figure 47. The volume of solid silica contained in a droplet is

$$m\frac{\pi}{6}x^3\frac{\rho}{\rho_s} \qquad \textbf{Eq. 48}$$

where m is the mass fraction of silica present in the liquid, x is the droplet diameter, ρ and ρ_s are the acidified sodium silicate and solid silica densities, respectively. The internal voidage of the particle is

$$\varepsilon_s = \frac{V_{voids}}{V_{voids} + V_{solid}} \qquad \textbf{Eq. 49}$$

where V_{voids} is the void volume and V_{solid} is the solid volume of the silica. The V_{voids} is the volume of the particle minus the volume of the solid silica:

$$V_{voids} = \frac{\pi}{6}(x_p{}^3 - m\frac{\rho}{\rho_s}x^3) \qquad \textbf{Eq. 50}$$

where x_p is the particle (xerogel or hydrogel) diameter. Combining Eq. (49) and Eq. (50) and rearranging provides the following equation for internal particle voidage:

$$\varepsilon_s = 1 - \frac{\rho}{\rho_s} m \left(\frac{x}{x_p} \right)^3 \qquad \textbf{Eq. 51}$$

Figure 47 provides values of the ratio of the particle size and droplet size for both hydrogel and xerogel particles. Using the ratios shown in the figure provides internal particle voidages of 88% and 64% for the hydrogel and xerogel particles, respectively. The latter compares favourably with the value of 63% obtained from the pore volume and density determination.

For comparison, Chen *et al.* (2008) used an approach similar to Carroll *et al.* (2008) (acidified TEOS as silica source, surfactant templating method in a microfluidic device) and determined the internal surface area of the produced silica particles to be 550–675 $m^2\ g^{-1}$ with the reported cumulative pore volume to be 1.1–2.6 $cm^3\ g^{-1}$, depending on experimental parameters. Chokkalingam *et al.* (2010) (acidified TMOS with ammonia as silica source, sol-gel method, microfluidic co-flow device) produced silica particles with internal surface area of 820 $m^2\ g^{-1}$ and the total reported pore volume of 0.93 $cm^3\ g^{-1}$. The highest pore volume created in this work measured by BET was 0.88 $cm^3\ g^{-1}$ (± 0.03 $cm^3\ g^{-1}$) and calculated from Eq. (50) and a material balance was found to be 0.86 $cm^3\ g^{-1}$. However, to date, no membrane emulsification synthesis route has been reported for production of porous silica particles larger than 5 μm. The increase in pore size in the case of the sample aged in acetone and produced from solution with higher pH (4.5) may be interpreted in two ways. According to Iler (1979), the increase of the pH increases the size of the primary silica particles too. Through condensation polymerization, particles bind together to form a gel structure, so that when bigger particles come together they form a less dense gel structure with larger pores. The xerogel structure is a collapsed and distorted version of the structure that originally existed at the gel point. During the drying the gel shrinks and the capillary force, which is directly proportional to the capillary pressure p_c, exerted on the network depends on the surface tension of the liquid φ, contact angle θ, and the pore size r_p:

$$p_c = 2\varphi \cos(\theta) / r_p \qquad \textbf{Eq. 52}$$

Since the pore size can be very small the capillary pressure, which collapses the initial gel structure can be enormous (Iler 1979). By using the acetone which has a 3 times lower surface tension than water during the drying step the capillary pressure is lower, hence the gel shrinks less and larger pores are created.

In Figure 56 (a) and (b) BJH approach (based on the Kelvin equation) was used to calculate pore size distribution

$$\ln\frac{P}{P_o} = -\frac{2\varphi\overline{V}}{r_p R_g T_s} \qquad \textbf{Eq. 53}$$

where R_g is universal gas constant, $\overline{V}$ is molar volume of condensed liquid, P is pressure and P_o is saturation pressure while T_s is saturation temperature.

Lowel *et al.* 2004 in their book about surface characterization gave a review of available methods (classic thermodynamic and modern microscopic) for determining the pore size distribution. The accuracy of the pore size distribution when classic BJH approach is applied depends on applicability and the deficiencies of the Kelvin equation. On the other hand modern macroscopic DFT (density function theory (Seaton & Walton 1989)) provides a microscopic treatment of sorption phenomena in micro-and mesopores on a molecular level, i.e. based on statistical mechanics. Complex mathematical modelling of gas-solid interactions plus geometrical considerations (pore geometry) leads to realistic density profiles for the confined fluid as a function of temperature and pressure. From these density profiles the amount adsorbed can be derived. Gas-solid interactions are ~~"c~~alibrated" against real isotherm data of non-porous material. In Figure 57 the pore size distribution applying DTF theory is applied. Again, as in Figure 56, two different pore size distributions are obtained and the smaller pores are present in the sample aged in water. From Figure 57 it is obvious that the BJH method was underestimating the pore sizes and for both samples the pore size distribution shifts toward larger pores.

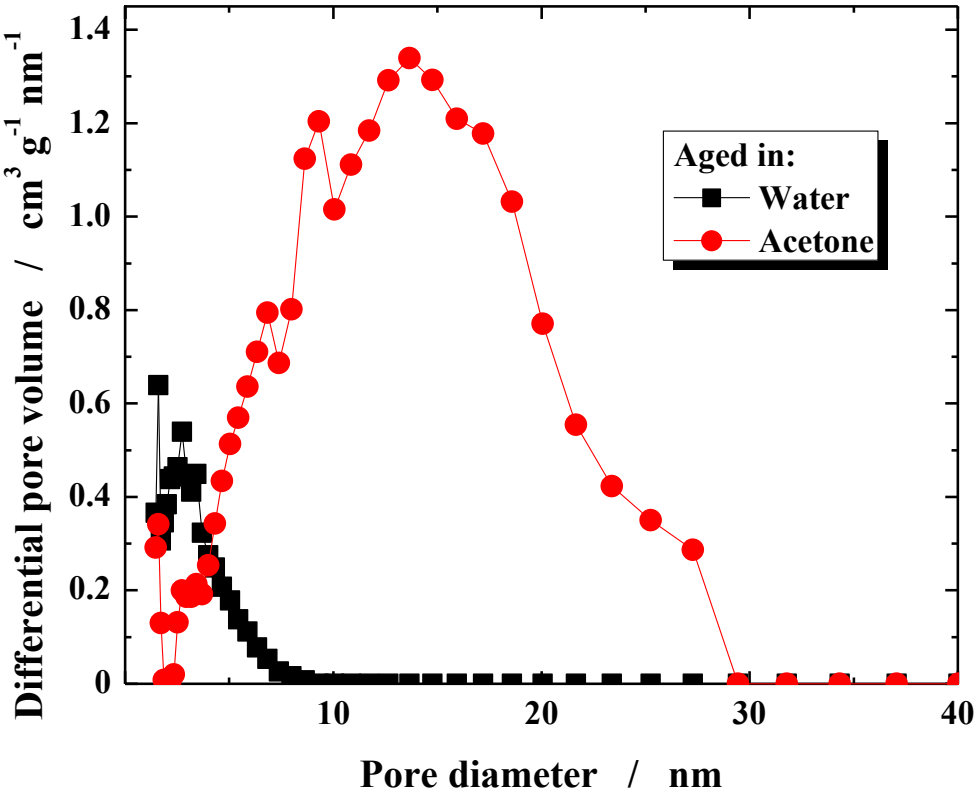

Figure 57 DFT (Density function theory) pore size distribution curve obtained from the sorption isotherm.

Silica particles produced using acidified sodium silicate aged in acetone were additionally functionalized according to the procedure described in Chapter 4.1.2.3.3 and tested for copper sorption (Chapter 5.2.3).

5.1.1.3.5 Attempt to influence the internal porosity using surfactant templating method

An attempt to regulate internal structure of the silica particles by the surfactant templating method was also tested. Figure 58 compares an experiment when no water soluble surfactant was used with two experiments when water soluble surfactants were used.

As it can be seen from Figure 58 the surfactant templating method was not successful since both when Tween 20 and Triton X were used final particles did not maintain a spherical shape. What is interesting is that when surfactant is dissolved a delay in solidification of the particles is observed (sticky phase starts after 3 days), and polymerization condensation reaction can also be followed by observing the turbidity of the solution.

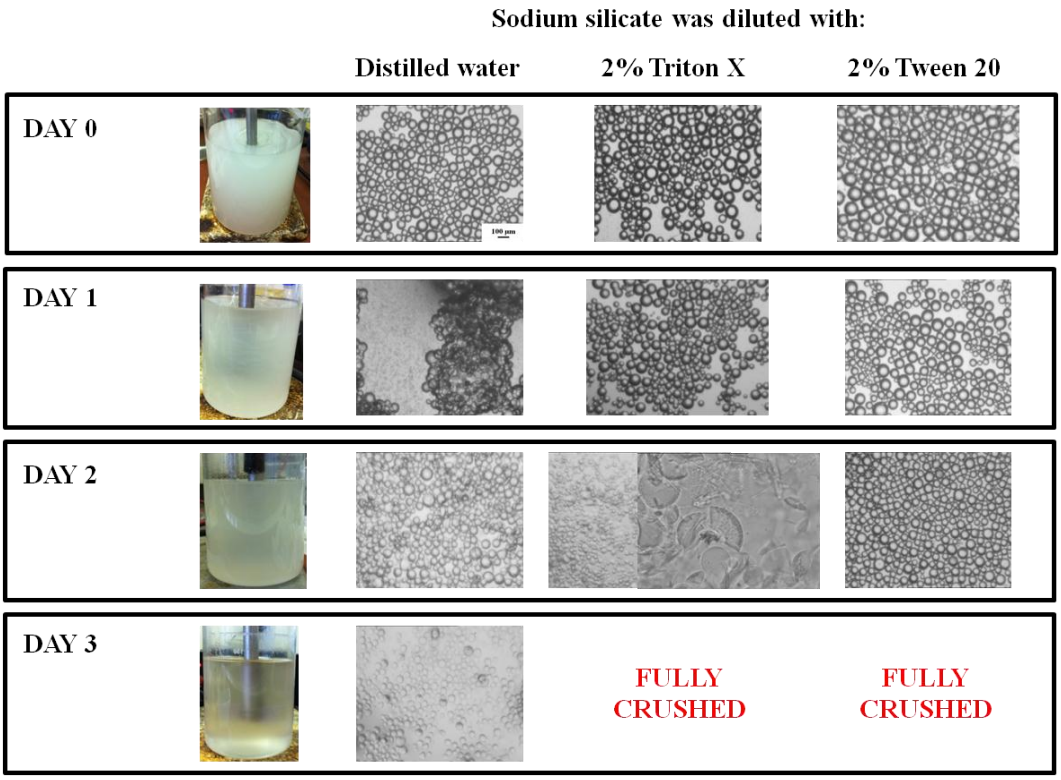

Figure 58 Use of 2% Triton X and 2% Tween 20 to tailor the internal structure of silica particles. pH of acidified sodium silicate was in all experiments 3.5. Droplets were produced using a rotation speed of 875 rpm and flow rate of 5 mL min^{-1}. Produced droplets were transferred into a beaker and stirred at 170 rpm until solidified.

In Figure 58 the glass beaker was used in order to be able to see the difference in the solution turbidity as the reaction condensation polymerization progresses. Photographs of the glass beaker (Figure 58) were taken for the case when the distilled water was used but similar trends in the change of turbidity was observed when the surfactants (both Tween and Triton X) were dissolved within the water phase. Once the acidified sodium silicate was injected into the kerosene the solution became milky white (day 0). With time as the condensation polymerization progressed kerosene solution became more and more transparent and by day 3 (in the case when acidified solution of sodium silicate had the pH of 3.5) the solution became almost completely transparent. All the photographs were taken with stirrer in operation. It is believed that the initial kerosene solution became milky due to the water released during the condensation reaction.

5.1.2 Oscillating system

The Dispersion Cell proved to be a valuable tool for laboratory investigations and formulation testing, but due to its limited size it is inadequate for industrial application. In order to bring nickel metal membranes and membrane emulsification closer to the industrial application an Oscillating system is proposed. In the Oscillating system it is the vertical oscillations of the membrane that governs the shear induced on the membrane surface. It is believed that the shear mainly governs the droplet size therefore no matter how the shear is induced it would produce droplets of a same size. To commission the system sunflower oil was used to produce O/W emulsions.

5.1.2.1 Influence of the shear stress (amplitude and frequency)

As an indication of the reproducibility of the results, and the drop size span, Figure 59 illustrates the data obtained from triplicate experiments for an oscillator frequency of 15 Hz and over the range where the drop size is a significant function of peak shear stress. At each shear condition the results from three experiments are reported as a circular marker. Where only a single marker is visible, it is because the markers all fall onto the same place. The results show that the experiments were reproducible and that there is a set of operating conditions that provide the narrowest drop size distribution. For this frequency, and injection rate, the most narrow drop size distribution was obtained at a peak shear stress of 3.6 Pa, giving a median drop size on a number distribution of just below 50 μm and a drop size span in the range of 0.37 – 0.45.

The transmembrane flux was kept at a value of only 30 L m^{-2} h^{-1} in the Oscillating membrane tests, so that the effects of ―push-off" and drop growth are again avoided. On increasing peak shear the droplet size decreases sharply and for most frequencies reaches a constant value after the peak shear is 4 Pa.

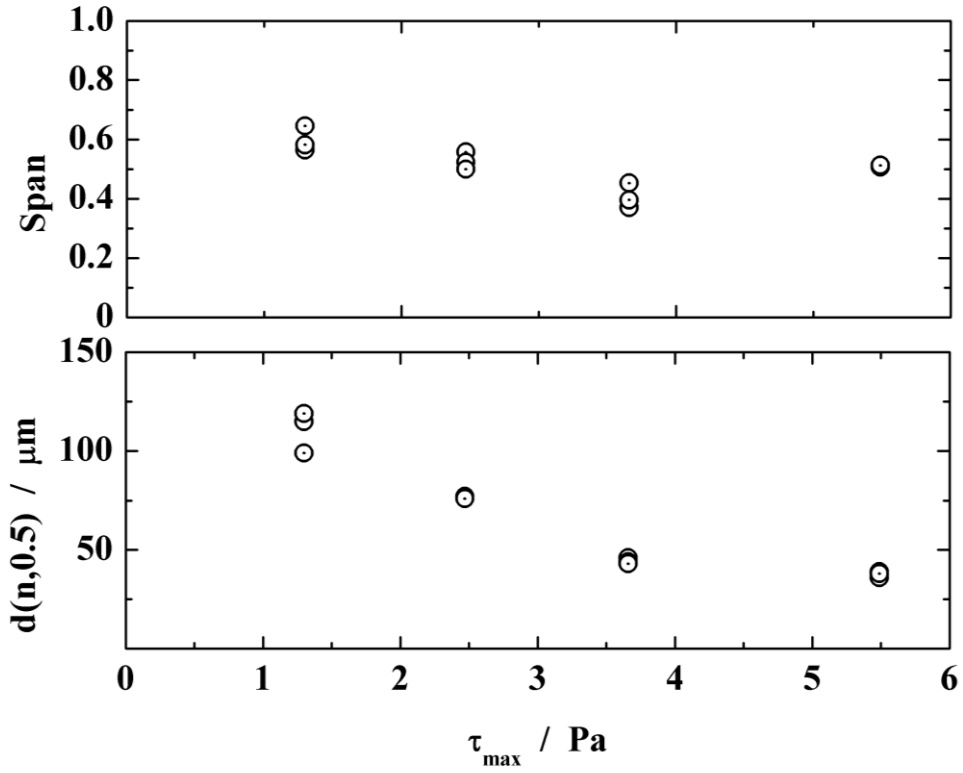

Figure 59 For each peak shear stress three experiments were performed to estimate the reproducibility of results, the frequency was kept constant 15 Hz and transmembrane flux was 30 L m^{-2} h^{-1}.

The influence of the shear condition on the degree of uniformity of the produced droplets is also illustrated in Figure 60, and Figure 61 which also supports the information contained in Figure 59. Optical microscope images are shown in Figure 60 at four values of peak shear stress: 1.3, 2.5, 3.6 and 5.5 Pa. It can be seen that the most uniform droplets are provided at a shear stress of 3.6 Pa, and in Figure 61 it is noticeable that the cumulative distribution curve at this peak shear (a=3.5 mm and f=15 Hz) is also the steepest – indicating the narrowest drop size distribution. Hence, it appears that the narrowest drop size distribution, i.e. lowest span value, is not simply determined by conditions of the highest shear, or lowest shear giving the smallest or largest droplets. It is likely that the most uniform drop distribution is provided by a complex function of all the parameters influencing the process, including: disperse phase injection rate, peak shear, membrane properties and the physical properties of the two immiscible liquids.

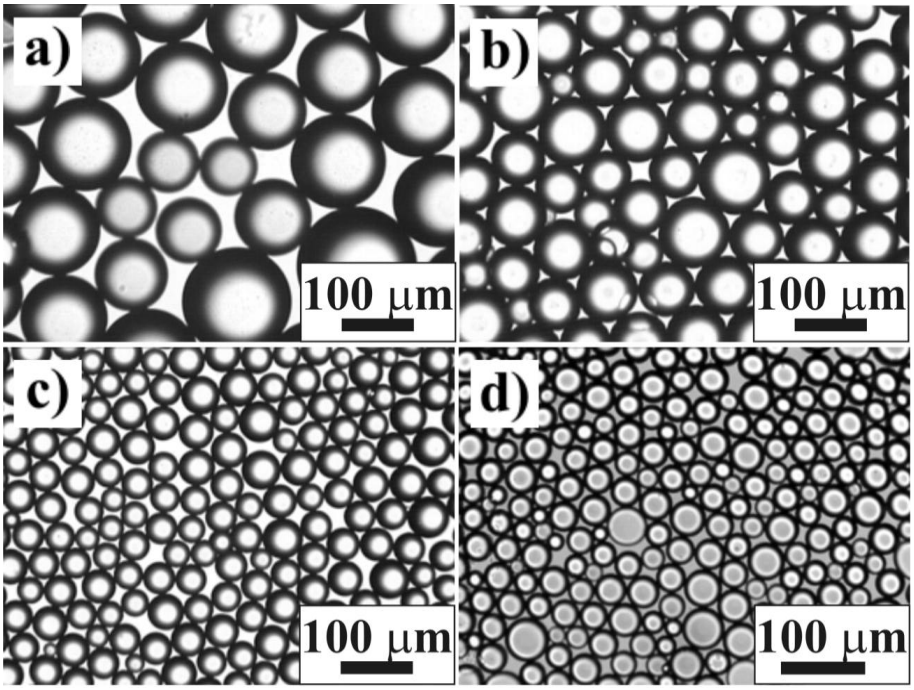

Figure 60 Photographs of emulsions produced by applying different peak shear stresses on the membrane surface is: a) 1.3 Pa; b) 2.5 Pa; c) 3.6 Pa and d) 5.5 Pa, while frequency was kept constant at 15 Hz and transmembrane flux was 30 L m^{-2} h^{-1}.

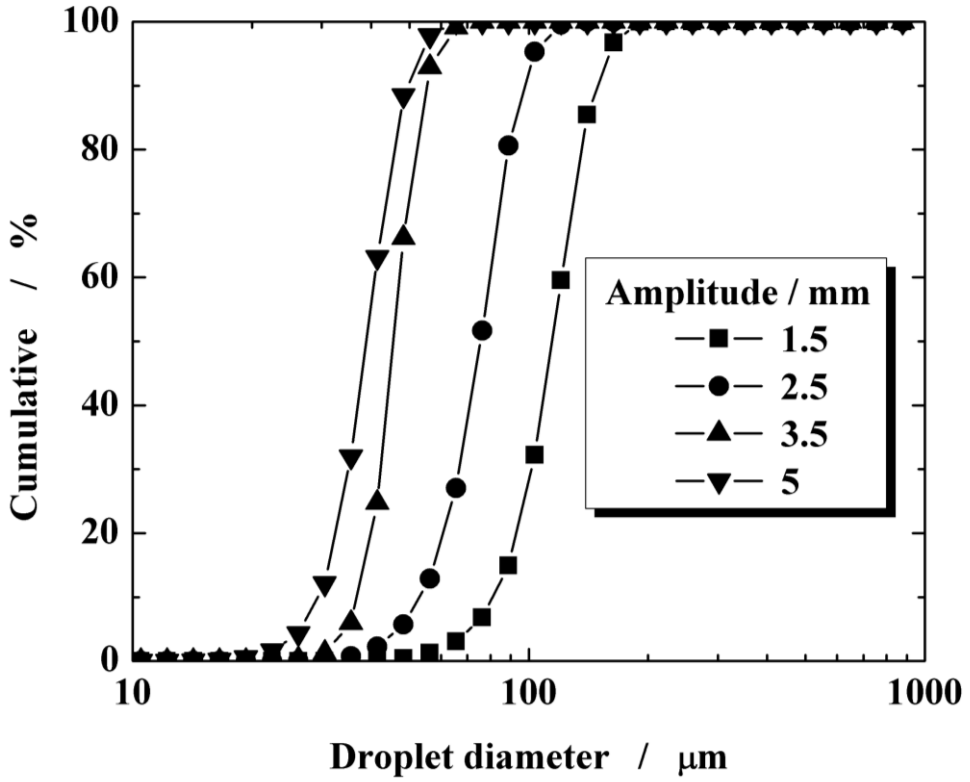

Figure 61 Cumulative distribution curves of produced emulsions presented in Figure 60, with constant frequency of 15 Hz and transmembrane flux of 30 L m^{-2} h^{-1}.

A similar comparison is illustrated in Figure 62, for the Oscillating membrane system. In this figure the curves for Models A and C (τ_{max}) are retained, so that a comparison between the results obtained in the Dispersion Cell (Figure 32) and Oscillating systems is possible – based on conditions of peak shear within either system. When stirring with a paddle stirrer the control of the shear is from the rotation speed of the stirrer, but for the Oscillating system varying shear can be obtained by varying the frequency, or the amplitude of oscillation. The data in Figure 62 records the frequency used to achieve the given peak shear stress and the corresponding amplitude can be estimated from Eqs. 22-24. Under identical conditions of shear stress, a higher frequency is compensated by using a lower amplitude of oscillation, where amplitude is half of the peak-to-peak displacement of the membrane motion. Apart from the very low frequency of 10 Hz, there does not appear to be any significance in the combination of the frequency and amplitude used: the resulting drop size is observed to be a function of the peak shear stress only and not the frequency used to achieve it. Also, there is a significant

difference between the most applicable model for the paddle stirred system, the average shear model, and the results from the Oscillating system. The droplets are significantly smaller than those obtained with the Dispersion Cell. Almost all the results from the Oscillating membrane system are placed between the peak shear model without any correction for neck formation (Model A) and peak shear model with correction for neck formation (Model C (τ_{max})). However, Model C fits the data better – but still does not represent the data well at intermediate values – where the drop sizes are smaller than the predicted ones.

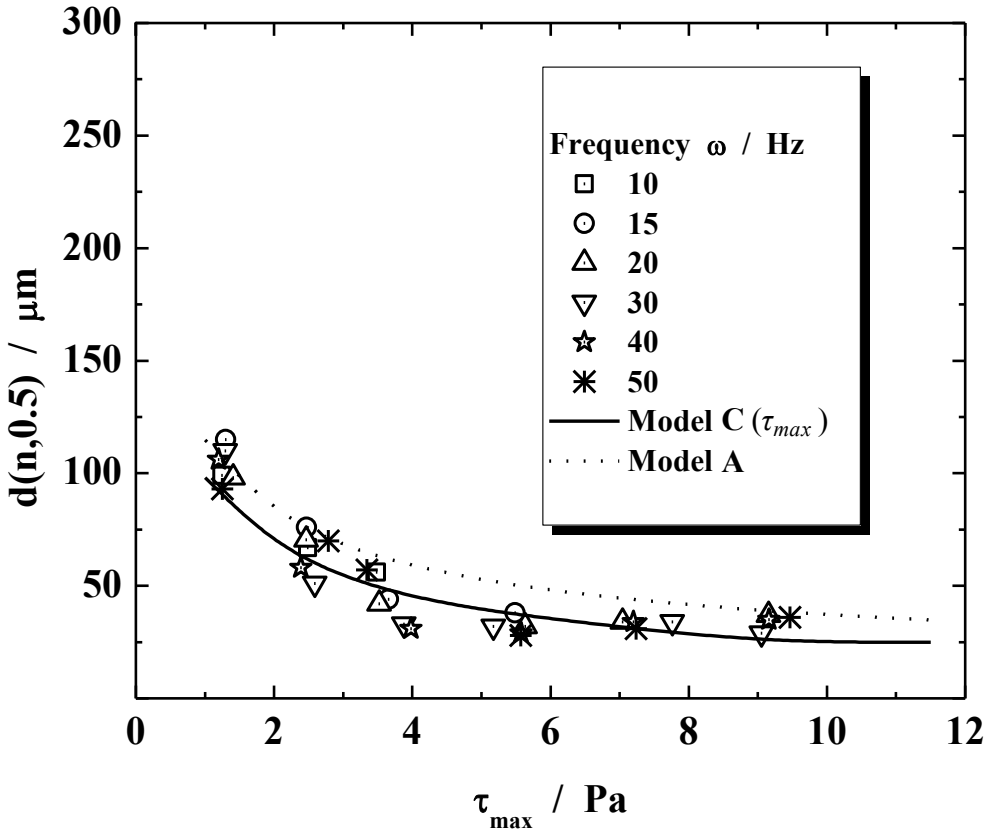

Figure 62 Comparison of experimental drop diameters produced in Oscillating system and predicted values using Model A (Eqs. 10 and 13), in which $\tau = \tau_{max}$ and Model C (Eqs. (17)-(20) and (13)), in which $\tau = \tau_{max}$ with correction for the neck: the values of *d(n,0.5)* were obtained at 30 L m^{-2} h^{-1}. 10 µm membrane, 200 µm pore spacing.

From Figure 62, it is evident that another droplet detachment force or factor supplements the peak shear detachment. As previously discussed, the inertial force is low: two orders of magnitude below the shear force for a 200 µm droplet, and this is consistent with a numerical study provided for high frequency membrane oscillation

(Kelder, Janssen & Boom 2007). However, the study presented here used much lower frequencies: 10 to 90 Hz, and the influence of frequency of oscillation was investigated. Figure 63 shows the median drop diameter as a function of frequency for a constant peak shear stress at the membrane surface. Shear stress is a function of frequency and amplitude, so an increasing frequency will be compensated by decreasing amplitude, in accordance with Eqs. (22) – (24), to maintain the same overall shear stress. It can be seen that the drop size is substantially independent of the frequency of oscillation used, at least for frequencies greater than 20 Hz, but depends on the peak shear stress at the membrane surface, τ_{max}, as anticipated by Models A and C described earlier.

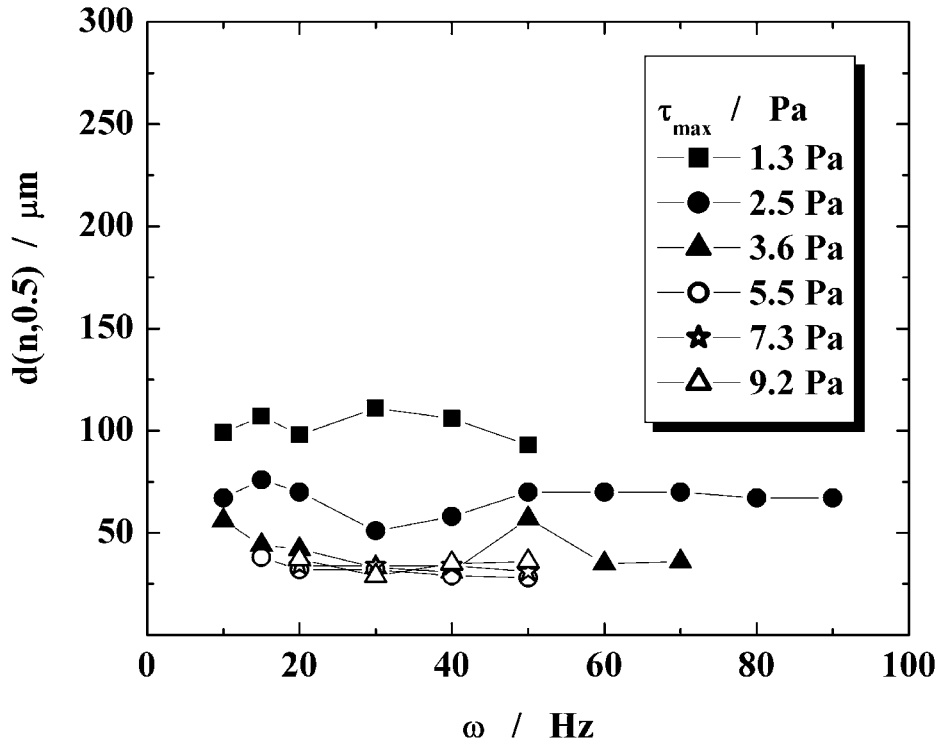

Figure 63 Influence of frequency on median droplet diameter under conditions of constant shear stress: varying amplitude.

In the Oscillating system where the droplets are displaced in two directions: upwards and downwards maximal shear stress model and model which applies maximal shear stress with neck formation are give better predictions.

Figure 64 illustrates how the shear rate varies at the membrane surface at two frequencies: 10 and 50 Hz. The amplitude is 2.61 and 0.2335 mm respectively, providing the same peak shear stress of 1.3 Pa. Also marked on Figure 64 is the average shear rate, as a dotted line, and this can be seen to be the same for the two different

conditions of frequency and amplitude. From Eqs. (22) – (24), the peak shear stress is given by:

$$\tau_{\max} = \omega_f^{3/2} a(\mu\rho)^{1/2} = (2\pi)^{3/2}(2)^{-1/2}(\mu\rho)^{1/2} a f^{3/2} \qquad \textbf{Eq. 54}$$

Therefore, in order to keep a constant peak shear for the two different conditions of amplitude and frequency 1 and 2, it is necessary to satisfy the following condition: $a_1/a_2 = (\omega_{f_2}/\omega_{f_1})^{3/2} = (f_2/f_1)^{3/2}$. This equation is satisfied for the sets of experimental conditions shown in Figure 64. A peak-shear-event will take place twice for every cycle: once during upward movement and again during downward movement. Hence, for the slowest frequency used, 10 Hz, the number of peak-shear-events is 20 per second; or a peak shears every 50 milliseconds. It is possible to compare this with the drop formation time; it is desirable to have a drop formation time in excess of a peak shear event time.

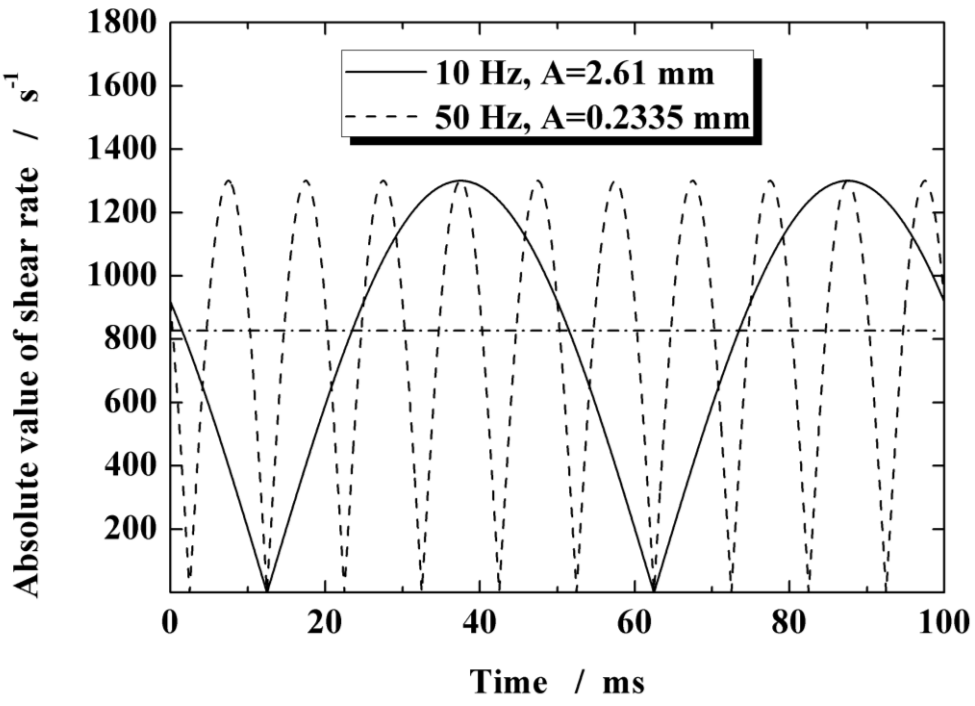

Figure 64 Shear rate with time where the maximal shear stress for both frequencies was 1.3 Pa, the dashed/dot line represents the average shear rate of 828 s^{-1}.

The drop formation time (Eq. (25)) depends on the number of active pores, which is known to be significantly lower than 100% (Vladisavljević & Schubert 2002). However, the number of active pores was not measured. Hence, the drop formation time has been estimated for a range of amounts of active pores, varying from 1% to 50%, and is

reported in Table 10. Eq. 25, based on continuity, was used to estimate the drop formation time for the range of drop sizes illustrated in Figure 62. Table 10 reports both the median by number and the mean by volume of the droplets. The latter spherical diameter is important in the calculation of the drop formation time based on a continuity balance. Drop formation times lower than 50 ms are highlighted in Table 10 in bold italic values. In these cases the formation time is less than the peak-shear time (based on 10 Hz oscillation frequency). Hence, this is not an appropriate frequency to use for the generation of the smallest droplets: median size of 32 μm. This low frequency was not used to generate droplets with this median size. However, it was used to generate droplets with a size slightly greater than 50 μm. At this size, the drop formation time is between 4.9 and 48 milliseconds, depending on the fraction of active pores used by the membrane (from 1 to 10% respectively). Hence, it is likely that the drop formation time is shorter than the peak-shear time under these conditions. This may explain why the median droplet diameter at 10 Hz and a peak shear stress of 3.6 Pa, illustrated in Figure 63, was slightly higher when compared to the other frequencies: i.e. the peak-shear-event time is too long and droplets can form and detach at shear conditions other than the peak value, which gives rise to larger droplets being formed.

Table 10 Droplet formation time from continuity and its dependence on amount of active pores.

		Percentage of active pores				
		1%	5%	10%	15%	50%
$d(n,0.5)$ (μm)	$d(v,0.5)$ (μm)	Droplet formation time, t_d (ms)				
32	34	***0.9***	***4.4***	***8.8***	***13***	***44***
56	60	***4.9***	***24***	***48***	73	240
99	112	***31***	160	310	470	1600
149	194	160	820	1600	2500	8200
198	265	420	2100	4200	6200	21000

5.1.2.2 Influence of the flow rate

Previous work of Egidi *et al.* (2008) showed that very monosized distributions can be obtained when the ―push-off" force is applicable. This occurs when the drop production

rate is large and droplets from adjoining pores may touch each other, leading to a distortion of the drop shape from spherical and an additional force to assist in droplet detachment. This touching between the droplets may also help the droplets grow to the same volume. In the previous work it was noticeable that under constant conditions, apart from dispersed phase injection rate, the drop size increased with injection rate until a certain value was achieved at which the drop size reduced again and the uniformity of the distribution became excellent. That work was performed with a membrane having spacing between the pores of 80 μm. In the work reported here the pore spacing was 200 μm, to ensure that the investigation was limited to that of surface shear and not –push-off". Nevertheless, an investigation of increasing injection rate was performed, to investigate if –push off" could be induced with the Oscillating system. It is worth noting that in the Oscillating system the droplets will be distorting from one direction to the other, rather than simply distorting within a consistent shear field such as that obtained in a stirred system. Clearly, –push-off" will be more likely when generating larger droplets; hence the test was performed for conditions of the lowest shear: frequency of 10 Hz and peak to peak displacement of 1.2 mm. The results are presented in Figure 65.

The dispersed phase flux was varied from 30 to 13900 L m^{-2} h^{-1} and median droplet diameter increased from 180 to 340 μm, falling back to just over 300 μm at the fastest injection rate. The span value (measure of uniformity of the distribution) dropped from 0.75 at the lowest injection rate to 0.5 at an intermediate rate and then up to 0.8 corresponding to the largest drop size, before rising to 0.9 at the fastest injection rate. It is likely that the lower median drop size and poorer span value at the highest injection rate is due to either some degree of jetting, and/or the break up of the larger droplets in the local shear field within the Oscillating membrane system. Given that the pore spacing was 200 μm, then it should be possible that the droplets, which were all greater than this size, could experience some form of –push off". However, the evidence for this is not strong: the span does reach a minimum at an injection rate of between 1000 and 2000 L m^{-2} h^{-1}, but the drop size continues to increase with injection rate until the fastest injection rate is achieved.

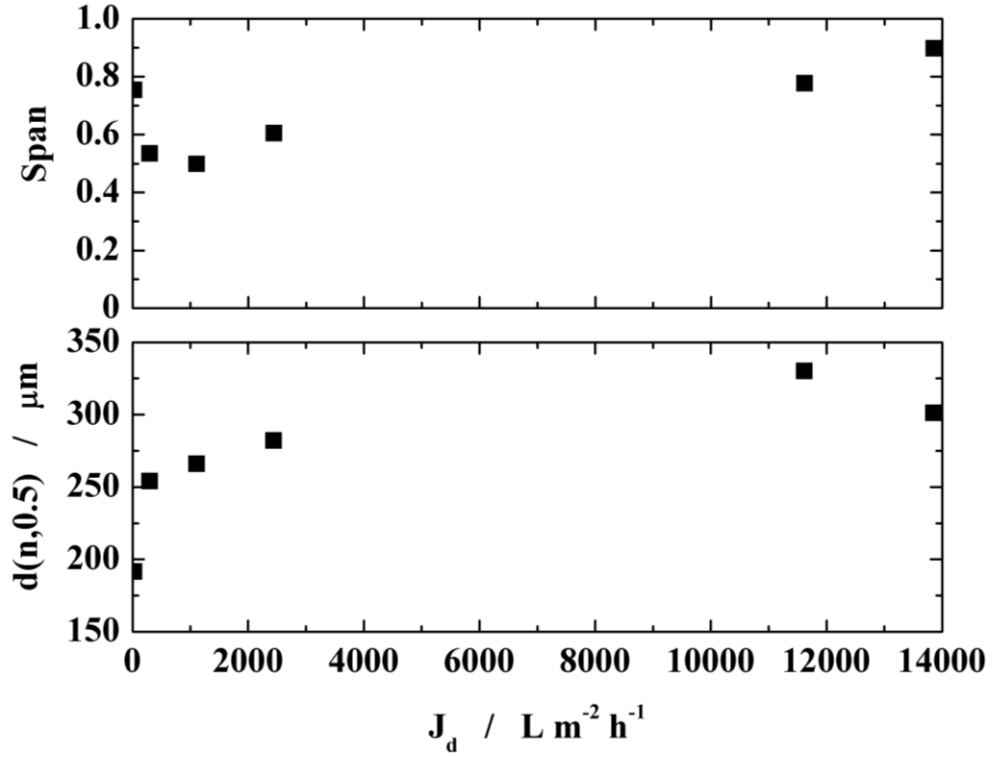

Figure 65 Variation of number based median diameter and span of a droplet size distribution with dispersed phase flux at 10 Hz frequency and peak to peak displacement of 1.2 mm: maximum peak shear stress in all experiments was 0.3 Pa.

5.1.3 Pulsating system

When compared with the Dispersion Cell, using the same conditions of the shear stress more uniform droplets were produced using the Oscillating system. Using the Oscillating system the productivity increased up to 13900 L m^{-2} h^{-1} but the emulsion was produced in a beaker meaning that the process was not continuous. It was possible to predict the droplet size in the Oscillating system using the force balance model based on the maximal shear stress. In the attempt to make a continuous system the horizontal tubular membrane was used in a cross-flow system where, beside the shear of the continuous phase shear, additional shear on the membrane surface was induced by pulsating the continuous phase. Again the system was commissioned using sunflower oil for production of O/W emulsions. Two different lengths of the membranes were used. A membrane with the glassed surface (that does not require wetting agent to increase the hydophilicity) was investigated too.

Having in mind potential industrial application of the system a feasibility test to produce complex coacervates was done.

5.1.3.1 O/W emulsion

5.1.3.1.1 Long membrane

5.1.3.1.1.1 Influence of the flow rate and shear stress

For each condition of peak shear stress two experiments were performed to estimate the reproducibility of results. Figure 66 illustrates the data obtained from duplicate experiments for amplitude of 0.5 mm over the range where the droplet size is a significant function of peak shear stress (Eq. (22)). At each shear condition the results from two experiments are reported as a square and a cross marker. Where only a single marker is visible, it is because the markers all fall onto the same place. The results show that the experiments were reproducible and that there is a set of operating conditions that provide the narrowest droplet size distribution. The most narrow droplet size distribution was obtained at a peak shear stress of 0.1 Pa (amplitude 0.5 mm and frequency 8 Hz), giving a median droplet size on a volume distribution of just above 260 μm.

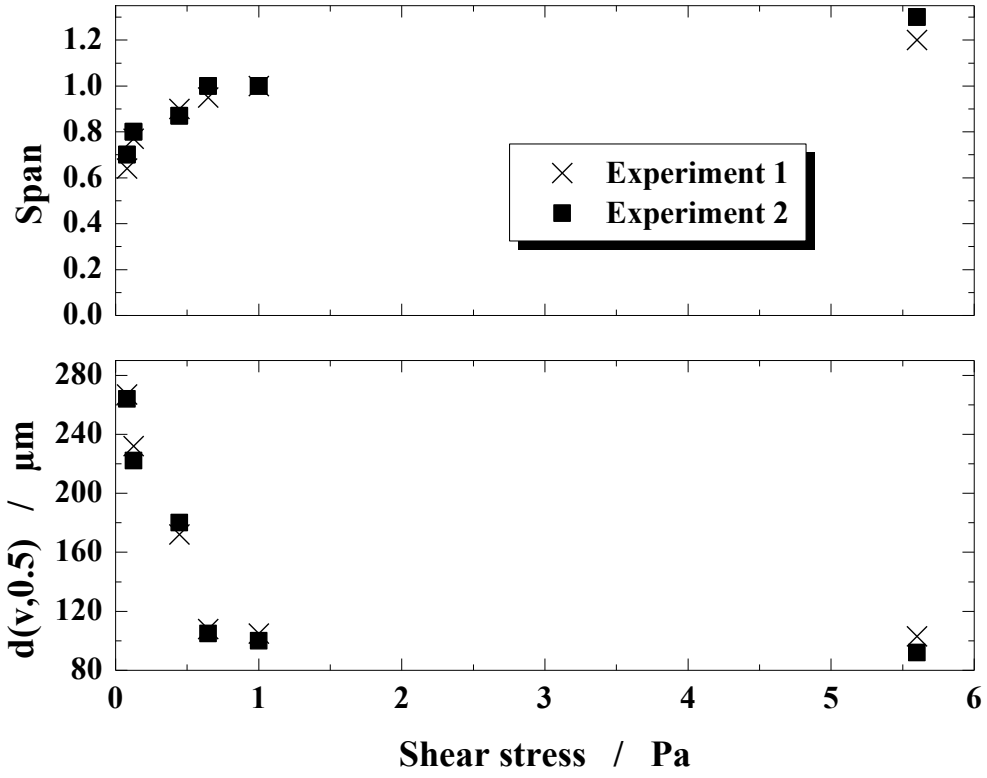

Figure 66 For each condition of peak shear stress two experiments were performed to estimate the reproducibility of results, the amplitude was kept constant 0.5 mm and transmembrane flux was 160 L m^{-2} h^{-1}. Pore size 20 µm and pore spacing 200 µm. Continuous phase flow rate 40 mL min^{-1}. 170 mm long non glassed membrane.

The flux of the dispersed phase and the shear stress are the most effective tools in regulating the droplet size in membrane emulsification. The influence of both of them was also investigated in the Pulsating system. As shown previously in the Dispersion Cell as well as in the Oscillating system, too low or too high flux of the dispersed phase is not suitable for production of the most uniform particles. Figure 67 shows the influence of the dispersed phase flux on the droplet size. With the increase of the dispersed phase flux from 40 to 1000 L m^{-2} h^{-1} the droplet size increased more than 6 times. Values of the span decreased with the increase of the flux but the most uniform droplets were produced using 40 L m^{-2} h^{-1}. Compared to the other systems the flux which gave the most uniform droplets in the Pulsating system was 10 times smaller than the one used in the Dispersion Cell and 20 times smaller compared to the one in Oscillating system. On the other hand the working area of the Pulsating membrane was

3 times greater than the candle membrane in Oscillating system and 10 times greater than the disk membrane used in the Dispersion Cell.

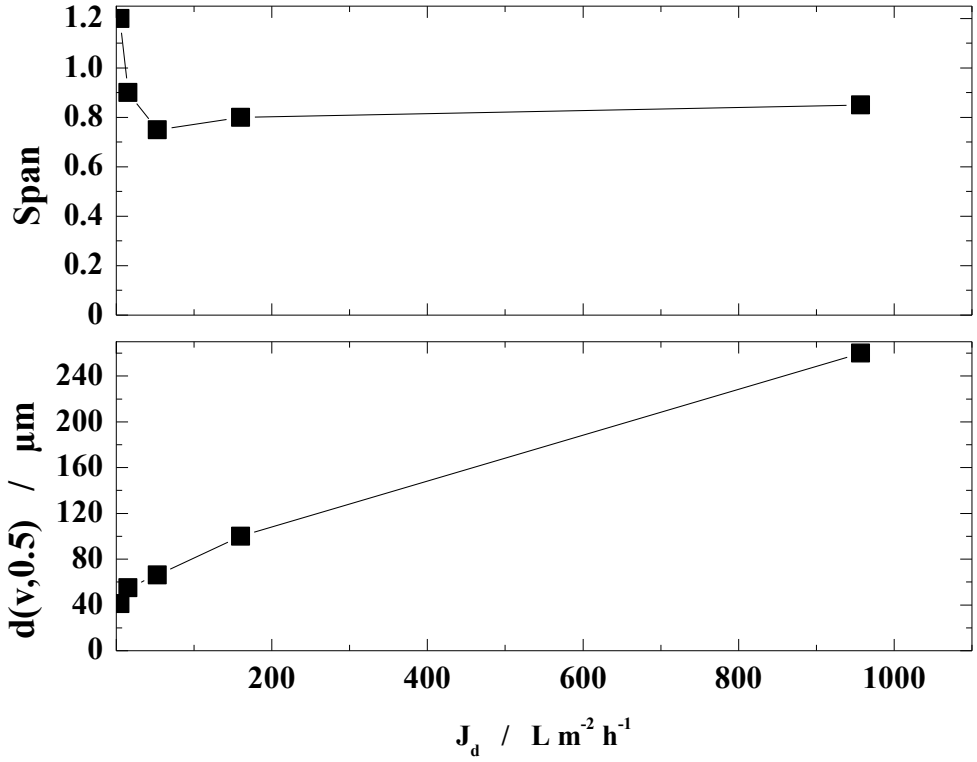

Figure 67 Variation of median diameter and span of a droplet size distribution with dispersed phase flux at 10 Hz frequency and 1 mm amplitude: maximum peak shear stress in all experiments was 0.5 Pa. Pore size 20 µm and pore spacing 200 µm. Continuous phase flow rate 40 mL min^{-1}. 170 mm long non glassed membrane.

The experimental data obtained using two different fluxes of the dispersed phase (40 and 160 L m^{-2} h^{-1}) have been compared with the models for predicting the droplet size and presented in Figure 68. In the experiments amplitude was kept constant (0.5 mm) while the frequency was varied between 8 and 100 Hz, and corresponding values of the shear on the membrane surface were calculated using Equ. (22). From Figure 68 it can be seen that the model that takes into maximal shear stress (Model A) describes well the results obtained using the 160 L m^{-2} h^{-1} while the droplets produced using 40 L m^{-2} h^{-1} drift off from the model implying that there must be an additional force acting on the droplets while formed. It also appears that when the low dispersed phase flux is used, shear did not influence greatly the droplet size. Uniformity of the droplets (span) produced using low dispersed phase flux at any shear was quite consistent and it was

just below 0.7. According to the results it is obvious that in the Pulsating system there could be an additional forces or factors influencing the droplets during the detachment. It is also possible that the membrane itself vibrates, due to its length when the pulsations are applied and therefore bounces the droplet off from the surface.

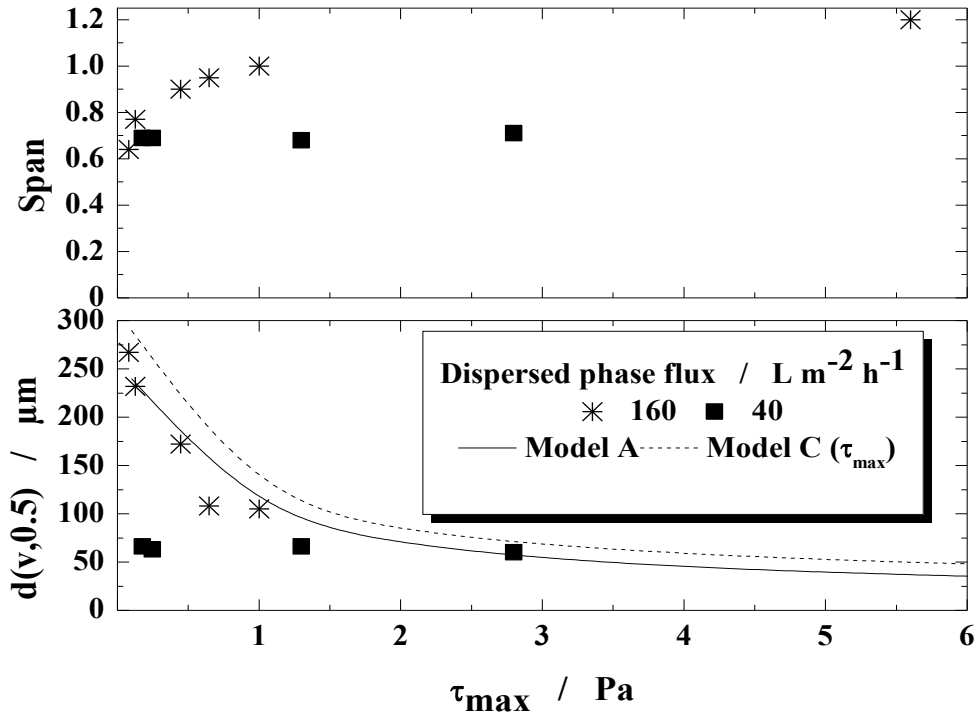

Figure 68 Comparison of the experimental droplet diameters produced in Pulsating system and predicted values using Model A and Model C (τ_{max}) with correction for the neck. a=0.5 mm; Continuous phase flow rate 40 mL min^{-1}. Pore size 20 µm and pore spacing 200 µm. 170 mm long non glassed membrane.

5.1.3.1.1.2 Influence of the membrane surface

The use of the wetting agent (for increasing the hydrophilicity of the membrane) in industrial applications is not very practical since it brings additional preparation step. In order to try to eliminate the need for the wetting agent, as well as to try to bring the values of the span of a droplet size distribution down, a membrane with the glassed surface (that does not acquire the soaking in the wetting agent prior to the experiment) was used and the results obtained from those experiments are presented in Figure 69.

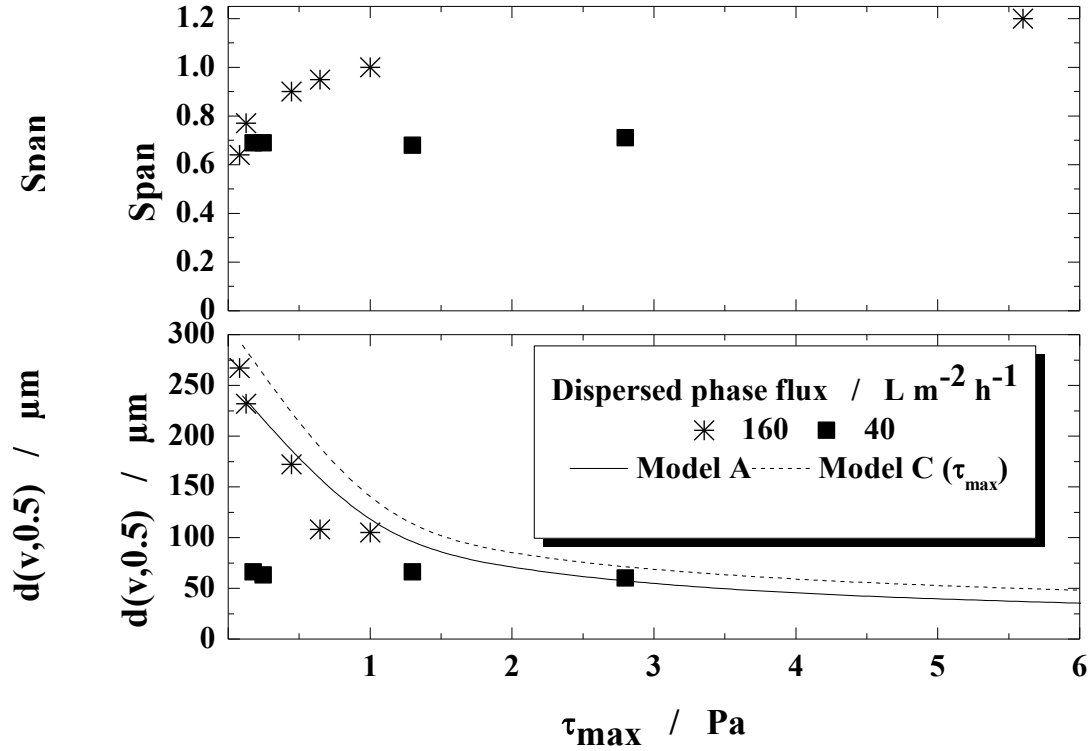

Figure 69 Comparison of the experimental droplet diameters and span of particle size distribution in Pulsating system using 170 mm long glassed and non glassed membrane. a=0.5 mm, continuous phase flow rate 40 mL min^{-1}. 20 µm membrane and 200 µm pore spacing.

An improvement of the span was visible for both fluxes when glassed membrane was used. The membrane with the glassed surface is therefore recommended for the industrial application.

5.1.3.1.2 Short membrane

5.1.3.1.2.1 Influence of the flow rate and shear stress

The span of particle size distribution when long glassed membrane (170 mm) was used in the Pulsating system (Figure 69) was higher than the span values obtained with the Oscillating system (Figure 59) and the Dispersion Cell (Figure 33). In order to investigate the membrane length effect on the uniformity of the droplets the additional experiments were done using the shorter tubular membrane (70 mm long). In Figure 70 results for the shorter membrane are presented. A slight improvement can be noticed compared to the long membrane (Figure 69) but still the Oscillating system appears to be superior providing the most uniform droplets in combination with high productivity

(up to 13900 L m^{-2} h^{-1}). The Dispersed phase flow rate that was used in the Pulsating system in combination with the short membrane, was 5 and 20 mL min^{-1} (corresponding to fluxes of 90 and 360 L m^{-2} h^{-1} respectively) while the continuous phase flow rate was 20 mL min^{-1} a final content of the dispersed phase gave 20 and 50%.

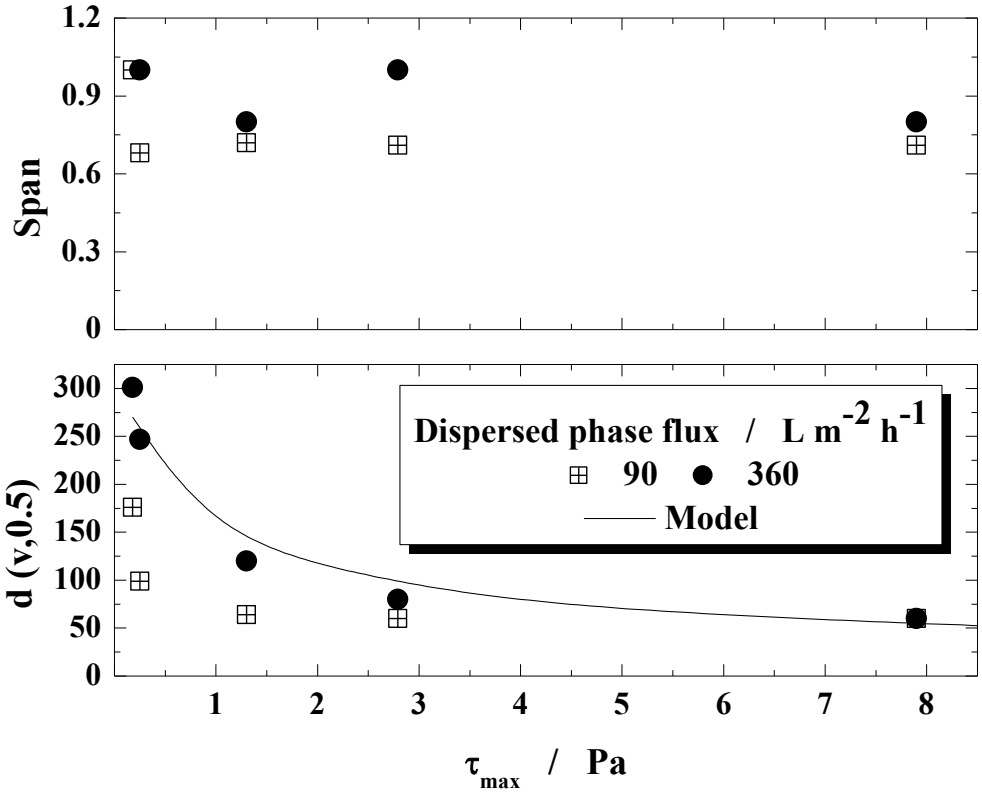

Figure 70 Experimental droplet diameters and span of particle size distribution as a function of shear stress on the membrane surface in the Pulsating system. 70 mm long tubular glassed membrane. Amplitude was kept constant at 0.5 mm while the frequency was varied in the range between 8 and 100 Hz. Continuous phase flow rate 20 mL min^{-1}. 20 µm membrane; 200 µm pore spacing.

5.1.3.2 Complex coacervation

Over the last decade, microencapsulation of functional food ingredients has attracted a great interest, and the coacervation is one of the methods how the microcapsules can be formed. Coacervation consists of the separation from solution of colloidal particles which then agglomerate into separate liquid phase called coacervates (Korus, 2001). Generally, the core material used in coacervation must be compatible with the recipient polymer and be insoluble (or slightly soluble) in coacervation medium. Coacervation can be simple or complex. Simple coacervation involves only one type of polymer with the addition of strongly hydrophilic agents to the colloidal solution. For complex coacervation at least two oppositely charged polymers are used (e.g. gelatine and Gum Arabic). The process is quite interesting especially for the food industry since it does not require surfactant for the stabilisation of the oil droplets. Preliminary test were done to investigate whether the Pulsating system would be suitable for production of complex coacervates and therefore interesting for the food industry. Prior to the test with the Pulsating system batch test was conducted in order to investigate the process of complex coacervation.

The fundamental principle of capsule formation by coacervation relies on electrostatic interactions between oppositely charged hydrocolloids. These interactions will, therefore, depend on the charges themselves, i.e. the net charge carried by both colloids. This in turn, will be modified depending on the pH, the type and amount of the colloids, the ratio of the two colloids (positive vs. negative charges), and the accessibility of the charges for interactions (Leclercq, Harlander & Reineccius 2008). In Figure 71 a general recipe for complex coacervation is given based on the recipes available in the literature (Leclercq, Harlander & Reineccius 2008).

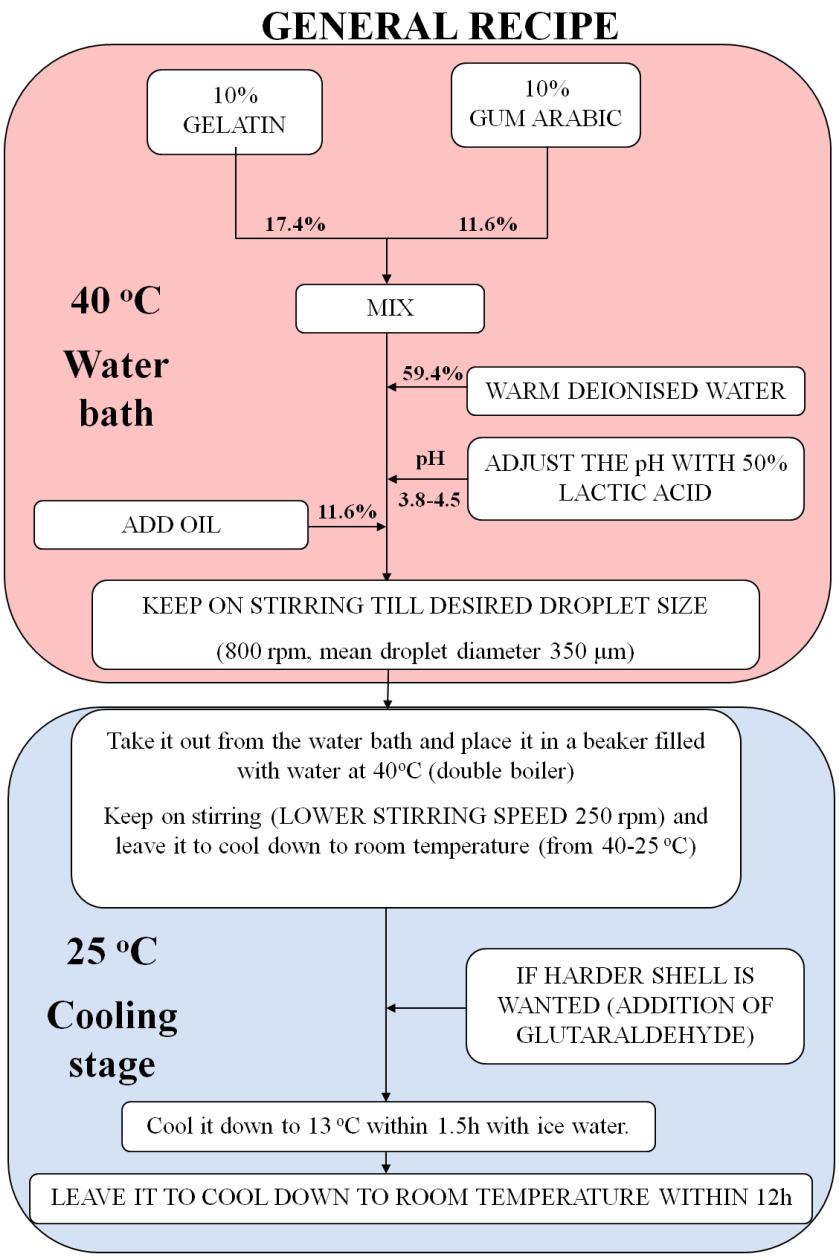

Figure 71 Formulation of the complex coacervates.

5.1.3.2.1 Batch test

According to Leclercq, Harlander & Reineccius (2008), the pH and the cooling temperature after the coacervate production are one of the most critical parameters for the formation of coacervate microcapsules. Due to that, both parameters have been investigated in the preliminary batch experiments. Gelatine type B with an isoelectric point between 4.7 and 5.2 was used in the experiments (Fisher Scientific, UK). The best coacervate yield is noted below the gelatine isoelectric point (Leclercq, Harlander &

Reineccius 2008). The fact that the optimum pH is below the isoelectric point, they explained by hydrocolloids carrying multiple ionizable functional side groups.

Therefore, the isoelectric point of the protein alone is a poor indicator of the charge density of the polymer (Leclercq, Harlander & Reineccius 2008). In addition, pH below the isoelectric point maximizes the surface tension of the gelatine which is critical during the coacervation stage (Leclercq, Harlander & Reineccius 2008). Complex coacervates were prepared when pH of the gelatine and Gum Arabic mixture was adjusted to 3.8 as it can be seen from Figure 72 (b) and (d). When the pH was 4.5 thin shells around the droplets was formed Figure 72 (a) and (c).

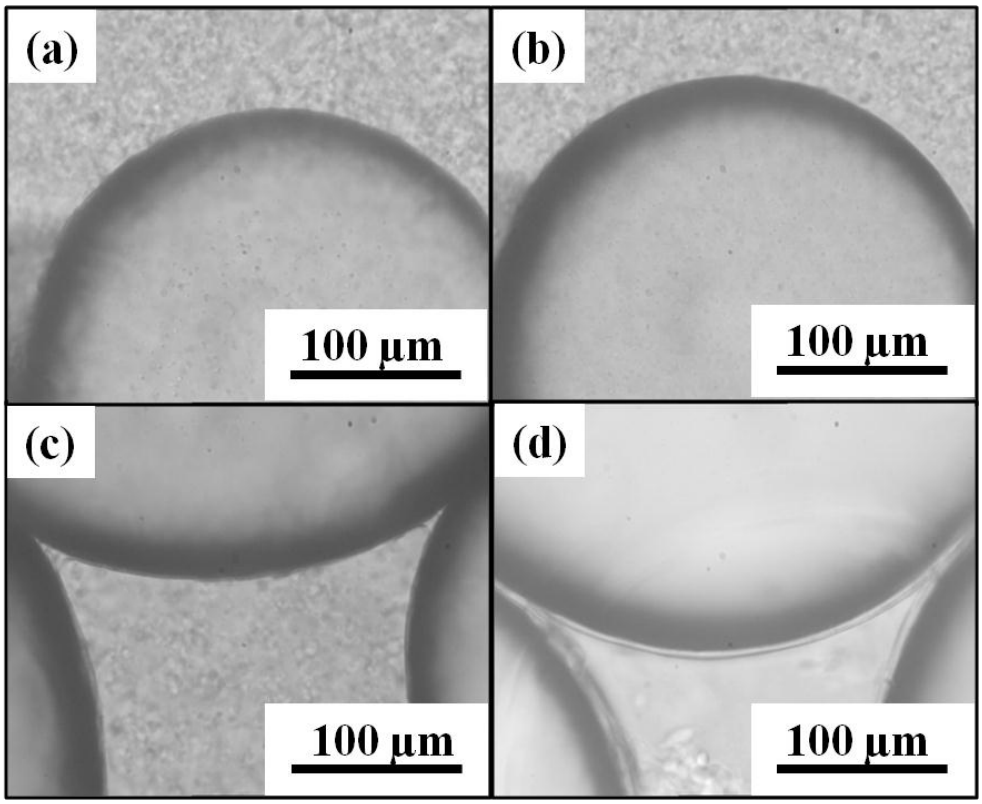

Figure 72 Oil droplets stabilized with the acidified mixture of Gum Arabic and gelatine: (a) pH = 4.5; 5 min after production. (c) pH = 4.5; 80 min after production. (b) pH = 3.8; 5 min after production. (d) pH = 3.8; 80 min after production. Batch experiment: stirring during the oil adding 800 rpm (final coacervate droplet size *d(v,0.5)* = 350 µm); stirring during the cooling stage 300 rpm.

Formation temperature is very important when it comes to the encapsulation of the flavours (losses due to the volatization) but may be of little importance in drug

encapsulation and pharmaceutical applications. Temperature of 40 °C was selected as formation temperature since it allowed maintenance of the gelatine in the solution limiting the volatilization of the volatile compound if dissolved in the oil phase. As mentioned earlier, coacervation occurs when the entangled wall material aggregates around the oil droplets. Therefore the system needs to be cooled down while stirred to 25 °C, at which temperature the colloid material is gelled (Leclercq, Harlander & Reineccius 2008). Fast and slow cooling was checked and temperature profile is given in Figure 73. And it was found that the cooling stage after the production of the coacervates had a significant effect on the thickness of the shell (Figure 74).

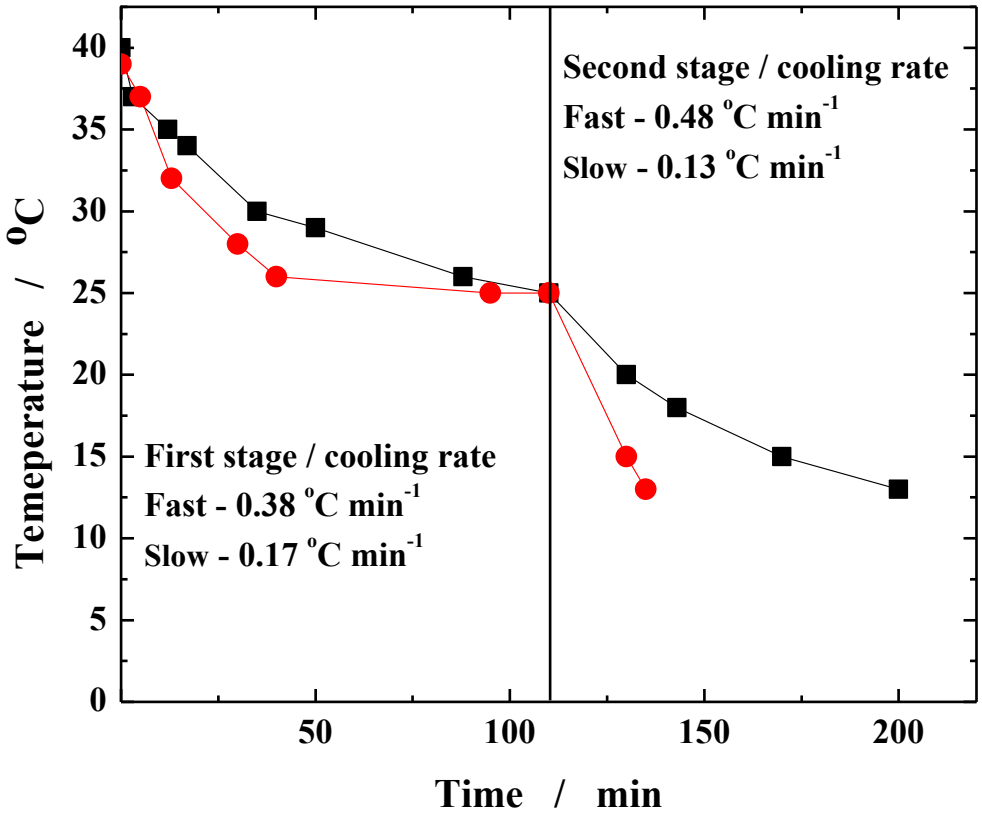

Figure 73 (■) Slow cooling rate. (●) Fast cooling rate. Stirring speed during the cooling was set to 300 rpm.

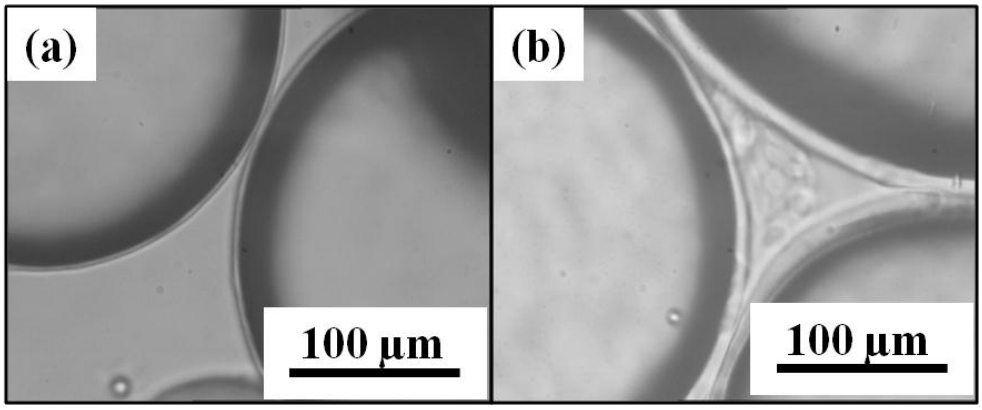

Figure 74 Thickness of the shell when cooling rate was: (a) fast or (b) slow.

From Figure 74 it is clear that the slow cooling rate produces thicker wall around the oil droplet (in some places up to 20 µm). The thicker wall in the case of the slow cooling rate can be explained with the fact that there is more time for the wall material to aggregate properly around the oil droplet. In the case of the fast cooling the wall thickness was less than 5 µm. Even if the oil droplets were left in the solution no increase in the wall thickness was observed. Similar observation was confirmed by Leclercq, Harlander & Reineccius (2008). As it can be seen in Figure 75 when slow cooling was applied and the pH of the solution was 3.8 the wall was successfully formed around the pumpkin seed oil droplets. Similar results were obtained in the case when peppermint oil was dissolved within the sunflower oil.

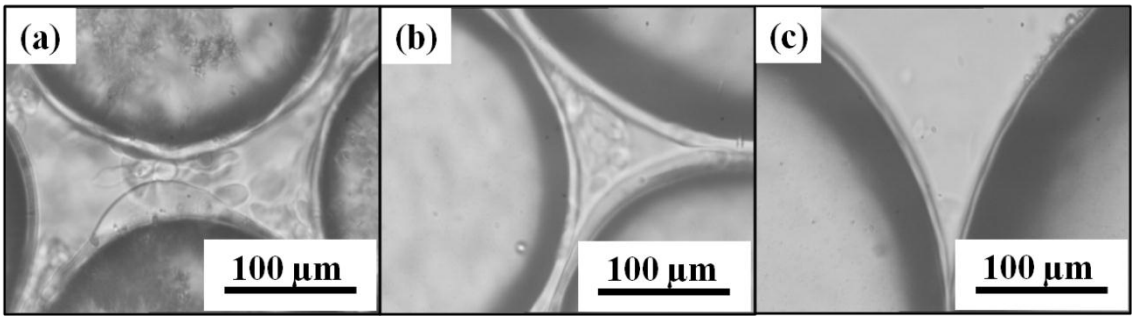

Figure 75 Complex coacervates with: (a) pumpkin seed oil, (b) sunflower oil and (c) 10 wt.% peppermint oil dissolved in sunflower oil.

The firmness of the wall can be increased by adding glutaraldehyde which acts as a crosslinking agent (Leclercq, Harlander & Reineccius 2008). Both complex coacervates produced using pumpkin seed oil, sunflower oil and 10 wt.% peppermint oil were crosslinked using glutaraldehyde (Figure 76).

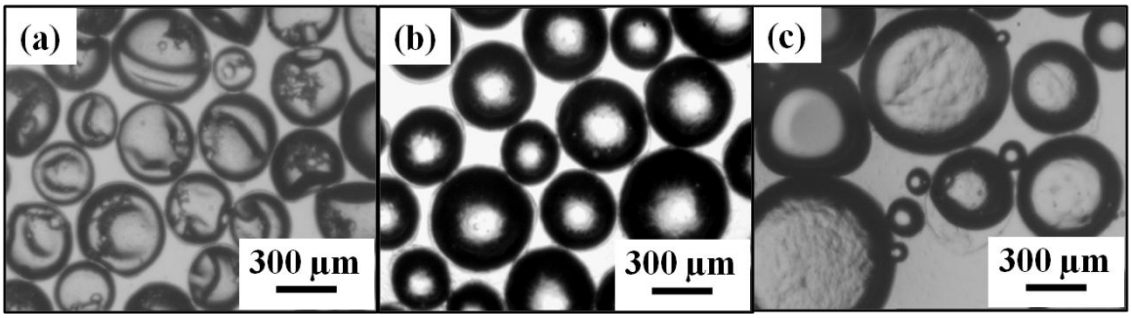

Figure 76 Complex coacervates with added glutaraldehyde: (a) pumpkin seed oil, (b) sunflower oil and (c) 10 wt.% peppermint oil dissolved in sunflower oil.

It can be noticed that the surface of the complex coacervates becomes ruff (corrugated); no matter the oil used (Figure 76). Once crosslinked the complex coacervates were washed with warm water (50 ^{o}C), and it was noticeable that the crosslinked complex coacervates did not burst while the ones that were not crosslinked bursted even when a wall was present.

5.1.3.2.2 Pulsating system

The Pulsating system was tested for production of the complex coacervates that contained 10 wt.% peppermint oil. According to Figure 68 droplets of sunflower oil of about 120 µm diameter can be produced if the shear stress of 0.5 Pa (f = 10 Hz, a = 0.5 mm) is applied in combination with the dispersed phase flux of 160 L m^{-2} h^{-1} corresponding to the flow rate of 20 mL min^{-1} and the continuous flow rate of 40 mL min^{-1}.

The setup of the Pulsating system for complex coacervation is presented in Figure 22. The pH value of the continuous phase was adjusted prior to the experiment to the value of 3.8 and the solution was kept warm at 50 ^{o}C (Figure 71). The reason for the higher temperature in the case of the Pulsating system compared to the batch experiments was just to make sure that when the continuous phase gets into contact with the dispersed phase (within the membrane) it has the temperature of 40 ^{o}C. A lipophilic dye - Nile Red (Sigma Aldrich, UK) was dissolved in the oil phase (10 wt.% peppermint oil dissolved in sunflower oil) purely to enhance the visual detection. Figure 77 (a) shows droplets of dispersed phase (10 wt.% peppermint oil in sunflower oil) produced using the Pulsating system immediately after the production; Figure 77 (b) is a different magnification of the same droplets. After fast cooling and stirring overnight the thin

wall was produced around the droplets (Figure 77 (c)). Produced complex coacervates (after solidification) were analyzed using Malvern Mastersizer S and mean droplet diameter was found to be 125 μm while the span was 0.67. The thickness of the shell was estimated to be 2 μm (as can be seen also from the Figure 77(c)).

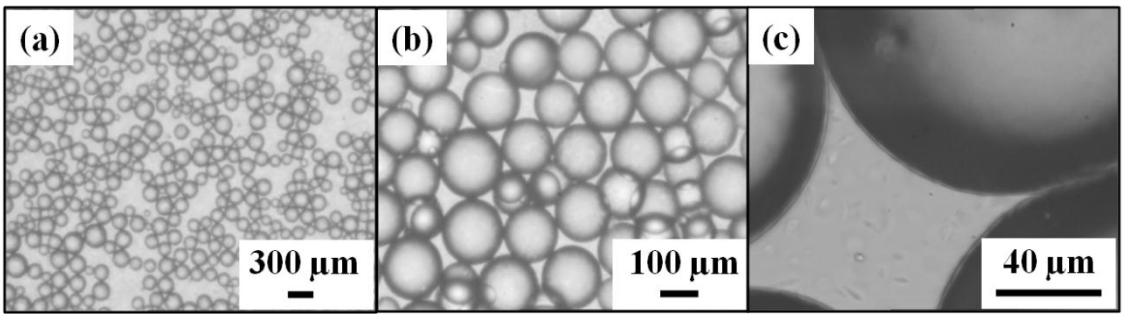

Figure 77 Flux of the dispersed phase 300 L m^{-2} h^{-1} corresponding to the flow rate of 20 mL min^{-1} while the continuous phase (Gum Arabic and gelatin, pH = 3.8) flow rate was 40 mL min^{-1} giving the final content of the dispersed phase to be 20 vol. %. Droplet were produced using the shear stress of 0.25 Pa (f = 10 Hz, a = 0.5 mm). (a) 10 min after the production; (b) 10 min after the production higher magnification; (c) 1 day after the production.

This experiment confirmed that Pulsating system would be applicable for the industrial application and that the model based on the maximal shear stress could be used for the prediction of the droplet size. If a thicker shell around the oil droplet is wanted then the higher control over the cooling step should be applied.

5.2 ION EXCHANGE

As a complementary project, relevant to the use of the functionalized silica particles and especially relevant to nuclear laboratory testing, the Dispersion Cell was used as a continuous stirred system (with slotted microporous filter) for determining the sorption capacity of ion exchange material. It is a technique employing microfiltration and ion exchange (or adsorption), of the engineered particles that could be produced by membrane emulsification. The system was commissioned using commercial ion exchange material DOWEX 50W-X8. Once commissioned, the system was used to test novel ion exchange material (copper hydroxide acetate) for the removal of iodide from water. Functionalized silica particles were also tested using the continuous stirred cell for removal of copper.

5.2.1 Dowex 50W-X8

5.2.1.1 Determination of the equilibrium parameters – batch experiments

Conventional batch sorption experiments require several days to determine the isotherm. Figure 78 shows the experimental results of the batch sorption of copper onto fresh resin at different concentrations of copper. The concentration of $NaNO_3$ in all flasks was 0.2 M which ensured that the resin was converted into Na^+ form and at the same time provided the ionic strength of ~0.2M during the experiment. The Langmuir isotherm (Eq. (4)) was used to fit the experimental data. The equilibrium parameters obtained by fitting are q_m = 0.116 g g^{-1} and b = 0.003 m^3 g^{-1}. The maximal sorption capacity q_m obtained in this work compares with the q_m value stated by the manufacturer (0.154 g g^{-1}) and reported by Awang (2001) (0.116 g g^{-1}) and Sing and Yu (1998) (0.104 g g^{-1}). The Langmuir constant b is very low as compared to 0.13 m^3 g^{-1} reported by Awang (2001) and 0.245 m^3 g^{-1} reported by Sing and Yu (1998), but they used resin in the H^+ form at very low ionic strength (~0 M) and this strongly influences the isotherm, as discussed later. A lower value indicates a lower affinity of copper for sorption.

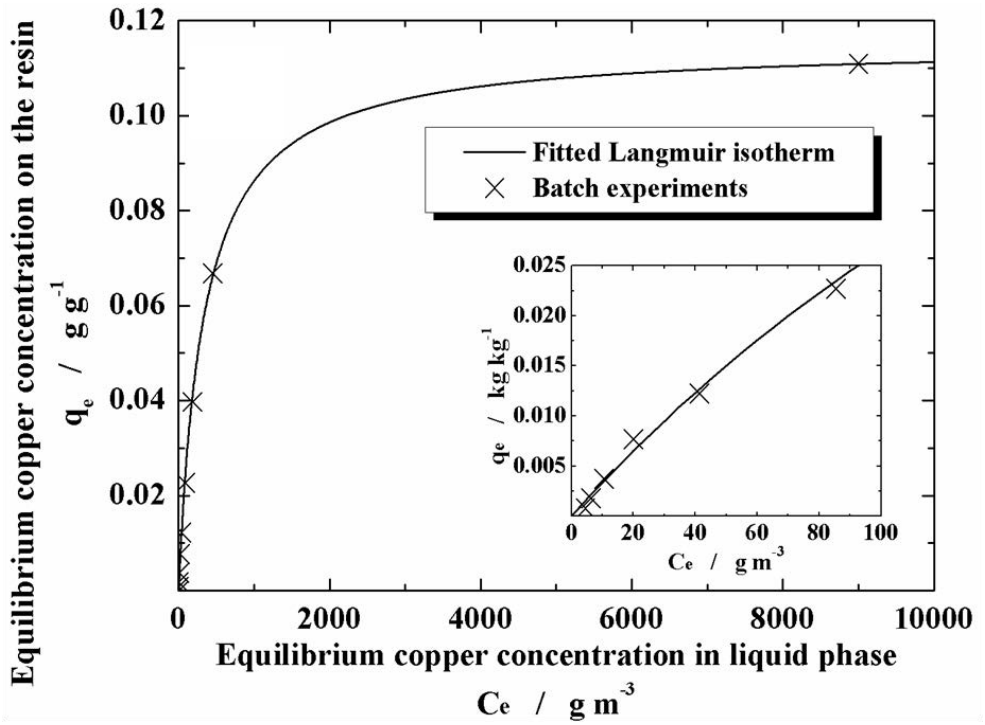

Figure 78 Langmuir isotherm for copper sorption on Dowex 50W-X8 determined by batch experiments. The inset represents the Langmuir isotherm at copper concentrations in the liquid phase below 100 g m^{-3}.

The maximal sorption capacity at high concentrations represented by a plateau on the Langmuir isotherm corresponds to monolayer coverage of the surface by the copper ions and this value can be used to estimate the specific surface area, S of the sorbent (Ho *et al.* 2002). Following equation can be used for estimating the specific surface area:

$$S = \frac{q_m N r_{Cu}^{\ 2} \pi}{M_{Cu}} \qquad \textbf{Eq. 55}$$

where S is the specific surface area of sorbent, N is Avogadro's number (6.02×10^{23} mol^{-1}), r_{Cu} is the empirical radius of copper ion (135×10^{-10} m) (Slater, 1964), and M_{Cu} is the molecular weight of copper ion (63.5 g mol^{-1}).

The specific surface of the Dowex 50W-X8 towards copper binding is 62.39 m^2 g^{-1}. The parameter of Hall R_L, for predicting the exchange efficiency of the process, was also calculated in order to confirm favourability of the sorption process (Hall et. al. 1966):

$$R_L = \frac{1}{1 + bC_o} \qquad \textbf{Eq. 56}$$

The R_L values ranged from 0.95 to 0.36 (for copper concentrations 19 to 625 g m^3). The parameter was lower than 1, which confirmed that sorption process is favourable (Helfferich, 1995). Experiments were done at room temperature.

5.2.1.2 Determination of equilibrium constants - continuous flow stirred cell

The sorption equilibrium parameters can be also estimated from the experiments in the stirred cell with continuous flow of the liquid phase. Comparing two experiments, one with and one without ion exchange resin, in the stirred cell it is possible to determine the amount of copper sorbed providing that the experimental time is long enough to ensure that the equilibrium is reached. In the absence of the ion exchange resin the concentration of copper in the effluent will be equal to that predicted by a continuous flow stirred tank model, validated in Figure 79. However, with ion exchange, or sorption, present in the cell the outlet concentration will be below that of the continuous flow stirred tank model. A mass balance for the continuous flow stirred cell if resin is not present can be expressed as follows:

$$C_o F dt - CF dt = V dC \qquad \textbf{Eq. 57}$$

where $C_o F dt$ represents the mass of copper that enters the cell, $CF dt$ is the mass of copper that leaves the cell and $V dC$ is the mass of copper accumulated in the cell (C_o is inlet concentration, F is flow rate and dt is time interval). If the resin is present in the cell (CST + resin) mass balance for the continuous flow stirred cell is:

$$C_o F dt - C_{IX} F dt = V dC + Acc_{IX} \qquad \textbf{Eq. 58}$$

$C_{IX} F dt$ is the mass of copper that leaves the cell and Acc_{IX} ($= m \frac{d\overline{q}}{dt}$ see Eq. (39)) is the mass of copper that enters the resin. Combining Eqs. (57) and (58) the mass of copper that enters the resin is

$$Acc_{IX} = CF dt - C_{IX} F dt \qquad \textbf{Eq. 59}$$

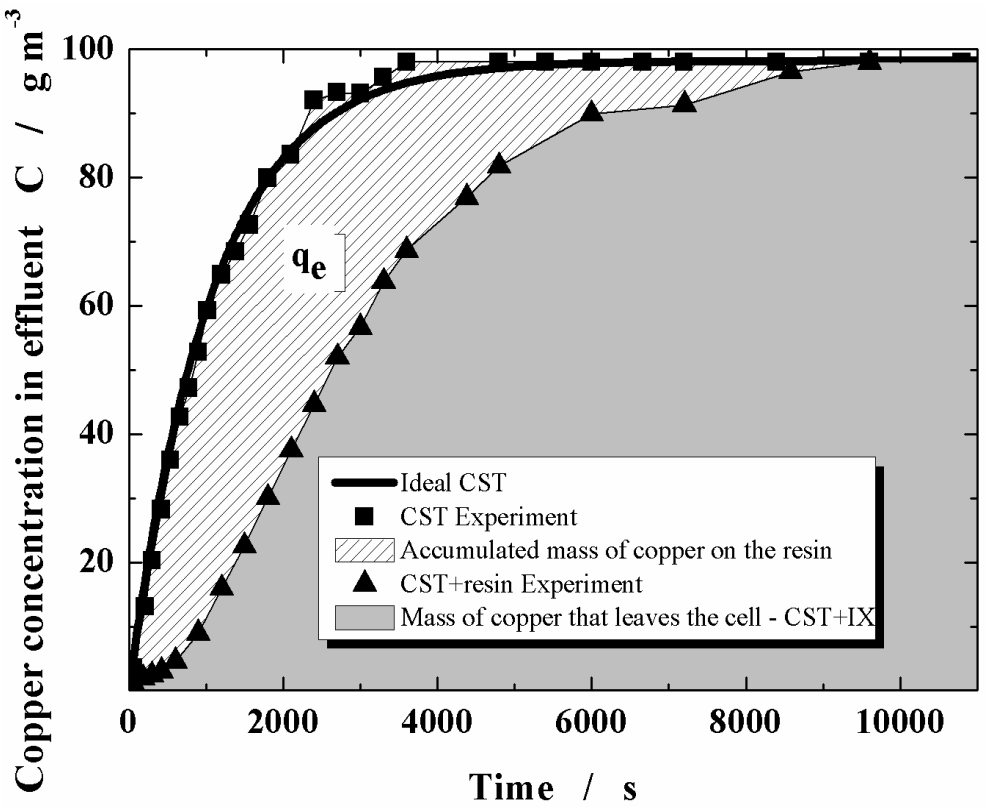

Figure 79 Graphical explanation for calculating the amount of sorbed copper q_e on the resin.

In Figure 79 $\int CFdt$ is the surface under the square marker curve and $\int C_{IX}Fdt$ is the surface under the triangle marker curve. The difference in mass of copper that leaves the cell with and without the resin represents the amount of copper that is sorbed on the resin (q_e) at the equilibrium concentration C_e (i.e. the inlet concentration C_o). In Figure 80 the amount of copper sorbed on the ion exchange resin deduced by this method is compared with the conventional batch experiments for isotherm determination. The equilibrium values obtained in the continuous experiments give the same isotherm as the batch experiments, for both sizes of beads used. The only data point off the single isotherm curve is one obtained when the resin was in H^+ form ($NaNO_3$ was not used therefore the resin maintained the H^+ form) and when background ionic strength was much lower (~0 M), which is consistent with the earlier discussion on literature values of the isotherm at H^+ form at low ionic strength, and the effect of this on mass transfer modelling will be investigated further later.

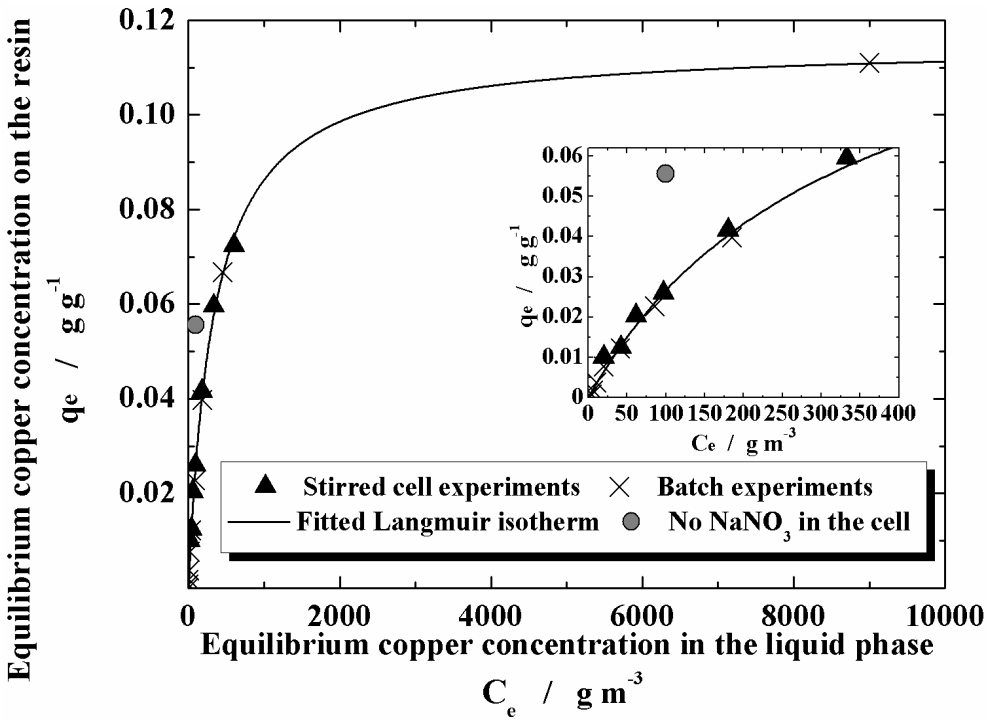

Figure 80 Comparison of the Langmuir isotherm obtained from the batch and the continuous experiments.

5.2.1.3 Effect of initial copper concentration

To study the effect of the initial copper concentration on sorption properties of Dowex 50W-X8 solutions were prepared in the range from 19 to 636 g m^{-3}. Concentration of $NaNO_3$ in all experiments was 0.2 M. The pH of the solutions was adjusted by adding a 0.4 M solution of NaOH, providing a constant pH of 4.5. The liquid flow rate was 7.8 mL min^{-1}. Copper concentration in all feed solutions was high, hence particle diffusion was the limiting step in the mass transfer. Resistance in the fluid phase (*1/k*) for both sizes of the used resins is not more than 5% of total resistance ($1/k+R/D_{eff}$) (for the smaller beads $k = 3.6\times10^{-5}$ m s^{-1} and for the larger beads $k = 3.74\times10^{-5}$ m s^{-1}). As the resistance in the particle R/D_{eff} is more than 95% the simplification used in the calculation of *k* (the slip velocity is equal to the terminal velocity) did not adversely influence the model accuracy. Figure 81 and Figure 82 represent the experimental results for Dowex 50W-X8 together with model curves (Eqs. 30 – 43).

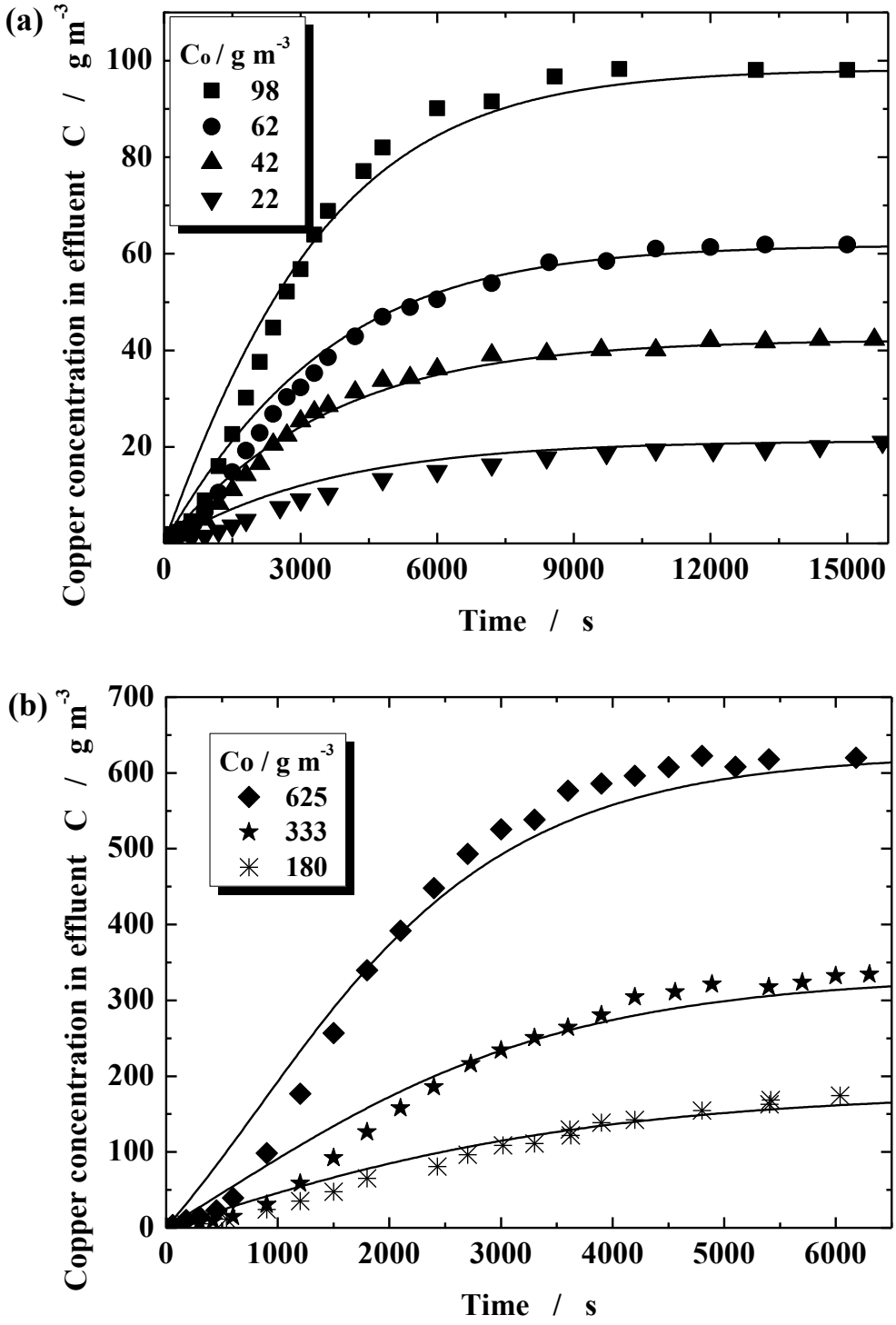

Figure 81 **Small beads (R = 42 µm).** Flow rate $F = 1.3\times10^{-7}$ m^3 s^{-1}. (a) Influence of the inlet copper concentration (22 – 98 g m^{-3}) on the copper concentration in effluent and mass transfer model Eqs. (30) – (43) (solid curves on figure). (b) Influence of the inlet copper concentration (180 – 625 g m^{-3}) on the copper concentration in effluent and mass transfer model Eqs. (30) – (43) (solid curves on figure).

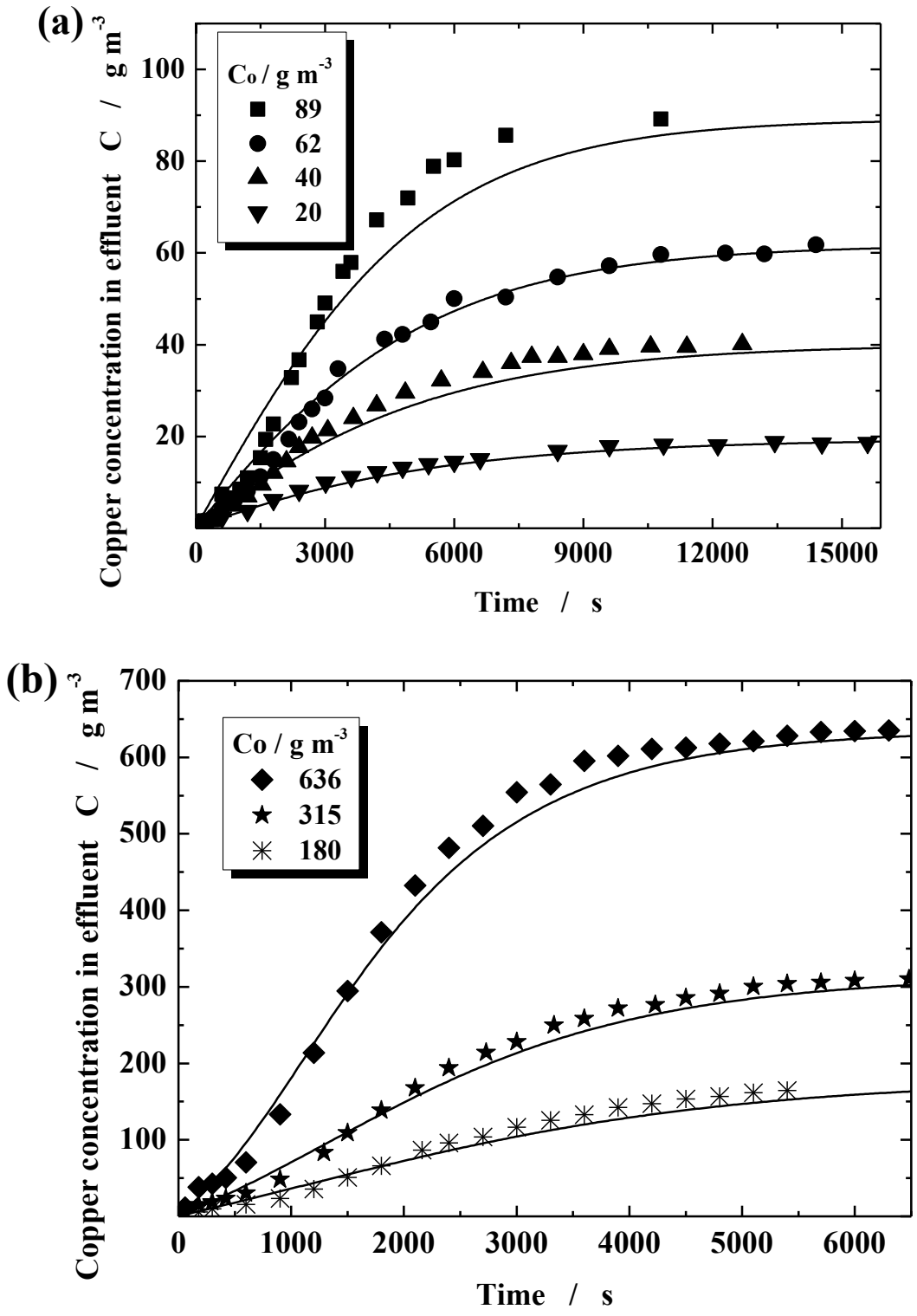

Figure 82 **Big beads (R = 87 µm).** Flow rate $F = 1.3\times10^{-7}$ m^3 s^{-1}. (a) Influence of the inlet copper concentration (20 – 89 g m^{-3}) on the copper concentration in effluent and mass transfer model Eqs. (30) – (43) (solid curves on figure). (b) Influence of the inlet copper concentration (180 – 636 g m^{-3}) on the copper concentration in effluent and mass transfer model Eqs. (30) – (43) (solid curves on figure).

Comparing the model and experimental data, the initial part of the experimental curves of the system showed a better mass transfer than the model predicted meaning that copper removal was more efficient. This type of behaviour of ion exchange beads can be referred to the nature of the ion exchange system: where the resin is converting between the hydrogen and sodium forms. The model assumes a uniform distribution of ion exchange sites within the bead; whereas it is most likely that the outer part of the bead has a higher number of sites than the inner part of the bead, a likely consequence of bead production, and contributing to the initial more efficient copper removal. The effective diffusion coefficient of copper inside the particle, D_{eff} that gave the best fit of the experimental results was 7×10^{-11} m^2 s^{-1}, used for both small and big beads and at all the copper concentrations used in this work.

When tried to minimise the number of experiments to determine the mass transfer parameters (effective diffusivity in the particle), care has to be exercised over the experimental conditions selected. For example, Figure 83 illustrates the mass transfer from 100 g m^{-3} copper solution into Dowex modelled by four different diffusion coefficients. Using the experimental data, a diffusivity of 10^{-13} is clearly incorrect, but under the experimental conditions selected there is a little difference in the model result for diffusivities from 10^{-12} upwards. The reported effective diffusivity of 7×10^{-11} m^2 s^{-1} has been deduced by modelling the wide range of experimental conditions tested.

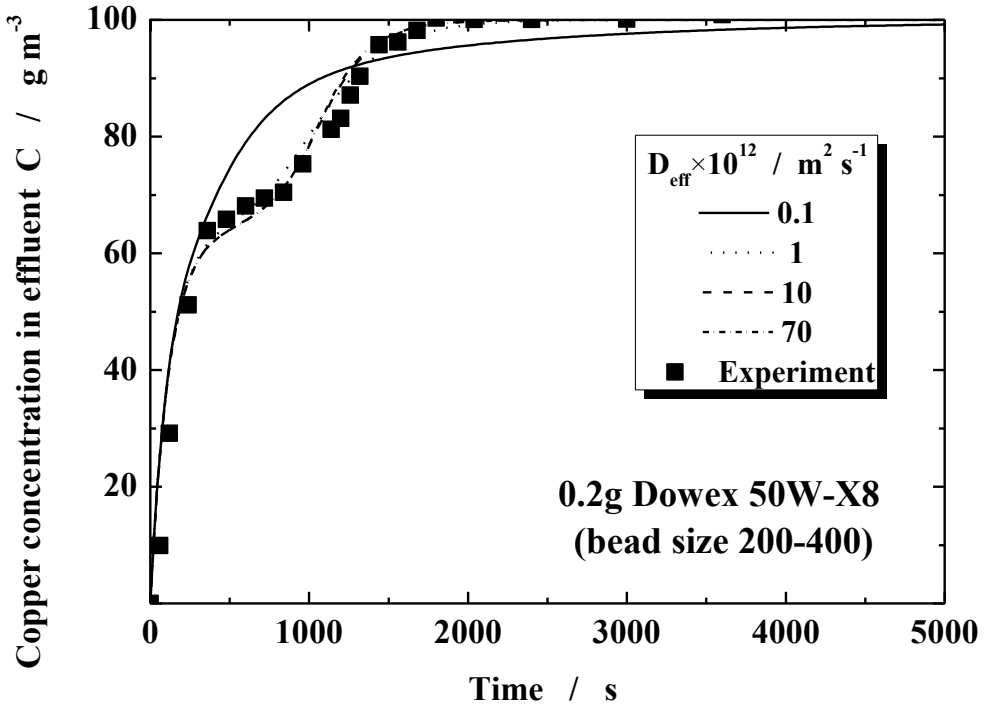

Figure 83 Influence of effective diffusivity on the shape of the mass transfer model curves (Eqs. 30 – 43, curves on the figure). Inlet copper concentration (100 g m^{-3}) – Small beads (R =42 μm). Flow rate F = 7.7×10^{-7} m^3 s^{-1}.

Using this technique for general IX studies it may be that tests at high concentration are required for isotherm determination and other tests are more appropriate for mass transfer analysis. However, model testing and verification should be achieved with all the tests.

The model is also quite valuable when predicting the performance of the beads with different sizes. At the beginning of the process, small beads have a better performance since the interfacial area and diffusion gradient is higher. However, after 3000s the diffusion gradient for both beads is the same since (crossing of model curves on Figure 84) the small beads have more uniform copper distribution hence the driving force for mass transfer (concentration difference) will decrease; in the big beads due to the greater distance to the bead centre, the concentration gradient will be higher leading a to a better performance at a longer period of time. At saturation, the same amount of copper is sorbed for both beads types.

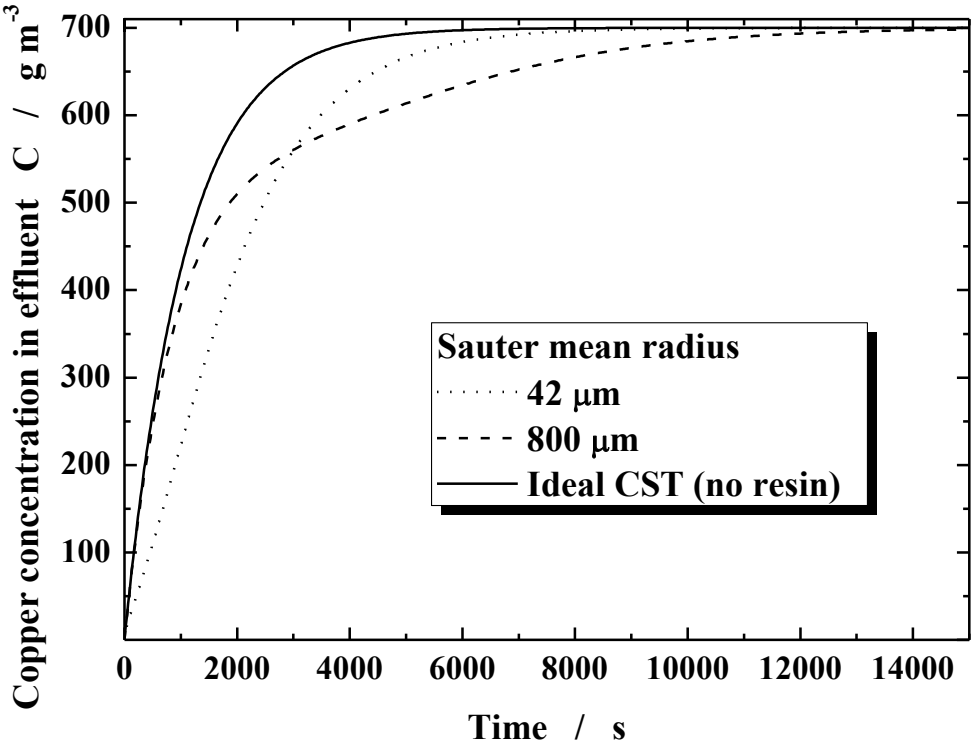

Figure 84 Influence of bead size on copper concentration in effluent (model). Constants used in modelling are: q_m = 0.116 g g^{-1}; b = 3 m^3 kg-^{1}; m = 1g; F = 1.3×10^{-7} m^3 s^{-1}; V = 0.14×10^{-3} m^3; R = 800×10^{-6} m or 42×10^{-6} m; μ = 0.001 Pa S ρ_s = 1443 kg m^{-3}, ρ = 1000 kg m^{-3}, D_{liq} = 1.2×10^{-9} m^2 s^{-1}.

Equilibrium parameters (q_m and b) as well as effective diffusivity (D_{eff}) obtained with the continuous stirred cell were used to model the sorption of copper in the fixed bed 10 cm high column (Sigma Aldrich, UK). The breakthrough curve for copper/Dowex system in a fixed bed column together with several model predictions is presented in Figure 85. Prediction of the concentration in the effluent used the fixed bed shock and saturation model, Glueckauf‘s model (Helfferich 1995) and a model that treated the fixed bed as a series of stirred tanks. As seen in Figure 85, the shock and saturation models did not predict the breakthrough curve, but did the starting and the end points of the curve. Such prediction is expected since the models do not take into consideration film or particle diffusion, only equilibrium data obtained from the isotherm. Glueckauf‘s model is based on the concept of ~~–e~~effective plates”. The plate height is calculated from the fundamental data and the model takes into consideration film and particle diffusion. The model gave quite good prediction of the lower part of the breakthrough curve but failed to predict closer to saturation.

Another model used was based on a series of identical continuous stirred cells. For the purposes of the modelling the bed was split into sections and each section was modelled as a stirred cell using Eqs. (31) and (43) had to be modified:

$$\frac{\varepsilon_b V_{bed}}{N}\frac{dC_i}{dt} = F(C_{i-1} - C_i) - \frac{m}{N}\frac{d\bar{q}_i}{dt} \qquad \textbf{Eq. 60}$$

ε_b is bed porosity (ε_b = 0.5 (Helfferich 1995)), V_b is bed volume, N is number of column sections (identical stirred cells) used in the model (N = 11) and i is bed section (i = 1,N). As it can be seen from Figure 85, the model gave a good prediction of the start and the end of the breakthrough curve using the mass transfer and equilibrium parameters obtained from the experiments in the stirred cell.

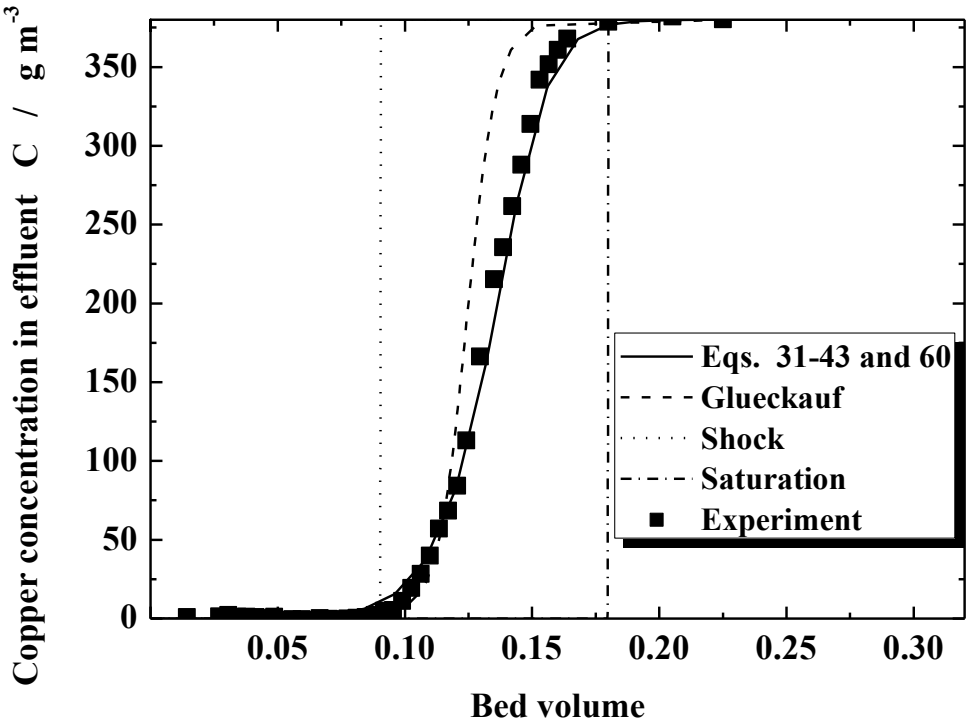

Figure 85 Breakthrough curve together with the different models predictions. Inlet copper concentration (380 g m^{-3}) – 3g of big beads (R = 87 μm). Flow rate F = 1.2×10^{-7} m^3 s^{-1}; pH = 4.5; ionic strength 0.2 M. Column Internal diameter×Length=1×10cm.

5.2.1.4 Effect of $NaNO_3$

The influence of $NaNO_3$ on copper sorption was also investigated. As a background for adjusting the ionic strength $NaNO_3$ was used coupled with adjusting the pH inside the

cell. In all experiments the buffer ionic strength of 0.2 M was maintained, so that during all experiments the variation in ionic strength due to ion exchange was less than 5%. Such a small change of ionic strength *I* during all experiments allows the assumption that activity coefficients are constant, hence concentration is used instead of activities in all modelling.

$$I = 0.5\sum_{i}^{n} C_i z_i^2 \qquad \textbf{Eq.61}$$

where C_i is the molar concentration of the ion *i*, z_i is the charge of the ion *i* and *n* is number of *i* ions present in the solution. A set of experiments in the stirred cell were performed in order to monitor the influence of sodium on the sorption of copper ions on the ion exchange (Figure 86). Inlet solutions contained different amounts of $NaNO_3$. A significant reduction in the sorption of copper was observed with an increase of $NaNO_3$ content in the inlet solution. The influence of $NaNO_3$ on copper sorption on the resin can also be seen on Figure 80, where one experiment in the continuous stirred cell was done without $NaNO_3$ in solution. When $NaNO_3$ was not present in the solution a much higher amount of copper was sorbed onto the resin.

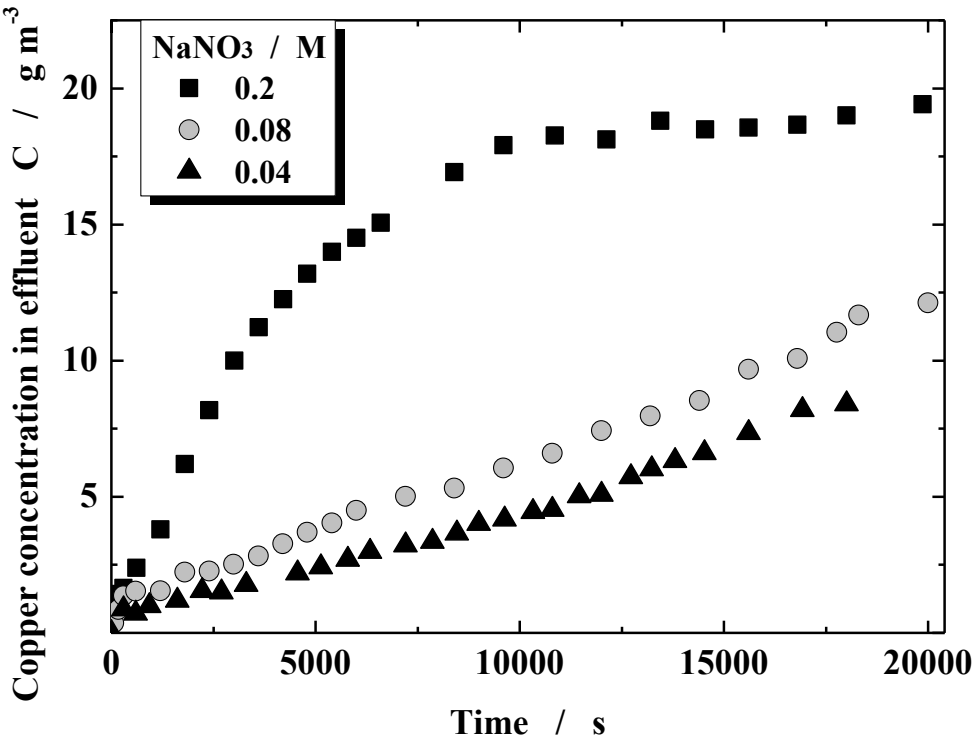

Figure 86 Influence of $NaNO_3$ on copper sorption on to Dowex 50W-X8. Inlet copper concentration in all experiments was 20 g m^{-3}.

To determine if there is a competitive sorption of sodium ions on the surface of the ion exchange resin the sorption of sodium ions was monitored. For this purpose the same samples from batch experiments used for determining the Langmuir isotherm were investigated. The samples were analysed before and after the sorption and a few results are presented in Table 11. In all cases reported in Table 11 the sodium concentration is higher after the batch isotherm experiment compared to before, due to the addition of sodium hydroxide for pH control (to maintain pH = 4.5). The amount of extra sodium matches that added. Hence, it can be concluded that sodium did not exchange onto the resin under the experimental conditions, and any influence of the sodium nitrate concentration on the copper extraction is probably due to decreasing copper ion activity with increasing ionic strength.

Table 11 Copper and sodium concentrations in the flasks during the batch experiments.

Equilibrium copper concentration	**Sodium concentration / g m^{-3}**	
q_e / g m^{-3}	**before sorption**	**after sorption**
10	3770	3980
230	3670	3990
430	3680	3870
870	3760	3990

5.2.2 Copper hydroxide acetate

Once the stirred cell was commissioned for determining the ion exchange capacity as well as mass transfer properties it was possible to use it to determine the properties of any ion exchange material. a A novel material, copper hydroxide acetate (Cu-Ac) produced by the Department of Chemistry (Loughborough University) was selected; no sorption capacity data nor mass transfer properties were available. The amount of the material was just a few grams therefore the experiments had to be carefully planned. Figure 87 shows the results from the batch experiments to determine the equilibrium parameters of the Cu-Ac.

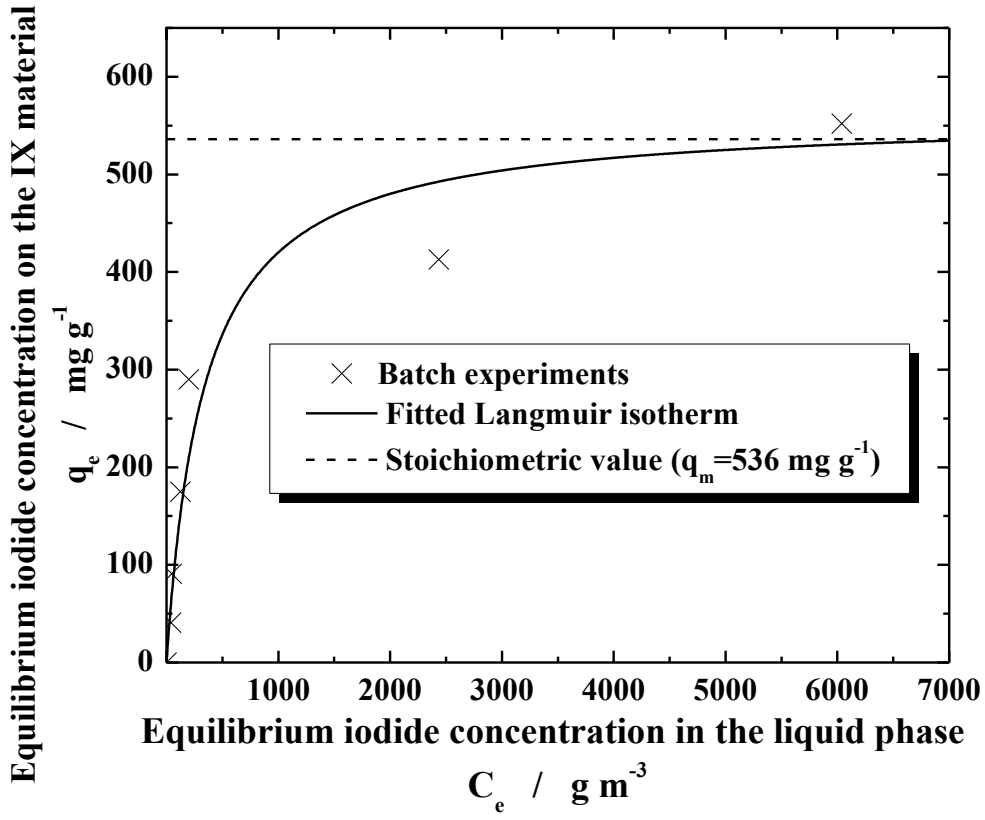

Figure 87 Langmuir isotherm for iodide sorption on Cu-Ac determined by batch experiments.

The Langmuir isotherm Eq. (4) was used to fit the experimental data, and the equilibrium parameters obtained by fitting are: q_m = 0.530 g g^{-1} and b = 0.003 m^3 g^{-1}. The q_m value obtained with the batch experiments compares well with the stoichiometric value (S) for iodide in reaction with Cu-Ac according to Eq. 62 ($S=M(I)/M(Cu_2(OH)_3CH_3COO=127/237 = 0.536$ g g^{-1})

$$Cu_2(OH)_3CH_3COO + KI \rightarrow Cu_2(OH)_3I + CH_3COOK \qquad \textbf{Eq. 62}$$

The equilibrium parameters were also determined using the stirred cell with continuous flow as described in Chapter 5.2.1.2. Figure 88 represents the case when initial iodide concentration was 2000 g m^{-3}.

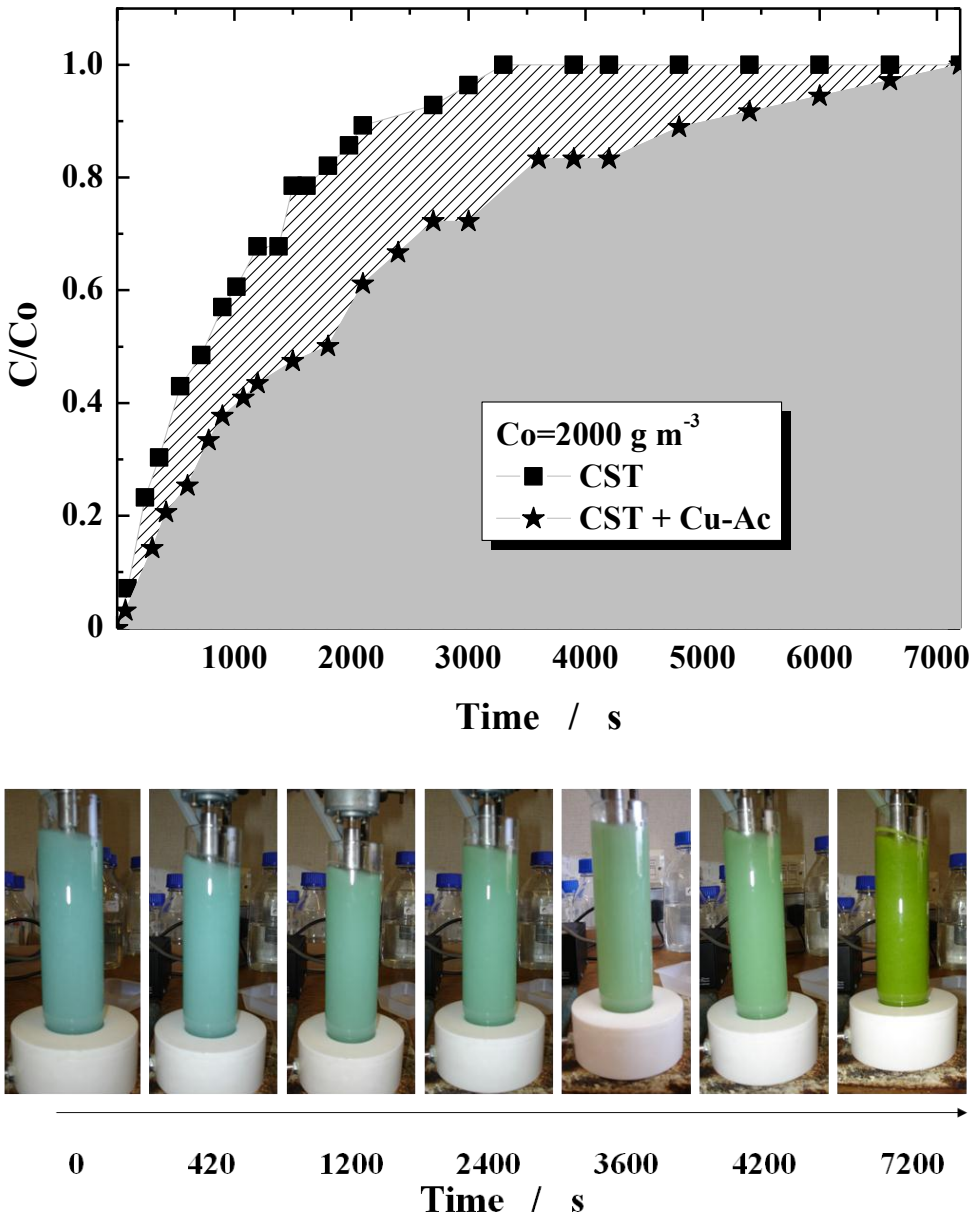

Figure 88 Graphical explanation for calculating the amount of sorbed iodide q_e on the resin and colour change of Cu-Ac with the progressing of the reaction.

It is interesting to notice that as the reaction progresses the Cu-Ac changes to Cu-I and the colour changes from blue to green. In Figure 89 the amount of iodide sorbed on the Cu-Ac, deduced by the method using the stirred cell, is compared with the conventional batch experiments for isotherm determination. Two points (one stirred cell and one batch experiment) are greater than stoichiometric value and a possible explanation for such behaviour might be that beside chemisorption physorption could take place.

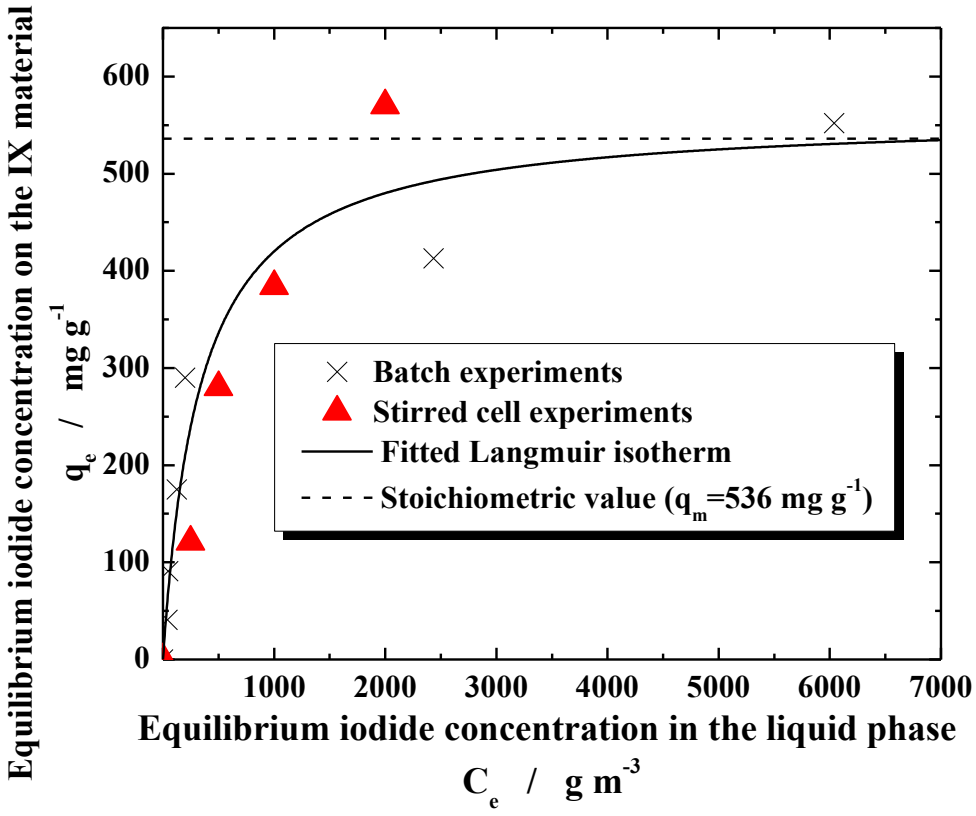

Figure 89 Comparison of the Langmuir isotherm obtained from the batch and the continuous experiments.

To study the effect of the initial iodide concentration on iodide sorption on Cu-Ac iodide solutions were prepared in the range from 250 to 2000 g m^{-3}. The pH was not regulated and in all experiments it was 6.3. The liquid flow rate was 7.8 mL min^{-1}. Iodide concentration in all feed solutions was high and the particle diffusion was the limiting step in the mass transfer. Figure 90 represents the experimental results for Cu-Ac together with model curves (Eqs. 30 – 43). The effective diffusion coefficient for iodide that gave the best fit of all experimental results was D_{eff}= 7×10^{-17} m^2 s^{-1}.

As it can be seen in Figure 31 Cu-Ac particles are not as uniform as Dowex 50W-X8 (Figure 25), Sauter mean diameter for Cu-Ac was 10 µm (obtained using Malvern) and Figure 91 shows the sensitivity of the model on the particle size.

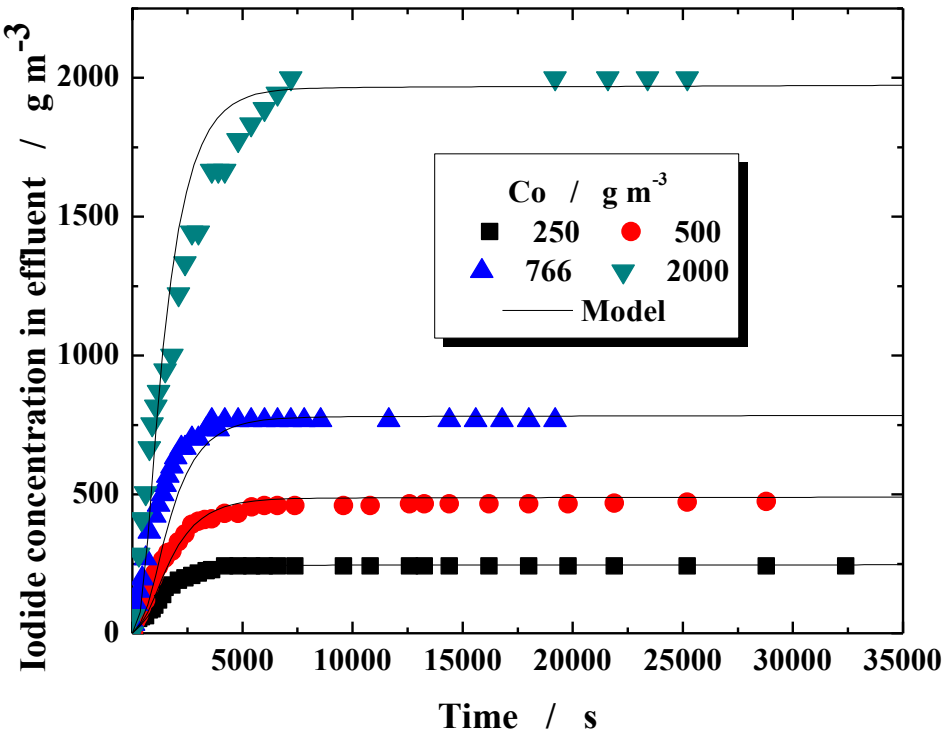

Figure 90 Influence of the inlet iodide concentration (250–2000 g m^{-3}) on the iodide concentration in effluent (markers are the experimental data) and mass transfer model Eqs. (30) – (43) (solid curves in figure). Flow rate F = 1.3×10^{-7} m^3 s^{-1}.

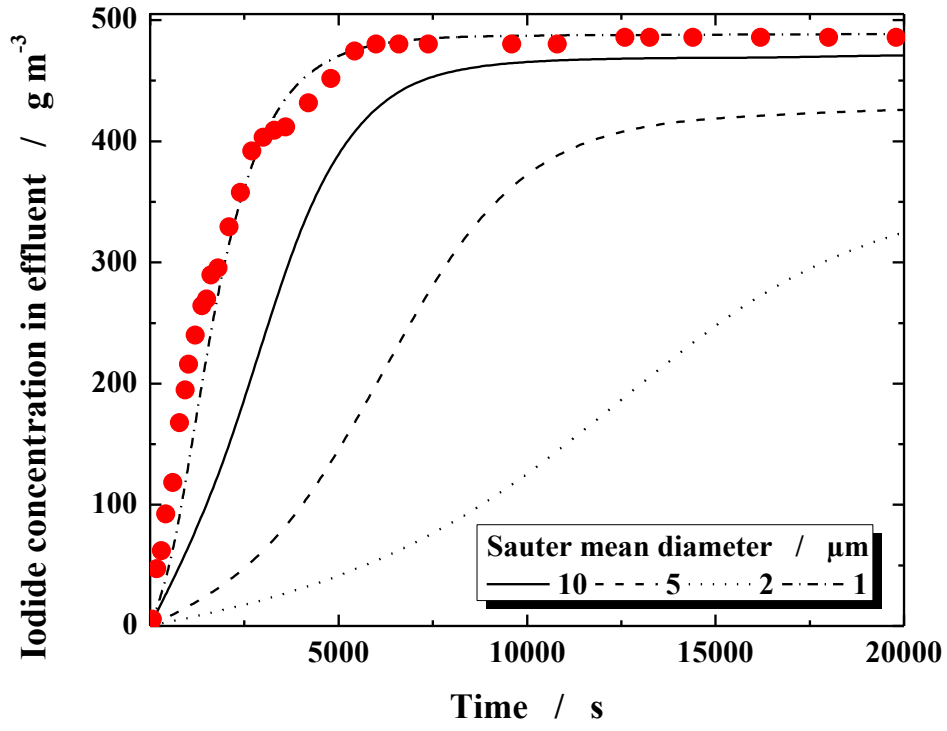

Figure 91 Influence of the Sauter mean diameter on the model. Red dots represent the experimental data.

It is clear from the results, based on the copper sorption in Dower 50W-X8 as well as copper hydroxide acetate, that the continuous flow stirred cell in combination with the modelling (based on diffusion within the particle) is valuable tool in designing the system for industrial application. The equilibrium and mass transfer parameters once obtained from the continuous stirred cell can be applied to any ion exchange process to predict its performance. But at the same time the model itself can be valuable tool in predicting for example the right size of the ion exchange material that should be used in order to achieve certain performance.

The continuous flow stirred cell is particularly relevant to instances when the mass of ion exchange material available for the testing is low (less than 1g) and when dealing with hazardous or expensive materials. It is a technique employing microfiltration and ion exchange (or sorption), of the engineered particles that could be produced by membrane emulsification.

5.2.3 Functionalized silica particles

Silica particles produced by membrane emulsification using acidified sodium silicate (aged in acetone with average internal pore size 6 nm and specific surface area of 320 m^{-2} g^{-1} Figure 56 (b)) were additionally functionalized according to the procedure described in Chapter 4.1.2.3.3 and tested for copper sorption.

The ability of functionalized particles to sorb Cu(II) was demonstrated in a continuous flow stirred cell. The aim of these experiments was solely to show that functional silica particles were capable to sorb copper. If equilibrium and mass transfer properties should be determined a set of experiments with different inlet concentrations should be performed. The volume of the liquid phase in the cell was 140 cm^3 and the stirrer speed was 270 rpm. The pH of the inlet solution was adjusted to 4.5 using 10% HCl (Fisher Scientific, UK). As can be seen from response curves in Figure 92, the functionalized silica particles had a higher binding affinity toward Cu(II) compared to the non-functionalized particles. After about 80 min, both non-treated and functionalized particles were fully saturated with Cu(II) and from that time the Cu(II) concentration in the effluent matched the Cu(II) content in the feed stream.

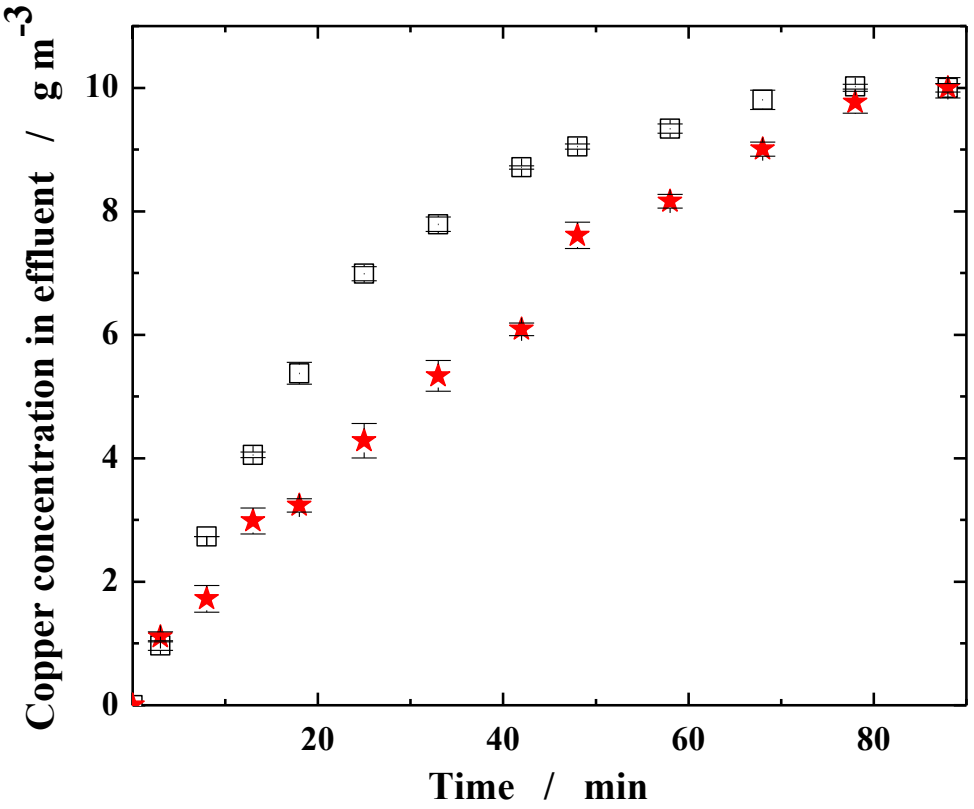

Figure 92 Sorption of $CuSO_4$ on silica gel in a continuous flow stirred cell with slotted pore membrane. The copper concentration in feed stream was 10 g m^{-3}, the flow rate of feed stream was 8 mL min^{-1}, and the particle loading in the cell was 3.5 g. (□) Non-functionalized silica particles. (★) Silica particles functionalized with 3-aminopropyltrimethoxysilane.

Experiments with non-functionalized and functionalized particles were repeated 2 times and in Figure 92 the markers represent the average value while the error bars represent the standard deviation of the experiments showing that the experiments were reproducible.

5.3 Results summary

Membrane emulsification using microengineered nickel membranes with cylindrical pores was successfully applied for production of larger droplets (greater than 10 μm) as well as solid particles. It was demonstrated that the Dispersion Cell represents a valuable laboratory technique for manufacturing the droplets of various emulsions. The droplets of acidified sodium silicate in kerosene stabilized with Span 80 (W/O), sunflower oil droplets stabilized with Tween 20 as well as mixture of Gum Arabic and Gelatine (O/W) and W/O droplets stabilized with Tween 20 (W/O/W) were successfully formed. Using the appropriate process parameters it was possible to control the droplet size.

If an additional step (drying, temperature adjustments, etc.) is applied with the right formulation it is possible to convert the liquid droplets into the solid particles. Highly spherical solid silica particles, with high surface area and internal structure, were successfully produced using a W/O emulsion route. The droplets of acidified sodium silicate, produced using the Dispersion Cell, were solidified due to the condensation polymerisation reaction taking place within the droplets. Additionally it was possible to tailor the internal structure of silica particles by aging the particles, when in the state of the xerogel, in different solvents. It was possible to functionalize the surface of produced silica particles with 3-aminopropyltrimethoxysilane. Once functionalized it was demonstrated that the silica particles were suitable for copper sorption.

An alternative field of application for the Dispersion Cell, relevant to the tests of functionalized silica particles, was investigated. The Dispersion Cell was modified into a continuous flow stirred cell with slotted nickel membrane on the bottom. The continuous flow stirred cell is shown to be an effective technique for both mass transfer kinetics as well as equilibrium data acquisition – combining both into a single step, and simplifying ion exchange analysis. The commercial ion exchange resin (Dowex 50W-X8) was used to commission the system. Once determined, the design parameters can readily be used to model any ion exchange processes. Performance of the fixed bed column filled with Dowex 50W-X8 was successfully modelled using the equilibrium and mass transfer properties obtained from the continuous stirred cell in the

combination with the appropriate equation for the mass balance taking into consideration the nature of the system.

Using the continuous flow stirred cell it was confirmed that the silica particles produced using the Dispersion Cell and functionalized using 3-aminopropyltrimethoxysilane were capable to sorb copper. Equilibrium and mass transfer parameters for the novel ion exchange material (copper hydroxide acetate suitable for iodide sorption) produced in Chemistry Department (Loughborough University) were successfully obtained too. The continuous flow stirred cell is particularly relevant to instances when the mass of ion exchange material available for the testing is low (less than 1g) and when dealing with hazardous or expensive materials (nuclear laboratory test).
Slotted nickel membrane proved to be valuable when it came to the filtration of the produced silica particles from kerosene. It was possible to quickly separate the spherical silica particles from the needle shaped silica particles which were also created during solidification of the acidified sodium silicate droplets. The slotted membrane retained the Dowex 50W-X8 particles within the continuous flow stirred cell, providing the operation without the pressure drop and membrane blocking. Also it was a good support for the cellulose nitrate membrane during the testing of copper hydroxide acetate.

Industrial application of membrane emulsification is very important but the Dispersion Cell cannot be scaled up. Two novel systems: Oscillating and Pulsating relevant for industrial application were developed and reported. Just by providing the larger membrane area both systems can be easily scaled up.

An attempt was also made to produce the particles using membrane emulsification but without surfactant, and edible oil droplets (pure and containing peppermint oil) were stabilized using gelatine and Gum Arabic (complex coacervates). Cooling of the complex coacervates had a great effect on the shell thickness that coated the oil droplets. Glutaraldehyde was successfully employed to harden the complex coacervates shell.

The Pulsating system was successfully used to produce the complex coacervates but better temperature control during the cooling should be applied if a thicker shell around the oil droplets is wanted. Therefore, the Pulsating system can have potential

application in the food industry or in any other industry where the surfactants are less wanted.

The model based on the simple force balance was used to predict the droplet sizes produced using all three systems. In the Dispersion Cell it was the average shear that gave better predictions while in the Oscillating and Pulsating system the maximal shear stress worked better but it was observed that an additional force or factor influences the droplet detachment. If higher flow rates of the dispersed phase were used the formation of the droplet neck had to be taken into consideration when predicting the final droplet size.

6. CONCLUSIONS AND RECOMMENDATIONS FOR FUTURE WORK

Dispersion cell

W/O/W emulsions

The Dispersion Cell and flat disc nickel membranes were used to produce narrow size distribution droplets of multiple emulsions containing unrefined pumpkin seed oil with controllable volume median diameters from 100 to 430 μm. For most of the work, membranes with 20 and 40 μm pores with 200 μm pore spacing were used, and it was possible to obtain fluxes up to 3200 L m^{-2} h^{-1} while the span in most cases did not exceed 0.5. Extreme cases (low rotation speed and high flux as well as high rotation speed and low flux) were not optimal conditions for production of multiple emulsions and in these few cases the span exceeded 1.4.

Bigger droplets were produced when PGPR with internal water phase were present suggesting that partial wetting of the membrane occurred, but the chemical cleaning of the membrane between tests showed that it was effective. The reproducibility of the experiments was good, showing no irreversible adsorption of the PGPR molecules and that after each experiment the membrane surface regained its hydrophilicity. With the addition of PVA as a thickening agent the droplet size increased, again due to the decrease of the diffusivity of surfactant molecules in the more viscous environment.

Shear stress was the most effective way to regulate the droplet size so with an increase of the rotation speed by 5.7 times the droplet size decreased 2.6 times.

W/O emulsions

Spherical silica particles with mean particle sizes controllable within a range between 30 and 70 μm have been produced from inexpensive sodium silicate solution. It was found that the solid silica particle size was a linear function of the initial droplet size of acidified sodium silicate. It was possible to control the internal structure, i.e. pore diameters and voidage, by an aging process of the particles in different solvents from which the final, xerogel, particles were produced. The starting point for the different

techniques was membrane emulsification: injecting the aqueous phase into an oil phase, kerosene, containing a surfactant to stabilize the droplets. Careful control of the stirring, after droplet formation, was required in order to maintain the spherical shape and to avoid droplet damage by the stirrer. Likewise, careful control of the pH of the aqueous phase being injected was required, as it controlled the rate of polymerization: at too high pH, the reaction was too fast risking blockage within the membrane emulsification equipment, and too low pH led to long polymerization times. Therefore, with long stirring times damage to the gelling particles is more likely to occur. Hence, the optimum pH for the process was determined to be 3.5. A coefficient of variation of the particle sizes formed of less than 20% was possible.

The BET pore size analysis indicated that the internal porosity, or voidage, of the particles produced was between 47% and 64%, depending on the solvent used for aging. A material balance based on the known starting mass of silica present and an analysis of the droplet and final (xerogel) particle size provided a very similar result for internal porosity, for all the different sizes of particles produced. The internal porosity of the hydrogel particles was close to 90%, and the shrinkage of the droplets as they changed from liquid to hydrogel, and then xerogel, was monitored by microscope analysis and confirmed the progression of the polymerization from liquid droplets, to hydrogel and then xerogel, where the xerogel size mass balance provided an internal voidage equal to the BET value. There was no further shrinkage between the air dried xerogel and the calcined particles that were used for the BET analysis. The particles produced in this work are suitable for use as supports of functional groups for selective separations of components within liquids. As a demonstration they were functionalized using 3-aminopropyltrimethoxysilane and were capable to sorb copper.

Overall the Dispersion Cell is valuable tool for investigation of the new formulations. The Dispersion Cell cannot be scaled up and therefore is not recommended for industrial application. Nevertheless it is a valuable laboratory technique, and other methods of applying shear at a membrane surface may be applicable for industrial use.

The continuous flow stirred cell

An alternative field of application for the Dispersion Cell, relevant to the tests of functionalized silica particles, was investigated. The Dispersion Cell was modified into the continuous flow stirred cell with slotted nickel membrane on the bottom. The technique was commissioned using Dowex 50W-X8 resins and equilibrium parameters (q_m =0.116 g g^{-1} and b = 0.003 m^3 g^{-1}) for a Langmuir isotherm were obtained from conventional batch experiments for the isotherm, and by tests in a continuous flow stirred cell. Good agreement using the two different methods was achieved.

Conventional batch experiments for determining the sorption equilibrium require several days while the length of the experiments in the continuous flow stirred cell can be controlled by selecting the mass of the resin to use and inlet concentrations of the solution. Hence, the experimental time in the continuous flow stirred cell can be much shorter and it is possible to use the continuous flow stirred cell experiments to replace the conventional batch equilibrium tests. Comparing the experimental results from the continuous flow stirred cell with the mass transfer model it is possible to find constant effective particle diffusion (for Dowex 50W-X8 D_{eff}= 7×10^{-11} m^{-2} s^{-1}). Mass transfer and equilibrium data from the continuous flow stirred cell were successfully used to model fixed bed operation.
Equilibrium and mass transfer properties for copper hydroxide acetate capable to sorb iodide were also determined using the continuous stirred cell (q_m = 0.536 g g^{-1}, b = 0.003 m^3 g^{-1}, D_{eff}= 7×10^{-17} m^{-2} s^{-1}.
Using the same cell it was confirmed that the silica particles produced using the Dispersion Cell and functionalized using 3-aminopropyltrimethoxysilane were capable to sorb copper.

Overall, it is shown that the continuous stirred cell represents an effective laboratory technique for determining both equilibrium and mass transfer parameters. After having achieved the mass transfer and equilibrium data, it is possible to use the same mathematical model to predict the performance of a seeded microfiltration process using larger volumes of liquid, filter area, etc. to enable the design of a combined ion exchange and microfiltration process, or other types of contactors, such as columns. It will be particularly relevant to instances when the mass of ion exchange particles

available for testing is low, less than 1 gram, and when dealing with hazardous or expensive materials.

Oscillating system

The median drop sizes obtained in the Oscillating membrane emulsification systems have been compared with the predicted values calculated using different force balance models. The drop sizes produced in the oscillating system were placed between the simple peak-shear model (Model A) and peak-shear model that takes into account the neck formation (Model C with τ_{max}) but both models overestimated the drop sizes at intermediate shear values suggesting the existence of another drop detachment force to supplement the shear-induced drag force. Under constant peak shear stress at the membrane surface, the drop size was essentially independent of the frequency of oscillation, because the effect of an increasing frequency was compensated by decreasing amplitude. On increasing peak shear the droplet size decreased sharply and for most frequencies reached a constant value at the peak shear stress of about 4 Pa. The most narrow drop size distribution with a span of 0.37 to 0.45 and a median drop size of just below 50 μm was obtained at a peak shear stress of 3.6 Pa. For the generation of droplets with a size lower than 56 μm the slowest frequency of 10 Hz was not appropriate, because the drop formation time for the amount of active pores of 10%, or less, was shorter than the peak-shear-event time. On increasing the dispersed phase flux from 30 to 13900 $L\,m^{-2}\,h^{-1}$ no significant improvement of the uniformity of distribution due to droplet "push off" effect was observed. The technique is applicable to the generation of larger droplets than can be reliably achieved by a cross-flow membrane emulsification process, where drop breakage after formation occurs. The oscillating membrane technique can be scaled up by providing a larger membrane area in the oscillating membrane assembly.

Pulsating system

Pulsating system was successfully used to generate the droplets of sunflower oil stabilized with Tween 20 but also complex coacervates with a thin shell were produced using only poor temperature control. The lowest value of the span was 0.68 and droplets between 40 and 260 μm were produced. The model taking into consideration the maximal shear stress overestimated the droplet size implying that an additional

force or factor must have influenced the droplets during the formation. The shear on the membrane surface comes from both pulsation and the continuous phase flow. But the values of the shear induced by the continuous phase flow are negligible compared to the shear of the pulsations. Therefore the smaller droplet size cannot be explained by the existence of the continuous flow.

When comparing Dispersion Cell, Oscillating and Pulsating system the most uniform droplets were produced using the Oscillating system. The highest productivity of reasonably uniform droplets was recorded for the Oscillating system. Nevertheless, the Pulsating system due to its continuous operation should be investigated more to find the optimal working conditions.

6.1 RECOMMENDATIONS AND FUTURE WORK

Dispersion Cell

The Dispersion Cell is easy to set up and handle as well as to dismantle and clean and it allows even less experienced operators to successfully generate the emulsions. Hence it is recommended that the Dispersion Cell be used every time when the new formulation for membrane emulsification is tried.

Stirred cell with continuous flow

Further tests with appropriately functionalized silica particles are required in order to determine the mass transfer and equilibrium parameters. The loading of the silica surface with amino groups can also be determined. Functionalising the silica surface using crown ethers (Jal, Patel, & Mishra 2004) suitable for removal of heavy metals (organic compounds with molecules containing large rings of carbon and oxygen atoms) should also be tried since they could have a potential application in nuclear industry. Also some inorganic materials used in nuclear industry i.e. clinoptilolite could be tested in order to determine equilibrium and mass transfer properties. Also ion exchange systems with clinoptilolite could be modelled.

Oscillating system

The Oscillating system produced the most uniform droplets but the production was in batches. Therefore it is highly recommended that a system with the continuous flow of the continuous phase is designed.

Pulsating system

Further experiments are needed to find the right combination of the dispersed phase flow rate and the shear applied on the membrane surface in order to achieve more uniform size distribution (both the Dispersion Cell as well as the Oscillating system had lower values for the span of the size distribution when compared to the Pulsating system). The effort to do so should be made since the productivity of the Pulsating system can be great industrial application due to its single pass and continues nature. Since the membrane with 200 μm pore spacing was used, smaller pore spacing should be tested which might lead to production of more uniform droplets.

Regarding the complex coacervation using the Pulsating system better temperature control during the production of oil droplets, as well as regulation of the cooling temperature after the production of the droplets, should be applied if a thicker shell of the particles is wanted.

Modelling

The model should be reconsidered when trying to predict the droplet size in the Pulsating system since it was clear that the additional force or factor was acting on the droplets. That would lead to better understanding of the system and more accurate predictions of droplet sizes in the Pulsating system. An effort should be made in order to include the dispersed phase flux in the existing model.

REFERENCES

Andersson, N., Kronberg, B., Corkery, R. & Alberius, P. 2007, "Combined emulsion and solvent evaporation (ESE) synthesis route to well-ordered mesoporous materials", *Langmuir,* vol. 23, no. 3, pp. 1459-1464.

Aryanti, N., Hou, R. & Williams, R.A. 2009, "Performance of a rotating membrane emulsifier for production of coarse droplets", *Journal of Membrane Science,* vol. 326, no. 1, pp. 9-18.

Barbé, C., Bartlett, J., Kong, L., Finnie, K., Lin, H.Q., Larkin, M., Calleja, S., Bush, A. & Calleja, G. 2004, "Silica particles: a novel drug-delivery system", *Advanced Materials,* vol. 16, no. 21, pp. 1959-1966.

Baacke, M., Kiss, A. 1991, "*Zeolites . In Ion Exchangers*", Berlin, Germany: de Gruyter, p. 473 .

Barret, E.P., Joyner, L.G. & Halenda, P.P. 1951, "The Determination of Pore Volume and Area Distributions in Porous Substances. I. Computations from Nitrogen Isotherms", *Journal of the American Chemical Society,* vol. 73, no. 1, pp. 373-380.

Becher, P. (ed) 2001, "*Emulsions: Theory and practice"*, 3rd edn, Oxford University Press, New York.

Blitz, I.P., Blitz, J.P., Gun'ko, V.M. & Sheeran, D.J. 2007, "Functionalized silicas: Structural characteristics and adsorption of Cu (II) and Pb (II)", *Colloids and Surfaces A: Physicochemical and Engineering Aspects,* vol. 307, no. 1-3, pp. 83-92.

Brunauer, S., Emmett, P.H. & Teller, E. 1938, "Adsorption of Gases in Multimolecular Layers", *Journal of the American Chemical Society,* vol. 60, no. 2, pp. 309-319.

Buranda, T., Huang, J., Ramarao, G.V., Linnea, K., Larson, R.S., Ward, T.L., Sklar, L.A. & Lopez, G.P. 2003, "Biomimetic molecular assemblies on glass and mesoporous silica microbeads for biotechnology", *Langmuir,* vol. 19, no. 5, pp. 1654-1663.

Butterworth, A.D., Dann, S.E. & Kirk, C.A. 2010, "Anion exchange materials for radiochemical application", DIAMOND Conference, 15th - 17th December, Manchester, United Kingdom.

Carroll, N.J., Rathod, S.B., Derbins, E., Mendez, S., Weitz, D.A. & Petsev, D.N. 2008, "Droplet-based microfluidics for emulsion and solvent evaporation synthesis of monodisperse mesoporous silica microspheres", *Langmuir,* vol. 24, no. 3, pp. 658-661.

Chen, C.C., Tu, Y.Y. & Chang, H.M. 1999, "Efficiency and protective effect of encapsulation of milk immunoglobulin G in multiple emulsion", *Jougnal of Agricultural and Food Chemistry,* vol. 47, no. 2, pp. 407-410.

Chen, Y., Wang, Y.J., Yang, L.M. & Luo, G.S. 2008, "Micrometer-sized monodispersed silica spheres with advanced adsorption properties", *AICHE Journal,* vol. 54, no. 1, pp. 298-309.

Cho, Y.H. & Park, J. 2003, "Evaluation of process parameters in the O/W/O multiple emulsion method for flavor encapsulation", *Journal of Food Science,* vol. 68, no. 2, pp. 534-538.

Chokkalingam, V., Weidenhof, B., Krämer, M., Maier, W.F., Herminghaus, S. & Seemann, R. 2010, "Optimized droplet-based microfluidics scheme for sol–gel reactions", *Lab on a Chip,* vol. 10, no. 13, pp. 1700-1705.

Christov, N.C., Ganchev, D.N., Vassileva, N.D., Denkov, N.D., Danov, K.D. & Kralchevsky, P.A. 2002, "Capillary mechanisms in membrane emulsification: oil-in-water emulsions stabilized by Tween 20 and milk proteins", *Colloids and Surfaces A: Physicochemical and Engineering Aspects,* vol. 209, no. 1, pp. 83-104.

Chu, L.Y., Utada, A.S., Shah, R.K., Kim, J.W. & Weitz, D.A. 2007, "Controllable monodisperse multiple emulsions", *Angewandte Chemie International Edition,* vol. 46, no. 47, pp. 8970-8974.

Clare, H.J., Pearson, C.A. & Shanks, I.A. 2003, *Method for controlling droplet size of an emulsion when mixing two immiscible fluids,* EP 1545754 A1.

Clearfield, A. & Stynes, J.A. 1964, "The preparation of crystalline zirconium phosphate and some observations on its ion exchange behaviour", *Journal of Inorganic and Nuclear Chemistry,* vol. 26, no. 1, pp. 117-129.

Cournarie, F., Savelli, M., Rosilio, V., Bretez, F., Vauthier, C., Grossiord, J. & Seiller, M. 2004, "Insulin-loaded W/O/W multiple emulsions: comparison of the performances of systems prepared with medium-chain-triglycerides and fish oil", *European Journal of Pharmaceutics and Biopharmaceutics,* vol. 58, no. 3, pp. 477-482.

Daisuke, W., Noriko, I. & Akira, U. 2004, "*Fat-soluble Vitamins-containing Food and Drink Product, and Method for Stabilizing Fat-soluble Vitamins [P]"*, Japan.

Dalgleish, D.G. 2006, "Food emulsions—their structures and structure-forming properties", *Food Hydrocolloids,* vol. 20, no. 4, pp. 415-422.

Dragosavac, M.M., Sovilj, M.N., Kosvintsev, S.R., Holdich, R.G. & Vladisavljević, G.T. 2008, "Controlled production of oil-in-water emulsions containing unrefined pumpkin seed oil using stirred cell membrane emulsification", *Journal of Membrane Science,* vol. 322, no. 1, pp. 178-188.

Dragosavac, M.M., Holdich, R.G. & Vladisavljević, G.T. 2011, "Continuous Flow Stirred Cell Microfiltration of Ion Exchange Media to Determine Mass Transfer Kinetics and Equilibrium Data", *Industrial & Engineering Chemistry Research,* vol. 50, no. 4, pp. 2408-2417.

Dubinin, M.M. 1968, "Porous structure of adsorbents and catalysts", *Advances in Colloid and Interface Science,* vol. 2, no. 2, pp. 217-235.

Egidi, E., Gasparini, G., Holdich, R.G., Vladisavljević, G.T. & Kosvintsev, S.R. 2008, "Membrane emulsification using membranes of regular pore spacing: Droplet size and uniformity in the presence of surface shear", Journal of Membrane Science, vol. 323, no. 2, pp. 414-420.

Fogler, H.S. 2005, *Elements of chemical reaction engineering,* 4th edn, Prentice Hall, Boston.

Frössling, N. 1938, "*Evaporation of Falling Droplet"s,* Gerlands Beitraäge zur Geophysik, vol. 52, pp. 170.

Fuchigami, T., Toki, M. & Nakanishi, K. 2000, "Membrane emulsification using sol-gel derived macroporous silica glass", *Journal of Sol-Gel Science and Technology,* vol. 19, no. 1, pp. 337-341.

Gañán-Calvo, A.M. & Gordillo, J.M. 2001, "Perfectly monodisperse microbubbling by capillary flow focusing", *Physical Review Letters,* vol. 87, no. 27, pp. 274.

Garti, N. 1997, "Double emulsions—scope, limitations and new achievements", *Colloids and Surfaces A: Physicochemical and Engineering Aspects,* vol. 123, pp. 233-246.

Gijsbertsen-Abrahamse, A.J., van der Padt, A. & Boom, R.M. 2004, "Status of cross-flow membrane emulsification and outlook for industrial application", *Journal of Membrane Science,* vol. 230, no. 1-2, pp. 149-159.

Giorno, L., Li, N. & Drioli, E. 2003, "Use of stable emulsion to improve stability, activity, and enantioselectivity of lipase immobilized in a membrane reactor", *Biotechnology and bioengineering,* vol. 84, no. 6, pp. 677-685.

Griffin, W.C. 1949, "Classification of surface active agents by HLB", *Journal of Cosmetic Chemists,* vol. 1, no. 311, pp. 97.

Hall, K.R., Eagleton, L.C., Acrivos, A. & Vermeulen, T. 1966, "Pore-and solid-diffusion kinetics in fixed-bed adsorption under constant-pattern conditions", *Industrial & Engineering Chemistry Fundamentals,* vol. 5, no. 2, pp. 212-223.

Harriott, P. 1962, "Mass transfer to particles: Part I. Suspended in agitated tanks", *AICHE Journal,* vol. 8, no. 1, pp. 93-101.

Hatate, Y., Ohta, H., Uemura, Y., Ijichi, K. & Yoshizawa, H. 1997, "Preparation of monodispersed polymeric microspheres for toner particles by the Shirasu porous glass membrane emulsification technique", *Journal of Applied Polymer Science,* vol. 64, no. 6, pp. 1107-1113.

Helfferich, F.G. 1995, "*Ion exchange",* Courier Dover Publications: Mineola, New York.

Heywood, H. 1948, "The Calculation of particle terminal velocities", *The Journal of the Imperial College Chemical Engineering Society,* pp. 140-257.

Higashi, S. & Setoguchi, T. 2000, " Hepatic arterial injection chemotherapy for hepatocellular carcinoma with epirubicin aqueous solution as numerous vesicles in iodinated poppy-seed oil microdroplets: clinical application of water-in-oil-in-water emulsion prepared using a membrane emulsification technique", *Advanced Drug Delivery Reviews,* vol. 45, no. 1, pp. 57-64.

Holdich R.G., Cumming I.W., Perni S. 2006, "Boron mass transfer during seeded microfiltration", *Chemical Engineering Research and Design,* vol. 84, no. 1, pp. 60-68.

Holdich, R.G., Dragosavac, M.M., Vladisavljevićc, G.T. & Kosvintsev, S.R. 2010, "Membrane emulsification with oscillating and stationary membranes", *Industrial & Engineering Chemistry Research,* vol. 49, no. 8, pp. 3810-3817.

Holdich, R.G., Cumming, I.W., Kosvintsev, S., Bromley, A.J. & Stefanini, G. 2003, "Clarification by slotted surface microfilters", *Minerals Engineering,* vol. 16, no. 2, pp. 121-128.

Holdich, R.G., Cumming, I.W., Streat, M. & Awang, A.R.B. 1998, "Seeded microfiltration of ionic copper with modified powdered activated carbon", *Proceedings of the 1998 IChemE Research Event*, The Institution of Chemical Engineers, Newcastle-upon-Tyne, 1998, CD Rom R.ec No 9623, ISBN 0 85295 400 X.

Hosoya, K., Bendo, M., Tanaka, N., Watabe, Y., Ikegami, T., Minakuchi, H. & Nakanishi, K. 2005, "An Application of Silica-Based Monolithic Membrane Emulsification Technique for Easy and Efficient Preparation of Uniformly Sized Polymer Particles", *Macromolecular Materials and Engineering,* vol. 290, no. 8, pp. 753-758.

Hutson, G.V. 1996, "Liquid effluent treatment research and development at BNFL Sellafield", *Nuclear Energy*, vol. 6, no. 35, pp. 393-398

Ide, M., Wallaert, E., Van Driessche, I., Lynen, F., Sandra, P. & Van Der Voort, P. 2010, "Spherical mesoporous silica particles by spray drying: doubling the retention factor of HPLC columns", *Microporous and Mesoporous Materials,* vol. 142, no 1.

Iler, R.K. 1979, "*The chemistry of silica: solubility, polymerization, colloid and surface properties, and biochemistry",* Wiley, New York.

Inglezakis, V.J. & Poulopoulos, S. 2006, "*Adsorption, ion exchange and catalysis: design of operations and environmental applications",* Elsevier Science, Amsterdam.

Jaffrin, M.Y. 2008, "Dynamic shear-enhanced membrane filtration: A review of rotating disks, rotating membranes and vibrating systems", *Journal of Membrane Science,* vol. 324, no. 1-2, pp. 7-25.

Jal, P.K., Patel, S. & Mishra, B.K. 2004, "Chemical modification of silica surface by immobilization of functional groups for extractive concentration of metal ions", *Talanta,* vol. 62, no. 5, pp. 1005-1028.

Joscelyne, S.M. & Trägårdh, G. 2000, "Membrane emulsification—a literature review", *Journal of Membrane Science,* vol. 169, no. 1, pp. 107-117.

Kandori, K., Kishi, K. & Ishikawa, T. 1992, "Preparation of uniform silica hydrogel particles by SPG filter emulsification method", *Colloids and surfaces,* vol. 62, no. 3, pp. 259-262.

Karbstein, H. & Schubert, H. 1995, "Developments in the continuous mechanical production of oil-in-water macro-emulsions", *Chemical Engineering and Processing,* vol. 34, no. 3, pp. 205-211.

Kawakatsu, T., Trägårdh, G. & Trägårdh, C. 2001, "Production of W/O/W emulsions and S/O/W pectin microcapsules by microchannel emulsification", *Colloids and Surfaces A: Physicochemical and Engineering Aspects,* vol. 189, no. 1, pp. 257-264.

Kawakatsu, T., Kikuchi, Y. & Nakajima, M. 1997, "Regular-sized cell creation in microchannel emulsification by visual microprocessing method", *Journal of the American Oil Chemists' Society,* vol. 74, no. 3, pp. 317-321.

Kelder, J.D.H., Janssen, J.J.M. & Boom, R.M. 2007, "Membrane emulsification with vibrating membranes: A numerical study", *Journal of Membrane Science,* vol. 304, no. 1, pp. 50-59.

Kobayashi, I., Lou, X., Mukataka, S. & Nakajima, M. 2005, "Preparation of monodisperse water-in-oil-in-water emulsions using microfluidization and straight-through microchannel emulsification", *Journal of the American Oil Chemists' Society,* vol. 82, no. 1, pp. 65-71.

Kobayashi, I. & Nakajima, M. 2002, "Effect of emulsifiers on the preparation of food-grade oil-in-water emulsions using a straight-through extrusion filter", *European journal of lipid science and technology,* vol. 104, no. 11, pp. 720-727.

Kobayashi, I., Nakajima, M. & Mukataka, S. 2003, "Preparation characteristics of oil-in-water emulsions using differently charged surfactants in straight-through microchannel emulsification", *Colloids and Surfaces A: Physicochemical and Engineering Aspects,* vol. 229, no. 1-3, pp. 33-41.

Korus, J. 2001, "Microencapsulation of flavours in starch matrix by coacervation method", *Polish Journal of Food and Nutrition Sciences,* vol. 10, no. 51, pp. 17-23.

Kosvintsev, S.R., Gasparini, G., Holdich, R.G., Cumming, I.W. & Stillwell, M.T. 2005, "Liquid− Liquid Membrane Dispersion in a Stirred Cell with and without Controlled Shear", *Ind.Eng.Chem.Res,* vol. 44, no. 24, pp. 9323-9330.

Kosvintsev, S.R., Gasparini, G. & Holdich, R.G. 2008, "Membrane emulsification: Droplet size and uniformity in the absence of surface shear", *Journal of Membrane Science,* vol. 313, no. 1-2, pp. 182-189.

Kukizaki, M. & Goto, M. 2007, "Preparation and evaluation of uniformly sized solid lipid microcapsules using membrane emulsification", *Colloids and Surfaces A: Physicochemical and Engineering Aspects,* vol. 293, no. 1-3, pp. 87-94.

Lambrich, U., van der Graaf, S., Dekkers, K., Schubert, H. & Boom, R.M. 2004, "Production of double emulsions using microchannel emulsification", *Proceeding of ICEF*, vo. 9 Monpellier.

Landau, L.D. & Lifshits, E.M. 1959, "*Fluid mechanics",* Pergamon.

Leclercq, S., Harlander, K.R. & Reineccius, G.A. 2009, "Formation and characterization of microcapsules by complex coacervation with liquid or solid aroma cores", *Flavour and Fragrance Journal,* vol. 24, no. 1, pp. 17-24.

Lehto, J. & Harjula, R. 1995, "Experimentation in ion exchange studies - the problem of getting reliable and comparable results", *Reactive and Functional Polymers,* vol. 27, no. 2, pp. 121-146.

Levenspiel, O. 1999, "*Chemical reaction engineering",* 3rd edn, Wiley, New York.

Liang, T., Hsu, C. 1993, "Sorption of cesium and strontium on natural mordenite", *Radiochimica acta,* vol. 61, p. 105-108.

Komarneni,S., Roy,R. 1988, "A cesium-selective ion sieve made by topotactic leaching of phlogopite mica", *Science*, vol. 239, 1286-1288.

Lieser, K.H. 1991 "Non-siliceous inorganic ion exchangers", *Ion Exchangers*, (K.Dorfner, ed.), Berlin, Germany: de Gruyter, p. 519.

Limousin, G., Gaudet, J., Charlet, L., Szenknect, S., Barthès, V. & Krimissa, M. 2007, "Sorption isotherms: A review on physical bases, modeling and measurement", *Applied Geochemistry,* vol. 22, no. 2, pp. 249-275.

Lin, H.P. & Mou, C.Y. 2002, "Structural and morphological control of cationic surfactant-templated mesoporous silica", *Accounts of Chemical Research,* vol. 35, no. 11, pp. 927-935.

Lowell, S., Shields, J.E., Thomas, M.A. & Thommes, T. 2004, "*Characterization of porous solids and powders: surface area, pore size, and density",* Kluwer Academic Publisher, Netherlands.

Luschtinetz, F. & Dosche, C. 2009, "Determination of micelle diffusion coefficients with fluorescence correlation spectroscopy (FCS)", *Journal of colloid and interface science,* vol. 338, no. 1, pp. 312-315.

Ma, G.H., Chen, A.Y., Su, Z.G. & Omi, S. 2003, "Preparation of uniform hollow polystyrene particles with large voids by a glass-membrane emulsification technique and a subsequent suspension polymerization", *Journal of Applied Polymer Science,* vol. 87, no. 2, pp. 244-251.

Ma, G.H., Nagai, M. & Omi, S. 1999, "Preparation of uniform poly (lactide) microspheres by employing the Shirasu Porous Glass (SPG) emulsification technique", *Colloids and Surfaces A: Physicochemical and Engineering Aspects,* vol. 153, no. 1-3, pp. 383-394.

Malik, D., Webb, C., Holdich, R., Ramsden, J., Warwick, G., Roche, I., Williams, D., Trochimczuk, A., Dale, J. & Hoenich, N. 2009, "Synthesis and characterization of size-selective nanoporous polymeric adsorbents for blood purification", *Separation and Purification Technology*, vol. 66, no. 3, pp. 578-585

Manu, V., Mody, H.M. & Bajaj, H.C. 2010, "Effect of Thermal Treatment of Silica Gels on Their Amino Functionalization and Subsequent Adsorption Properties for Cu^{2+} from Aqueous Solution of Copper Sulfate", *Industrial & Engineering Chemistry Research,* vol. 49, no. 17, pp 8184–8191.

Merchant, Z.M., Gaonkar, A.G., Nicholson, V.J. & Tufts, H.M. 1998, *Flavor delivery system*, EP 815743 A3.

Michaels, A.S. 1968, "New separation technique for the chemical process industry", *Chemical Engineering Progress,* vol. 64, pp. 31.

Morig, C.R. & Gopala Rao, M. 1965, "Diffusion in ion exchange resins: sodium ion-strontium ion system", *Chemical Engineering Science,* vol. 20, no. 10, pp. 889-893.

Murkovic, M., Piironen, V., Lampi, A.M., Kraushofer, T. & Sontag, G. 2004, "Changes in chemical composition of pumpkin seeds during the roasting process for

production of pumpkin seed oil (Part 1: non-volatile compounds)", *Food Chemistry,* vol. 84, no. 3, pp. 359-365.

Muñoz-Aguado, M.J., Gregorkiewitz, M. & Bermejo, F.J. 1995, "Structural characterization of silica xerogels", *Journal of Non-Crystalline Solids,* vol. 189, no. 1-2, pp. 90-100.

Muñoz-Aguado, M. & Gregorkiewitz, M. 1997, "Sol–Gel Synthesis of Microporous Amorphous Silica from Purely Inorganic Precursors", *Journal of colloid and interface science,* vol. 185, no. 2, pp. 459-465.

Muschiolik, G. 2007, "Multiple emulsions for food use", *Current Opinion in Colloid & Interface Science,* vol. 12, no. 4-5, pp. 213-220.

Nadav, N. 1999, "Boron removal from seawater reverse osmosis permeate utilizing selective ion exchange resin", *Desalination,* vol. 124, no. 1-3, pp. 131-135.

Nagata, S. (ed) 1975, *Mixing: Principles and Applications*, Kodansha, Tokyo, Japan.

Nakano, M. 2000, "Places of emulsions in drug delivery", *Advanced Drug Delivery Reviews,* vol. 45, no. 1, pp. 1-4.

Nakashima, T., Shimizu, M. & Kukizaki, M. 2000, "Particle control of emulsion by membrane emulsification and its applications", *Advanced Drug Delivery Reviews,* vol. 45, no. 1, pp. 47-56.

Nakashima, T., Shimizu, M. & Kukizaki, M. 1991, "Membrane emulsification by microporous glass", *Key Engineering Materials,* vol. 61, no. 62, pp. 513-516.

Okonogi, S., Kato, R., Asano, Y., Yuguchi, H., Kumazawa, R., Sotoyama, K., Takahashi, K. & Fujimoto, M. 1994, , Google Patents.

Okushima, S., Nisisako, T., Torii, T. & Higuchi, T. 2004, "Controlled production of monodisperse double emulsions by two-step droplet breakup in microfluidic devices", *Langmuir,* vol. 20, no. 23, pp. 9905-9908.

Ouki,S.K., Kavannagh, M.1997, "Performance of natural zeolites for the treatment of mixed metal contaminated effluents", *Waste Management& Research*, vol. 15, pp. 383-394

Owusu, R.K., Zhu, W. & Dickinson, E. 1992, "Controlled release of L-tryptophan and Vitamin B2 from model water/oil/water multiple emulsions", *Food Hydrocolloids,* vol. 6, no. 5, pp. 443-453.

Ozmen, M., Can, K., Akin, I., Arslan, G., Tor, A., Cengeloglu, Y. & Ersoz, M. 2009, "Surface modification of glass beads with glutaraldehyde: Characterization and their adsorption property for metal ions", *Journal of hazardous materials,* vol. 171, no. 1-3, pp. 594-600.

Peng, S. & Williams, R.A. 1998, "Controlled Production of Emulsions Using a Crossflow Membrane", *Particle & Particle Systems Characterization,* vol. 15, no. 1, pp. 21-25.

Popuri, S.R., Vijaya, Y., Boddu, V.M. & Abburi, K. 2009, "Adsorptive removal of copper and nickel ions from water using chitosan coated PVC beads", *Bioresource technology,* vol. 100, no. 1, pp. 194-199.

Schadler, V. & Windhab, E. 2006, "Continuous membrane emulsification by using a membrane system with controlled pore distance", *Desalination,* vol. 189, no. 1-3, pp. 130-135.

Schramm, L.L. 2005, *Emulsions, foams, and suspensions: fundamentals and applications,* Wiley-Vch Verlagsgesellschaft Mbh.

Schröder, V., Behrend, O. & Schubert, H. 1998, "Effect of dynamic interfacial tension on the emulsification process using microporous, ceramic membranes", *Journal of colloid and interface science,* vol. 202, no. 2, pp. 334-340.

Schröder, V. & Schubert, H. 1999, "Production of emulsions using microporous, ceramic membranes", *Colloids and Surfaces A: Physicochemical and Engineering Aspects,* vol. 152, no. 1-2, pp. 103-109.

Schubert, H. & Armbruster, H. 1992, "Principles of formation and stability of emulsions", *International Chemical Engineering,* vol. 32, no. 1, pp. 14-28.

Seaton, N.A. & Walton, J. 1989, "A new analysis method for the determination of the pore size distribution of porous carbons from nitrogen adsorption measurements", *Carbon,* vol. 27, no. 6, pp. 853-861.

Seifriz, W. 1925, "Studies in emulsions", *Journal of Phisical Chemistry,* vol. 29, pp. 738-749.

Sing, C. & Yu, J. 1998, "Copper adsorption and removal from water by living mycelium of white-rot fungus Phanerochaete chrysosporium", *Water research,* vol. 32, no. 9, pp. 2746-2752.

Sing, K.S.W., Everett, D.H., Haul, R.A.W., Moscou, L., Pierotti, R.A., Rouquerol, J. & Siemieniewska, T. 1985, "Reporting physisorption data for gas/solid systems with special reference to the determination of surface area and porosity (Recommendations 1984)", *Pure and Applied Chemistry,* vol. 57, no. 4, pp. 603-619.

Soong, R., Nieh, M.P., Nicholson, E., Katsaras, J. & Macdonald, P.M. 2010, "Bicellar Mixtures Containing Pluronic F68: Morphology and Lateral Diffusion from Combined SANS and PFG NMR Studies", *Langmuir,* vol. 26, no. 4, pp. 2630-2638.

Stillwell, M.T., Holdich, R.G., Kosvintsev, S.R., Gasparini, G. & Cumming, I.W. 2007, "Stirred Cell Membrane Emulsification and Factors Influencing Dispersion Drop Size and Uniformity", *Industrial & Engineering Chemistry Research,* vol. 46, no. 3, pp. 965-972.

Sugiura, S., Nakajima, M., Iwamoto, S. & Seki, M. 2001, "Interfacial tension driven monodispersed droplet formation from microfabricated channel array", *Langmuir,* vol. 17, no. 18, pp. 5562-5566.

Sugiura, S., Nakajima, M., Yamamoto, K., Iwamoto, S., Oda, T., Satake, M. & Seki, M. 2004, "Preparation characteristics of water-in-oil-in-water multiple emulsions using microchannel emulsification", *Journal of colloid and interface science,* vol. 270, no. 1, pp. 221-228.

Surh, J., Vladisavljevićc, G.T., Mun, S. & McClements, D.J. 2007, "Preparation and characterization of water/oil and water/oil/water emulsions containing biopolymer-gelled water droplets", *Journal of Agricultural and Food Chemistry,* vol. 55, no. 1, pp. 175-184.

Suzuki, K., Shuto, I. & Hagura, Y. 1996, "Characteristics of the membrane emulsification method combined with preliminary emulsification for preparing corn oil-in-water emulsions", *Food Science and Technology International, Tokyo,* vol. 2, no. 1, pp. 43-47.

Suzuki, T.M., Yamamoto, M., Fukumoto, K., Akimoto, Y. & Yano, K. 2007, "Investigation of pore-size effects on base catalysis using amino-functionalized monodispersed mesoporous silica spheres as a model catalyst", *Journal of Catalysis,* vol. 251, no. 2, pp. 249-257.

Tarleton, E.S. & Wakeman, R.J. 1994, "Understanding Flux Decline in Cross-Flow Microfiltration. 3. Effects of Membrane Morphology", *Chemical Engineering Research & Design,* vol. 72, no. 4, pp. 521-529.

Tarleton, E.S. & Wakeman, R.J. 1993, "Understanding Flux Decline In Crossflow Microfiltration-Part I-Effects Of Particle And Pore Size", *Chemical Engineering Research and Design,* vol. 71, no. a, pp. 399-410.

Thompson, K.L., Armes, S.P. & York, D.W. 2011, "Preparation of Pickering Emulsions and Colloidosomes with Relatively Narrow Size Distributions by Stirred Cell Membrane Emulsification", *Langmuir,* vol. 27, no. 6, pp. 2357-2363.

Thorsen, T., Roberts, R.W., Arnold, F.H. & Quake, S.R. 2001, "Dynamic pattern formation in a vesicle-generating microfluidic device", *Physical Review Letters,* vol. 86, no. 18, pp. 4163-4166.

Titulaer, M.K., Jansen, J.B.H. & Geus, J.W. 1994, "The preparation and characterization of sol-gel silica spheres", *Journal of Non-Crystalline Solids,* vol. 168, no. 1-2, pp. 1-13.

Tong, J., Nakajima, M., Nabetani, H. & Kikuchi, Y. 2000, "Surfactant effect on production of monodispersed microspheres by microchannel emulsification method", *Journal of Surfactants and Detergents,* vol. 3, no. 3, pp. 285-293.

Umbanhowar, P.B., Prasad, V. & Weitz, D.A. 2000, "Monodisperse emulsion generation via drop break off in a coflowing stream", *Langmuir,* vol. 16, no. 2, pp. 347-351.

Utada, A.S., Lorenceau, E., Link, D.R., Kaplan, P.D., Stone, H.A. & Weitz, D.A. 2005, "Monodisperse double emulsions generated from a microcapillary device", *Science,* vol. 308, no. 5721, pp. 537.

van der Graaf, S., Schroën, C.G.P.H. & Boom, R.M. 2005, "Preparation of double emulsions by membrane emulsification—a review", *Journal of Membrane Science,* vol. 251, no. 1-2, pp. 7-15.

van der Graaf, S., Schroën, C.G.P.H., van der Sman, R.G.M. & Boom, R.M. 2004, "Influence of dynamic interfacial tension on droplet formation during membrane emulsification", *Journal of colloid and interface science,* vol. 277, no. 2, pp. 456-463.

van der Graaf, S., Steegmans, M.L.J., van der Sman, R.G.M., Schroën, C.G.P.H. & Boom, R.M. 2005, "Droplet formation in a T-shaped microchannel junction: A model system for membrane emulsification", *Colloids and Surfaces A: Physicochemical and Engineering Aspects,* vol. 266, no. 1-3, pp. 106-116.

van Dijke K.C., Boom R.M., Schroën K. 2008, "Microchannel emulsification: From computational fluid dynamics to predictive analytical model", *Langmuir* , vol. 24, pp. 10107–10115.

van Dijke, K.C, Kobayashi, I., Schroën, K., Uemura, K., Nakajima, M. & Boom, R. 2010, "Effect of viscosities of dispersed and continuous phases in microchannel oil-in-water emulsification", *Microfluidics and Nanofluidics,* vol. 9, no. 1, pp. 77-85.

van Rijn, C.J.M., Nijdam, W., Kuiper, S., Veldhuis, G.J., van Wolferen, H. & Elwenspoek, M. 1999, "Microsieves made with laser interference lithography for

micro-filtration applications", *Journal of Micromechanics and Microengineering,* vol. 9, pp. 170-172.

Van Nguyen, N., Lee, J., Jha, M.K., Yoo, K. & Jeong, J. 2009, "Copper recovery from low concentration waste solution using Dowex G-26 resin", *Hydrometallurgy,* vol. 97, no. 3-4, pp. 237-242.

Vasudevan, T.V. & Naser, M.S. 2002, "Some Aspects of Stability of Multiple Emulsions in Personal Cleansing Systems", *Journal of colloid and interface science,* vol. 256, no. 1, pp. 208-215.

Vladisavljević, G.T., Holdich, R.G., Dragosavac, M.M. & Weitz, D.A. 2010, "Recent developments in manufacturing multiple emulsions using membrane and micro fluidic devices", 5th World Congress on Emulsions, 12th-14th October, Lyon, France.

Vladisavljević, G.T. & Williams, R.A. 2005, "Recent developments in manufacturing emulsions and particulate products using membranes", *Advances in Colloid and Interface Science,* vol. 113, no. 1, pp. 1-20.

Vladisavljević, G.T., Lambrich, U., Nakajima, M. & Schubert, H. 2004, "Production of O/W emulsions using SPG membranes, ceramic α-aluminium oxide membranes, microfluidizer and a silicon microchannel plate—a comparative study", *Colloids and Surfaces A: Physicochemical and Engineering Aspects,* vol. 232, no. 2-3, pp. 199-207.

Vladisavljević, G.T. & Schubert, H. 2003, "Influence of process parameters on droplet size distribution in SPG membrane emulsification and stability of prepared emulsion droplets", *Journal of Membrane Science,* vol. 225, no. 1-2, pp. 15-23.

Vladisavljević, G.T. & Schubert, H. 2003b, "Preparation of Emulsions with a Narrow Particle Size Distribution Using Microporous α-Alumina Membranes", *Journal of Dispersion Science and Technology,* vol. 24, no. 6, pp. 811-819.

Vladisavljević, G.T. & Schubert, H. 2002, "Preparation and analysis of oil-in-water emulsions with a narrow droplet size distribution using Shirasu-porous-glass (SPG) membranes", *Desalination,* vol. 144, no. 1-3, pp. 167-172.

Vladisavljević, G.T., Shimizu, M. & Nakashima, T. 2006a, "Production of multiple emulsions for drug delivery systems by repeated SPG membrane homogenization: Influence of mean pore size, interfacial tension and continuous phase viscosity", *Journal of Membrane Science,* vol. 284, no. 1-2, pp. 373-383.

Vladisavljević, G.T., Shimizu, M. & Nakashima, T. 2005, "Permeability of hydrophilic and hydrophobic Shirasu-porous-glass (SPG) membranes to pure liquids and its microstructure", *Journal of Membrane Science,* vol. 250, no. 1-2, pp. 69-77.

Vladisavljević, G.T., Shimizu, M. & Nakashima, T. 2004, "Preparation of monodisperse multiple emulsions at high production rates by multi-stage premix membrane emulsification", *Journal of Membrane Science,* vol. 244, no. 1-2, pp. 97-106.

Vladisavljević, G.T. & Williams, R.A. 2006, "Manufacture of large uniform droplets using rotating membrane emulsification", *Journal of colloid and interface science,* vol. 299, no. 1, pp. 396-402.

Wagdare, N.A., Marcelis, A.T.M., Ho, O.B., Boom, R.M. & van Rijn, C.J.M. 2010, "High throughput vegetable oil-in-water emulsification with a high porosity micro-engineered membrane", *Journal of Membrane Science,* vol. 347, no. 1-2, pp. 1-7.

Wagner, J. 2001, *Membrane Filtration Handbook Practical Tips and Hints*, Osmonic Inc. USA.

Weiss, A., Sextl, E. 1991, "Clay minerals as ion exchangers", *Ion Exchangers* (K.Dorfner, ed.) Berlin, Germany: de Gruyter, p. 494.

Walcarius, A., Etienne, M. & Bessière, J. 2002, "Rate of access to the binding sites in organically modified silicates. 1. Amorphous silica gels grafted with amine or thiol groups", *Chemistry of materials,* vol. 14, no. 6, pp. 2757-2766.

Weiss, J., Scherze, I. & Muschiolik, G. 2005, "Polysaccharide gel with multiple emulsion", *Food Hydrocolloids,* vol. 19, no. 3, pp. 605-615.

Weng, C.H., Tsai, C.Z., Chu, S.H. & Sharma, Y.C. 2007, "Adsorption characteristics of copper (II) onto spent activated clay", *Separation and Purification Technology,* vol. 54, no. 2, pp. 187-197.

Wulff-Pérez, M., Torcello-Gómez, A., Gálvez-Ruíz, M.J. & Martín-Rodríguez, A. 2009, "Stability of emulsions for parenteral feeding: Preparation and characterization of o/w nanoemulsions with natural oils and Pluronic f68 as surfactant", *Food Hydrocolloids,* vol. 23, no. 4, pp. 1096-1102.

Xu, J.H., Luo, G.S., Chen, G.G. & Wang, J.D. 2005, "Experimental and theoretical approaches on droplet formation from a micrometer screen hole", *Journal of Membrane Science,* vol. 266, no. 1-2, pp. 121-131.

Yiacoumi, S. & Tien, C. 1995, "Modeling Adsorption of Metal Ions from Aqueous Solutions: II. Transport-Controlled Cases", *Journal of colloid and interface science,* vol. 175, no. 2, pp. 347-357.

Yanagishita, T., Tomabechi, Y., Nishio, K. & Masuda, H. 2004, "Preparation of monodisperse SiO_2 nanoparticles by membrane emulsification using ideally ordered anodic porous alumina", *Langmuir,* vol. 20, no. 3, pp. 554-555.

Yilmaz Ipek, I., Holdich, R., Kabay, N., Bryjak, M. & Yuksel, M. 2007, "Kinetic behaviour of boron selective resins for boron removal using seeded microfiltration system", *Reactive and Functional Polymers,* vol. 67, no. 12, pp. 1628-1634.

Zagorodni, A.A. 2007, *Ion exchange materials: properties and applications,* Elsevier Science, Netherland.

Zhou, Q., Ma, G. & Su, Z. 2009, "Effect of membrane parameters on the size and uniformity in preparing agarose beads by premix membrane emulsification", *Journal of Membrane Science,* vol. 326, no. 2, pp. 694-700.

APPENDIX

A. Atomic absorbance Spectrophotometer

In order to determine the concentration of copper or sodium ions in water solutions an Atomic Absorbance Spectrophotometer (SpectrAA 2000, Varian) was used. Relative standard deviation also referred as a precision (i.e. the standard deviation divided by the mean based as a percentage) was set to 1% (PROMT mode of operation was selected). When the precision of the instrument is selected as an operating parameter the instrument records many absorbance values for the single sample being analysed until the desired precision is achieved. The absorbance data given as a result of the measurement represents a mean reading. Prior to the measurement of the samples, the calibration had to be performed in order to relate the measured absorbance with the concentration of the metal ions in water solution. The maximal concentration of the standard solution was chosen to be the maximal concentration that should be measured (the inlet concentration). For each calibration ten standards were used. Thermal drift is a common occurrence during analysis by atomic absorption; hence a single calibration performed at the start of the analysis may not be valid for the samples taken towards the end of the analysis. The calibration was repeated after 10 measurements and also at the end of the analysis. In general the calibration curves were not that different (both for copper and sodium). Figure 93 shows three calibration curves taken for copper ions at the start, after 10 samples and then at the end (after another 15 samples). According to the ion analysed as well as the concentration working range the wave length of the instrument had to be selected according to the manufacturer recommendations. When sodium nitrate was used to adjust the ionic strength standards were also prepared with the same ionic strength in order to get the same background.

Each sample was then measured three times and in Chapter 5.2 the average values are reported. Here Figure 94 and Figure 95 report the same values as Figure 81 (a) and Figure 82 (b), but this time the error bars are included in order to demonstrate the level of uncertainty when measuring the concentrations. The error bars represent the highest and the lowest value measured. Almost identical results are obtained when higher concentrations were used.

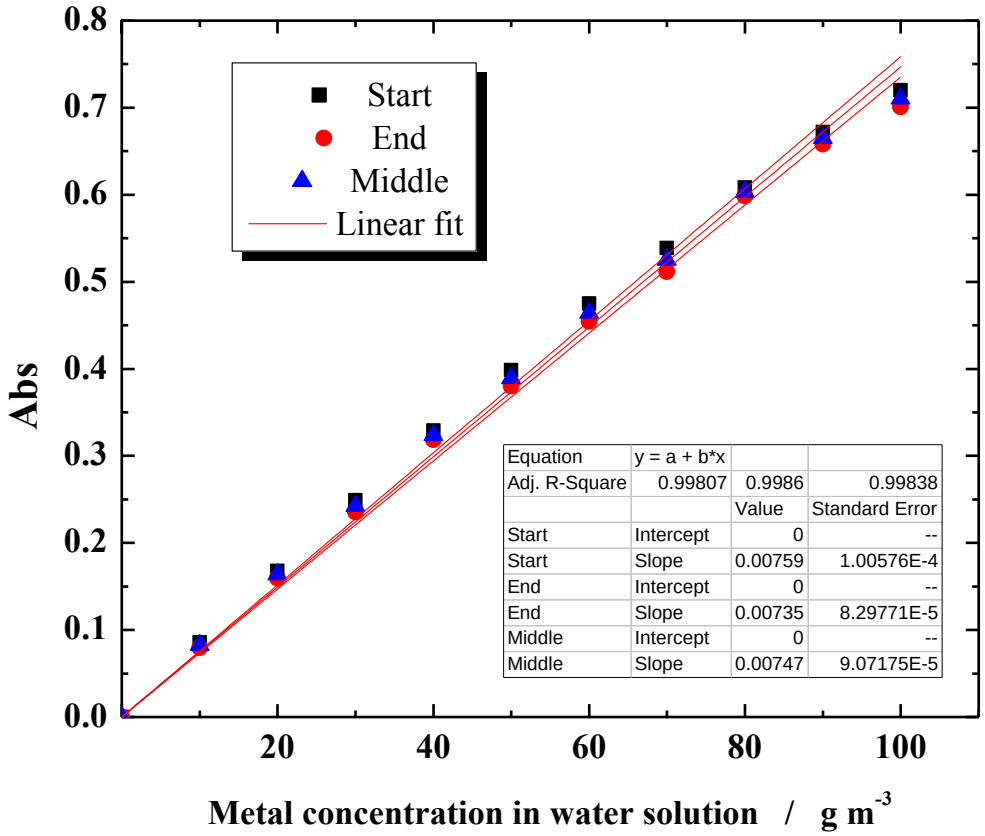

Figure 93 Calibration for SpectrAA, for copper concentration between 0 and 100 g m^{-3}.

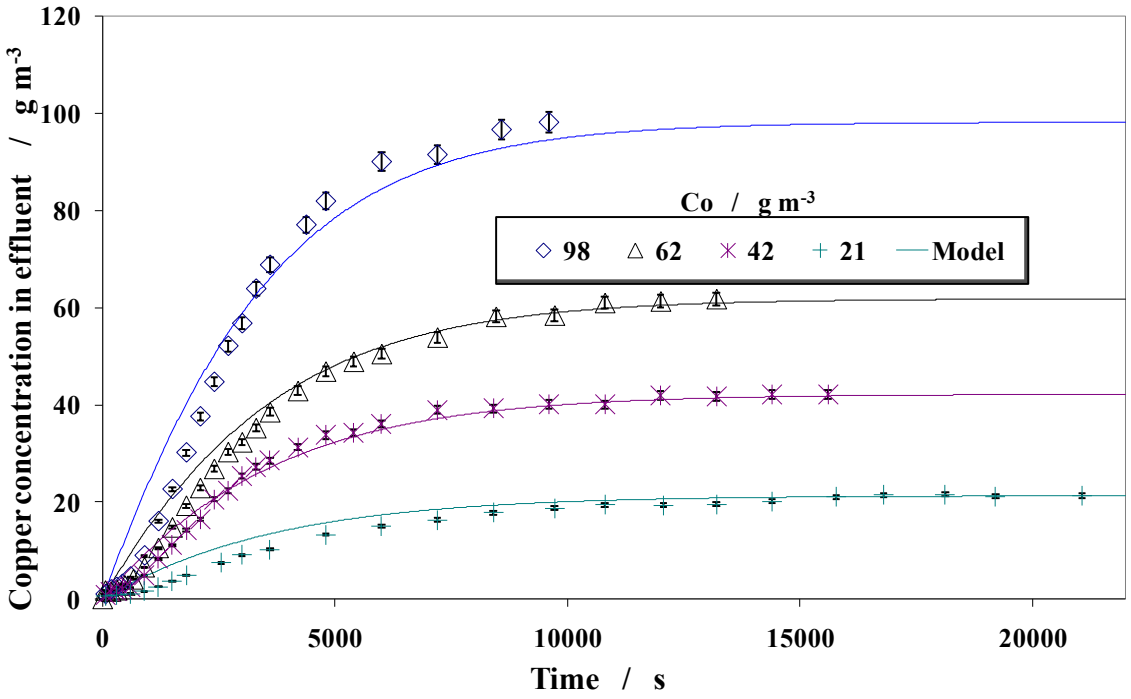

Figure 94 Small beads (R =4 2 µm). Flow rate $F = 1.3\times10^{-7}$ m^3 s^{-1}. (a) Influence of the inlet copper concentration (21 – 98 g m^{-3}) on the copper concentration in effluent and mass transfer model Eqs. (30) – (43) (solid curves in figure). Error bars represent the lowest and the highest value of concentration obtained during the measurements.

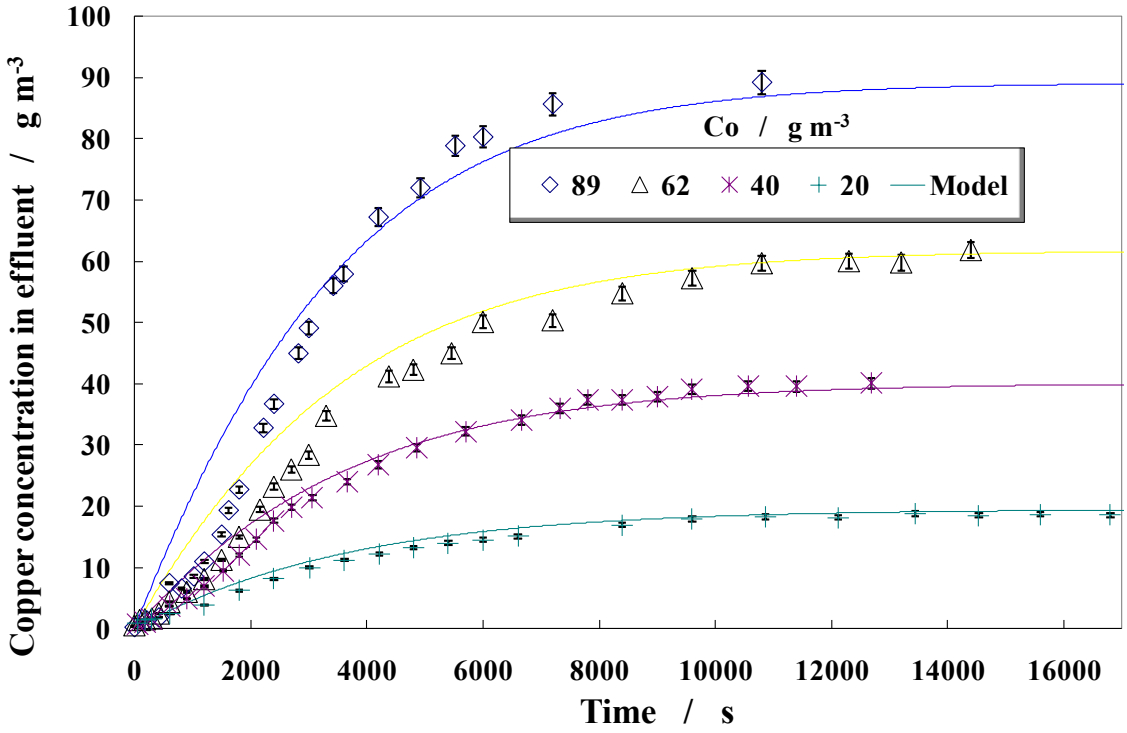

Figure 95 Big beads (R = 87 µm). Flow rate $F = 1.3\times10^{-7}$ m^3 s^{-1}. (a) Influence of the inlet copper concentration (20 – 89 g m^{-3}) on the copper concentration in effluent and mass transfer model Eqs. (30) – (43) (solid curves in figure). Error bars represent the lowest and the highest value of concentration obtained during the measurements.

B. Image J

When analyzing the W/O emulsions for production of the silica particles Malvern Mastersizes S could not be used since it had only a water sampling cell. Therefore a different method of analysis to determine the particle size as well as their uniformity had to be applied. A Leitz Ergolux optical microscope with attached Pulnix TM-6CN monochrome camera was available therefore the most convenient method was to use ImageJ (a public Java-based image processing program http://rsb.info.nih.gov/ij/) for size analysis.

The final silica particles (after drying and calcining) could be analyzed with the Malvern Mastersizer S but in order to be consistent the sizes of freshly prepared droplets of dispersed phase in kerosene (W/O emulsion), hydrogel as well as xerogel (fully dried hydrogel) particles were determined using ImageJ. The number of particles to count is regulated by the British standard but it changes considerably from publication to publication. In this thesis for each experiment (which needed to be analyzed by ImageJ), numerous random photos were taken and at least 700 droplets or particles were measured for representative measurements of size.

The droplets tended to burst when placed on a microscopic slide due to surface tension effects, so microphotographs had to be taken very quickly. A similar problem occurred with the hydrogel where due to the acetone evaporation the hydrogel was solidifying and shrinking forming the xerogel. It was important that the microphotographs of the droplets and xerogel are taken very quickly. Figure 96 (a-c) shows the image transformation suitable for ImageJ analysis as well as the result of the analysis Figure 96 (d).

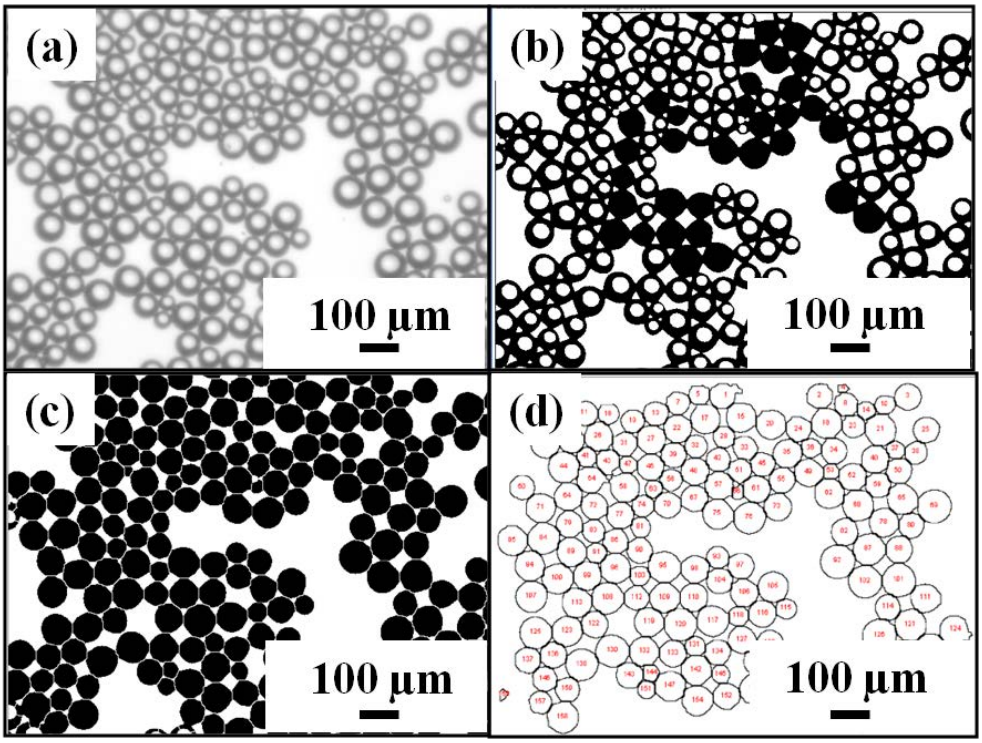

Figure 96 (a) Microphotograph of W/O emulsions. (b) Conversion to the binary image and filling of the droplets. (c) Outlined droplets ready for analysis. (d) Summary of the droplets calculated by the software. Average droplet size of W/O emulsions 90 µm. *CV* = 23 %.

Initially the microphotograph had to be imported into ImageJ (Figure 96 (a)) and scale had be set based on the microphotograph of the graticule. Contrast of the image was adjusted followed by the conversion into the binary image and threshold adjustments. Once the image was black and white all circles have to be filled with black (Figure 96 (b)). Droplets usually touched each other therefore it was necessary to use watershed function within ImageJ to separate the borders of the droplets and Figure 96 (c) represents the image ready for the analysis. The conversion into the binary image as well as the separation of the droplets was performed automatically. Manual corrections are also possible, and were done if mistakes were noticed. Before the analysis those droplets, touching the edges of the microphotograph, were excluded from the analysis. Figure 96 (d) represents the outlines of the droplets which are actually considered by ImageJ. Each droplet is numbered in order to be able to link it with the calculated size in the calculation worksheet. ImageJ reports Feret‘s Diameter, which is indeed the droplet diameter as the droplets are spherical.

Once obtained the results were exported to an Excel spreadsheet; the mean droplet diameter is calculated and as an indication of the droplet size distribution, the coefficient of variation ($CV = \frac{\sigma}{d} \times 100$) is calculated from the standard deviation ($\sigma = \sqrt{\frac{\sum_{i=1,n}^{n} (d_i - d)^2}{n-1}}$) and mean droplet diameter (*d*). Figure 97 represents ImageJ analysis of the SEM image of the silica particles.

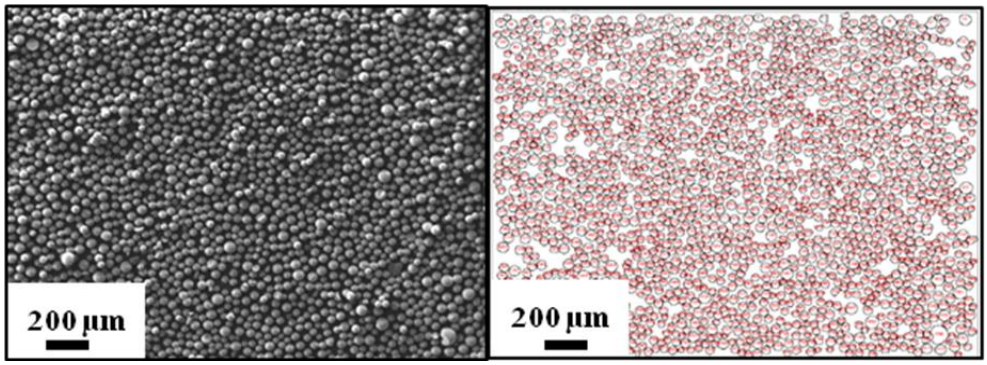

Figure 97 SEM image and outlined particles for ImageJ analysis of silica particles with average particle size of 30 µm.

C. PDSOL file

PDSOL file is given here together with the resulting graph for initial copper concentration of 100 g m^{-3}. Ion exchange material used was DOWEX 50W-X8 (100-200 mesh).

'CONSTANTS

qm=116e-3 'Langmuir maximum q value g/g

b=0.003' Langmiur parameter b m3/g of boron

m=1 'mass resin used g

V=.14e-3 'volume of cell in m3

radius=87e-6 'm

mu=0.001 'viscosity of liquid

rhos=1.443' specific gravity of solid

rhol=1 'specific gravity of liquid

diff=1.2e-9 'm2/s Diffusivity of transferring species in water

Deff=7e-11 'm2/s Internal diffusivity of transferring species in bead

cfeed=100 'g/m3 Incoming concentration of species in feed (also ppm)

Flow=1.3e-7 'm3/s Incoming flow rate

'CALCULATED CONSTANTS

rho=rhos*1e+6 'g/m3

deltarho=(rhos-rhol)*1000 'density difference in kg/m3

'vel_ter=9.8*(2*radius)^2*deltarho/(18*mu) 'Terminal settling velocity - Stokes

vel_ter= 0.00286

Re= 2*radius*rhol*1000*vel_ter/mu 'Particle Reynolds number

Sc=1e-3/1000/diff 'Scmidt number

Sh=2+.6*Re^.5*Sc^.33 'Sherwood number

K=2*Sh*diff/(2*radius) 'Mass transfer coefficient

'INITIAL CONDITIONS

q@t0=0

C@t0=0

'EQUATIONS

Cequ=q@xU/(b*(qm-q@xU))

q_x=dx(q)

q_x@xL = 0

q_x@xU = (K*(C - Cequ))/(rho*Deff)

C_t = Flow*(cfeed-C)/V-m*3*Deff*q_x@xU/(radius*V)

q_t = 1/(x>1e-6)^2*dx(Deff*x^2*q_x)

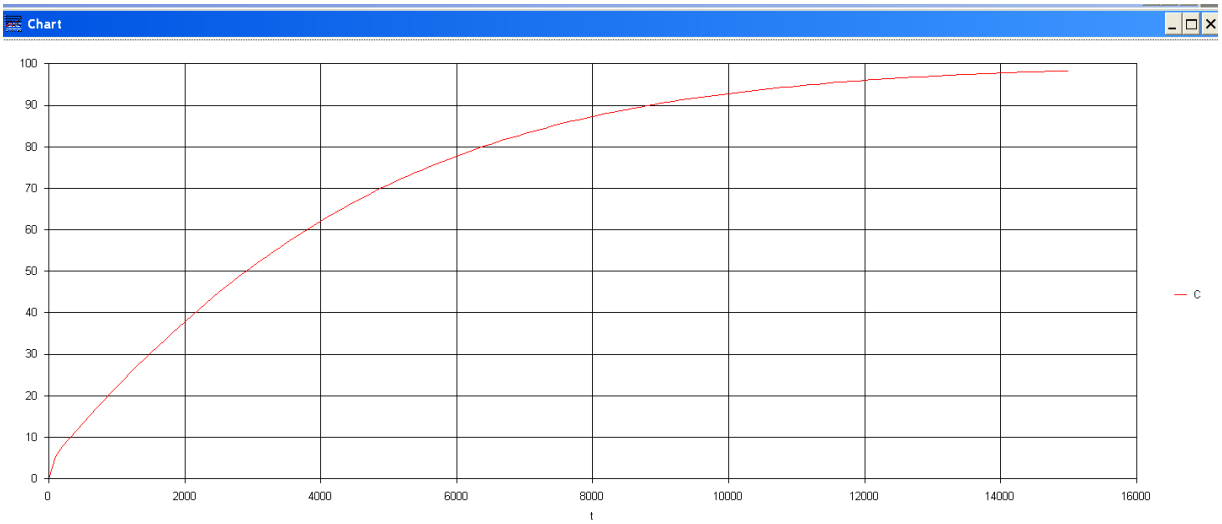

Figure 98 Model curve generated by the PDSOL.

D PUBLISHED WORK

PAPERS ACCEPTED IN PEER REVIEWED JOURNALS:

- Dragosavac, M.M., Sovilj, M.N., Kosvintsev, S.R., Holdich, R.G. & Vladisavljević, G.T. 2008, "**Controlled production of oil-in-water emulsions containing unrefined pumpkin seed oil using stirred cell membrane emulsification**", *Journal of Membrane Science,* vol. 322, no. 1, pp. 178-188.

- Holdich, R.G., Dragosavac, M.M., Vladisavljevićc, G.T. & Kosvintsev, S.R. 2010, "**Membrane emulsification with oscillating and stationary membranes**", Industrial & Engineering Chemistry Research, vol. 49, no. 8, pp. 3810-3817.

- Dragosavac, M.M., Holdich, R.G. & Vladisavljević, G.T. 2011, "**Continuous Flow Stirred Cell Microfiltration of Ion Exchange Media to Determine Mass Transfer Kinetics and Equilibrium Data**", Industrial & Engineering Chemistry Research, vol. 50, no. 4, pp. 2408-2417.

PAPERS SUBMITTED TO THE PEER REVIEWED JOURNALS:

- Dragosavac, M.M., Holdich, R.G., Vladisavljević, G.T. & Sovilj, M.N., "**Stirred cell membrane emulsification for multiple emulsions containing unrefined pumpkin seed oil with uniform droplet size**"
  Submitted to *Journal of Membrane Science* (26 August 2011)

- Dragosavac, M.M., Vladisavljević, G.T., Holdich, R.G. & Stillwell, M.T., " **Production of porous silica microparticles by membrane emulsification**"
  Submitted to *Langmuir* (29 Jul 2011)

ORAL PRESENTATIONS:

- **"Oscillating membrane emulsification",** 10th UK particle Technology Forum, held at Birmingham University on 1st and 2nd July 2009.
  - **Shortlisted as finalist for "Young Researcher Award 2009".**

- **"Combined ion exchange and microfiltration",** Diamond conference, Decommissioning, Immobilisation and Management of Nuclear Waste for Disposal, 9-10 September 2009, York, UK

- **"Stirred cell and oscillating membrane emulsification for particle production",** PARTICLES (of all shapes and sizes) INTO LIQUIDS, 23 September 2009, GSK Stevenage, UK

- **"Novel oscillating membrane emulsification for production of food emulsions and microcapsules"**, 4th EFCE workshop, May 27-28, 201, Belgrade, Serbia.
  - **Chosen as a selected speaker to be a UK representative – Travel award**

- **"Stirred cell and oscillating membrane emulsification for particle production"** World Conference on Particle Technology 2010, WCPT6 Student Conference, April 22-25, 2010, Delft, Holland.

- **"Combined ion exchange and microfiltration",** Diamond conference, Decommissioning, Immobilisation and Management of Nuclear Waste for Disposal, 15-16 December 2010, Manchester, UK
  Also the poster was presented at the conference – First prize for the poster

- **"Novel method of producing highly uniform silica particles using inexpensive silica sources**", UK Colloids 2011, 4-7 July 2011, London

- **–Production of silica particles using membrane emulsification**", PSA 2011, 4-7 September 2011, Edinburgh

  The best student presentation (The Brian Scarlett Memorial and Beckman Coulter Prize)